Elucidating the olfactory pathways within and beyond the antennal lobe in *Drosophila melanogaster*

Dissertation

To Fulfill the

Requirements for the Degree of

„doctor rerum naturalium“ (Dr. rer. nat.)

Submitted to the Council of the Faculty

of Biology and Pharmacy

of the Friedrich Schiller University Jena

by Dipl. Biochemikerin Amelie Erika Elfriede Baschwitz

Born on May 9th 1985 in Altenburg (Thüringen), Germany

Reviewers

1. Prof. Bill S. Hansson, Jena

2. Prof. Rolf G. Beutel, Jena

3. Prof. André Fiala, Göttingen

Date of public defense

July 18, 2017

Research is an expedition into the unknown - that´s why it is so exciting.

- The risks of playing safe -

Gottfried Schatz

(Jeff´s view on science and scientists,

Essays from FEBS Letters; 2006)

Table of Contents

Introduction

Every day we sense a plethora of different odors, each of those either being pleasant, really disgusting or being seemingly not recognized at all. Odorant pleasantness, or hedonic valence, influences our behavior, for example approaching a source by following an odor plume of freshly baked cake or freshly brewed coffee. This is true for humans as well as for insects, like the tiny vinegar fly *Drosophila melanogaster*. The preferred food sources for this fly are decaying and fermented fruits, which flies locate easily when hidden in the abundance of unsuitable food sources in the kitchen or the orchard (Becher, 2012; Begon, 1982; Stökl et al., 2010). To fulfil this essential task they mainly rely on their sense of smell. Furthermore, they use their sense of smell for interacting socially, i.e. finding conspecifics, good mating partners and oviposition sites, as well as avoiding predators. Insects in general are very sensitive to odors and respond specifically to some odors: for example, the male silk moth *Bombyx mori* starts searching behavior after encountering only a few molecules of the female pheromone bombykol (Butenandt and Hecker, 1961; Schneider et al., 1968). From the reception of an odor by olfactory sensory neurons (OSNs) to the elicited odor-guided behavior the relevant odor information is extracted through processing, carried out within the brain by the interplay of different neuronal populations. But how do neurons perform the processing of information from the outer world via versatile senses such as vision, audition or smell? To unravel fundamental principles scientists have to choose simple models to test their assumptions: for example the sea hare *Aplysia* was – due to its large accessible cells – used to study neuron spiking properties during learning, sensitization and habituation (Kandel et al., 2014). To investigate genetic inheritance Thomas Hunt Morgan established *Drosophila melanogaster* as a valuable organism (Morgan, 1910). Since that time several genes and the function of their transcription products were identified in the vinegar fly (Venken et al., 2011). Furthermore, due to the insertion of exogenous genes, the improvement of genetic tools and the completely sequenced genome, *Drosophila* has become a valuable model organism to study neural systems, and especially the olfactory neural circuits (Adams et al., 2000; Luo et al., 2008; Olsen and Wilson, 2008a; Venken et al., 2011).

In the last years the odor response spectra of sensory neurons and higher-order neurons were thoroughly investigated (Bhandawat et al., 2007; de Bruyne et al., 1999; de Bruyne et al., 2001; Dweck et al., 2013; Fiala et al., 2002; Goldman et al., 2005; Hallem and Carlson, 2006; Honegger et al., 2011; Knaden et al., 2012; Kreher et al., 2005; Li et al., 2013; Ng et al., 2002; Perez-Orive et al., 2002; Schubert et al., 2014; Seki et al., 2010; Silbering and Galizia, 2007; Silbering et al., 2008; Silbering et al., 2011; Stensmyr et al., 2012; Stensmyr et al., 2003; Turner et al., 2008; Wang et al., 2003a). Moreover, the representations of odors in the primary olfactory processing center and the relay to the higher brain center involved in learning and memory have been investigated. But the

olfactory neural circuitry is still not fully understood (Hansson et al., 2010; Liang and Luo, 2010; Stocker, 1994; Su et al., 2009). This is also the case for the neural circuitry underlying innate odor-guided behavior (Li and Liberles, 2015; Schultzhaus et al., 2016). Thus, the aim of this thesis is the investigation of functional properties of second-order output neurons in the higher-brain center presumably mediating innate preference to odors by using the model organism *Drosophila melanogaster.* In addition, the neuropil structure in the primary olfactory processing center and the impact of neuron populations on the architecture of the neuropil substructures, the olfactory glomeruli, were examined.

Olfaction in *Drosophila melanogaster*

Drosophila perceives odors through two olfactory organs located on the fore-head: the maxillary palp and the antenna, more precisely the third antennal segment, the so-called funiculus (Figure 1A). The surface of the maxillary palp and the funiculus is equipped with hair-like structures, so-called sensilla. On the funiculus four different types of olfactory sensilla – basiconic, coeloconic, intermediate and trichoid – are stereotypically distributed, whereas on the maxillary palp basiconic sensilla are intermingled with mechanosensitive *sensilla chaetica* (Figure 1B) (Stocker, 1994). Each sensillum houses up to four OSNs as well as three auxiliary cells (thecogen, tormogen, and trichogen cells). Their cell bodies lay at the sensillum base and the dendrites of OSNs lay in the sensillum shaft protected in aqueous sensillum lymph. Into this lymph auxiliary cells secrete odorant binding proteins (OBPs), odor degrading enzymes (ODEs) and chemosensory proteins (CSPs) (Leal, 2013; Pelosi et al., 2014; Shanbhag et al., 1999; Stocker, 1994; Swarup et al., 2011; Vieira and Rozas, 2011; Vogt et al., 2002; Xu et al., 2005). Through pores in the sensillum wall odor molecules enter the sensillum and bind to OBPs. This complex mediates by an unknown mechanism the activation of specific chemoreceptors integrated in the cell membrane of OSN dendrites. OSNs express either one of about 63 olfactory receptors (ORs) encoded by about 60 OR genes or one of the more ancient ionotropic receptors (IRs) encoded by 60 IR genes (Benton et al., 2009; Clyne et al., 1999; Gao and Chess, 1999; Robertson et al., 2003; Vosshall et al., 1999; Vosshall et al., 2000). But few cases of OSN types with expression of two ORs or IRs per neuron exist (Abuin et al., 2011; Couto et al., 2005; Dobritsa et al., 2003; Fishilevich and Vosshall, 2005; Goldman et al., 2005; Larsson et al., 2004; Vosshall, 2001). Exceptions are OSNs that neither express ORs nor IRs but the two gustatory receptors GR21a and GR63a, which in combination detect carbon dioxide (Jones et al., 2007; Kwon et al., 2007; Suh et al., 2004). Distinct sensilla subtypes house always an identical combination of OSNs expressing a specific chemoreceptor (Benton et al., 2009; Couto et al., 2005). OSNs housed in coeloconic sensilla mostly express IRs that detect mainly acids and amines (Abuin et al., 2011; Ai et al., 2010; Benton et al., 2009; Silbering et al., 2011; Yao et al., 2005). ORs form complexes with the ubiquitous olfactory receptor co-receptor (Or-

co, formerly called OR83b) constituting a heteromeric receptor ion channel complex for the signal transduction in OSNs (Larsson et al., 2004; Neuhaus et al., 2005). This OR-Orco complex depolarizes OSNs after odor binding via ionotropic and metabotropic pathways (Sato et al., 2008; Wicher et al., 2008). Likewise, IRs form complexes with IR8a or IR25a as co-receptor (Abuin et al., 2011).

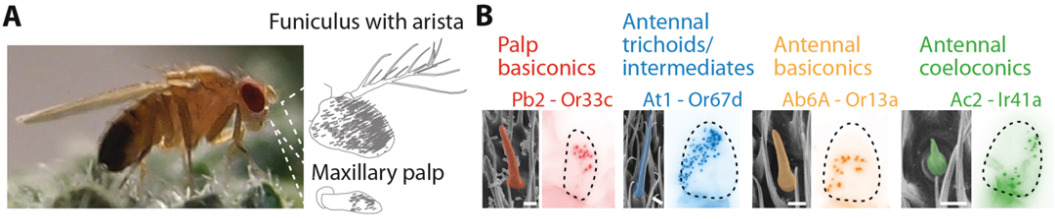

Figure 1 | Olfactory sensory organs of *Drosophila melanogaster*

(A) The olfactory organs, maxillary palp and the third antennal segment, the funiculus (with the mechanosensory arista), are located on the fore-head of the fly. On the surface of both olfactory appendages olfactory sensilla are distributed. (B) For each different type of sensillum (trichoid/ intermediate, coeloconic, antennal and palp basiconic) a representative scanning electron micrograph is shown (on the left) and the distribution of the sensilla by labeling of OSNs expressing a specific chemoreceptor (on the right). Scale bars equal 20 µm. Adopted from manuscript 3.

To comprehensively analyze the odor response profiles of OSNs several studies using single sensillum recordings (SSR) were performed (de Bruyne et al., 1999; de Bruyne et al., 2001; Dweck et al., 2013; Goldman et al., 2005; Hallem and Carlson, 2006; Kreher et al., 2005; Silbering et al., 2011; Stensmyr et al., 2012; Stensmyr et al., 2003; van der Goes van Naters and Carlson, 2007) (Manuscript 3). This continuously increasing knowledge on odor response profiles of almost all *Drosophila* olfactory chemoreceptors is available online at the DoOR data base (http://neuro.uni-konstanz.de/DoOR/2.0/) (Münch and Galizia, 2016). Furthermore, these studies revealed that the expressed chemoreceptor determines the odor response profile of OSNs, their spontaneous firing rate, the response dynamic, as well as their signaling mode – exhibiting inhibitory or excitatory responses (Hallem et al., 2004). Some ORs are activated by several odors, i.e. they are broadly tuned, whereas some ORs are excited by single or few odorants with a specific ecological relevance (Hallem and Carlson, 2006). To those odors belong pheromones (Dweck et al., 2015b; Ha and Smith, 2006; Kurtovic et al., 2007), cues indicating either suitable (Dweck et al., 2013) or unsuitable oviposition sites (Ebrahim et al., 2015), the stress signal carbon dioxide (Suh et al., 2004), as well as food infested with harmful microbes (Babin et al., 2014; Stensmyr et al., 2012). The selectivity of a receptor can be described by calculating the lifetime sparseness based on the odor response profile tested for a large set of odors. Higher lifetime sparseness values signify a higher degree of OR specificity (Bhandawat et al., 2007; Perez-Orive et al., 2002; Vinje and Gallant, 2000) (Manuscript 3).

Perceived odors, either being monomolecular odorants or complex mixtures, elicit stereotypic behaviors in flies, like the approach of food sources or its avoidance. This innate odor-guided behavior of flies can be analyzed in behavioral assays such as the trap-assay, the Flywalk, the wind tunnel, the tethered flight arena or the T-maze assay (Budick and Dickinson, 2006; Frye and Dickinson, 2004; Larsson et al., 2004; Steck et al., 2012; Suh et al., 2004; Tully and Quinn, 1985). Those assays evaluate the hedonic valence, i.e. the pleasantness, of a single odor or complex mixtures as a strong or weak attractant or repellent. However, the innate odor-guided response can be modulated by the internal state of the fly, the context, or the fly´s experience (Beshel and Zhong, 2013; Bräcker et al., 2013; Heisenberg, 2015; Lin et al., 2014b; Owald and Waddell, 2015; Root et al., 2011; Su and Wang, 2014). Innate and experience-dependent odor-guided behaviors are the result of complex neural processing in different neuropils. The current knowledge about the olfactory neural circuitry is briefly reviewed in the next section.

Neural circuitry in the *Drosophila* olfactory system

About 1,200 OSNs of the antennae converge to the antennal nerve and innervate the primary olfactory processing center, the antennal lobe (AL). About 120 OSNs of the maxillary palps converge to the labial nerve, passing through the suboesophageal ganglion, also innervate the AL (Figure 2A). Most OSNs innervate both ipsi- and contralateral ALs via an axonal commissure (Shanbhag et al., 1999, 2000; Stocker, 1994, 2001; Stocker et al., 1990). Within the AL the OSNs expressing the same chemoreceptor converge onto one (in rare cases two) spherical subunit, called glomerulus (Fishilevich and Vosshall, 2005; Gao et al., 2000; Vosshall et al., 2000). 54 glomeruli are described for *Drosophila melanogaster*, four of which are non-olfactory glomeruli: they are thermosensitive or hygrosensitive (Enjin et al., 2016; Gallio et al., 2011). Position, size and shape of glomeruli are invariant across flies and thus create a topographic map (Couto et al., 2005; Fishilevich and Vosshall, 2005; Laissue et al., 1999) (Manuscript 2). In each glomerulus OSNs synapse on a specific number of second-order neurons, so-called projection neurons (PNs), and local interneurons (LNs) (Manuscript 3). Three cell clusters attached to the anterodorsal, lateral and ventral surface of the AL contain the cell bodies of about 150 PNs, whereas the cell bodies of about 200 LNs lie between as well as within these three cell clusters (Chou et al., 2010; Das et al., 2011; Seki et al., 2010; Stocker et al., 1990). LNs exhibit various innervation patterns in the AL either innervating all glomeruli, most glomeruli, glomeruli in specific clusters, discontinuous regions or only a few glomeruli. Furthermore, LNs display a diverse neurotransmitter repertoire releasing the neurotransmitters acetylcholine, gamma-aminobutyric acid (GABA), glutamate, or neuropeptides as well as combinations of neurotransmitters and neuropeptides, which elicit excitatory and inhibitory effects on the postsynaptic targets (Chou et al., 2010; Das et al., 2011; Ignell et al., 2009; Liu and Wilson, 2013; Seki et al., 2010; Shang et al., 2007;

Wilson and Laurent, 2005). Additionally, LNs are connected with PNs via electrical synapses (Huang et al., 2010; Yaksi and Wilson, 2010). By means of lateral excitation or lateral inhibition or both LNs modulate the odor responses transferred from OSNs to PNs (Olsen et al., 2007, 2010; Olsen and Wilson, 2008b; Root et al., 2008; Root et al., 2007; Shang et al., 2007; Silbering and Galizia, 2007; Wilson and Laurent, 2005; Yaksi and Wilson, 2010). This causes for some odors almost identical OSN and PN responses or broader PN responses (Bhandawat et al., 2007; Kazama and Wilson, 2008; Knaden et al., 2012; Ng et al., 2002; Root et al., 2008; Schlief and Wilson, 2007; Semmelhack and Wang, 2009; Silbering et al., 2008; Wang et al., 2003a; Wang et al., 2014; Wilson et al., 2004). The modulated input signal is transferred by the PNs to higher brain centers. Two major populations of PNs can be distinguished based on their innervation of one (uniglomerular) or several glomeruli (multiglomerular), as well as on their secreted neurotransmitter being either acetylcholine or GABA (Okada et al., 2009; Yasuyama and Salvaterra, 1999). Excitatory uniglomerular PNs (ePNs) have their cell bodies in the anterodorsal and the lateral cell cluster. They convey odor information via the medial antennal lobe tract or the lateral antennal lobe tract to the higher brain centers mushroom body calyx and lateral horn (LH) (Jefferis et al., 2007; Stocker et al., 1997; Tanaka et al., 2012). Inhibitory, multiglomerular PNs (iPNs) have their cell bodies in the ventral cell cluster and they innervate directly and solely the LH via the mediolateral antennal lobe tract (Ito et al., 1997; Jefferis et al., 2007; Lai et al., 2008; Liang et al., 2013; Okada et al., 2009; Stocker et al., 1990; Tanaka et al., 2004; Tanaka et al., 2012).

The mushroom body is involved in learning and memory as well as context-dependent odor evaluation (Bräcker et al., 2013; Davis, 2005; Heisenberg, 2003; Lin et al., 2014b; Owald and Waddell, 2015). Within the mushroom body calyx ePNs form boutons synapsing on several third-order neurons called Kenyon cells (KCs) (Butcher et al., 2012; Stocker, 1994). Approximately 2,500 cell bodies of KCs are densely packed around the mushroom body calyx. The KCs project via the peduncle to the mushroom body lobes where they synapse on relatively few mushroom body output neurons (Aso et al., 2014a; Aso et al., 2014b; Sejourne et al., 2011; Tanaka et al., 2008). Furthermore, KCs are connected to apparently random sets of ePN types supporting a combinatorial odor response pattern in distinct KCs (Caron et al., 2013; Masuda-Nakagawa et al., 2005; Murthy et al., 2008). KCs exhibit a sparse coding since they need input by several PNs to get excited (Honegger et al., 2011; Perez-Orive et al., 2002; Turner et al., 2008). The random organization of the ePN-KC connections as well as the overall sparse coding of odors by KCs permits associations of any perceived odor with experiences – the basic feature for learning. In studies ablating the mushroom body the ability to perform olfactory associative learning tasks is abolished but innate behavioral responses are not affected suggesting a role of the LH in innate olfactory behaviors (de Belle and Heisenberg, 1994; Heimbeck et al., 2001; Heisenberg et al., 1985; Kido and Ito, 2002). The stereo-

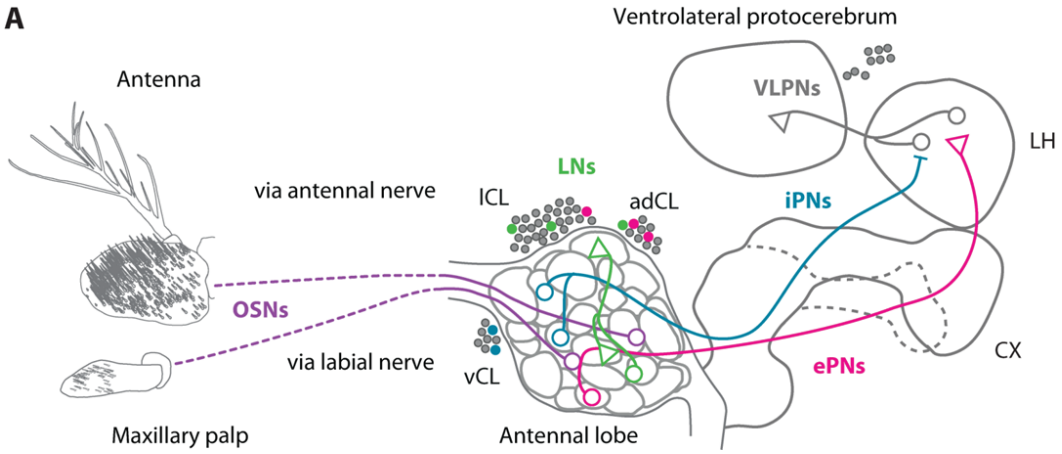

Figure 2 | The neural circuitry of the olfactory system in *Drosophila*

(A) Olfactory sensory neurons (OSNs) housed in sensilla located on the peripheral olfactory organs, antenna and maxillary palp, innervate via the antennal and labial nerve distinct glomeruli of the primary olfactory processing center, the antennal lobe. Within glomeruli OSNs synapse onto local interneurons (LNs), as well as excitatory and inhibitory projection neurons (ePNs and iPNs). Somata of LNs, ePNs and iPNs are located in different cell clusters ventral (vCL), lateral (lCL) and anterodorsal (adCL) on the surface of the AL. The two types of projection neurons innervate via different tracts the higher brain centers, the mushroom body calyx (CX) or the lateral horn (LH) or both. Within the LH projection neurons synapse onto third order neurons of the ventrolateral protocerebrum (VLPNs). Adopted from manuscripts 3 and 4.

typed innervation patterns of ePNs in the LH as well as the stereotyped connectivity to specific third-order lateral horn neurons (LHNs) support the notion of the LH being responsible for hard-wired innate odor-guided behavior (Fişek and Wilson, 2014; Jefferis et al., 2007; Lin et al., 2007; Marin et al., 2002; Wong et al., 2002). Odor representations for either few tested or simulated odors revealed different coding strategies either of separation of food and pheromone odors or aversive and attractive odors (Jefferis et al., 2007; Liang et al., 2013; Min et al., 2013). Using a set of 18 odors including acids, lactones, terpenes, aromatics, alcohols, esters, ketones and the blend balsamic vinegar we expanded the investigation on odor representations of ePNs and iPNs in the LH and revealed a spatial coding of odor valence and intensity (Manuscripts 1 and 4). This reduction of odor information to ecological relevance appears to be the basic feature to elicit innate behavior.

Transgenic flies and applied methods

Using the model-organism *Drosophila melanogaster* provides several advantages such as short reproduction cycles, easy and cheap breeding, a huge number of isogenic siblings, a fully sequenced genome, and most important a plethora of genetic tools (Adams et al., 2000; Duffy, 2002; Luo et al., 2008; Venken et al., 2011). Those tools allow the

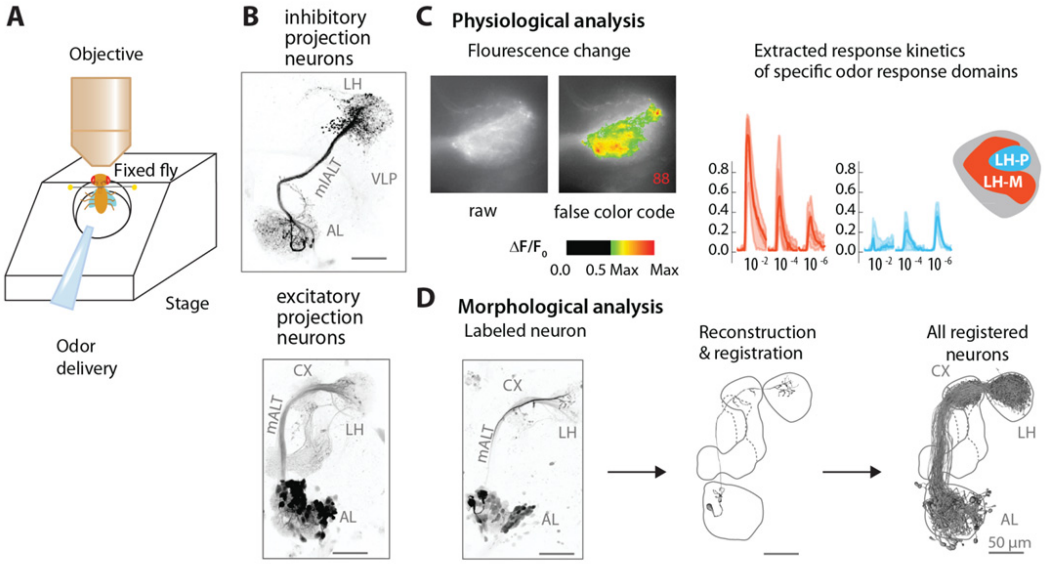

Figure 3 | Morphological and physiological analysis of the neural circuitry in *Drosophila*

(A) Fixed fly in a custom-made stage for *in vivo* preparation. (B) Overview of the innervation of the inhibitory (top) and excitatory neuron populations (bottom). (C) Physiological analysis using functional calcium imaging. Representative images of responses to benzaldehyde by excitatory projection neurons (left raw image, right false color coded fluorescence change).Time traces of the response to benzaldehyde in different concentrations in the two different odor response domains (LH-M and LH-P) (D) Morphological analysis of labeled single neurons by reconstruction and registration to a reference brain enables comparison with all registered neurons. Scale bars equal 50 µm. Abbreviations: AL antennal lobe, CX mushroom body calyx, LH lateral horn. Adopted from manuscript 4.

analysis of an unbelievably wide array of cellular processes of interest. Commonly used important tools are the binary transcription systems like GAL4-UAS (Brand and Perrimon, 1993), the Q-system (Potter et al., 2010) and LexA-LexAop (Lai and Lee, 2006). We chose the GAL4-UAS system in all experiments (Manuscripts 1 to 4). It is based on the brewer's yeast its (*Saccharomyces cerevisiae*) transcriptional activator GAL4 integrated in the genome of a driver fly line in front of an endogenous promotor sequence and the GAL4 binding site downstream of the target sequence integrated in the genome of the responder fly line. The binding of GAL4 to its binding site, the upstream activating sequence (UAS), initiates the transcription of the downstream gene of interest (Duffy, 2002). The binary transcription systems thus enable via crossing of distinct transgenic lines a temporally and spatially selective integration and expression of reporter proteins, like fluorescent proteins, to investigate for example neuron populations. One of the most frequently used fluorescent proteins is the green fluorescent protein (GFP) of the jellyfish *Aequorea victoria* and its derivatives (van Thor, 2009). To label single neurons we expressed the photoactivatable green fluorescent protein (pa-GFP), which fluorescence signal increases 100-fold after irradiation with visible or infrared light

(Datta et al., 2008; Patterson and Lippincott-Schwartz, 2002; Ruta et al., 2010). This permits the specific labeling of single or several neurons, as well as whole neuron populations of interest, and thus allows their morphological analysis *in vivo*. We used this approach to characterize the morphology of single neurons of the enhancer trap lines GH146-GAL4 (Stocker et al., 1997) and MZ699-GAL4 (Ito et al., 1997) that label most of the ePNs and iPNs, respectively (Figure 3B; Manuscripts 1, 3 and 4).

Another approach is the use of genetically encoded calcium (or chloride) indicators (GECIs) to monitor neuronal activity (Hires et al., 2008; Miyawaki et al., 1997; Riemensperger et al., 2012). Those indicators rely on the increased fluorescence emission by the GFP fluorophore due to a conformational change after calcium binding to the calcium binding sites (Akerboom et al., 2009). The expression of calcium-sensitive proteins, such as GCaMP and GECO, enables the visualization of excited neurons due to the increase in cytoplasmic calcium concentration resulting in stronger emission of fluorescence (Chen et al., 2013; Nakai et al., 2001; Tian et al., 2009; Zhao et al., 2011). In combination with the GAL4-UAS system GECIs support the analysis of responses of defined neuron populations, whereas electrophysiological techniques are limited to recordings from single neurons or up to a dozen of neurons. Gained spatiotemporal activity patterns in calcium imaging experiments can be used to extract through computational analysis the time traces for the different odor responses and spatial patterns that can be clustered to odor response domains (Figure 3C). For calcium imaging in the LH we used wide-field fluorescence microscopy to record the fluorescence light emitted of neurons in a thick plane. This allows measuring the responses of the whole PN population in the LH simultaneously to get a global perspective on the odor representation (Manuscripts 1 and 4).

To analyze synaptic connections between specific neuron populations the GFP reconstitution across synaptic partners (GRASP) was used (Feinberg et al., 2008). In this approach the GFP-protein is split in two parts and these parts are fused to synaptic proteins. The fused proteins are expressed in distinct neuron types accomplished by the use of different binary transcription systems. If the two parts of the GFP are located in connected synapses they can reconstitute and emit fluorescence. Applying this approach, we analyzed the synaptic connections of ePNs, iPNs and third-order neurons (Manuscript 4).

For anatomical analysis of single neurons obtained in our studies the spatial resolution was increased by the use of multiphoton confocal laser scanning microscopy. This enables the activation of a single focal plane to reduce photobleaching and improves the signal-to-noise ratio due to the reduction of scattered photons. Moreover, multiphoton microscopy uses light of longer wavelength with lower energy to excite fluorophores, thus further reducing the photobleaching of the fluorophores and the photodamage of the

tissue (Denk et al., 1990). In addition, the use of longer wavelength permits the imaging of tissues *in vivo* in up to 200 µm depth (Masters et al., 1997). The use of multiphoton confocal laser scanning microscopy provides higher precision for the photoactivation experiments. In contrast, for laser ablation the laser intensity was increased deliberately to damage the tissue but restricted precisely to a small region of interest (Manuscripts 1 and 4).

Investigations of neuron populations described in the manuscripts 1 and 4 aimed at connecting morphological characterizations of single projection neurons with their physiological properties (Figure 3A). To reliably identify neuropil structures *in vivo*, we developed a protein construct called END1-2 that mimics the neuropil staining obtained with the antibody nc82 (Hofbauer, 1991) (Manuscript 2). END1-2 consists of the protein ELAV (embryonic lethal abnormal vision), which is involved in the development of the central nervous system in *Drosophila melanogaster*, combined with the neuronal synaptic vesicle protein *n*-synaptobrevin and the red fluorescent protein DsRed found in the coral *Discosoma striata* (DiAntonio et al., 1993; Matz et al., 1999; Yao et al., 1993). This construct was integrated in the genome of *Drosophila* and thus can be combined with the GAL4-UAS system. Confocal scans of specific neurons with the neuropil staining by END1-2 facilitate subsequent 3D-reconstruction and registration of the *in vivo* anatomy, enabling a thorough investigation of neuropil structures and neuronal arborizations (Rybak et al., 2010) (Figure 3D; Manuscripts 1 to 4).

Aim of this thesis

This thesis aimed at investigating the relay of odor information from the primary olfactory processing center to the higher brain center, presumably mediating innate odor-guided behavior, the LH. This was accomplished by comparing the morphology of two types of projection neurons and by analyzing the characteristics of their odor representations in the higher brain to reveal the strategies of odor coding in the LH. Furthermore, the impact of quantitive abundance of different neuron types on the neuropil structure and on the importance of different odor processing channels was examined.

Several studies analyzed the representation of odors in the AL revealing a combinatorial map (Knaden et al., 2012; Ng et al., 2002; Root et al., 2007; Schubert et al., 2014; Wang et al., 2003a). For the mushroom body it was shown that odors are represented as a combinatorial but sparse code (Honegger et al., 2011; Ito and Awasaki, 2008; Lin et al., 2014a; Perez-Orive et al., 2002; Turner et al., 2008; Wang et al., 2004). Yet, the LH is poorly investigated regarding the representation of odors. In the LH odor responses of projection neurons were simulated or measured only for few odors (Jefferis et al., 2007; Liang et al., 2013; Parnas et al., 2013). Furthermore, a few studies analyzed the activity of subsets of third-order neurons in the LH (Fişek and Wilson, 2014; Kohl et al., 2013;

Ruta et al., 2010; Yu et al., 2010). Therefore, we analyzed the innervation patterns of ePNs and iPNs in the LH as well as their global representation of several odors. In addition, the connectivity of ePNs and iPNs on a subset of third-order neurons of the VLP was investigated (Manuscripts 1 and 4).

Available atlases of the AL glomeruli are generated based on *in vitro* data and consequently suffer from fixation artefacts (Chiang et al., 2011; Couto et al., 2005; Laissue et al., 1999; Ma et al., 2008; Rein et al., 2002). However, the *in vivo* analysis of the glomerular innervation pattern of multiglomerular iPNs required the use of an atlas based on morphological *in vivo* data (Manuscript 1). Therefore, we generated such an *in vivo* atlas of the fly AL and investigated the impact of *in vitro* processing onto this neuropil (Manuscript 2). Furthermore, this *in vivo* atlas was also applied to determine the glomerulus of interest for the specific labeling of all ePNs innervating this distinct glomerulus (Manuscripts 3 and 4).

Moreover, the characteristics of the glomerular morphology were studied as well as the impact of the neuronal composition. This enabled to correlate the glomerular neural circuit with the ecological relevance of the processed odor information. Thus, we could show that the number of neurons innervating a specific glomerulus varies and that these numbers correlate with the breadth of the odor tuning profile of the glomerulus (Manuscript 3).

Overview of Manuscripts

Manuscript 1

Decoding Odor Quality and Intensity in the *Drosophila* brain

Antonia Strutz, Jan Soelter, Amelie Baschwitz, Abu Farhan, Veit Grabe, Jürgen Rybak, Markus Knaden, Michael Schmuker, Bill S. Hansson, Silke Sachse

eLife 2014; 3:e04147

Published, 16 December 2014 (DOI: 10.7554/eLife.04147)

In this study we investigated the morphological, functional and behavioral properties of multiglomerular inhibitory projection neurons. Due to their segregated innervation patterns in the antennal lobe and lateral horn as well as due to their odor representation in the lateral horn, either coding odor valence or intensity, we describe two subpopulations of inhibitory projection neurons. Furthermore, diminishing neuronal activity in inhibitory projection neurons results in increased odor avoidance behavior as well as in disinhibition of third-order neurons of the ventrolateral protocerebrum. These results indicate the contribution to odor attraction.

Author contributions:

Built on an idea conceived by all authors.

Designed experiments: A. Strutz, S. Sachse, B. S. Hansson

Performed physiological experiments: A. Strutz, V. Grabe

Performed behavioral experiments: A. Farhan

Performed single neuron labeling and 3D-reconstruction: A. Baschwitz

Performed morphological analysis: A. Baschwitz (50%), S. Sachse

Performed bioinformatic analysis: J. Soelter, M. Schmuker

Performed physiological analysis: A. Strutz, S. Sachse

Wrote the manuscript: A. Strutz, J. Soelter, S. Sachse, B. S. Hansson

Manuscript 2

Digital *in vivo* 3D atlas of the antennal lobe of *Drosophila melanogaster*

Veit Grabe*, Antonia Strutz*, Amelie Baschwitz, Bill S. Hansson, Silke Sachse

* These authors contributed equally

The Journal of Comparative Neurology; 523, 530-544

Published, 15 February 2015 (DOI: 10.1002/cne.23697)

Establishing a genetically encoded fluorescent neuropil staining allowed us to generate an atlas of the antennal lobe representing the *in vivo* situation. Furthermore, this enabled analyses of the actual impact of fixation artifacts on the flexible antennal lobe structure. Unequal volumetric differences and dislocations of the neuropil in the *in vitro* situation emphasized the importance of using morphological *in vivo* data to compare and assign with physiological studies.

Author contributions:

Built on an idea conceived by all authors.

Designed experiments: V. Grabe, A. Strutz, B. S. Hansson and S. Sachse

Performed immunohistochemistry and confocal scans: V. Grabe, A. Baschwitz (30%)

Generated fly line: A. Strutz

Analyzed the data: V. Grabe and S. Sachse

Wrote the manuscript: V. Grabe, S. Sachse and B. S. Hansson

Revised the article: all authors

Manuscript 3

Elucidating the neuronal architecture of olfactory glomeruli in the *Drosophila* antennal lobe

Veit Grabe*, Amelie Baschwitz*, Hany K. M. Dweck, Sofia Lavista-Llanos, Bill S. Hansson and Silke Sachse

* These authors contributed equally

Cell Reports 16, 3401–3413

Published, 20 September 2016 (DOI: 10.1016/j.celrep.2016.08.063)

Olfactory glomeruli in the antennal lobe exhibit stereotypic shapes and sizes. Investigating the numerical proportions of sensory neurons, projection neurons, as well as local interneurons revealed varying numbers for all neuron types for the single glomeruli and the correlation of the glomerular volume to the number of sensory and projection neurons. Furthermore, functional consideration of all neuron types highlights a dependence of glomerular wiring to the odor tuning profile. The connection of morphological and functional properties emphasizes the uniqueness of each glomerulus and allows predictions of the significance of the detected odor in less characterized glomeruli.

Author contributions:

Built on an idea conceived by V. Grabe, B. S. Hansson and S. Sachse

Designed experiments: V. Grabe, A. Baschwitz (30%) and S. Sachse

Performed neuron labeling and quantification: V. Grabe, A. Baschwitz (50%)

Performed SSR: H. K. M. Dweck

Analyzed the data: V. Grabe, A. Baschwitz (25%), H. K. M. Dweck and S. Sachse

Wrote the manuscript: V. Grabe, S. Sachse and B. S. Hansson

Revised the article: all authors

Manuscript 4

Parallel olfactory pathways support odor valence and intensity coding in the lateral horn of *Drosophila melanogaster*

Amelie Baschwitz*, Jan Soelter*, Natalia Marquez, Jürgen Rybak, Michael Schmuker, Bill S. Hansson, Silke Sachse

* These authors contributed equally

In preparation for eLife

In this study we analyzed the morphological and functional properties of excitatory projection neurons in the lateral horn. Stereotypic innervations of excitatory projection neurons retain the topographic map of the antennal lobe. Moreover, odor representations in the lateral horn separate in two domains coding either aversive odors and high odor concentration or attractive odors. Comparing these findings of ePNs with those of iPNs supports a parallel but antagonizing pathway from the primary olfactory center to the second-order brain center presumably mediating innate olfactory-driven behavior.

Author contributions:

Built on an idea conceived by A. Baschwitz, J. Soelter, B. S. Hansson and S. Sachse.

Designed experiments: A. Baschwitz (60%) and S. Sachse

Performed morphological and physiological experiments: A. Baschwitz

Performed bioinformatic analysis: J. Soelter, M. Schmuker

Performed data analysis: A. Baschwitz (40%), J. Soelter, S. Sachse

Performed GRASP experiments and analysis: N. Marquez

Wrote the manuscript: A. Baschwitz (60%), B. S. Hansson and S. Sachse

Revised the article: all authors

Manuscript 1

Decoding Odor Quality and Intensity in the *Drosophila* brain

Antonia Strutz, Jan Soelter, Amelie Baschwitz, Abu Farhan, Veit Grabe, Jürgen Rybak, Markus Knaden, Michael Schmuker, Bill S. Hansson, Silke Sachse

eLife 2014; 3:e04147

Published, 16 December 2014 (DOI: 10.7554/eLife.04147)

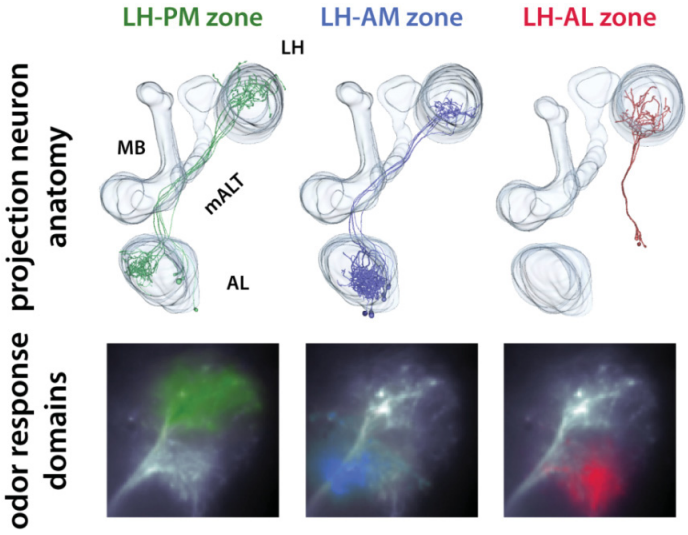

eLIFE elifesciences.org

RESEARCH ARTICLE

Decoding odor quality and intensity in the *Drosophila* brain

Antonia Strutz[1], Jan Soelter[2], Amelie Baschwitz[1], Abu Farhan[1], Veit Grabe[1], Jürgen Rybak[1], Markus Knaden[1], Michael Schmuker[2†], Bill S Hansson[1], Silke Sachse[1]*

[1]Department of Evolutionary Neuroethology, Max Planck Institute for Chemical Ecology, Jena, Germany; [2]Department for Biology, Pharmacy and Chemistry, Free University Berlin, Neuroinformatics and Theoretical Neuroscience, Berlin, Germany

Abstract To internally reflect the sensory environment, animals create neural maps encoding the external stimulus space. From that primary neural code relevant information has to be extracted for accurate navigation. We analyzed how different odor features such as hedonic valence and intensity are functionally integrated in the lateral horn (LH) of the vinegar fly, *Drosophila melanogaster*. We characterized an olfactory-processing pathway, comprised of inhibitory projection neurons (iPNs) that target the LH exclusively, at morphological, functional and behavioral levels. We demonstrate that iPNs are subdivided into two morphological groups encoding positive hedonic valence or intensity information and conveying these features into separate domains in the LH. Silencing iPNs severely diminished flies' attraction behavior. Moreover, functional imaging disclosed a LH region tuned to repulsive odors comprised exclusively of third-order neurons. We provide evidence for a feature-based map in the LH, and elucidate its role as the center for integrating behaviorally relevant olfactory information.
DOI: 10.7554/eLife.04147.001

***For correspondence:** ssachse@ice.mpg.de

Present address: †School of Engineering and Informatics, University of Sussex, Brighton, United Kingdom

Competing interests: See page 19

Funding: See page 19

Received: 24 July 2014
Accepted: 09 November 2014
Published: 16 December 2014

Reviewing editor: Mani Ramaswami, Trinity College Dublin, Ireland

Introduction

To navigate the environment in a way that optimizes their survival and reproduction, animals have evolved sensory systems. These have three essential tasks: First, the external world has to be translated into an internal representation in the form of an accurate neural map. Second, the neural map has to be readable and interpretable, that is, the generated neural code must allow common attributes to be extracted across stimuli to enable the animal to make the best decisions. Third, the animal has to be able to adapt to environmental changes and to form a sensory memory of new stimuli. Many studies have been dedicated to unraveling the primary transformation from a stimulus into an initial neural representation within various sensory systems (***Manni and Petrosini, 2004***; ***Vosshall and Stocker, 2007***; ***Sanes and Zipursky, 2010***) and to elucidating neuronal plasticity and sensory memory formation in higher-level processing centers (***Heisenberg, 2003***; ***Pasternak and Greenlee, 2005***). The ability to extract features and integrate stimulus modalities have so far mainly been studied in the visual system (***Livingstone and Hubel, 1988***; ***Bausenwein et al., 1992***; ***Nassi and Callaway, 2009***). We addressed the question of how stimulus features such as odor valence and intensity are coded and integrated within the olfactory system using the model organism *Drosophila melanogaster*.

The olfactory system of the vinegar fly provides an excellent model system for deciphering olfactory processing mechanisms, since it displays remarkable similarities to the mammalian system but is less complex and highly genetically tractable. Like other sensory systems, the olfactory system employs a spatio-temporal map to translate the variables in chemosensory space into neuronal activity patterns in the brain. This map emerges when the olfactory sensory neurons (OSNs) with the same chemosensory receptors converge into one exclusive glomerulus in the antennal lobe (AL) which represents the

eLife digest Organisms need to sense and adapt to their environment in order to survive. Senses such as vision and smell allow an organism to absorb information about the external environment and translate it into a meaningful internal image. This internal image helps the organism to remember incidents and act accordingly when they encounter similar situations again. A typical example is when organisms are repeatedly attracted to odors that are essential for survival, such as food and pheromones, and are repulsed by odors that threaten survival.

Strutz et al. addressed how attractiveness or repulsiveness of a smell, and also the strength of a smell, are processed by a part of the olfactory system called the lateral horn in fruit flies. This involved mapping the neuronal patterns that were generated in the lateral horn when a fly was exposed to particular odors.

Strutz et al. found that a subset of neurons called inhibitory projection neurons processes information about whether the odor is attractive or repulsive, and that a second subset of these neurons process information about the intensity of the odor. Other insects, such as honey bees and hawk moths, have olfactory systems with a similar architecture and might also employ a similar spatial approach to encode information regarding the intensity and identity of odors. Locusts, on the other hand, employ a temporal approach to encoding information about odors.

The work of Strutz et al. shows that certain qualities of odors are contained in a spatial map in a specific brain region of the fly. This opens up the question of how the information in this spatial map influences decisions made by the fly.

DOI: 10.7554/eLife.04147.002

equivalent to the mammalian olfactory bulb (***Hildebrand and Shepherd, 1997***; ***Vosshall et al., 2000***; ***Vosshall and Stocker, 2007***). Glomeruli, the functional and morphological units of the AL, are microcircuits comprising OSNs, multiglomerular local interneurons (LNs) and uniglomerular output neurons, so-called excitatory projection neurons (ePNs) (***Wilson and Mainen, 2006***; ***Vosshall and Stocker, 2007***) that convey the olfactory information to higher brain centers, as the mushroom body calyx (MBc) and the lateral horn (LH) (***Stocker et al., 1997***). The stringent spatial arrangement of OSNs and ePNs in the AL generates a spatial map containing characteristic combinatorial glomerular activity patterns for all odorants (***Fiala et al., 2002***; ***Wang et al., 2003a***; ***Couto et al., 2005***; ***Fishilevich and Vosshall, 2005***). The MBc is involved in olfactory memory formation (***Heisenberg, 2003***) and enables a contextualization of the odor space (***Caron et al., 2013***). By exclusion, the LH is believed to be involved in innate olfactory behavior (***de Belle and Heisenberg, 1994***; ***Jefferis et al., 2007***). Excitatory PNs retain the sensory information encoded in the AL and form glomerulus-dependent, stereotypic axonal terminal fields in the LH (***Marin et al., 2002***; ***Wong et al., 2002***; ***Tanaka et al., 2004***). Compartmentalization in the LH has been observed in form of a spatial segregation of ePNs innervating specific glomerular subgroups (***Tanaka et al., 2004***), fruit and pheromone odor information processing ePNs (***Jefferis et al., 2007***) as well as ammonia and amine vs carbon dioxide coding ePNs (***Min et al., 2013***).

Like many other sensory networks, the olfactory circuit of the fly contains spatially distinct pathways to the higher brain, namely the inner, middle and outer antennocerebral tract (iACT, mACT and oACT) (***Stocker et al., 1990***). Notably, the mACT projects from the AL to the LH exclusively and consists of inhibitory PNs (iPNs), which exhibit also uniglomerular but mainly multiglomerular AL innervations (***Ito et al., 1997***; ***Jefferis et al., 2007***; ***Lai et al., 2008***; ***Okada et al., 2009***; ***Liang et al., 2013***). Both PN populations have been attributed different coding properties: Although both PN populations exhibit odor responses to overlapping odor ligands, iPNs seems to be broader tuned than ePNs (***Wang et al., 2014***). Furthermore, while ePNs encode rather odor identity (***Wang et al., 2003a***; ***Wilson et al., 2004***; ***Silbering et al., 2008***), iPNs have been shown to enhance innate discrimination of closely related odors (***Parnas et al., 2013***). Together, these PN populations process information on dual olfactory pathways (***Liang et al., 2013***; ***Wang et al., 2014***), as do processing mechanisms in other sensory modalities (***Nassi and Callaway, 2009***), and most likely accomplish different olfactory behaviors. The mainly multiglomerular AL pattern of iPNs suggests that these neurons extract characteristic stimulus features from the AL code and re-integrate this information into the LH to mediate innate odorant-guided behavior. This assumption is further supported by two recent studies showing that the

inhibitory input from the AL to the LH is module-specific, that is, selective for food odors and pheromones (***Liang et al., 2013***; ***Fisek and Wilson, 2014***), while the connectivity in the MBc is rather probabilistic (***Murthy et al., 2008***; ***Caron et al., 2013***).

However, it still remains open if and how different odor features as hedonic valence or intensity are functionally coded and integrated in the LH. In this study, we characterized and dissected the iPN olfactory processing pathway regarding the coding of odor quality and intensity at morphological, functional and behavioral levels. By linking odor-evoked activity patterns in the LH to odor-guided behavior, we provide evidence that iPNs mediate odor attraction. Furthermore, our data demonstrate a feature-based, spatially segregated activity map in the LH comprised of iPNs and third-order neurons and thus expand its role as a center for integrating behaviorally relevant olfactory information.

Results

Dendrites of iPNs innervate two-thirds of olfactory glomeruli

Cell bodies of iPNs are exclusively located in the ventral cell cluster which consists of ~50 iPNs (***Lai et al., 2008***) that project via the mACT to the LH, thereby bypassing the MBc (***Ito et al., 1997***) (***Figure 1A,B***). In contrast, ePN somata are located anterodorsally and laterally of the AL, and their axons project through the iACT or oACT to the MBc and the LH (***Stocker et al., 1997***; ***Marin et al., 2002***; ***Wong et al., 2002***; ***Lai et al., 2008***). To analyze the innervation patterns of iPNs and ePNs, we labeled both PN populations simultaneously in vivo using the enhancer trap lines *GH146-QF* and *MZ699-GAL4* that label the majority of ePNs (60%) and iPNs (86%), respectively (***Lai et al., 2008***). Double-labeling shows that both PN types innervate overlapping regions in the AL and the LH, while a small posterior-lateral LH area is targeted only by ePNs (***Figure 1A***, ***Figure 1—figure supplement 1***). In GH146-positive (GH146+) PNs, immunolabeling reveals GABA production in all ~6 PNs of the ventral cell cluster (***Wilson and Laurent, 2005***), whereas ePNs of this line are exclusively cholinergic (***Shang et al., 2007***). For the ~45 MZ699-positive (MZ699+) iPNs (***Lai et al., 2008***), GAD1 (glutamic acid decarboxylase) in situ hybridizations imply GABA synthesis (***Okada et al., 2009***), which was recently verified via immunostaining (***Liang et al., 2013***; ***Parnas et al., 2013***). The polarity of both PN populations has been studied in detail, showing that both possess dendritic regions in the AL, indicating the AL as their cholinergic input site, while the LH represents their major output site (***Jefferis et al., 2001***; ***Okada et al., 2009***; ***Liang et al., 2013***; ***Parnas et al., 2013***).

To further characterize PNs labeled by *MZ699-GAL4* and *GH146-GAL4*, we analyzed their precise glomerular innervation to unravel how selectively they acquire information in the AL. To allow glomerulus identification in vivo, we employed a transgenic fly carrying elav-n-synaptobrevin:DsRed (END1-2) to express the presynaptically targeted fusion protein under the control of the neuron-specific elav promotor (***Figure 1—figure supplement 2A***) (***Grabe et al., 2014***). The reconstruction and identification of all AL glomeruli provided 53 glomeruli, of which 75% were innervated by MZ699+ iPNs (40) while 70% (37) were covered by GH146+ ePNs (***Figure 1C***, ***Figure 1—figure supplement 2B***). 55% of all glomeruli were innervated by both lines. Notably, dendritic *MZ699-GAL4* innervation density was not homogeneous. Certain glomeruli were densely innervated (e.g., DM2, DM4 and DM5), while others did not reveal any postsynaptic sites (e.g., DL1, DL4 and DL5). Hence MZ699+ iPNs target specific glomerular subsets selectively, which suggests that these neurons have a particular function within the olfactory network.

Calcium signals in the lateral horn spatially segregate into distinct response domains

Probabilistic synaptic density maps of GH146+ PNs predicted a regionalized neuronal activity in the LH (***Jefferis et al., 2007***). Do iPNs functionally segregate in a comparable way? To address this question, we expressed the Ca^{2+}-sensitive reporter G-CaMP3.0 (***Nakai et al., 2001***; ***Tian et al., 2009***) in iPNs using *MZ699-GAL4* and performed functional imaging in the LH (***Figure 2A–C***). We initially tested three odors with potential relevance for *Drosophila* at different concentrations: acetoin acetate, an attractive byproduct of the yeast fermentation process, balsamic vinegar, an attractive natural odor mixture, and benzaldehyde, a well-known fly repellant (***Magee and Kosaric, 1987***; ***Keene et al., 2004***; ***Semmelhack and Wang, 2009***). We observed that odor evoked Ca^{2+} responses separate in certain regions of the LH in an odor-specific and concentration-dependent manner (***Figure 2C***). Acetoin acetate and balsamic vinegar evoked Ca^{2+} activity in spatially similar regions. At higher concentrations, an

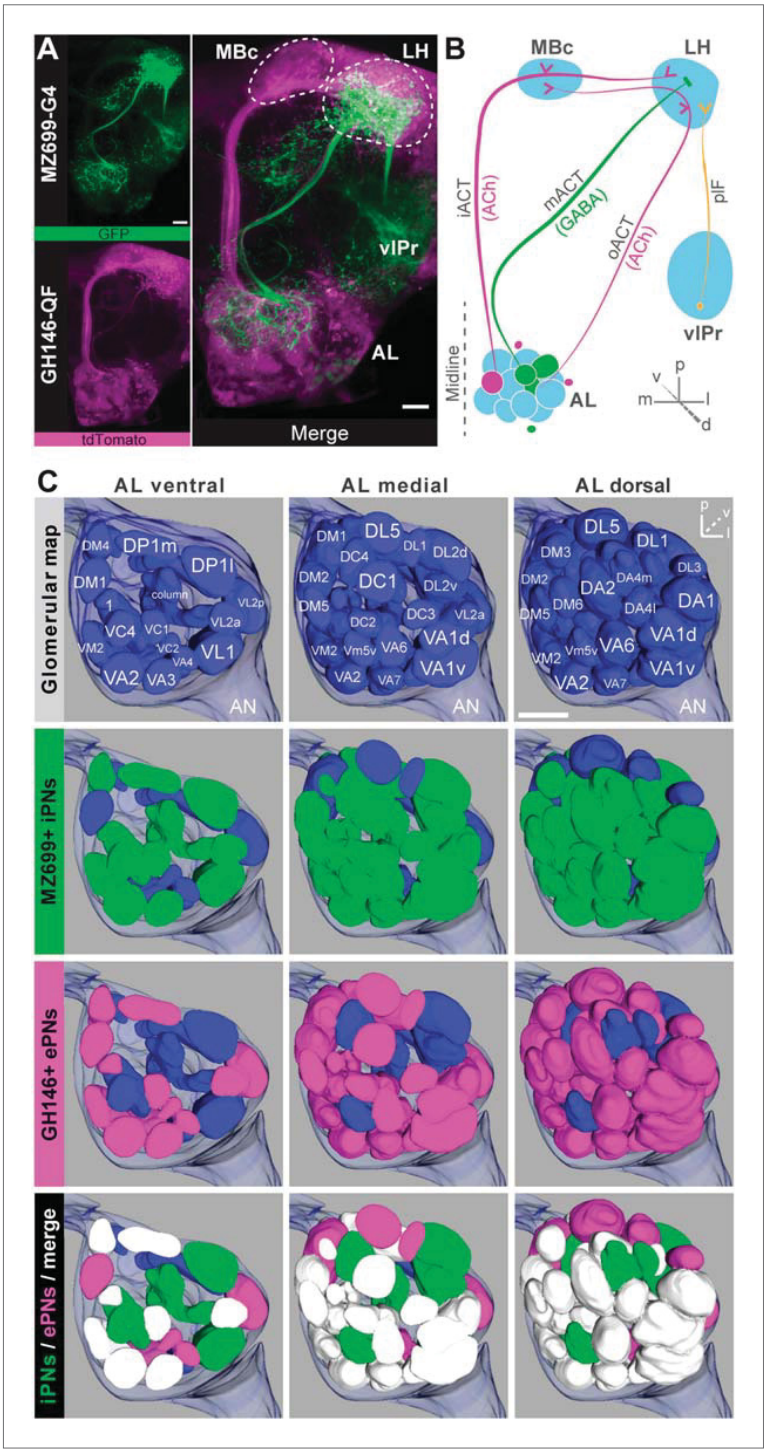

Figure 1. Detailed glomerular innervations of excitatory and inhibitory projection neurons in the AL. (**A**) Simultaneous labeling of inhibitory projections neurons (iPNs, labeled by *MZ699-GAL4;G-CaMP*) and excitatory projection neurons (ePNs, labeled by *GH146-QF;tdTomato*) in vivo reveals distinct projections to the lateral horn (LH). All iPNs

Figure 1. Continued on next page

Figure 1. Continued

bypass the mushroom body calyx (MBc) and innervate the LH exclusively. The MZ699 line labels a few ventrolateral protocerebral neurons (vlPr neurons) projecting via the posterior lateral fascicle (plF) from the ventrolateral protocerebrum (vlPr) to the LH. (**B**) Schematic of the PN connectivity relay from the antennal lobe (AL) to higher brain centers (ePNs in magenta, iPNs in green, and vlPr neurons in orange). (**C**) Above, complete glomerular assignment of the AL neuropil (right AL), labeled with elav-*n*-synaptobrevin:DsRed (END1-2). Below, glomerular innervations of both PN populations related to in vivo images in ***Figure 1—figure supplement 2***. Depicted are the ventral level (~−40 µm), the medial level (~−20 µm) and the dorsal view onto the AL. Color annotation: blue glomeruli are not innervated by any of the used GAL4-lines; green glomeruli are innervated by MZ699+ iPNs and magenta by GH146+ ePNs; white glomeruli are innervated by both enhancer trap lines. Scale bar, 20 µm.

DOI: 10.7554/eLife.04147.003

The following figure supplements are available for figure 1:

Figure supplement 1. Characterization of excitatory and inhibitory projection neurons.

DOI: 10.7554/eLife.04147.004

Figure supplement 2. Glomerular innervations of ePNs and iPNs.

DOI: 10.7554/eLife.04147.005

additional region was recruited. Benzaldehyde elicited no response at very low concentrations, but induced clear activity at median and high concentrations in a third region, which was completely separate from the regions activated by the other two odors. Observed patterns were highly reproducible within one animal and stereotypic among different individuals, as shown for the stimulation with 1-octen-3-ol (***Figure 2D***) as well as other odors (***Figure 2—figure supplement 1***).

Due to the lack of morphological landmarks in the LH, functional data were analyzed using the pattern recognition algorithm Non-Negative Matrix Factorization (NNMF) (***Lee and Seung, 1999***), which automatically extracts spatial areas possessing a common distinct time-course, further termed LH odor response domains (ORDs). The NNMF analysis extracted three clearly reproducible and spatially robust ORDs (***Figure 2E***, see NNMF part in the 'Materials and methods' section). Notably, ORDs occupying common temporal kinetics exhibited highly stereotypic spatial patterns. We termed the ORDs LH-PM (LH-posterior-medial), LH-AM (LH-anterior-medial) and LH-AL (LH-anterior-lateral) according to their anatomical positions. To validate our observations, we extended our stimulus array to 11 additional odorants and applied each at three concentrations. Odorants were chosen according to chemical classes, hedonic valence and biological value. Hence, the odor set included acids, lactones, terpenes, aromatics, alcohols, esters, ketones and the natural blend, balsamic vinegar. Remarkably, analysis of the additional odorants revealed neuronal activity exclusively within the three described ORDs (***Figure 2F***, ***Figure 2—figure supplements 2,3***). Furthermore, median NNMF-extracted Ca^{2+} response traces with indicated statistical quartiles illustrate very low variability and highly reproducible LH signals. The LH-PM area chiefly revealed robust odor-evoked responses across concentrations, while the LH-AM and LH-AL were mainly activated at very high odor concentrations by distinct odorants. The global responsiveness within separate ORDs in the LH substantiates our finding of a relatively broad AL input to MZ699+ iPNs which converges into three spatially regionalized and stereotypic LH activity domains.

iPNs can be divided into two morphological classes

We next investigated if the spatially regionalized odor-evoked response patterns are reflected in the axonal terminal fields of MZ699+ iPNs in the LH. To analyze these neurons at the single neuron level, we performed neural tracing by employing a genetically encoded photoactivatable GFP (PA-GFP) (***Patterson and Lippincott-Schwartz, 2002***; ***Datta et al., 2008***; ***Ruta et al., 2010***). The photoconversion of all MZ699+ neurons leaving the AL confirmed the homogeneous distribution of iPN neurites in the LH and the sparse innervation of the posterior-lateral region as mentioned above (***Figure 3A***). Next we illuminated PA-GFP in single somata to selectively label individual MZ699+ iPNs from the soma up to the farthest axonal terminals in the LH. Individual iPNs were reconstructed and transformed into a reference brain using the END1-2 background (***Grabe et al., 2014***) to align neurons of different individuals. Based on their innervation pattern in the LH, MZ699+ iPNs could be assigned to two major morphological classes (***Figure 3B,C***). As expected from the extracted ORDs, one iPN group diverged to the LH-PM region (8/25 of iPNs), while a second group extended their axonal terminations within the LH-AM area (10/25 of iPNs). In order to statistically substantiate our observation, we

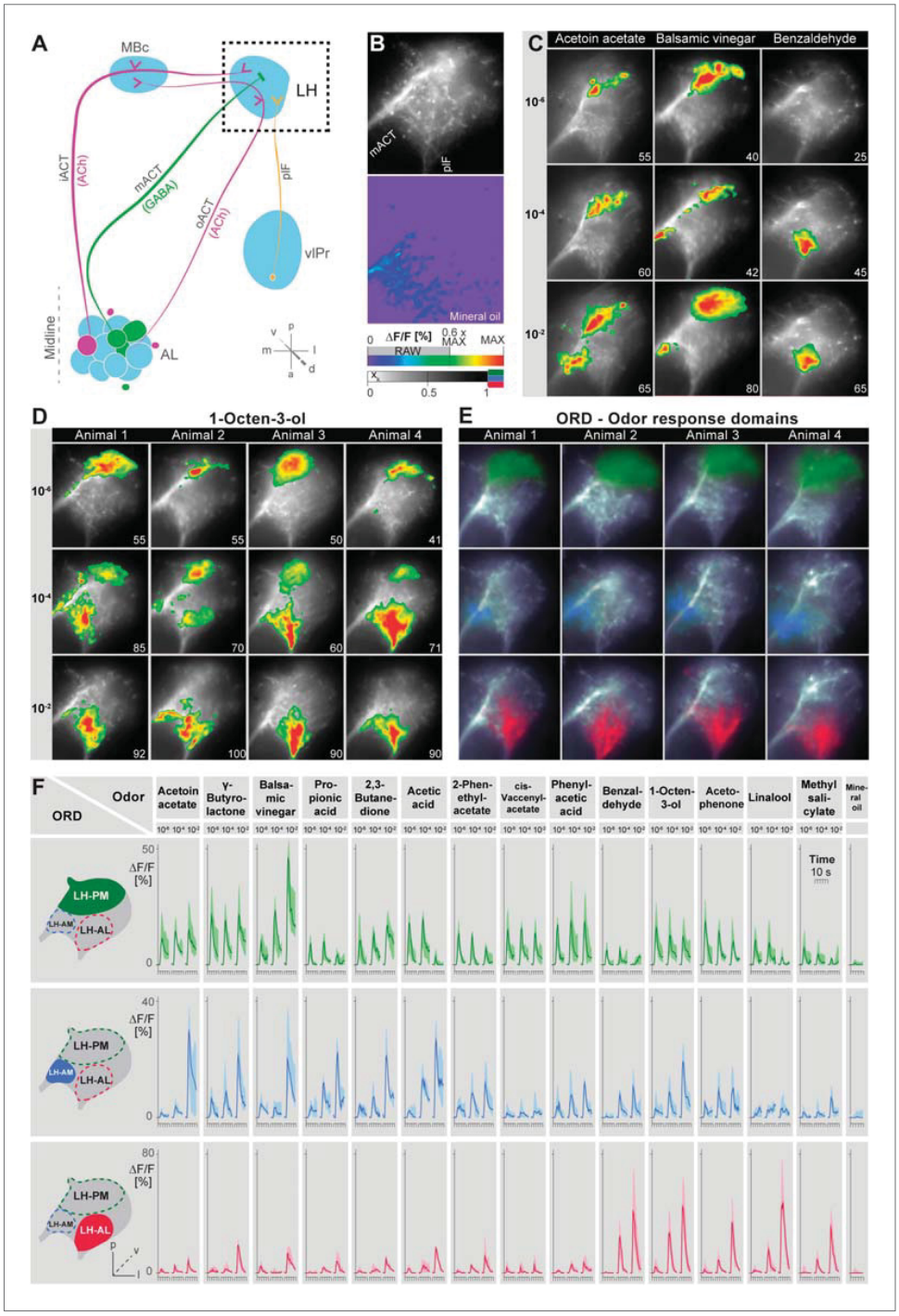

Figure 2. Odors evoke specific and stereotypic calcium responses in the LH subdivided into three distinct odor response domains. (**A**) Schematic of the olfactory circuit with the investigated area highlighted. (**B**) RAW image of the LH (top picture) depicting the recorded area of figures (**C**–**E**) and the false color image (bottom picture) during the solvent application. The ΔF/F scale bar applies for all false color-coded pictures; the alpha-bar for the pixel

Figure 2. Continued on next page

Figure 2. Continued

participation x_k of the indicated colors applies for (**E**–**F**). (**C**) Representative LH Ca^{2+} responses (ΔF/F%) of acetoin acetate, balsamic vinegar and benzaldehyde at three concentrations. Numbers in the lower right corner indicate individual maxima. (**D**) Odor-evoked Ca^{2+} responses (ΔF/F%) are exemplarily depicted for 1-octen-3ol- at three concentrations in four animals. (**E**) NNMF-extracted LH odor response domains (ORD) of four representative animals: three LH ORDs were fully reproducible after being extracted from all measured animals. Domains classified as identical are similarly color-coded: the green ORD is located in the posterior-medial region of the LH (LH-PM); blue, in the anterior-medial (LH-AM), and red in the anterior-lateral LH area (LH-AL). The alpha-bar for green, blue and red shades is placed in (**B**). (**F**) Left, schematic outlines of the LH with indicated ORDs. Right, median activity traces of all odors at three concentrations are depicted for each colored ORD. Shadows represent lower and upper quartiles (n = 6–7).

DOI: 10.7554/eLife.04147.006

The following figure supplements are available for figure 2:

Figure supplement 1. Odor-evoked activity patterns in the LH are reproducible and stereotypic.

DOI: 10.7554/eLife.04147.007

Figure supplement 2. Odor-evoked activity patterns in the LH can be reconstructed with five components.

DOI: 10.7554/eLife.04147.008

Figure supplement 3. Odor-evoked activity patterns in the LH cluster into three components.

DOI: 10.7554/eLife.04147.009

performed a cluster analysis based on a similarity score (***Kohl et al., 2013***) of the target areas of all terminals of each iPN in the LH (for details see 'Materials and methods'). The dendrogram of morphological similarity between each individual iPN shows that all, except one iPN, could be clustered according to their target region in either the LH-AM or LH-PM area (***Figure 3D***) which confirms the classification into two major categories. Additionally, we performed a principal component analysis based on the distances of the similarity scores showing that both neuronal classes possess significantly different target areas in the LH (***Figure 3—figure supplement 1A***; $p < 0.001$, one-way ANOSIM).

We did not observe any clear panglomerular innervations of individual MZ699+ iPNs that spanned the entire AL, consistent with ***Liang et al. (2013)***. Instead, MZ699+ iPNs develop mainly oligoglomerular patterns innervating on average 5.4 ± 3.9 glomeruli (mean ± SD), which are not necessarily in close proximity. It is important to note here, that the glomerular innervations of iPNs are rather sparse in comparison to the innervation of ePNs which complicates the identification of truly innervated glomeruli. After classifying all registered neurons according to their LH zones along with their glomerular innervations, we noted a spatial subdivision of MZ699+ iPN dendritic fields in the AL (***Figure 3—figure supplement 2***). Whereas LH-PM iPNs extended dendrites mainly into glomeruli from the ventro- or dorsomedial area of the AL (e.g., DM4, DM2, VM7, VM5d), iPNs targeting the LH-AM zone innervated glomeruli ranging from the ventro- and dorsoanterior to the dorsocentral region (e.g., DC3, VC1, VA6, VL1). We observed that a glomerulus is typically innervated by only LH-PM iPNs or LH-AM iPNs. However, we also found a few cases where a glomerulus can be innervated by both iPN types (e.g., glomeruli D and DC2). In order to analyze whether the two categories of iPNs can also be statistically separated according to their glomerular innervations in the AL, we performed a cluster analysis based on the glomeruli innervated by each individual iPN (***Figure 3E***). Notably, the two iPN classes could be clearly clustered into two groups due to their specific AL innervations. This finding is further supported by a principal component analysis showing that iPNs targeting the LH-PM region innervate a significant different glomerular subset than iPNs that send their axonal terminals to the LH-AM area (***Figure 3—figure supplement 1B***; $p < 0.001$, one-way ANOSIM). In accordance with our finding of two major iPN categories is the study by ***Lai et al. (2008)*** who observed several different stereotyped projection patterns of multiglomerular MZ699+ single-cell clones that could be broadly categorized into two groups based on the dendritic and axonal projection patterns. While we observed corresponding innervated areas in the AL, the described target areas in the LH seem to differ. However, due to the lack of 3D reconstruction of the single-cell clone data, the innervation patterns cannot be compared in detail.

In addition to the oligoglomerular iPNs, we observed a few uniglomerular MZ699+ iPNs innervating either glomerulus DA1 or VL1 (4/25 of iPNs), consistent with ***Lai et al. (2008)***, which target the LH-AM region (***Figure 3—figure supplement 2***). Moreover, we identified three other MZ699+ neurons that did not innervate the AL and sent their axons through the mACT to the LH and/or the MBc.

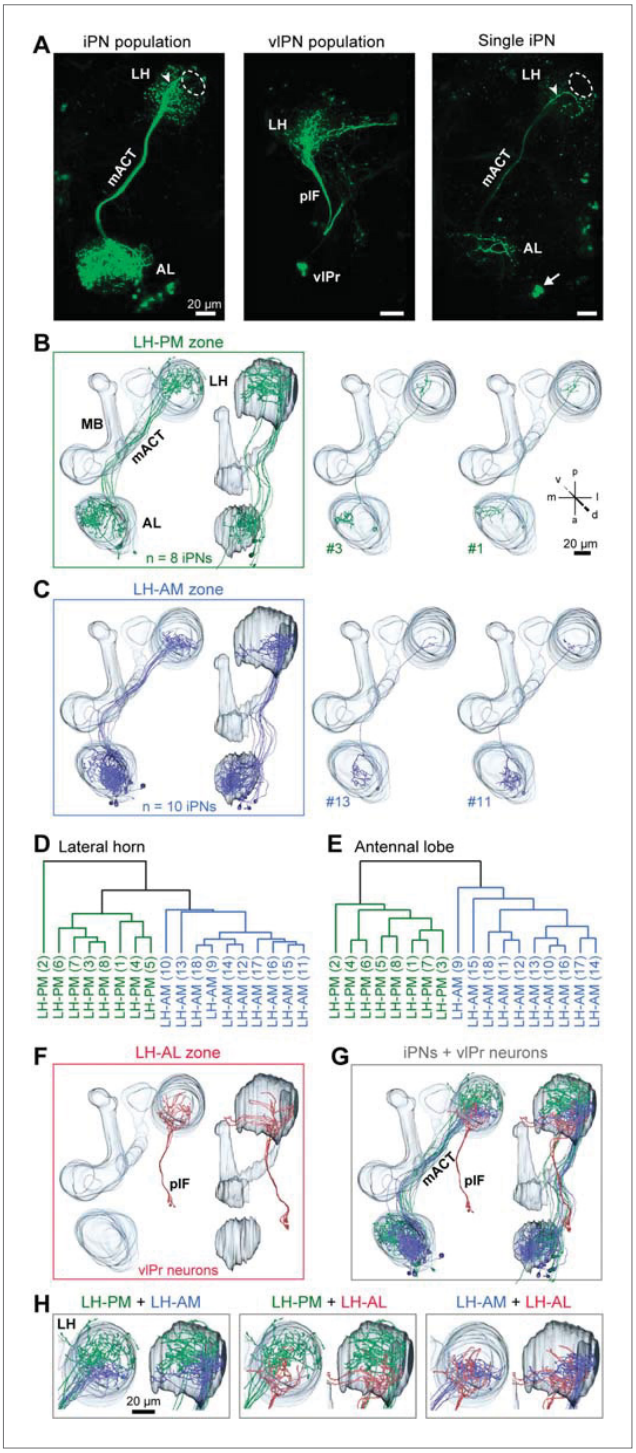

Figure 3. iPNs can be classified according to their projection pattern in three distinct LH zones. (**A**) Complete population of MZ699+ iPNs labeled using PA-GFP (left image), the posterior-lateral LH region is encircled, arrowhead indicates the final common projection point of iPN axons. Middle image: photoactivation of all vlPr

Figure 3. Continued on next page

Figure 3. Continued

neurons of the MZ699-GAL4 line that project from the LH to the vlPr via the plF. Right image: exemplary single iPN, labeled by photoconverting PA-GFP in a single soma (arrow). Scale bar, 20 μm. (**B**) Framed images: neuronal reconstructions of all iPNs projecting to the LH-PM zone (n = 8) with outlined olfactory neuropils. View from dorsal (left) and lateral (right). Right part represents two exemplary registered individual iPNs. (**C**) Neuronal reconstructions of all iPNs projecting into the LH-AM zone (n = 10), images are arranged as in (**B**). (**D** and **E**) Cluster analyses based on the target areas of all terminals of each iPN in the LH (**D**) or based on the innervated glomeruli in the AL (**E**). The dendrograms are split into colored subclusters. Below each dendrogram, each individual iPN is specified according to the labels in ***Figure 3—figure supplement 2***. Note, that iPNs can be morphologically clustered according to their target or input regions. (**F**) Neuronal reconstruction of vlPr neurons projecting through the plF to the LH-AL zone. (**G**) Combination of all registered neurons. (**H**) Dual combinations of all registered neurons with their projections in the LH.

DOI: 10.7554/eLife.04147.010

The following figure supplements are available for figure 3:

Figure supplement 1. iPNs can be morphologically segregated according to their target and input region.

DOI: 10.7554/eLife.04147.011

Figure supplement 2. Glomerular innervations of individual iPNs.

DOI: 10.7554/eLife.04147.012

Since the *MZ699-GAL4* line labels also neurons connecting the LH and the ventrolateral protocerebrum (vlPr) (***Ito et al., 1997***; ***Liang et al., 2013***; ***Parnas et al., 2013***), we illuminated a small fraction of the posterior lateral fascicle (plF) to target these putative third-order neurons (***Figure 3A***). The plF comprised axons of ventrolateral protocerebral neurons (vlPr neurons), which bifurcated within the LH-AL (***Figure 3F***). Combinations of all registered neuron types within the assigned zones revealed that iPNs of the LH-AM area and vlPr neurons of the LH-AL region intermingle (***Figure 3G,H***).

Odor response domains contain the activity of distinct neuronal populations

To illustrate higher-order connectivity, we labeled the three major neuron types, that is, MZ699+ iPNs, GH146+ ePNs and vlPr neurons, targeting the LH within the olfactory circuitry using PA-GFP (***Figure 4A***). Since our observed Ca^{2+} responses in the LH-AL region might reflect activity from vlPr neurons rather than iPNs, we dissected the neuronal contributions within each extracted ORD by conducting transection experiments using two-photon laser-mediated microdissection (***Figure 4B***). By transecting the mACT, we aimed at abolishing LH-responses deriving from MZ699+ iPNs, while cutting the plF connection should eliminate potential odor-evoked vlPr neuron activity. To achieve unambiguous and comparable results, functional imaging was performed in both brain hemispheres simultaneously. Immediately after the intact brain areas were imaged, the tracts were selectively transected on one brain side each (***Figure 4C***) and the imaging procedure was repeated. We applied a reduced odor set that elicited activity in all ORDs and performed NNMF for pre- and post-lesion recordings. Transecting the mACT significantly reduced responses in the LH-PM and LH-AM region, whereas LH-AL responses were significantly abolished by plF-ablation (***Figure 4D***). Notably, we observed that LH-AL responses to some odors were significantly increased after mACT transection as a consequence of the suppression of iPN inhibition of vlPr neurons confirming the study by ***Liang et al. (2013)***. Hence, activity in the LH-PM and LH-AM domain can be assigned to MZ699+ iPNs, while LH-AL activity is mainly evoked by vlPr neurons (***Figure 4E***).

iPN activity in the lateral horn mediates flies' attraction to odors

We next addressed the behavioral relevance of MZ699+ iPN activity in the LH for innate odor-guided behavior. To precisely target iPN function, we expressed an RNAi construct against glutamic acid decarboxylase 1 (GADi) to selectively knock-down the GABA synthesis in MZ699+ iPNs (***Figure 5A***). We confirmed the reduction in GABA production via immunostaining (***Figure 5B***). Since vlPr neurons are not GABAergic, they were not affected by the RNAi expression (***Liang et al., 2013***; ***Parnas et al., 2013***). Using wild-type flies and parental controls, we conducted T-maze assays (***Tully and Quinn, 1985***; ***Chakraborty et al., 2009***) with nine of the odorants applied in functional imaging experiments at medium and high concentrations. Notably, flies with silenced MZ699+ iPN GABA production revealed a neutral or aversive behavioral response to attractive odors, while repellent odors

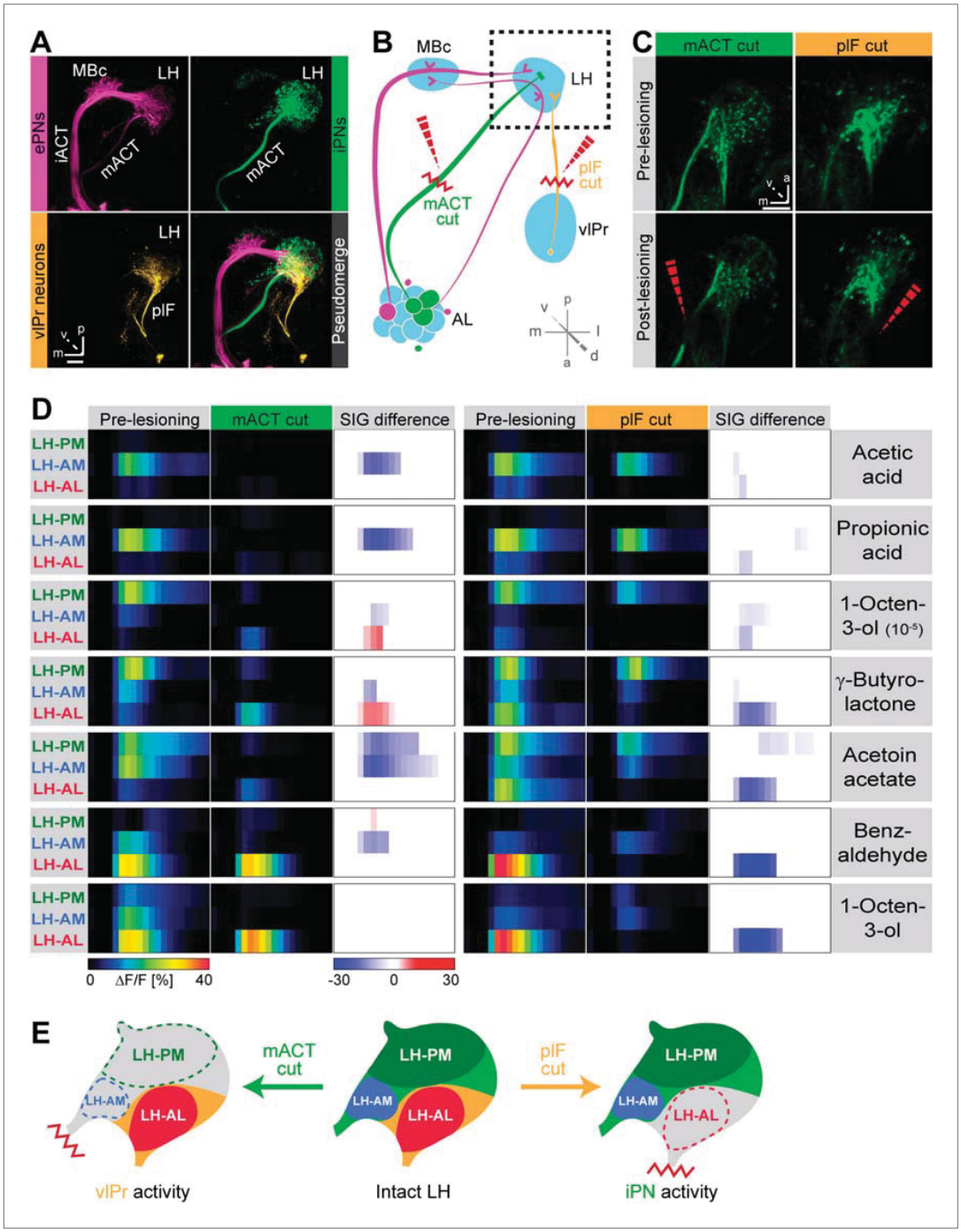

Figure 4. Distinct odor response domains in the LH constitute neuronal activity of iPNs and vlPr neurons. (**A**) Representation of all ePNs (magenta) and iPNs (green) labeled by *GH146-GAL4* and *MZ699-GAL4* using PA-GFP, respectively. Photoactivation of vlPr neurons (orange, MZ699-GAL4) connecting the LH and the vlPr via the pIF. The overlay image depicts a pseudo-merge image of the different GAL4-driver lines. (**B**) Schematic of the olfactory circuit with integrated layout of the transection experiment. After simultaneous Ca^{2+} imaging of bilateral LHs, the ipsilateral pIF and contralateral mACT was transected (red zigzag line) with an infrared laser (dashed red arrow). (**C**) Projection images of a 7 µm stack of the LH area prior and post transection. Left

Figure 4. Continued on next page

Figure 4. Continued

images, mACT transected; right image, plF transected. The ablated region is indicated by the dashed red arrow. Scale bar, 20 μm. (**D**) Median time traces displaying percental change of ΔF/F values for indicated ORDs prior to post transection of the mACT (green, left) and the plF (orange, right) for different odorants. Significant changes of odor-evoked Ca^{2+} signals due to transection are shown in the column SIG difference. Differences were tested with a two-tailed paired Student's *t* test ($p < 0.05$). Color codes are indicated by the corresponding scale bar below, n = 4–5. Transecting the mACT eliminates Ca^{2+} signals in the LH-PM and LH-AM domain, while lesioning the plF significantly abolishes LH-AL responses. Notably, the LH-AL domain is significantly stronger activated after mACT transection following application of 1-octen-3-ol and γ-butyrolactone. (**E**) Summarized cartoon of the neuron populations contributing to ORD activity prior and post transection of axons of iPNs or vlPr neurons.

DOI: 10.7554/eLife.04147.013

evoked an even stronger aversion (***Figure 5C***). To compare the T-maze data more accurately, we calculated the average change of behavioral response indices (RIs) between GADi flies and parental controls (***Figure 5D***). Indeed, all responses changed in a negative direction, indicating MZ699+ iPNs play a crucial role in mediating attraction behavior. The sole exception involved high concentrations of the most repulsive odor, acetophenone, since this odor had already induced maximum aversion. Overall, these experiments reveal a crucial function of MZ699+ iPNs in mediating attraction behavior by releasing GABA in the LH.

The lateral horn integrates hedonic valence and odor intensity into separate domains

The behavioral effect of the iPN knock-down suggests that MZ699+ iPNs encode positive hedonic valences. To correlate the complete ORD pattern array with innate behavioral preferences, we assigned behavioral RIs for all odors at median and high odor concentrations using the T-maze assay as in our previous experiment (***Figure 6A***). Since extremely low concentrations rarely evoked any behavioral response, we excluded the 10^{-6} concentration in this analysis. It is important to note here, that different behavioral assays for testing olfactory preferences in flies might lead to contradictory results. However, the majority of odors used here was also tested in two other behavioral paradigms, the trap assay (***Stökl et al., 2010***; ***Knaden et al., 2012***) and the FlyWalk (***Steck et al., 2012***) (pers. comm. M Knaden) and yielded similar results (see ***Figure 6—figure supplement 1***). When we plotted median odor-evoked activity in a three-dimensional space defined by the three ORDs, we saw a clear clustering of responses evoked by aversive and attractive odorants (***Figure 6B***). The LH-AL domain, constituted mainly by vlPr neurons, is coding aversive odors, while attractive odors activated only the LH-PM and LH-AM domains that derive from MZ699+ iPNs. This result is in accordance with our finding that iPNs mediate odor attraction.

We next correlated ORD activity to odor valence separately for all ORDs. This evaluation enabled us to analyze iPN and vlPr neuron coding properties apart from each other (***Figure 6C***). As expected, the analysis revealed a significant correlation between positive valence and the LH-PM domain, whereas Ca^{2+} responses in the LH-AL were strongly negatively correlated to hedonic valence. The LH-AM domain exhibited a positive but not significant correlation for odor valence. Remarkably, activity within the LH-PM was totally independent of concentration, whereas activity in both anterior domains was significantly correlated to odor intensity (***Figure 6D***). Hence, MZ699+ iPNs integrate odor attraction information into the LH-PM domain independent of odor intensity, confirming behavioral experiments. Intensity coding is in turn conducted separately by distinct iPNs within the LH-AM domain. In contrast, putative third-order vlPr neurons projecting into the LH-AL area code both negative valence and odor intensity.

Finally, we wondered if this valence-specific LH representation is already reflected at the primary level of olfactory processing. The odor-evoked responses in iPNs are generally similar to those in OSNs (***Wang et al., 2014***), indicating a straight forward transduction of cholinergic OSN responses. We therefore performed functional imaging of odor-evoked Ca^{2+} dynamics at the AL input level by expressing G-CaMP3.0 in OSNs using Orco-GAL4 (***Larsson et al., 2004***) (***Figure 6—figure supplement 2***). In order to compare the activity patterns at both processing levels, we calculated correlation distances for all pair-wise combinations of odor-evoked response patterns and plotted these with respect to maximal ORD pattern similarity in the LH (***Figure 6E***). As expected, odor representations in the LH clearly clustered within three separated parts of the matrix, reflecting our observed ORDs. However, this coding similarity could not predict AL activity patterns, even if the correlation matrix was sorted with respect to pattern similarity in the AL (***Figure 6—figure supplement 3***).

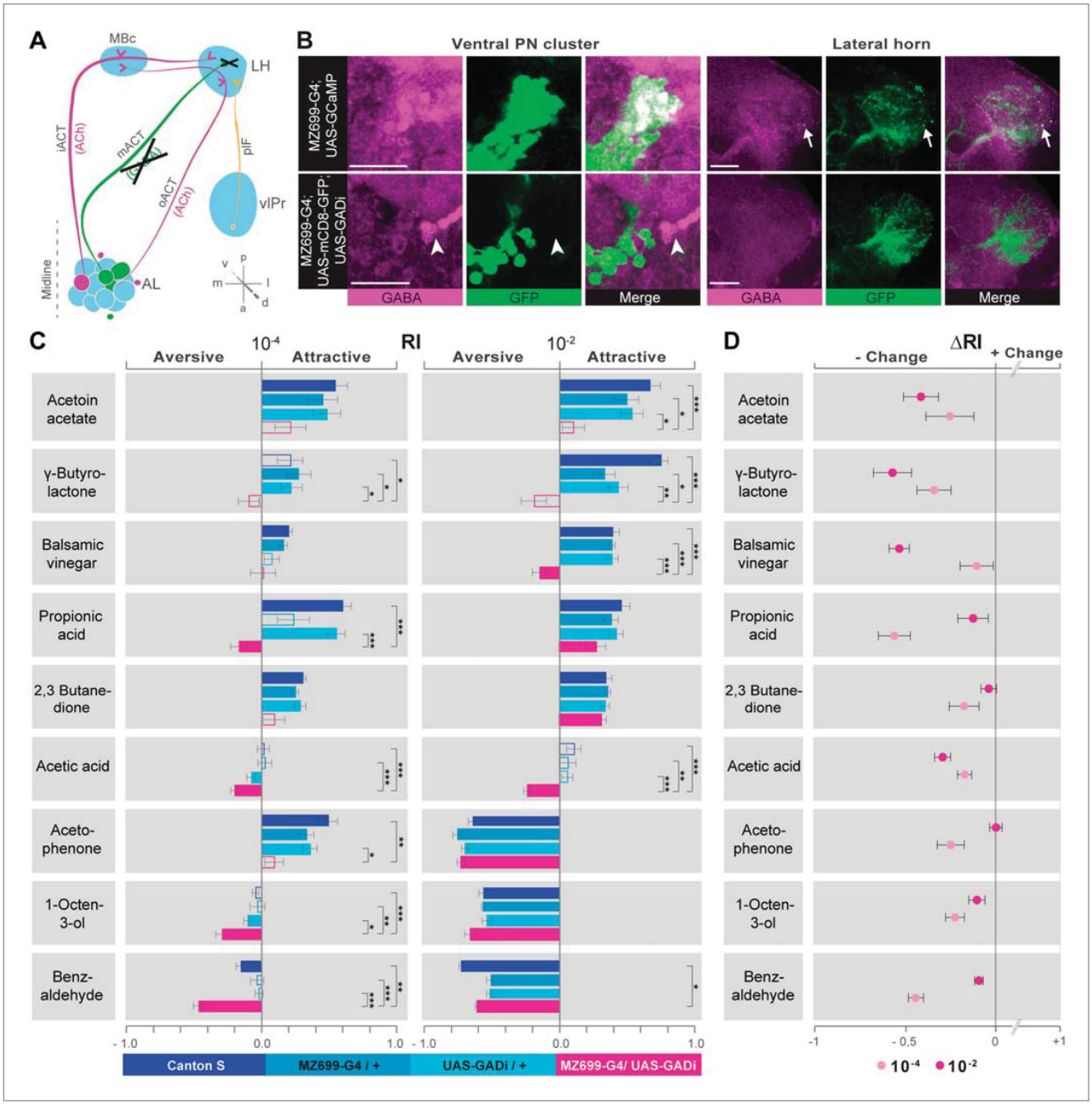

Figure 5. iPN GABA release in the LH mediates odor attraction behavior. (**A**) Experimental layout: iPN GABA production was selectively silenced via GADi expression in MZ699+ iPNs; ePN and vlPr neuron activity remained unaffected. (**B**) Immunostaining against GABA and GFP within AL somata (left) and LH neurites (right) of iPNs with intact (top) and silenced GABA production (bottom). GADi flies show GABA signals in somata of iPNs labeled by *GH146-GAL4* only (arrowhead). The arrow head points to an exemplary GABA-positive bouton in the LH. Scale bar, 20 μm. (**C**) Averaged behavioral response indices (RIs) determined with a T-maze assay for wild-type flies (dark blue), parental controls (light blue) and experimental animals (magenta) for nine odorants at two concentrations. Empty boxes display no response (Wilcoxon signed-rank test). Dunn's Multiple Comparison Test was used for global differences in the dataset followed by a posthoc test for selected pairs ($p^* < 0.05$; $^{**}p < 0.01$; $^{***}p < 0.001$). Error bars represent SEM. (**D**) RI differences between GADi flies and averaged parental controls. RI differences are negative for all but one odor indicating that GADi expression shifts odor-guided behavior towards aversion. Error bars indicate SEM.

DOI: 10.7554/eLife.04147.014

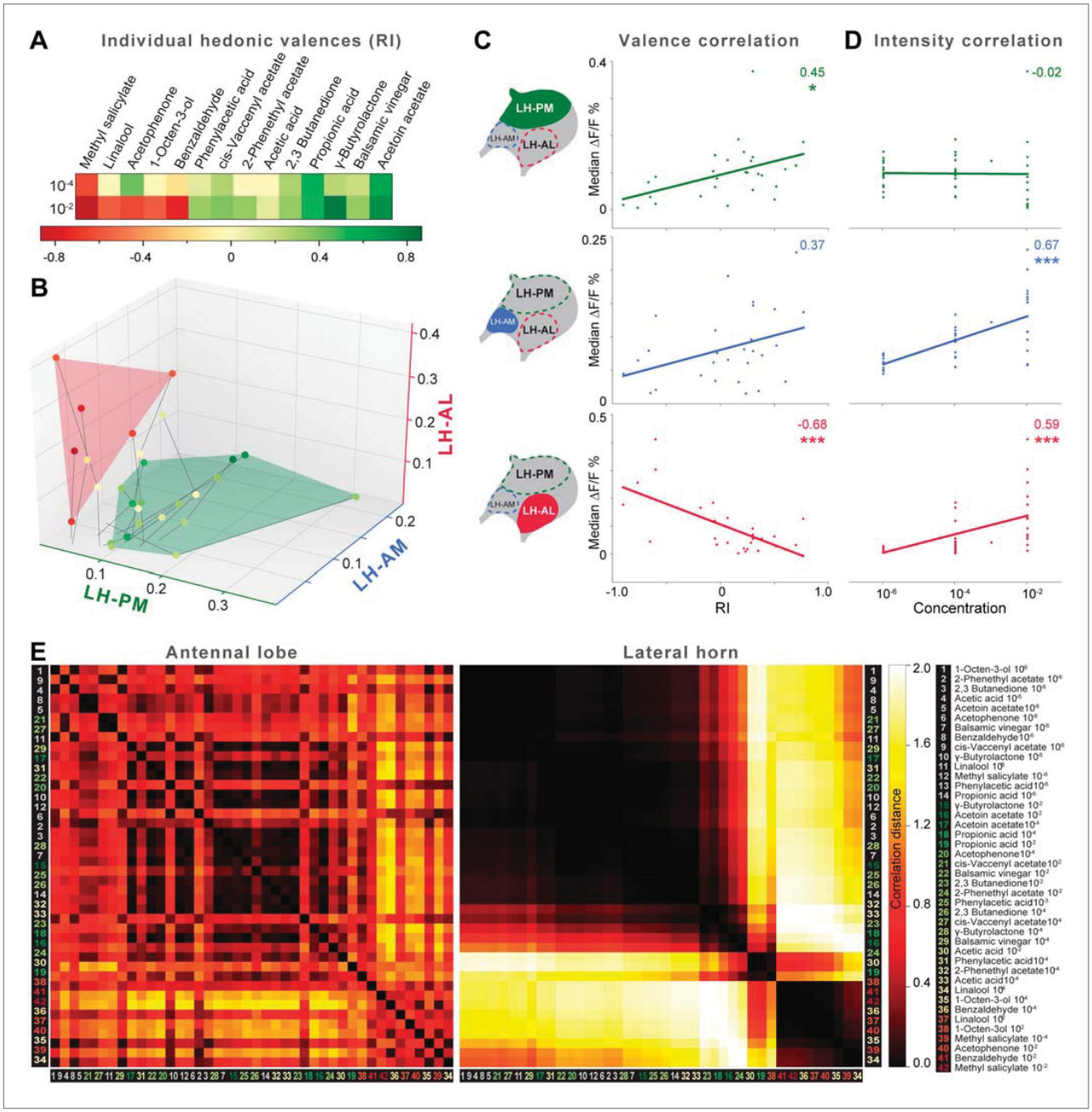

Figure 6. Integration of hedonic valence and odor concentration into ORDs. (**A**) Response indices of wild type flies for all odors at median and high concentrations. Odors are sorted from highly aversive (−1, red) to highly attractive (+1, green). (**B**) 3D-scatter plot of median Ca^{2+} responses of all odors based on the three ORDs. Odor-dots are labeled due to their RI shown in (**A**). Same odors at different concentrations are connected with a line: the dot at the end depicts 10^{-2}, the centered dot 10^{-4}, and the end of the line 10^{-6}. Attractive and aversive odor representations form separate clusters. (**C** and **D**) Left, schematic LH outlines with colored ORDs corresponding to data on the right. Correlation score r (upper right corner) between median activity and measured RI in T-maze experiments or odor concentration, respectively, with significance denoted below. Student's *t* test, *p < 0.05, ***p < 0.001. (**E**) Complete correlation matrices for Ca^{2+} response patterns of OSNs in the AL (left) and iPNs in the LH (right). The odors are arranged according to single linkage clustering of the LH activity patterns. Heatmap color-code refers to the correlation distance scale bar on the right. Correlation distance is

Figure 6. Continued on next page

Figure 6. Continued

defined as 1 − r, where r is the Pearson correlation coefficient between the response patterns of two odorants. Odor letters are color-coded according to hedonic valence; 10^{-6} RI values are labeled in grey (complete list right hand).

DOI: 10.7554/eLife.04147.015

The following figure supplements are available for figure 6:

Figure supplement 1. Odor valences determined with three different behavioral assays.

DOI: 10.7554/eLife.04147.016

Figure supplement 2. Calcium responses of OSNs.

DOI: 10.7554/eLife.04147.017

Figure supplement 3. Correlation matrices for odor-evoked responses in the AL and LH.

DOI: 10.7554/eLife.04147.018

Discussion

We augment our present understanding of the *Drosophila* olfactory circuitry by elucidating the coding properties of a parallel and behaviorally relevant higher-order processing pathway to the LH. Morphological, functional and behavioral approaches provide strong evidence for a functional subdivision of iPNs into neurons coding either odor attraction or odor intensity. Our behavioral experiments reveal that inhibitory properties of iPNs are necessary for innate odor-guided attraction. In addition, we characterize a third neural pathway coding odor repellence.

Do MZ699+ iPNs fulfill anatomical requirements to constitute a distinct processing channel in addition to ePNs? A remarkable anatomical feature of MZ699+ iPNs is their glomerular innervation pattern in the AL. Whereas GH146+ ePNs are uniglomerular and retain the topographic code in their axonal arrangement (***Marin et al., 2002***; ***Wong et al., 2002***; ***Jefferis et al., 2007***), most MZ699+ iPNs possess oligoglomerular innervations suggesting that these neurons might not convey precise odor-identity information. In addition, MZ699+ iPNs in the AL diverge only into specific glomerular subsets, and so might be pre-determined to selectively extract common features of distinct odors. We have previously shown that the AL map at the PN level exhibits a spatial segregation of valence representation (***Knaden et al., 2012***). Certain glomeruli, which have been classified as aversion coding at the GH146+ ePN level, are omitted by MZ699+ iPNs, whereas most glomeruli classified as attraction coding are particularly densely innervated. These results suggest that within the MZ699+ iPN population, mainly positive odor traits are extracted, whereas the odor information of negative valence is neglected. This conclusion is consistent with the recent finding that one type of LH neurons is receiving input from PNs that mainly innervate glomeruli coding fruity-smelling acetates (***Fisek and Wilson, 2014***) which represent attractive odor cues (***Knaden et al., 2012***). We furthermore demonstrate that the MZ699+ iPN population is split into two major morphological classes possessing a clear spatial segregation in the AL which is strictly maintained within the LH. It has to be kept in mind that we do not cover all iPNs by using *MZ699-GAL4*. Further experiments characterizing the ~6 missing MZ699–iPNs, which are labeled by *GH146-GAL4* (***Wilson and Laurent, 2005***; ***Lai et al., 2008***), will elucidate if our assumptions apply for the whole iPN population.

So far only a handful neuroanatomical studies targeting GH146+ ePNs have dealt with the question of how olfactory information is integrated and read out by higher brain structures, in particular the LH (***Marin et al., 2002***; ***Wong et al., 2002***; ***Tanaka et al., 2004***; ***Jefferis et al., 2007***). A recent study that traced the projection pattern of PNs coding ammonia and amines as attractive stimuli and carbon dioxide and acids as repulsive signals suggests that sensory stimuli of opposing valence are represented in spatially distinct areas within the LH (***Min et al., 2013***). In addition the study by ***Liang et al. (2013)*** showed that MZ699+ iPNs selectively suppress the activity of vlPr neurons to food odors, while pheromone responses were not affected verifying the assumption that different odor features are processed separately. However, functional evidence for a feature-based, spatially segregated activity map in the LH was so far missing.

To unravel the coding properties of MZ699+ iPNs within the LH, we conducted Ca^{2+} imaging experiments of MZ699+ iPNs in the LH to odorants having different hedonic valences and intensities, and could classify the LH into three functional ORDs. Our neuronal tracing and transection experiments validated the LH segmentation into two medial domains that derive from MZ699+ iPNs, and the LH-AL domain formed by vlPr neurons. In line with our observations are morphological studies on ePNs and third-order LH neurons revealing a similarly tight constriction into three zones within the

LH (**Tanaka et al., 2004**), while single-cell labeling combined with image registration resulted in five ePN target zones (**Jefferis et al., 2007**). However, the ePN terminal zones do not necessarily correspond to the target domains of iPNs, since it has recently been shown that MZ699+ iPNs do not inhibit odor responses of GH146+ ePNs (**Liang et al., 2013**) and that the presynaptic sites of iPNs are spatially separated from those of ePNs (**Wang et al., 2014**). Hence both PN populations represent parallel processing pathways that most likely accomplish distinct processing tasks analogous to the honeybee olfactory system which possesses dual olfactory pathways to the higher brain that accomplish parallel processing of similar odors (**Brill et al., 2013**).

Silencing MB function revealed that the LH alone is sufficient for basic olfactory behavior (**de Belle and Heisenberg, 1994**; **Connolly et al., 1996**; **Heimbeck et al., 2001**). Our behavioral results demonstrate that selectively silencing MZ699+ iPNs severely reduced the flies' odor attraction behavior. Hence our results suggest that MZ699+ iPNs are capable of extracting specific features from the combinatorial code emerging in the AL. A behavioral study revealed that silencing MBc neurons impairs odor attraction but not repulsion (**Wang et al., 2003b**). The authors drew the conclusion that the LH is involved in mediating innate repulsion rather than attraction. These results are not necessarily contradictory to ours since some ePNs might activate the LH-AL domain exclusively (i.e., vlPr neurons). On the other hand, **Wang et al. (2003b)** did not include highly concentrated attractive odors. Therefore it is possible that in their experiments, the odor detection threshold was simply reduced, so that only highly concentrated odors, which induced odor aversion, could be distinguished. Our behavioral results, in contrast, revealed the constant influence of the MZ699+ iPNs in mediating attraction for odorants over a range of concentrations.

Our data suggests that odors with opposing hedonic valences are encoded by an interplay of distinct processing pathways. The study by **Liang et al. (2013)** showed that GABA release from MZ699+ iPNs directly inhibits responses of vlPr neurons to food odors as mentioned above. This finding fits well to our observations that iPNs are activated mainly by attractive odors while vlPr neurons are not, likely due to the inhibitory input from iPNs. VlPr neurons are, on the other hand, almost solely activated by repellent odors, which do hardly activate iPNs and therefore do not induce a strong inhibition to vlPr neurons. Repellent odors most likely activate vlPr neurons via ACh release of ePNs which is supported by immunostainings with pre- and postsynaptic markers indicating that vlPr neurons receive input in the LH, while the vlPr represents their major output region (**Parnas et al., 2013**). The vlPr is supposedly also a target of visual neurons from the optic lobe (**Tanaka et al., 2004**) implying that a certain integration of different sensory modalities takes place at this central processing relay. Given that iPNs are inhibitory neurons, the underlying mechanism of odor attraction behavior might therefore be an inhibition of aversive neuronal circuits from the LH to the vlPr that are mainly composed of vlPr neurons. However, this assumption needs to be verified with further experiments elucidating if vlPr neurons are sufficient and necessary to mediate odor aversion.

What is known about odor coding in the LH in other insect species? Notably, in locusts it has been shown that LH neurons receiving convergent PN input appeared to encode stimulus intensity in their net firing rates and in the phases of their spikes (**Gupta and Stopfer, 2012**). Hence these results support the idea that within the LH, general stimulus features such as odor intensity are extracted, which is well in line with our observation of the anterior LH domains whose activity is also significantly correlated to odor intensity. Also in line with our results is a study from honeybees which shows that the representation of different pheromone types is spatially segregated in the LH (**Roussel et al., 2014**), indicating that odors eliciting specific behaviors are coded according to their biological values.

In conclusion, our study provides an important step in unraveling higher olfactory processing mechanisms that are crucial for mediating innate behaviors in *Drosophila*. We provide functional evidence for a feature-based spatial arrangement of the LH decoding opposing hedonic valences and odor intensity. The role of the LH as a center for integrating biological values towards innate decisions by computing conveyed information of two processing pathways is thus expanded.

Materials and methods

Drosophila stocks

All fly stocks were maintained on conventional cornmeal-agar-molasses medium under L:D 12:12, RH = 70% and 25°C. For wild-type controls *D. melanogaster* of the Canton-S strain was used. Transgenic lines were obtained from Bloomington Stock Center (http://flystocks.bio.indiana.edu/) and Vienna

RNAi stock center (http://www.vdrc.at). Other fly stocks were kindly provided by Kei Ito (*MZ699-GAL4*) and Maria Luisa Vasconcelos (*UAS-C3PA*). The END1-2 fly line is published in ***Grabe et al. (2014)***.

Immunohistochemistry

Whole-mount immunofluorescence staining was carried out as described (***Laissue et al., 1999***; ***Vosshall et al., 2000***). Initially brains were dissected in Ringer's solution (130 mM NaCl, 5 mM KCl, 2 mM $MgCl_2$, 2 mM $CaCl_2$, 36 mM saccharose, 5 mM HEPES, [pH 7.3]) (***Estes et al., 1996***) and fixed in 4% PFA in PBS-T (PBS, 0.2–1% Triton-X). After washing with PBS-T brains were blocked with PBS-T, 5% normal goat serum (NGS). Primary antibodies were diluted in blocking solution or PBS-T and incubated at 4°C for 2–3 days. Secondary antibody incubation lasted 1–2 days. Brains were mounted in VectaShield (Vector Labs, Burlingame, CA). The following primary antibodies were used: rabbit α-GABA (1:500) (Sigma), mouse α-GFP (1:500) (Invitrogen). The following secondary antibodies were used: Alexa Fluor 488, goat anti-mouse (1:500); Alexa Fluor 546, goat anti-rabbit (1:500); (all IgG Invitrogen).

Functional imaging

Fly preparation and functional imaging of the AL was conducted as previously described (***Stökl et al., 2010***; ***Strutz et al., 2012***). LH imaging was conducted similarly, except for the higher resolution achieved with a 60× water immersion objective (LUMPlanFl 60×/0.90 W Olympus). The optical plane was ~30 μm below the most dorsal entrance point of the iPN tract into the LH. Binning on the CCD-camera chip resulted in a resolution of 1 pixel = 0.4 × 0.4 μm. For bilateral LH imaging during transection a 20× water immersion objective (NA 0.95, XLUM Plan FI, Olympus) was employed. All recordings lasted 10 s with a frame rate of 4 Hz. Odors included acids (propionic acid, acetic acid), lactones (γ-butyrolactone), terpenes (linalool), aromatics (acetophenone, methyl salicylate, benzaldehyde, phenylacetic acid), alcohols (1-octen-3-ol), esters (acetoin acetate, cis-vaccenyl acetate, 2-phenethyl acetate), ketones (2,3 butanedione) and balsamic vinegar diluted in mineral oil (all from Sigma Aldrich). Odors were applied during frame 8–14 (i.e., after 2 s, lasting for 2 s). Flies were imaged for up to 1 hr, with a minimum inter-stimulus interval of one minute. We selected conventional widefield Ca^{2+} imaging as the method of choice, since we were able to obtain single bouton resolution with this technique.

Imaging data analysis

Calcium imaging data of AL were analyzed with custom-written IDL software (ITT Visual Information Solutions) provided by Mathias Ditzen as previously described (***Stökl et al., 2010***; ***Strutz et al., 2012***). Regarding the Ca^{2+} imaging data in the LH, we repeated recordings of each odor at each concentration two to three times to ensure the reliability of the extracted domain information. To execute NNMF analysis (see below), at least 6–7 valid measurements, that is, animals with repeated identical recordings, were collected for each odor and employed for the analysis. Individual odor measurements were aligned using ImageJ (Fiji) to correct movement artifacts. Fluorescence changes (ΔF/F) for each odor were calculated in relation to background fluorescence using frames 0–6 (i.e., 2–0.5 s before odor application). A Gaussian low-pass filter (ó = 1px) was applied to compensate for remaining movement artifacts and pixel noise. To reduce the computational load, the frame rate was averaged by two consecutive frames, and recordings were spatially down-sampled by a factor of two. The resulting concatenated time-series of the recordings is denoted as measurement matrix Y with element $Y_{t,p}$ being the t^{th} observed value of pixel p.

NNMF—Non-Negative Matrix Factorization

In contrast to the AL, which consists of highly ordered glomerular subunits, the LH comprises a mainly homogenous neuropil which does not provide spatial or functional landmarks. Therefore, we used the automatic method NNMF to extract Ca^{2+} signals that exhibit common spatial or temporal features. NNMF, like other matrix factorization techniques (e.g., Principal Component Analysis (PCA) and Independent Component Analysis (ICA)), decompose the measurement matrix Y into *k* components, $Y = \sum_k x_k * a_k^T + R$. The time-course a_k of each component contains a common underlying time-courses of all pixels and each pixel participation x_k declares how strongly each pixel is involved in this time-course. The residual matrix R contains the unexplained data. In order to perform NNMF, we implemented the HALS algorithm in Python including a spatial smoothness constraint (a_{sm} = 0.1) (***Cichocki and Phan, 2009***) and an additional spatial decorrelation constraint (a_{de} = 0.1) (***Chen and Cichocki, 2005***).

In PCA decomposition is performed such that either timecourses a_k or pixel participation x_k are uncorrelated, whereas ICA aims for timecourses (temporal ICA) or pixel participation (spatial ICA) to be independent. Although spatial ICA is able to segregate signals into functional similar neuropils (***Reidl et al., 2007***), we chose the NNMF approach, because it is known to achieve even a better parts-based representation compared to the more holistic results of PCA or ICA (***Lee and Seung, 1999***). In contrast to PCA and ICA, NNMF constrains both the extracted time-courses and pixel participations to be positive. Positive pixel participation enabled us to make a straightforward physiological interpretation, reading the participation values as the contribution strength of an underlying physiological domain. The restriction to positive time-courses reflects the fact that we did not observe any significant decrease of fluorescence in response to an odor in the original measurement data. For each animal we performed decomposition into $k = 5$ components. This was sufficient to explain most of the data's variance (88% + 8%, error is standard deviation across individuals). The remaining variance in the residual matrix R contained no additional domains but rather reflected remaining movement artifacts of the measurements (***Figure 2—figure supplement 2***). Of the five components extracted by NNMF, three stood out prominently (***Figure 2—figure supplement 3***): First, they were extracted in all animals at very clearly defined anatomical positions. Second, their responses to stimuli repetitions were highly reproducible in contrast to the other two components, that is, they exhibited a significant ($p < 2*10^{-8}$, *t* test) higher trial-to-trial correlation of 0.72 ± 0.20 in contrast to 0.52 ± 0.26 for the remaining components; third, the odorant spectra of their responses were characteristic across animals.

Though we cannot completely rule out that the remaining components of the factorization are ORDs of their own, there are several indications that they are not. On the one hand, they exhibit a lower trial-to-trial correlation than the three selected components. Second, those components did not consistently appear at similar anatomical position. Third, they were spatially overlapping with the selected three components. Instead of independent ORDs, these regions might convey fluorescence changes independent of odor stimulation or an overlapping region of two of the reliable ORDs. A validation of our NNMF-based results with spatial ICA yielded very similar, but slightly worse results. Whereas the three reliable ORDs from NNMF were also extracted in spatial ICA, the two remaining components exhibited much higher variability than when obtained with NNMF. Hence, we conclude that the LH area comprising MZ699+ neurons consists of three ORDs. We labeled those three components according to the anatomical position of their pixel participation within the LH.

Statistical analysis of imaging data

To determine the coding properties of extracted odor response domains (ORDs), we calculated the mean response of each animal within a time window of 1–4 s after stimulus onset. Hence, median responses over all animals defined the standard stimulated response r^o_{ORD} of an ORD to an odor *o*. Initially, regions were evaluated individually, and correlations were calculated between standard response spectra and the behavioral response index (RI), or odor concentration, respectively, using the 'linregress' function of the Python scipy.stat module. To analyze the combined ORD representations of odor patterns $p_o = \left(r^o_{PM}, r^o_{AM}, r^o_{AL}\right)$ we calculated for all odor pairs the pattern similarity as correlation distance $d_{o1,o2} = 1 - corr(p_{o1}, p_{o2})$. In order to visualize the correlation matrix in a comprehensible way, we then arranged odors according to the single linkage clustering of the Python scipy.cluster.hierarchy module. To compare the representation in the LH to those of the AL, we applied the same procedure to the dorsal glomerular odor activation pattern.

2-Photon photoactivation and neuronal reconstructions

For in vivo photoactivation experiments, 1–6 day old flies (genotype: END1-2,UAS-C3PA;MZ699-GAL4) were dissected as in the imaging experiments except that tracts of the salivary glands were cut to prevent movement. Photoactivation was accomplished via continuous illumination with 760 nm for 15–25 min. After a 5-min break to permit full diffusion of the photoconverted molecules, 925 nm z-stacks of the whole brain were acquired and subsequently used for neuronal 3D-reconstruction. For all 3D reconstructions, the segmentation software AMIRA 4.1.1 & 5.3.3 (FEI Visualization Sciences Group, Burlington, MA) was used. Neurons of different individuals were embedded into the reference brain using a labelfield registration as previously described (***Rybak et al., 2010***). Briefly, segmented labels of brain neuropils (AL, MBc, LH) were registered onto a reference brain image using affine registration followed by elastic warping. In a second step, the calculated

transformation matrix was applied to the respective neuron morphology that was then aligned to the reference brain image.

For morphological analysis of reconstructed iPNs, we first determined all terminal points of each iPN in the LH area. For each combination of terminals we calculated a similarity score (*s*) in analogy to (***Kohl et al., 2013***) as follows:

$$s(t_1,t_2) = \sqrt{e^{-\Delta(t_1,t_2)^2/2\sigma^2}},$$

where *t* is the terminal position, Δ*(t1,t2)* is the Euclidean distance and *σ* is a free parameter that determines how close in space terminal points must be to be considered similar; analogue to ***Kohl et al. (2013)*** we set this parameter to 3 µm. Finally we calculated the pairwise similarity score between two neurons as their average all-to-all terminal similarity scores, normalized to their self-scores as follows:

$$S(n_1,n_2) = \sum_{t_1,t_2} s(t_1,t_2) / \sqrt{\sum_{t_1} s(t_1,t_1) * \sum_{t_2} s(t_2,t_2)}$$

Effectively this quantifies the relative overlap of the target area of all pairs of iPNs. For clustering, the similarity scores were converted to distances (i.e., *1-S*) and a hierarchical clustering was performed using UPGMA method. Principal component analysis and one-way ANOSIM was performed using the statistical software PAST 3.x (Paleontological statistics software package for education and data analysis).

2-Photon-mediated transection

Transections of either the plF tract or the mACT were conducted in one brain hemisphere, each of the same fly. The target area was monitored with 925 nm and chosen to be close to the LH but distant enough not to affect neurites ramifying in the LH neuropil. For both tracts, lesioned areas had an average size of 34 µm and were illuminated with short pulses of 710 nm every 40 ms for 250 ms in 60 (plF) to 80 (mACT) cycles in a single focal plane. After a fast z-stack with 925 nm to confirm complete lesion, a 5-min neuronal recovery interval followed before continuing the imaging procedure. Data were analyzed using NNMF.

Image acquisition

Photoactivation and transection procedures as well as image acquisition following immunohistochemistry were accomplished with a 2-photon confocal laser scanning microscope (2PCLSM, Zeiss LSM 710 NLO) equipped with a 40× (W Plan-Apochromat 40×/1.0 DIC M27, Zeiss) or 20× (W N-Achroplan 20×/0.5 M27, Zeiss). The 2PCLSM was placed on a smart table UT2 (Newport Corporation, Irvine, CA, USA) and equipped with an infrared Chameleon Ultra diode-pumped laser (Coherent, Santa Clara, CA, USA). Z-stacks were performed with argon 488 nm and helium-neon 543 nm laser or the Chameleon Laser 925 nm (BP500-550 for G-CaMP and LP555 for DsRed/tdTomato) and had a resolution of 1024 or 512 square pixels. The maximum step size for immuno-preparations or single neuron projections was 1 µm and for AL reconstructions 2 µm.

Behavioral assay

Flies carrying P[GAD1-RNAi];P[MZ699-GAL4] were crossed just before the experiment to prevent dosage compensation effects. T-maze experiments were performed as described (***Stensmyr et al., 2012***). WT, parental controls (P[GAD1-RNAi] or P[MZ699-GAL4]) and test flies carrying both insertions were tested separately under identical conditions. The response index (RI) was calculated as (O-C)/T, where O is the number of flies in the odor arm, C is the number of flies in the control arm, and T is the total number of flies used in the trial. Hence, the RI ranges from −1 (complete avoidance) to 1 (complete attraction). Each experiment was carried out on 30 flies and was repeated 12 times. Dunn's Multiple Comparison Test was used for global differences in the dataset. Whenever the Multiple Comparison Test was significant (i.e., $p < 0.05$), a posthoc test for selected pairs was performed, that is, between the GADi-flies and the other three control lines as we were not interested in differences among the different control lines. All RI were tested against 0 (no response) by using the Wilcoxon-rank-sum test.

Acknowledgements

We thank Silke Trautheim, Regina Stieber, Linda Gummlich and Sascha Bucks for excellent technical assistance and Emily Wheeler for editorial assistance.

Additional information

Competing interests

BSH: Vice president of the Max Planck Society, one of the three founding funders of *eLife*, and a member of *eLife*'s Board of Directors. The other authors declare that no competing interests exist.

Funding

Funder	Grant reference number	Author
Bundesministerium für Bildung und Forschung		Silke Sachse
Max-Planck-Gesellschaft		Bill S Hansson
Deutsche Forschungsgemeinschaft	Priority program SPP1392 (SCHM2474/1-1 and 1-2)	Michael Schmuker, Jan Soelter

The funders had no role in study design, data collection and interpretation, or the decision to submit the work for publication.

Author contributions

AS, Conception and design, Acquisition of data, Analysis and interpretation of data, Drafting or revising the article; JS, Analysis and interpretation of data, Drafting or revising the article; AB, VG, JR, Acquisition of data, Analysis and interpretation of data; AF, Performed behavioral experiments; MK, Supervision of Abu Farhan, Analysis and interpretation of data; MS, Supervision of Jan Soelter, Analysis and interpretation of data; BSH, Provided intellectual and financial support, Conception and design; SS, Conception and design, Analysis and interpretation of data, Drafting or revising the article

Author ORCIDs

Amelie Baschwitz, http://orcid.org/0000-0003-0614-1667
Michael Schmuker, http://orcid.org/0000-0001-6753-4929

References

Bausenwein B, Dittrich AP, Fischbach KF. 1992. The optic lobe of *Drosophila melanogaster*. II. Sorting of retinotopic pathways in the medulla. *Cell and Tissue Research* **267**:17–28. doi: 10.1007/BF00318687.

Brill MF, Rosenbaum T, Reus I, Kleineidam CJ, Nawrot MP, Rössler W. 2013. Parallel processing via a dual olfactory pathway in the honeybee. *The Journal of Neuroscience* **33**:2443–2456. doi: 10.1523/jneurosci.4268-12.2013.

Caron SJ, Ruta V, Abbott LF, Axel R. 2013. Random convergence of olfactory inputs in the *Drosophila* mushroom body. *Nature* **497**:113–117. doi: 10.1038/nature12063.

Chakraborty TS, Goswami SP, Siddiqi O. 2009. Sensory correlates of Imaginal conditioning in *Drosophila melanogaster*. *Journal of Neurogenetics* **23**:210–219. doi: 10.1080/01677060802491559.

Chen Z, Cichocki A. 2005. Nonnegative matrix factorization with temporal smoothness and/or spatial decorrelation constraints. *Signal Processing*.

Cichocki A, Phan A. 2009. Fast local algorithms for large scale nonnegative matrix and tensor factorizations. *IEICE Transactions on Fundamentals of Electronics, Communications and Computer Sciences* **E92-A**:708–721. doi: 10.1587/transfun.E92.A.708.

Connolly JB, Roberts IJ, Armstrong JD, Kaiser K, Forte M, Tully T, O'Kane CJ. 1996. Associative learning disrupted by impaired Gs signaling in *Drosophila* mushroom bodies. *Science* **274**:2104–2107. doi: 10.1126/science.274.5295.2104.

Couto A, Alenius M, Dickson BJ. 2005. Molecular, anatomical, and functional organization of the *Drosophila* olfactory system. *Current Biology* **15**:1535–1547. doi: 10.1016/j.cub.2005.07.034.

Datta SR, Vasconcelos ML, Ruta V, Luo S, Wong A, Demir E, Flores J, Balonze K, Dickson BJ, Axel R. 2008. The *Drosophila* pheromone cVA activates a sexually dimorphic neural circuit. *Nature* **452**:473–477. doi: 10.1038/nature06808.

de Belle JS, Heisenberg M. 1994. Associative odor learning in *Drosophila* abolished by chemical ablation of mushroom bodies. *Science* **263**:692–695. doi: 10.1126/science.8303280.

Estes PS, Roos J, van der Bliek A, Kelly RB, Krishnan KS, Ramaswami M. 1996. Traffic of dynamin within individual *Drosophila* synaptic boutons relative to compartment-specific markers. *The Journal of Neuroscience* **16**:5443–5456.

Fiala A, Spall T, Diegelmann S, Eisermann B, Sachse S, Devaud JM, Buchner E, Galizia CG. 2002. Genetically expressed cameleon in *Drosophila melanogaster* is used to visualize olfactory information in projection neurons. *Current Biology* **12**:1877–1884. doi: 10.1016/S0960-9822(02)01239-3.

Fisek M, Wilson RI. 2014. Stereotyped connectivity and computations in higher-order olfactory neurons. *Nature Neuroscience* **17**:280–288. doi: 10.1038/nn.3613.

Fishilevich E, Vosshall LB. 2005. Genetic and functional subdivision of the *Drosophila* antennal lobe. *Current Biology* **15**:1548–1553. doi: 10.1016/j.cub.2005.07.066.
Grabe V, Strutz A, Baschwitz A, Hansson BS, Sachse S. 2014. Digital in vivo 3D atlas of the antennal lobe of *Drosophila melanogaster*. *The Journal of Comparative Neurology* doi: 10.1002/cne.23697.
Gupta N, Stopfer M. 2012. Functional analysis of a higher olfactory center, the lateral horn. *The Journal of Neuroscience* **32**:8138–8148. doi: 10.1523/jneurosci.1066-12.2012.
Heimbeck G, Bugnon V, Gendre N, Keller A, Stocker RF. 2001. A central neural circuit for experience-independent olfactory and courtship behavior in *Drosophila melanogaster*. *Proceedings of the National Academy of Sciences of USA* **98**:15336–15341. doi: 10.1073/pnas.011314898.
Heisenberg M. 2003. Mushroom body memoir: from maps to models. *Nature Reviews. Neuroscience* **4**:266–275. doi: 10.1038/nrn1074.
Hildebrand JG, Shepherd GM. 1997. Mechanisms of olfactory discrimination: Converging evidence for common principles across phyla. *Annual Review of Neuroscience* **20**:595–631. doi: 10.1146/annurev.neuro.20.1.595.
Ito K, Sass H, Urbach J, Hofbauer A, Schneuwly S. 1997. GAL4-responsive UAS-tau as a tool for studying the anatomy and development of the *Drosophila* central nervous system. *Cell and Tissue Research* **290**:1–10. doi: 10.1007/s004410050901.
Jefferis GS, Marin EC, Stocker RF, Luo L. 2001. Target neuron prespecification in the olfactory map of *Drosophila*. *Nature* **414**:204–208. doi: 10.1038/35102574.
Jefferis GS, Potter CJ, Chan AM, Marin EC, Rohlfing T, Maurer CR, Maurer CR Jnr, Luo L. 2007. Comprehensive maps of *Drosophila* higher olfactory centers: spatially segregated fruit and pheromone representation. *Cell* **128**:1187–1203. doi: 10.1016/j.cell.2007.01.040.
Keene AC, Stratmann M, Keller A, Perrat PN, Vosshall LB, Waddell S. 2004. Diverse odor-conditioned memories require uniquely timed dorsal paired medial neuron output. *Neuron* **44**:521–533. doi: 10.1016/j.neuron.2004.10.006.
Knaden M, Strutz A, Ahsan J, Sachse S, Hansson BS. 2012. Spatial representation of odorant valence in an insect brain. *Cell Reports* **1**:392–399. doi: 10.1016/j.celrep.2012.03.002.
Kohl J, Ostrovsky AD, Frechter S, Jefferis GS. 2013. A bidirectional circuit switch reroutes pheromone signals in male and female brains. *Cell* **155**:1610–1623. doi: 10.1016/j.cell.2013.11.025.
Lai SL, Awasaki T, Ito K, Lee T. 2008. Clonal analysis of *Drosophila* antennal lobe neurons: diverse neuronal architectures in the lateral neuroblast lineage. *Development* **135**:2883–2893. doi: 10.1242/dev.024380.
Laissue PP, Reiter C, Hiesinger PR, Halter S, Fischbach KF, Stocker RF. 1999. Three-dimensional reconstruction of the antennal lobe in *Drosophila melanogaster*. *The Journal of Comparative Neurology* **405**:543–552. doi: 10.1002/(SICI)1096-9861(19990322)405.
Larsson MC, Domingos AI, Jones WD, Chiappe ME, Amrein H, Vosshall LB. 2004. *Or83b* encodes a broadly expressed odorant receptor essential for *Drosophila* olfaction. *Neuron* **43**:703–714. doi: 10.1016/j.neuron.2004.08.019.
Lee DD, Seung HS. 1999. Learning the parts of objects by non-negative matrix factorization. *Nature* **401**:788–791. doi: 10.1038/44565.
Liang L, Li Y, Potter CJ, Yizhar O, Deisseroth K, Tsien RW, Luo L. 2013. GABAergic projection neurons route selective olfactory inputs to specific higher-order neurons. *Neuron* **79**:917–931. doi: 10.1016/j.neuron.2013.06.014.
Livingstone M, Hubel D. 1988. Segregation of form, color, movement, and depth: anatomy, physiology, and perception. *Science* **240**:740–749. doi: 10.1126/science.3283936.
Magee RJ, Kosaric N. 1987. The Microbial production of 2,3-butanediol. *Advances in Applied Microbiology* **32**:89–161. doi: 10.1016/S0065-2164(08)70079-0.
Manni E, Petrosini L. 2004. A century of cerebellar somatotopy: a debated representation. *Nature Reviews. Neuroscience* **5**:241–249. doi: 10.1038/nrn1347.
Marin EC, Jefferis GS, Komiyama T, Zhu H, Luo L. 2002. Representation of the glomerular olfactory map in the *Drosophila* brain. *Cell* **109**:243–255. doi: 10.1016/S0092-8674(02)00700-6.
Min S, Ai M, Shin SA, Suh GSB. 2013. Dedicated olfactory neurons mediating attraction behavior to ammonia and amines in *Drosophila*. *Proceedings of the National Academy of Sciences of USA* **110**:E1321–E1329. doi: 10.1073/pnas.1215680110.
Murthy M, Fiete I, Laurent G. 2008. Testing odor response stereotypy in the *Drosophila* mushroom body. *Neuron* **59**:1009–1023. doi: 10.1016/j.neuron.2008.07.040.
Nakai J, Ohkura M, Imoto K. 2001. A high signal-to-noise Ca(2+) probe composed of a single green fluorescent protein. *Nature Biotechnology* **19**:137–141. doi: 10.1038/84397.
Nassi JJ, Callaway EM. 2009. Parallel processing strategies of the primate visual system. *Nature Reviews. Neuroscience* **10**:360–372. doi: 10.1038/nrn2619.
Okada R, Awasaki T, Ito K. 2009. Gamma-aminobutyric acid (GABA)-mediated neural connections in the *Drosophila* antennal lobe. *The Journal of Comparative Neurology* **514**:74–91. doi: 10.1002/cne.21971.
Parnas M, Lin AC, Huetteroth W, Miesenböck G. 2013. Odor discrimination in *Drosophila*: from neural population codes to behavior. *Neuron* **79**:932–944. doi: 10.1016/j.neuron.2013.08.006.
Pasternak T, Greenlee MW. 2005. Working memory in primate sensory systems. *Nature Reviews. Neuroscience* **6**:97–107. doi: 10.1038/nrn1603.
Patterson GH, Lippincott-Schwartz J. 2002. A photoactivatable GFP for selective photolabeling of proteins and cells. *Science* **297**:1873–1877. doi: 10.1126/science.1074952.
Reidl J, Starke J, Omer DB, Grinvald A, Spors H. 2007. Independent component analysis of high-resolution imaging data identifies distinct functional domains. *Neuroimage* **34**:94–108. doi: 10.1016/j.neuroimage.2006.08.031.

Roussel E, Carcaud J, Combe M, Giurfa M, Sandoz JC. 2014. Olfactory coding in the honeybee lateral horn. *Current Biology* **24**:561–567. doi: 10.1016/j.cub.2014.01.063.
Ruta V, Datta SR, Vasconcelos ML, Freeland J, Looger LL, Axel R. 2010. A dimorphic pheromone circuit in *Drosophila* from sensory input to descending output. *Nature* **468**:686–690. doi: 10.1038/nature09554.
Rybak J, Kuß A, Hans L, Zachow S, Hege HC, Lienhard M, Singer J, Neubert K, Menzel R. 2010. The digital bee brain: integrating and managing neurons in a common 3D reference system. *Frontiers in Systems Neuroscience* **4**:30. doi: 10.3389/fnsys.2010.00030.
Sanes JR, Zipursky SL. 2010. Design principles of insect and vertebrate visual systems. *Neuron* **66**:15–36. doi: 10.1016/j.neuron.2010.01.018.
Semmelhack JL, Wang JW. 2009. Select *Drosophila* glomeruli mediate innate olfactory attraction and aversion. *Nature* **459**:218–223. doi: 10.1038/nature07983.
Shang Y, Claridge-Chang A, Sjulson L, Pypaert M, Miesenböck G. 2007. Excitatory local circuits and their implications for olfactory processing in the fly antennal lobe. *Cell* **128**:601–612. doi: 10.1016/j.cell.2006.12.034.
Silbering AF, Okada R, Ito K, Galizia CG. 2008. Olfactory information processing in the *Drosophila* antennal lobe: anything goes? *The Journal of Neuroscience* **28**:13075–13087. doi: 10.1523/jneurosci.2973-08.2008.
Steck K, Veit D, Grandy R, Badia SBi, Mathews Z, Verschure P, Hansson BS, Knaden M. 2012. A high-throughput behavioral paradigm for *Drosophila* olfaction - the Flywalk. *Scientific Reports* **2**:361. doi: 10.1038/srep00361.
Stensmyr MC, Dweck HK, Farhan A, Ibba I, Strutz A, Mukunda L, Linz J, Grabe V, Steck K, Lavista-Llanos S, Wicher D, Sachse S, Knaden M, Becher PG, Seki Y, Hansson BS. 2012. A conserved dedicated olfactory circuit for detecting harmful microbes in *Drosophila*. *Cell* **151**:1345–1357. doi: 10.1016/j.cell.2012.09.046.
Stocker RF, Heimbeck G, Gendre N, de Belle JS. 1997. Neuroblast ablation in *Drosophila* P[GAL4] lines reveals origins of olfactory interneurons. *Journal of Neurobiology* **32**:443–456. doi: 10.1002/(SICI)1097-4695(199705)32.
Stocker RF, Lienhard MC, Borst A, Fischbach KF. 1990. Neuronal architecture of the antennal lobe in *Drosophila melanogaster*. *Cell and Tissue Research* **262**:9–34. doi: 10.1007/BF00327741.
Stökl J, Strutz A, Dafni A, Svatos A, Doubsky J, Knaden M, Sachse S, Hansson BS, Stensmyr MC. 2010. A deceptive pollination system targeting Drosophilids through olfactory mimicry of yeast. *Current Biology* **20**:1846–1852. doi: 10.1016/j.cub.2010.09.033.
Strutz A, Voeller T, Riemensperger T, Fiala A, Sachse S. 2012. Calcium imaging of neural activity in the olfactory system of *Drosophila*. In: Martin JR, editor. *Genetically encoded functional indicators*. New York, USA: Springer Science+Business Media, LLC. p. 43–70. doi: 10.1007/978-1-62703-014-4_3.
Tanaka NK, Awasaki T, Shimada T, Ito K. 2004. Integration of chemosensory pathways in the *Drosophila* second-order olfactory centers. *Current Biology* **14**:449–457. doi: 10.1016/j.cub.2004.03.006.
Tian L, Hires SA, Mao T, Huber D, Chiappe ME, Chalasani SH, Petreanu L, Akerboom J, McKinney SA, Schreiter ER, Bargmann CI, Jayaraman V, Svoboda K, Looger LL. 2009. Imaging neural activity in worms, flies and mice with improved GCaMP calcium indicators. *Nature Methods* **6**:875–881. doi: 10.1038/nmeth.1398.
Tully T, Quinn WG. 1985. Classical conditioning and retention in normal and mutant *Drosophila melanogaster*. *Journal of Comparative Physiology A, Sensory, Neural, and Behavioral Physiology* **157**:263–277. doi: 10.1007/BF01350033.
Vosshall LB, Stocker RF. 2007. Molecular architecture of smell and taste in *Drosophila*. *Annual Review of Neuroscience* **30**:505–533. doi: 10.1146/annurev.neuro.30.051606.094306.
Vosshall LB, Wong AM, Axel R. 2000. An olfactory sensory map in the fly brain. *Cell* **102**:147–159. doi: 10.1016/S0092-8674(00)00021-0.
Wang JW, Wong AM, Flores J, Vosshall LB, Axel R. 2003a. Two-photon calcium imaging reveals an odor-evoked map of activity in the fly brain. *Cell* **112**:271–282. doi: 10.1016/S0092-8674(03)00004-7.
Wang K, Gong J, Wang Q, Li H, Cheng Q, Liu Y, Zeng S, Wang Z. 2014. Parallel pathways convey olfactory information with opposite polarities in *Drosophila*. *Proceedings of the National Academy of Sciences of USA* **111**:3164–3169. doi: 10.1073/pnas.1317911111.
Wang Y, Chiang AS, Xia S, Kitamoto T, Tully T, Zhong Y. 2003b. Blockade of neurotransmission in *Drosophila* mushroom bodies impairs odor attraction, but not repulsion. *Current Biology* **13**:1900–1904. doi: 10.1016/j.cub.2003.10.003.
Wilson RI, Laurent G. 2005. Role of GABAergic inhibition in shaping odor-evoked spatiotemporal patterns in the *Drosophila* antennal lobe. *The Journal of Neuroscience* **25**:9069–9079. doi: 10.1523/JNEUROSCI.2070-05.2005.
Wilson RI, Mainen ZF. 2006. Early events in olfactory processing. *Annual Review of Neuroscience* **29**:163–201. doi: 10.1146/annurev.neuro.29.051605.112950.
Wilson RI, Turner GC, Laurent G. 2004. Transformation of olfactory representations in the *Drosophila* antennal lobe. *Science* **303**:366–370. doi: 10.1126/science.1090782.
Wong AM, Wang JW, Axel R. 2002. Spatial representation of the glomerular map in the *Drosophila* protocerebrum. *Cell* **109**:229–241. doi: 10.1016/S0092-8674(02)00707-9.

eLife, 2014, 3

Supplemental Information

Decoding odor quality and intensity in the *Drosophila* brain

Antonia Strutz, Jan Soelter, Amelie Baschwitz, Abu Farhan, Veit Grabe, Jürgen Rybak, Markus Knaden, Michael Schmuker, Bill S Hansson, Silke Sachse

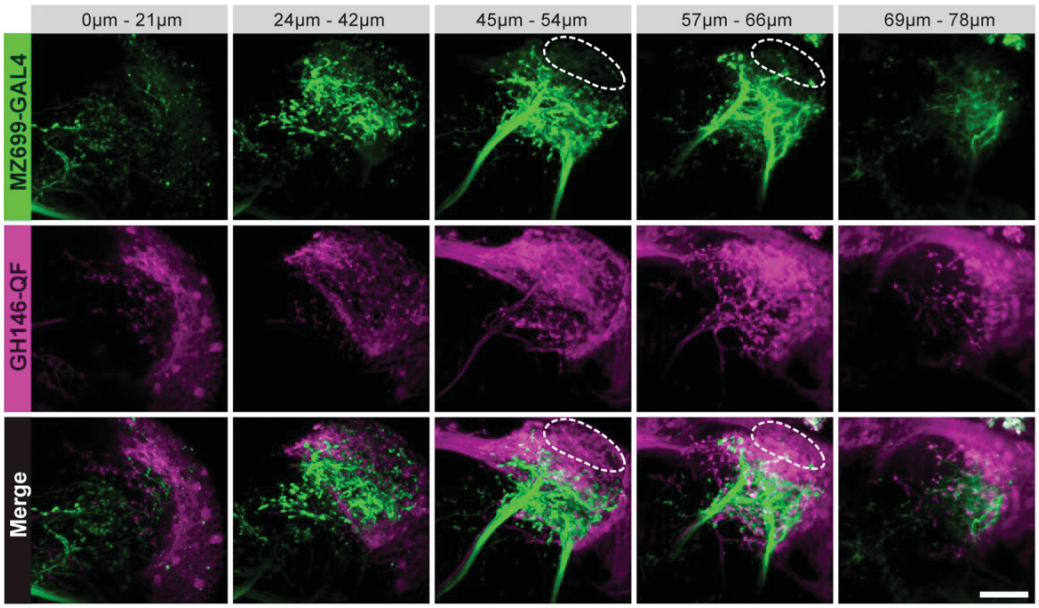

Figure 1—figure supplement 1.**Characterization of excitatory and inhibitory projection neurons.**

Overlap of ePNs (QUAS-tdTomato) and iPNs (UAS-GCaMP3.0) in the LH area. The circle indicates the posterior lateral region, which is sparsely innervated by iPNs and dominated by ePN axonal terminal fields. Scale bar, 20 µm.

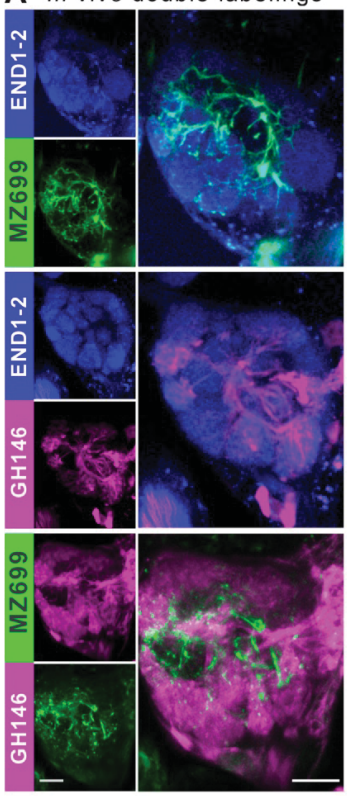

B

Glomerulus	MZ699	GH146	Merge
D			X
DA1			X
DA2			X
DA3			
DA4l			X
DA4m			
DC1			X
DC2			X
DC3			X
DC4			
DL1			
DL2d			
DL2v			
DL3			
DL4			X
DL5			
DM1			
DM2			X
DM3			X
DM4			X
DM5			X
DM6			X
DP1l			
DP1m			X
V			
VA1d			X
VA1v			X
VA2			X
VA3			X
VA4			
VA5			X
VA6			X
VA7l			X
VA7m			X
VC1			X
VC2			
VC3			
VC4			
VC5			
VL1			
VL2p			
VL2a			X
VM1			
VM2			X
VM3			X
VM4			
VM5d			
VM5v			
VM7d			X
VM7v			X
VP1			
VP4			
52	**40**	**37**	**28**
	76.92 %	**71.15 %**	**53.85 %**

Figure 1—figure supplement 2.**Glomerular innervations of ePNs and iPNs.**

(**A**) Representative *in vivo* images of glomerular innervations. *MZ699-* and *GH146-GAL4* lines have been reconstructed with the END1-2 background staining (two upper planes) and dual labeling via the Q-system and the GAL4-UAS expression system (lowest plane). Scale bar, 20 µm. (**B**) Detailed glomerular AL innervation. Green filled cells indicate innervation by *MZ699-GAL4*, magenta *GH146-GAL4* innervation, respectively and grey, no innervation by the indicated line. Bottom rows, total number of innervated glomeruli with percentage share indicated below. Merge column: white filled with ‘x’ indicates glomeruli innervated by both lines, grey only one line. Blue filled rows are glomeruli labeled by none of the enhancer trap lines.

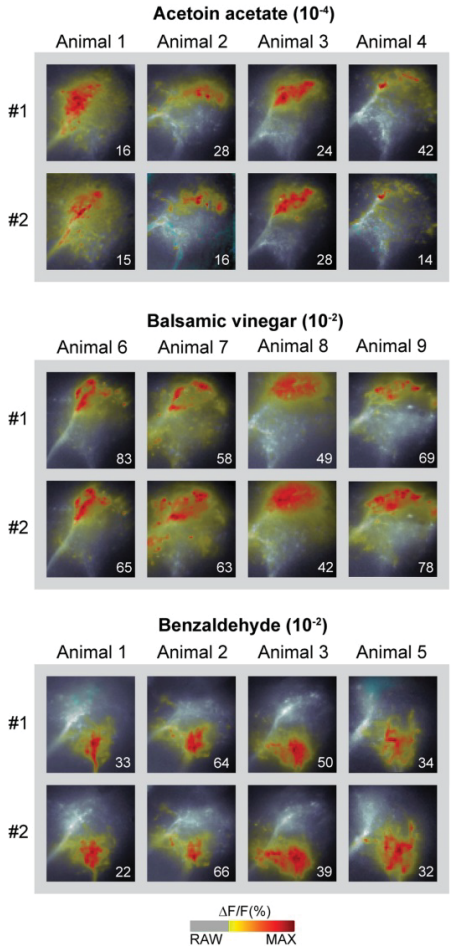

Figure 2—figure supplement 1.**Odor-evoked activity patterns in the LH are reproducible and stereotypic.**

Odor-evoked Ca^{2+} responses (ΔF/F%) in the LH for the three odors acetoin acetate, balsamic vinegar and benzaldehyde in four animals are shown as false-color coded images. Two measurements in each animal are given to reveal that the activity patterns are highly reproducible within one animal. Comparison between the patterns among individuals shows that the activity regions are stereotypic. Numbers in the lower right corner indicate individual maxima. The ΔF/F scale bar is shown at the bottom.

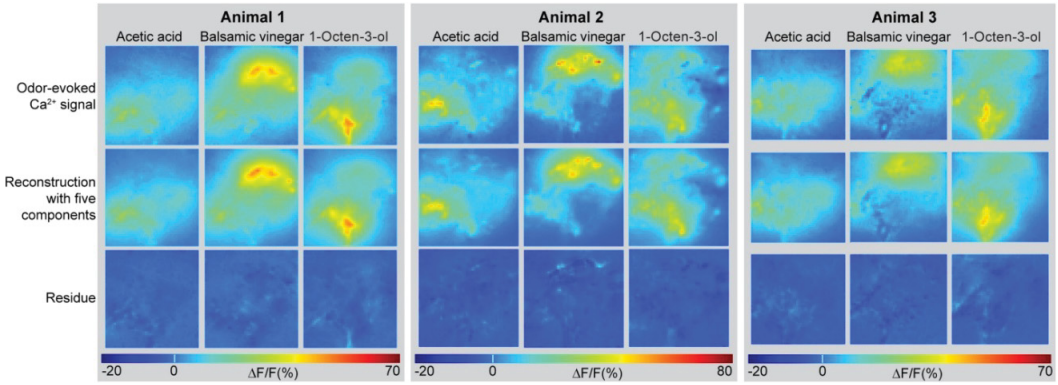

Figure 2—figure supplement 2.**Odor-evoked activity patterns in the LH can be reconstructed with five components.**

Above, Odor-evoked Ca^{2+} responses (ΔF/F%) in the LH for the three odors acetic acid, balsamic vinegar and 1-octen-3-ol in three animals are shown as false-color coded images. The ΔF/F scale bar is shown at the bottom. Middle, activity patterns were reconstructed using NNMF with five components. Below, residue of the pattern reconstructions with five components (as shown in the middle panel) revealing that no stimulus related activity remained.

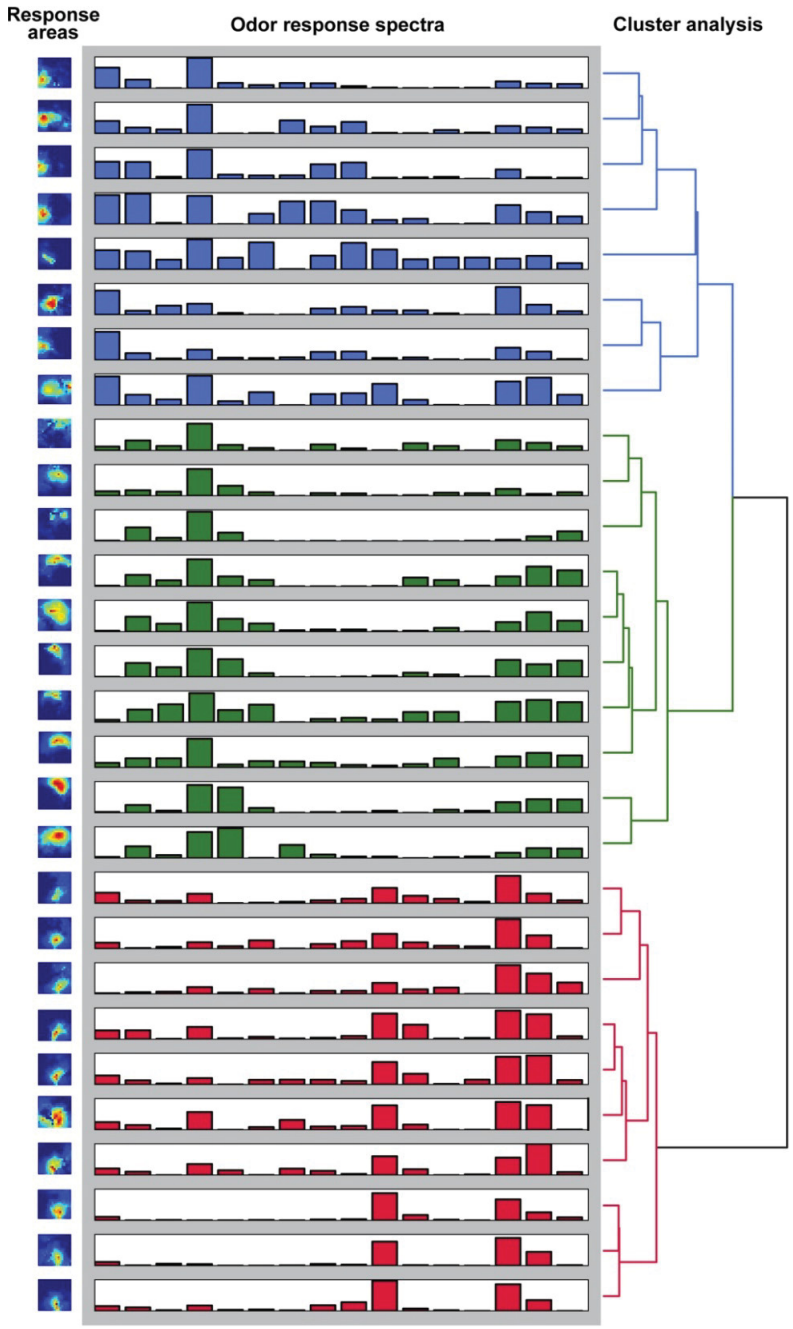

Figure 2—figure supplement 3.**Odor-evoked activity patterns in the LH cluster into three components.**

Hierachichal clustering (UMPGA) of the odor response spectra of the NNMF components with a reliable stimulus response (trial-to-trial correlation >0.7, that is, 28 out of 35 components in seven animals). The response spectra segregate into three distinct clusters according to their stimulus response spectra. The corresponding response areas (left pictures) are located in similar regions of the LH.

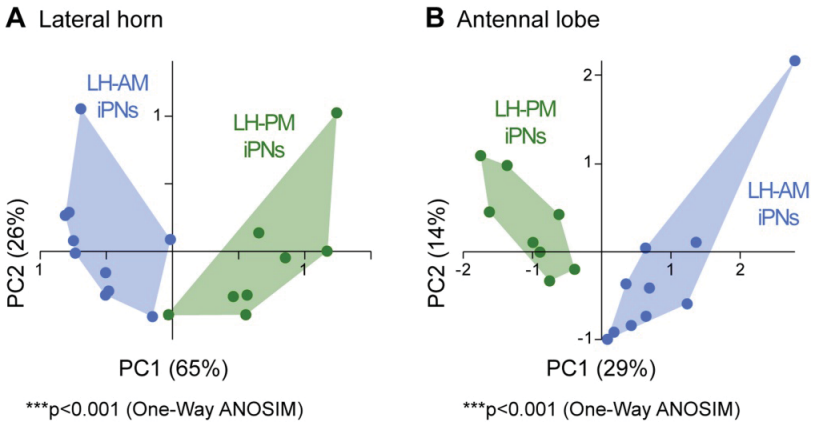

Figure 3—figure supplement 1.**iPNs can be morphologically segregated according to their target and input region.**

(**A**) Principal component analysis based on the distances of the similarity scores of all terminal points of each individual iPN in the LH (for details see 'Materials and methods'). LH-AM iPNs (blue) and LH-PM iPNs (green) form significantly distinct clusters (***p < 0.001, One-Way ANOSIM, Bray–Curtis). (**B**) Principal component analysis based on the glomerular innervations of each individual iPN in the AL. Again, LH-AM iPNs (blue) and LH-PM iPNs (green) form significantly distinct clusters (***p < 0.001, One-Way ANOSIM, Bray–Curtis).

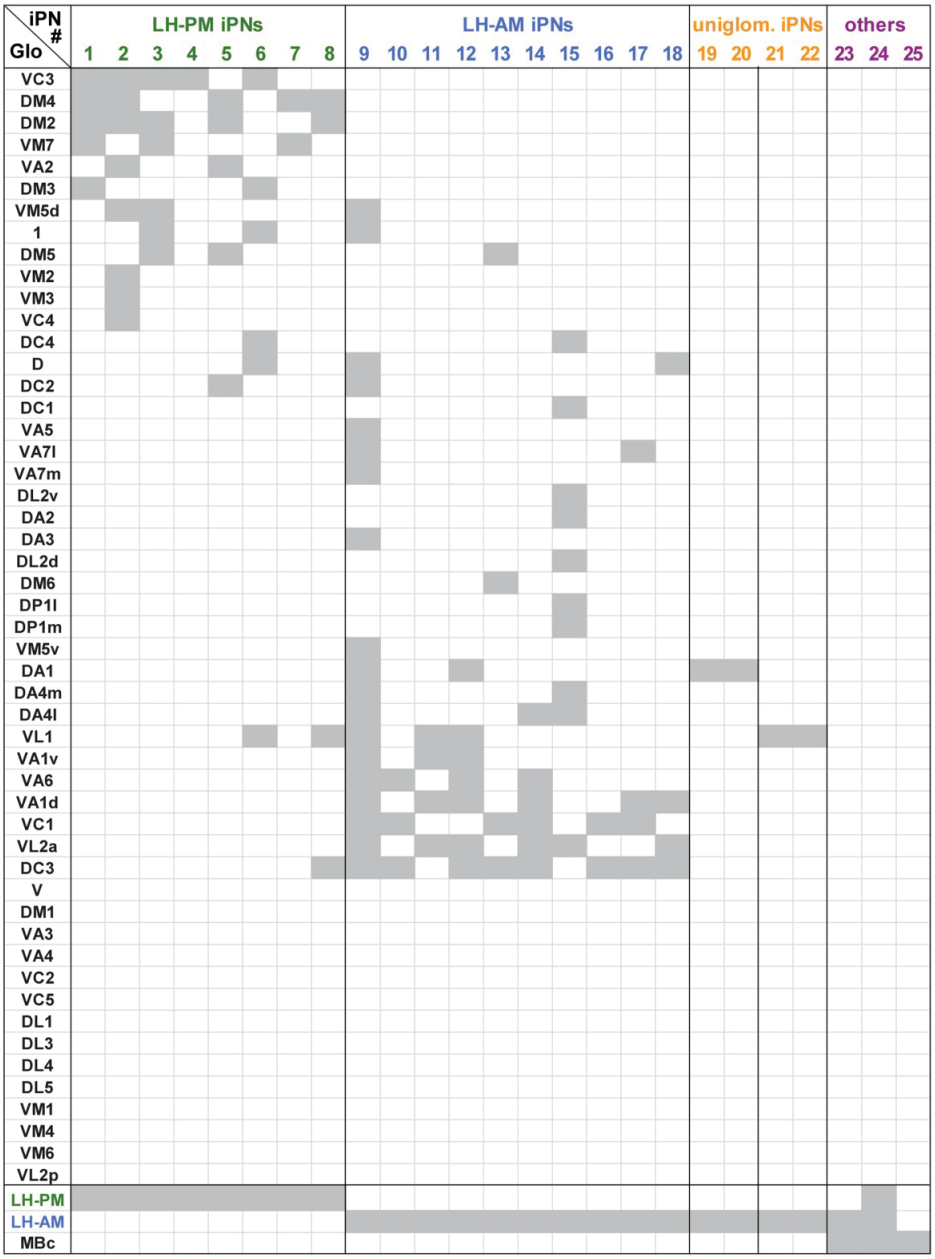

Figure 3—figure supplement 2.**Glomerular innervations of individual iPNs.**

Binary innervation patterns of 25 individually labeled MZ699+ iPNs using PA-GFP. Columns represent innervation patterns of individual neurons which have been grouped according to their innervation properties; rows represent 51 glomeruli in the AL along with the innervation in the specific odor response domains in the LH (LH-PM, LH-AM) and/or the mushroom body calyx (MBc). Glomeruli have been sorted according to their iPN innervation. Grey, innervated; white, not innervated.

Odor	T-maze	Trap assay	Fly Walk
Methyl salicylate			
Linalool			
Acetophenone			
1-Octen-3-ol			
Benzaldyhde			
Phenylacetic acid		N/T	N/T
cis-Vaccenyl acetate		N/T	
2-Phenylacetic acid			N/T
Acetic acid			N/T
2,3 Butanedione			
Propionic acid			N/T
γ-Butyrolactone			N/T
Balsamic vinegar			
Acetoin acetate		N/T	N/T

attractive aversive neutral N/T not tested

Figure 6—figure supplement 1.**Odor valences determined with three different behavioral assays.**

Odor-evoked behavioral responses of wild type flies for the 14 odors used in this study determined by T-maze assay, trap assay and the FlyWalk. The color denotes an attractive (green), aversive (red) or a neutral (light yellow) behavioral response. N/T, not tested. The majority of odors yielded similar results independent of the behavioral assay used. In a few cases an attractive odor evoked a neutral response (i.e., no response), but never induced an aversive response in another assay.

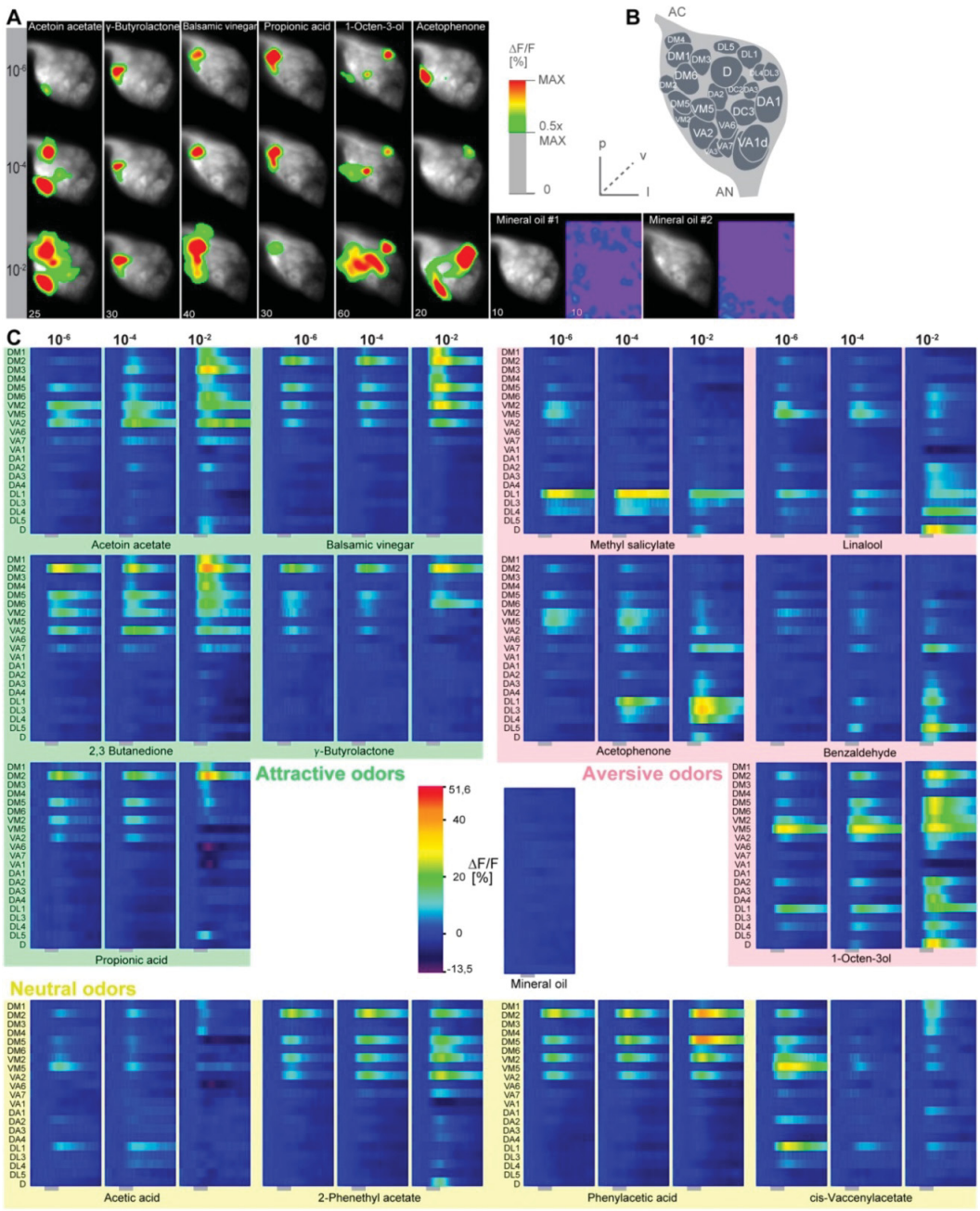

Figure 6—figure supplement 2.**Calcium responses of OSNs.**

(**A**) Representative glomerular Ca^{2+}-responses of OSNs in the AL for a subset of odorants at three concentrations. Scale bar to the right. Control (mineral oil) recordings are shown additionally as full false-color coded images. (**B**) Glomerular AL atlas used for glomerular identification. (**C**) Median Ca^{2+}-activity traces of all glomeruli for all odorants at the three indicated concentrations. Scale bar and control measurement in the center. Odor application is indicated by the grey bar below the heatmaps (n = 6–7).

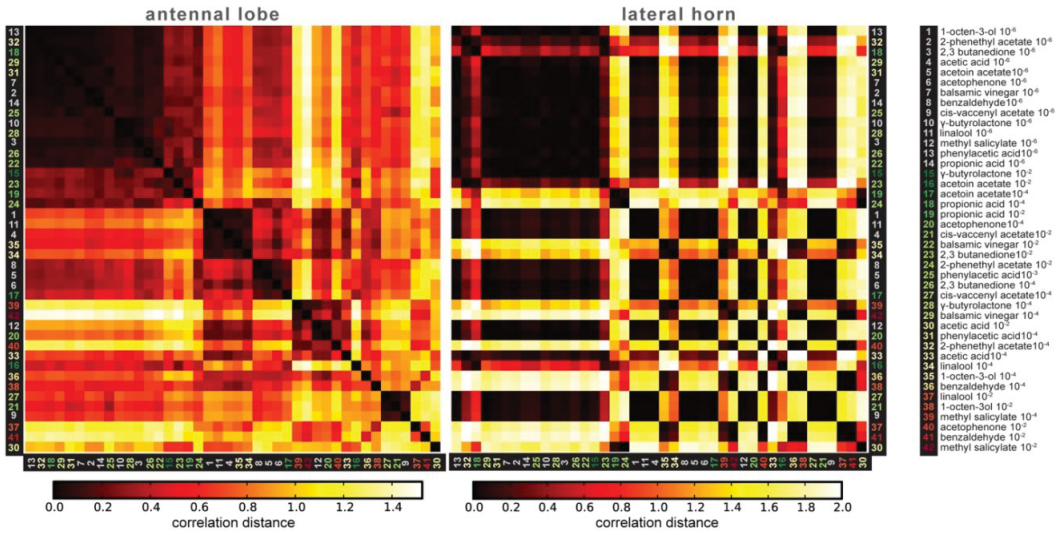

Figure 6—figure supplement 3.**Correlation matrices for odor-evoked responses in the AL and LH.**

Complete correlation matrices for calcium activity patterns of OSNs in the AL (left) and iPNs in the LH (right). The odors are arranged according to single linkage clustering of the AL activity patterns. Heatmap color-code refers to the correlation distance scale bar below each matrix. Odor letters are color-coded according to hedonic valence; 10^{-6} RI values are labeled in grey (complete list right hand).

Manuscript 2

Digital *in vivo* 3D atlas of the antennal lobe of *Drosophila melanogaster*

Veit Grabe, Antonia Strutz, Amelie Baschwitz, Bill S. Hansson, Silke Sachse

The Journal of Comparative Neurology; 523, 530-544.

Published, 15 February 2015 (DOI: 10.1002/cne.23697)

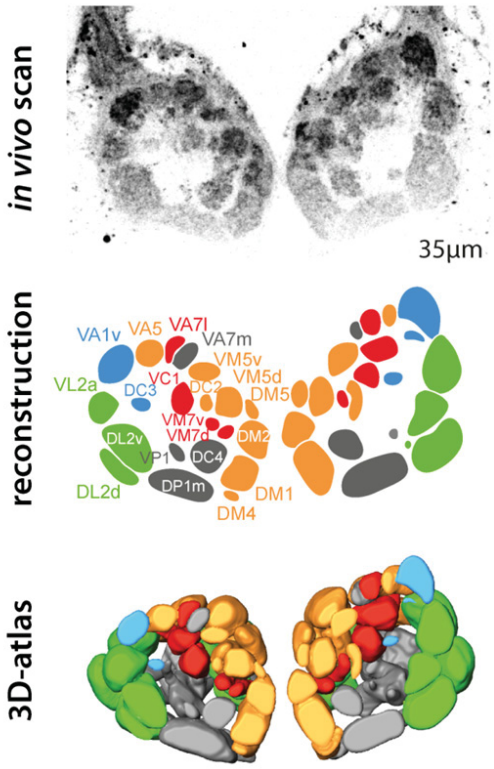

RESEARCH ARTICLE

Digital *In Vivo* 3D Atlas of the Antennal Lobe of *Drosophila melanogaster*

Veit Grabe, Antonia Strutz, Amelie Baschwitz, Bill S. Hansson, and Silke Sachse*

Department of Evolutionary Neuroethology, Max Planck Institute for Chemical Ecology, 07745 Jena, Germany

ABSTRACT

As a model for primary olfactory perception, the antennal lobe (AL) of *Drosophila melanogaster* is among the most thoroughly investigated and well-understood neuronal structures. Most studies investigating the functional properties and neuronal wiring of the AL are conducted *in vivo*, although so far the AL morphology has been mainly analyzed *in vitro*. Identifying the morphological subunits of the AL—the olfactory glomeruli—is usually done using *in vitro* AL atlases. However, the dissection and fixation procedure causes not only strong volumetric but also geometrical modifications; the result is unpredictable dislocation and a distortion of the AL glomeruli between the *in vitro* and *in vivo* brains. Hence, to characterize these artifacts, which are caused by *in vitro* processing, and to reliably identify glomeruli for *in vivo* applications, we generated a transgenic fly that expresses the red fluorescent protein DsRed directly fused to the presynaptic protein *n*-synaptobrevin, under the control of the pan-neuronal promotor elav to label the neuropil in the live animal. Using this fly line, we generated a digital 3D atlas of the live *Drosophila* AL; this atlas, the first of its kind, provides an excellent geometric match for *in vivo* studies. We verified the identity of 63% of AL glomeruli by mapping the projections of 34 GAL4-lines of individual chemosensory receptor genes. Moreover, we characterized the innervation patterns of the two most frequently used GAL4-lines in olfactory research: Orco- and GH146-GAL4. The new *in vivo* AL atlas will be accessible online to the neuroscience community. J. Comp. Neurol. 000:000–000, 2014.

INDEXING TERMS: *Drosophila melanogaster*; olfactory system; glomeruli; *in vivo* neuropil marker; *in vitro* artifacts

The chemical environment consists of a vast and quickly changing array of volatile cues, each of which has different ecological relevance. To orient itself within this complex environment, the vinegar fly *Drosophila melanogaster* possesses an elaborate olfactory system consisting on the periphery of a set of four classes of sensilla present in stereotypical patterns on the third antennal segment and the maxillary palp (Vosshall and Stocker, 2007). Each type of sensillum—antennal basiconic, trichoid, coeloconic, or palp basiconic—houses from one to four olfactory sensory neurons (OSNs). Each OSN expresses a repertoire of one or two chemosensory receptors (CRs); each CR has a unique molecular receptive range (Shanbhag et al., 1999; de Bruyne et al., 2001; Hallem and Carlson, 2006; Silbering et al., 2011). The information gathered on volatile odorants intercepted by the antenna is forwarded to the primary center of the olfactory pathway, the antennal lobe (AL). The *Drosophila* AL represents one of the most comprehensively investigated neuronal structures in nature (Stocker et al., 1990; Masse et al., 2009; Galizia and Sachse, 2010; Hansson et al., 2010; Wilson, 2013). It consists of discrete neuropil subunits, called olfactory glomeruli, which are conserved among individuals and can be identified by their specific position and size (Laissue et al., 1999). Each glomerulus collects OSN axons of only one type due to the strict convergence of OSNs expressing the same CR type (Gao et al., 2000; Vosshall et al., 2000).

In order to study the odor-coding mechanisms of the AL, a broad spectrum of *in vivo* or *ex vivo* techniques, such as the photolesioning of specified tracts (Liang et al., 2013), the photoactivation of single neurons

The first two authors contributed equally to this work.

Grant sponsor: Federal Ministry of Research and Education (BMBF); Grant sponsor: Max Planck Society (MPG).

*CORRESPONDENCE TO: Silke Sachse, Department of Evolutionary Neuroethology, Max Planck Institute for Chemical Ecology, Hans-Knöll-Str. 8, 07745 Jena, Germany. E-mail: ssachse@ice.mpg.de

Received September 4, 2014; Revised October 6, 2014;
Accepted October 14, 2014.
DOI 10.1002/cne.23697
Published online Month 00, 2014 in Wiley Online Library (wileyonlinelibrary.com)

(Datta et al., 2008; Ruta et al., 2010; Caron et al., 2013), patch clamp recordings (Wilson et al., 2004; Chou et al., 2010; Seki et al., 2010), as well as functional imaging (Fiala et al., 2002; Ng et al., 2002; Wang et al., 2003; Silbering et al., 2008; Stökl et al., 2010; Schubert et al., 2014) has been established over the last years. All these techniques demand an adequate atlas for the identification of the anatomical substructures—the glomeruli—so that they can be applied *in vivo*. However, all previous 3D atlases of the *Drosophila* AL have derived from *in vitro* data (Stocker et al., 1983; Laissue et al., 1999; Couto et al., 2005; Endo et al., 2007; Silbering et al., 2011; Tanaka et al., 2012). Since the dissection and fixation procedure causes not only strong volumetric but also geometric modifications (Ma et al., 2008), the result is the unpredictable dislocation and distortion of the AL glomeruli between the *in vitro* and *in vivo* brains. In order to reliably identify glomeruli in the live fly brain, an atlas of the *in vivo* AL is essential.

In this study we present the first digital 3D atlas of the live *Drosophila* AL. To identify glomeruli *in vivo*, we generated a transgenic fly that expresses the red fluorescent protein DsRed directly fused to the presynaptic protein *n*-synaptobrevin, under the control of the panneuronal promotor elav (Yao et al., 1993) to selectively label the neuropil in the live animal. In addition, we expressed a green fluorescent protein under the control of 34 individual chemosensory receptor genes (Couto et al., 2005; Fishilevich and Vosshall, 2005; Silbering et al., 2011) to confirm the correct identification of most glomeruli by its type of OSN innervation. Once quantified and compared to *in vitro* data, the new *in vivo* data were used to demonstrate nontrivial and unexpected structural deformations and distortions of the majority of glomeruli caused by *in vitro* processing. These results support the need for a digital *in vivo* 3D atlas of the fly AL to find geometric matches for *in vivo* studies. Furthermore, we characterized the glomerular innervation patterns of the two most frequently used GAL4-lines in olfactory research: Orco-GAL4 as well as GH146-GAL4. The new *in vivo* 3D AL atlas will be publicly accessible to the neuroscience community through our website (www.ice.mpg.de/ext/invivoALatlas.html).

MATERIALS AND METHODS

Fly lines

P[END1-2] (elav *n*-synaptobrevin-DsRed 1-2) was generated using a modified pCaST-elav-GAL4AD vector (plasmid 15307, Addgene, Cambridge, MA). The GAD domain present in the original vector was excised using NotI and FspAI enzymes; the FspAI recognition site was located within the DsRed coding sequence. A DNA oligonucleotide containing a modified *n*-synaptobrevin-coding ORF (*n*-syb) (DiAntonio et al., 1993), upstream of a sequence identical to the excised DsRed fragment, and a *Drosophila* Kozak site (caaaATG) and recognition sites for NotI and FspAI were synthesized and inserted into the vector. The *n*-syb contains one silent mutation (C168T) to eliminate an FspAI-recognition site within the fragment. Excision, synthesis, and ligation were performed by MWG Eurofins (Ebersberg, Germany). The resulting plasmid was amplified in *E. coli* (One Shot Top10 *E. coli*, Invitrogen, Eugene, OR) and purified using a Qiagen midi-prep kit (Qiagen, Hilden, Germany). Embryo transformation to generate transgenic lines was performed by Aktogen (Cambridge, UK).

All fly stocks were maintained on conventional cornmeal-agar-molasses medium under a 12-hour light: dark cycle at 25°C. Transgenic lines used were as follows: Gr21a-GAL4 (Scott et al., 2001), Ir40a-GAL4 (RRID:BDSC_41727), Ir41a-GAL4 (RRID:BDSC_41749), Ir75a-GAL4 (RRID:BDSC_41748 (Silbering et al., 2011)), Ir76a-GAL4 (RRID:BDSC_41735 (Benton et al., 2009)), Ir92a-GAL4 (RRID:BDSC_41733 (Abuin et al., 2011)), Or10a-GAL4 (RRID:BDSC_9944), Or13a-GAL4 (RRID:BDSC_23886), Or22a-GAL4 (RRID:BDSC_9951), Or33c-GAL4 (RRID:BDSC_9966), Or35a-GAL4 (RRID:BDSC_9968), Or42a-GAL4 (RRID:BDSC_9969), Or42b-GAL4 (RRID:BDSC_9972), Or43a-GAL4 (RRID:BDSC_9973), Or43b-GAL4 (RRID:BDSC_23895), Or46aA-GAL4 (RRID:BDSC_9979), Or47a-GAL4 (RRID:BDSC_9982), Or47b-GAL4 (RRID:BDSC_9984), Or49a-GAL4 (RRID:BDSC_9985), Or56a-GAL4 (RRID:BDSC_23896), Or59b-GAL4 (RRID:BDSC_23897), Or59c-GAL4 (RRID:BDSC_23899), Or67a-GAL4 (RRID:BDSC_23904), Or67c-GAL4 (RRID:BDSC_24856), Or69a-GAL4 (RRID:BDSC_10000), Or71a-GAL4 (RRID:BDSC_23121), Or83c-GAL4 (RRID:BDSC_23132), Or85a-GAL4 (RRID:BDSC_24461), Or85b-GAL4 (RRID:BDSC_23912), Or85d-GAL4 (RRID:BDSC_24148), Or88a-GAL4 (RRID:BDSC_23137), Or92a-GAL4 (RRID:BDSC_23139), Or98a-GAL4 (RRID:BDSC_23141 (Vosshall et al., 2000; Fishilevich and Vosshall, 2005)), Or67d-GAL4 (RRID:BDSC_23906 (Kurtovic et al., 2007)), UAS-GCaMP3.0 (RRID:BDSC_32116 (Tian et al., 2009)), GH146-GAL4 (RRID:BDSC_30026 (Stocker et al., 1997)), Orco-GAL4 (RRID:BDSC_26818 (Larsson et al., 2004)).

In vivo antenna and brain preparation

Between 3 to 6 days after hatching, female flies were anesthetized with CO_2. In order to scan labeled OSN somata on the third segment of the antenna (Fig. 1D), the whole antenna was gently severed using forceps and transferred to a drop of saline with Triton-X on an object holder. The antennae were then gathered

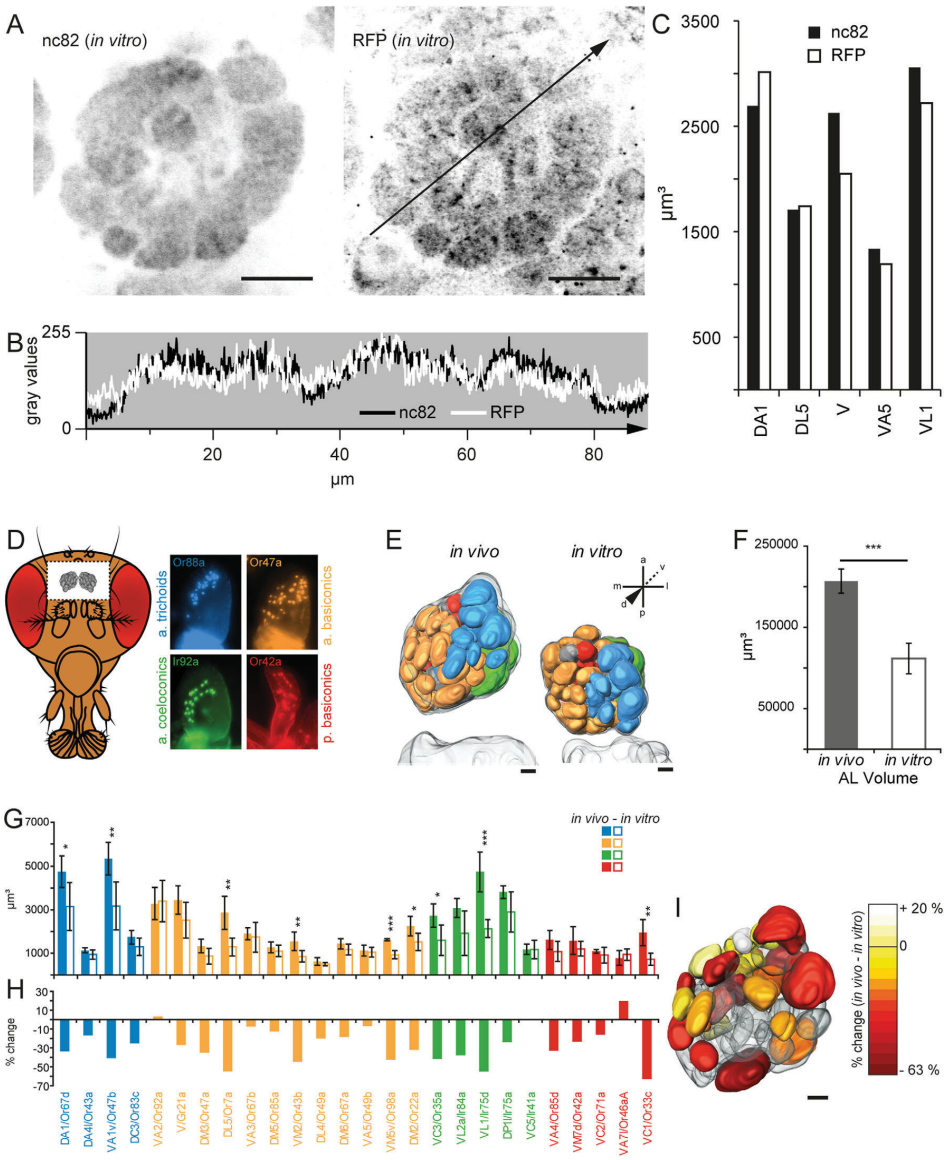

Figure 1. Characterization of volumetric differences between *in vivo* and *in vitro* antennal lobes. **A:** Immuno double staining of an *in vitro Drosophila* antennal lobe (AL) with nc82 (left) and anti-RFP (right) in inverted gray values. Both stainings visualize the glomerular borders in a comparable manner. **B:** Profile of gray values along a transverse line across the AL as shown in (A) of the nc82 (black line) and anti-RFP (white line) double-stained AL. **C:** Volume comparison of a subset of five glomeruli between the nc82 (black) and anti-RFP (white) staining in one animal. **D:** Left, schematic of the head of *D. melanogaster* with a superimposed window depicting the *in vivo* dissection area and position of the ALs. Right, images of the olfactory organs showing the distribution of four sensillum types representative for the different classes of sensilla acquired with specific GAL4 receptor lines (blue: antennal trichoids (Or88a-GAL4 / type: At4), yellow: antennal basiconics (Or47a-GAL4 / type: Ab5), green: antennal coeloconics (Ir92a-GAL4 / type: Ac1), red: palp basiconics (Or42a-GAL4 / type: Pb1)). **E:** Dorsal view on two 3D-reconstructed ALs with individual glomeruli. The left AL derives from an *in vivo* scan of the END1-2 neuropil labeling; the one on the right represents an AL after *in vitro* processing and nc82 antibody staining. The color code denotes the glomerular innervation by the four sensilla classes as shown in (D). **F:** Comparison of the averaged whole AL volume *in vivo* ($n = 4$) and *in vitro* ($n = 7$) based on 3D-reconstructions as shown in (E). Error bars represent SD; $***P < 0.001$, unpaired *t*-test. **G:** Comparison of the glomerulus-specific volume of *in vivo* (filled columns, $n = 4$) and *in vitro* processed ALs (empty columns, $n = 7$) based on 3D-reconstructions as shown in (E). Error bars represent SD; $*P < 0.5$, $**P < 0.1$, $***P < 0.001$, unpaired *t*-test. The color code indicates the classes of sensilla as shown in (D). **H:** Percentage of the glomerulus-specific volume change between the *in vivo* and *in vitro* datasets indicating an unequal fixation effect. **I:** Glomerulus-specific volume changes are heat-mapped onto the reconstructed *in vivo* AL. White represents an increase, yellow no change, and red a decrease in volume. For glomerular identities please see Fig. 5E. Scale bars = 20 µm.

and embedded in VectaShield (Vector Laboratories, Burlingame, CA) between a 22 × 22 mm and a 24 × 60 mm object slide. Scans were carried out with an Axio Imager.Z1 (Carl Zeiss, Jena, Germany) using a 20× water immersion objective (W Plan-Apochromat 20×/0.8, Carl Zeiss) from both sides of each antenna. The *in vivo* fly brain dissection was carried out as previously described (Strutz et al., 2012) in saline (130 mM NaCl, 5 mM KCl, 2 mM $MgCl_2$, 2 mM $CaCl_2$, 36 mM saccharose, and 5 mM Hepes) at pH 7.3 adjusted with 1 M NaOH.

In vitro immunohistochemistry

Female flies aged between 3 to 6 days after hatching were used. Fly brains were dissected and stained as described by Wu and Luo (2006) and scanned with a Zeiss LSM 710 NLO confocal microscope (Carl Zeiss, Jena, Germany) set on a Smart Table UT2 (Newport, Irvine, CA) using a 40× water immersions objective (W Plan-Apochromat 40×/1.0 DIC M27; Carl Zeiss). Primary antibodies were rabbit α-RFP (1:100, Invitrogen, Eugene, OR; Molecular Probes Cat. no. R10367 RRID:AB_2315269) against DsRed and mouse α-nc82 (1:30; Developmental Studies Hybridoma Bank [DSHB], Iowa City, IA; Cat. no. nc82 RRID:AB_528108). All primary antibodies are characterized below. Secondary antibodies were Alexa Fluor 633, goat anti-rabbit IgG (Invitrogen, Eugene, OR, Life Technologies; Cat. no. A21070 RRID:AB_10562894) and Alexa Fluor 488, goat anti-mouse IgG (both 1:250, Invitrogen, Life Technologies Cat. no. A11001 RRID:AB_10566289) (Fig. 1A-C). For the generation of the *in vitro* AL atlas (Fig. 1E), primary antibody was mouse α-nc82 (1:30; DSHB), secondary antibody was Alexa Fluor 488, goat anti-mouse IgG (1:200, Invitrogen). Z-stacks were scanned at 1-µm intervals at 512 × 512 or 1024 × 1024 pixel resolution.

We used monoclonal nc82 raised in a hybridoma screen against fly head homogenate. It was characterized by Daniels et al. (2008) with respect to labeling neuropil compartments in larval and adult *Drosophila*. Polyclonal RFP antibody was raised against full-length recombinant denatured and nondenatured TagRFP and characterized by Marcucci et al. (2011). No immunolabeling was observed with wildtype fly brains (data not shown).

3D reconstruction and identification of glomeruli

Confocal scans were obtained with a ZEISS LSM 710 NLO using a 40× water immersions objective (W Plan-Apochromat 40×/1.0 DIC M27; Carl Zeiss). Individual glomeruli were reconstructed using the segmentation software AMIRA 5.5.0 (FEI Visualization Sciences Group, Burlington, MA; Advanced 3D Visualization and Volume Modeling, RRID:nif-0000-00262). The identification of glomeruli was verified by *in vivo* scans using 34 specific receptor GAL4-lines crossed to UAS-GCaMP3.0 and combined with the END1-2 neuropil labeling. We analyzed scans of at least three specimens for each GAL4 receptor line. Using information on the voxel size from the LSM scans as well as the number of voxels labeled for each neuropil, we calculated the volume of the glomeruli and the whole AL.

We reconstructed *in vivo* ALs including all glomeruli of four female flies and selected one representative AL on the basis of the best signal-to-noise ratio, i.e., the clearest END1-2 staining, as the template for the *in vivo* AL atlas. The other specimens were used as references. All 54 glomeruli that are included in the *in vivo* atlas could be identified unambiguously in all reference specimens. Although our *in vivo* AL atlas derives from a female AL, it can be used as a template for male flies as well, since it has been shown that the glomerular identity is not clearly sexually dimorphic (Laissue et al., 1999). The sexual dimorphism that has been observed so far affects the volume of the three glomeruli DA1, VA1v, and VL2a (Kondoh et al., 2003; Stockinger et al., 2005). These glomeruli are innervated by OSNs that express the male-specific fruitless gene and are larger in males than in females. However, since these studies derive from *in vitro* brain dissections, it still remains to be elucidated whether the described dimorphism holds true for the *in vivo* condition or whether more striking effects will be observed.

Generation of a 3D PDF of the *in vivo* AL atlas followed the described procedure (Ruthensteiner and Heβ, 2008; Rybak et al., 2010). Reconstructed surfaces from AMIRA were imported to FIJI (ImageJ 1.48r, National Institutes of Health, Bethesda, MD; Fiji, RRID:SciRes_000137) and transformed into wavefront format (.obj). Sorting and grouping of the glomerular materials was done in Deep Exploration (5.0.5, Right Hemisphere, San Ramon, CA) saved in u3d-format. Final adjustments of visualization parameters were done in Adobe Acrobat X Pro (Adobe Systems, San Jose, CA).

Statistical analyses

Central coordinates (xyz) for each glomerulus were extracted from the reconstructed specimens' 3D labels via the "MaterialStatistics" tool in AMIRA. Reconstructed ALs were aligned beforehand by inverting corresponding axes, turning all ALs into right ones facing the same direction. Furthermore, distribution along the x-, y-, and z-axes was aligned, i.e., all *in vivo* and *in vitro* ALs were registered in a Cartesian coordinate

system of the same dimensions. The single axes are oriented in mediolateral (x), anteroposterior (y), and dorsoventral (z) directions through the AL. We calculated the minimal and maximal glomerular central coordinates along each axis for each individual AL as well as the average of these minimal and maximal coordinates across all *in vivo* and *in vitro* ALs separately. The difference between the individual and average minimal and maximal values was averaged per specimen, displaying the necessary shift along all three axes for every glomerulus per specimen to align the entire AL. This was done by subtracting the average per axis per specimen from each of its central glomerular coordinates. The same procedure was carried out for the averaged *in vivo* and *in vitro* ALs. Distances between central glomeruli coordinates were calculated as Euclidean distances in the Cartesian coordinate system for the *in vivo* and *in vitro* averaged ALs:

$$ED=\sqrt{(x_2-x_1)^2+(y_2-y_1)^2+(z_2-z_1)^2}$$

To eliminate the impact of the overall shrinkage of the ALs on the relative change, distances were normalized to the maximum distance in the average *in vivo* and *in vitro* AL datasets, respectively. To calculate the position change between a pair of glomeruli from *in vivo* to *in vitro* we placed one of the two glomeruli in the center of the coordinate system ($glom_0$) by subtracting its xyz coordinates from all other glomeruli in all specimens of the *in vivo* and *in vitro* dataset. Then we calculated the cosine of the angle of the position vector between $glom_0$ and another glomerulus *in vivo* ($coor_1$) and *in vitro* ($coor_2$). Based on the cosine we calculated the radian measure of the angle using the arc cosine and multiplied the radian with $180/\pi$, converting it to degree. All analyses were done in Excel.

$$\cos\varphi=\frac{coor_1 * coor_2}{|coor_1| * |coor_2|}$$

$$\cos\varphi=\frac{(x_1 * x_2+y_1 * y_2+z_1 * z_2)}{\sqrt{x_1{}^2+y_1{}^2+z_1{}^2} * \sqrt{x_2{}^2+y_2{}^2+z_2{}^2}}$$

RESULTS

In vivo neuropil labeling

We generated a transgenic fly line that expresses the presynaptic protein *n*-synaptobrevin directly fused to the red fluorescent protein DsRed under the control of the pan-neuronal promotor elav (Yao et al., 1993), subsequently called END1-2. Our *in vivo* END1-2 labeling features a comparable neuropil staining as the most commonly used neuropil-specific monoclonal antibody nc82 *in vitro* (Hofbauer, 1991; Laissue et al., 1999; Rein et al., 2002). In order to show that the END1-2 neuropil labeling correlates with the nc82 antibody staining, we carried out a double *in vitro* immunostaining with anti-RFP against DsRed and nc82 (Fig. 1A). Both antibodies show a distinct but comparable staining of glomeruli. To quantify the distribution of tagged antibodies, we analyzed gray values across the AL. Although the stains are not completely overlapping, in their gray value profiles similar glomerular borders can be seen (Fig. 1B). In addition, staining nc82 and anti-RFP results in similar glomerular volumes as analyzed for a subset of five glomeruli (Fig. 1C).

We next verified that the protein DsRed itself is not influencing the glomerular volume *in vivo*, since it has been shown to oligomerize (Baird et al., 2000). In order to visualize individual glomeruli in flies that are END1-2 negative, we selectively expressed UAS-GCaMP3.0 in Or22a-OSNs. Subsequently, we compared the volume of the respective glomerulus DM2 with and without the expression of END1-2. The results do not reveal any significant difference in volume ($n = 3$, data not shown).

Volumetric fixation effects on the antennal lobe

In order to analyze the effects caused by *in vitro* processing, we first quantified volumetric differences between the *in vivo* and *in vitro* AL morphology. To reduce the preparatory artifacts onto the brain to a minimum, we executed an *in vivo* preparation usually used for functional imaging (Silbering et al., 2012; Strutz et al., 2012). By immobilizing the fly in a Plexiglas stage and opening the head capsule under saline, we were able to remove the tracheal sacks and fat tissue to gain free access to the ALs; during this time, the brain was retained in the head capsule and the antennal nerves remained intact (Fig. 1D). Using the *n*-synaptobrevin::DsRed labeling as a neuropil marker in the live fly, we scanned the brain with the confocal microscope and reconstructed the whole AL, including all glomeruli, *in vivo* (Fig. 1E, left). In parallel, we carried out antibody staining according to Wu and Luo (2006) with the neuropil marker nc82 *in vitro* as well as scanned and reconstructed these *in vitro* ALs using the same procedures as for the *in vivo* data (Fig. 1E, right). In addition, to facilitate the comparison between the *in vivo* and *in vitro* generated datasets, we reconstructed the mushroom body β/β'- and γ lobes as anatomical landmarks. As a quantitative measure, we used the number of voxels in the reconstructed ALs and calculated the total AL volume based on their dimensions (Fig. 1F). A comparison of the *in vivo* and *in vitro* datasets shows that the AL volume decreased by about 43% due to the dissection and fixation procedure. The shrinkage of the whole AL neuropil *in vitro*

would not impair the identification of glomeruli for *in vivo* experiments, if the glomeruli were evenly affected. We therefore quantified and compared the volume of individual glomeruli for the *in vivo* and *in vitro* dataset.

Glomerulus-specific analysis of volumetric differences between *in vivo* and *in vitro* brains

In order to ensure correct glomerulus identification, the END1-2 flies were recombined with UAS-GCaMP3.0 and crossed with 34 receptor GAL4-lines each, i.e., two-thirds of glomeruli were thus labeled according to their corresponding OSN innervation (Couto et al., 2005; Fishilevich and Vosshall, 2005; Silbering et al., 2011). For the detailed quantification of the fixation artifacts, we selected a group of 26 representative glomeruli spanning throughout the AL neuropil and covering different classes of sensilla. Notably, we observed a clear unequal reduction of these glomerular volumes due to fixation (Fig. 1G). Whereas some glomeruli revealed a volume reduction of up to 60% (e.g., VC1) due to *in vitro* processing, other glomeruli shrank by 30% (e.g., DA1) or retained their volume (e.g., VA2) (Fig. 1H). By mapping these glomerulus-specific volumetric effects onto the reconstructed *in vivo* AL, it is obvious that the shrinkage correlates neither with the specific position nor with the total volume of the individual glomeruli (Fig. 1I). Since every glomerulus is shrinking to a different degree, in the next step we analyzed whether the *in vitro* processing caused any geometrical modifications of the glomerular arrangement.

Effect of fixation on the AL geometry

To evaluate possible dislocations of glomeruli following *in vitro* processing (Fig. 2A), we determined Euclidean distances by giving each glomerulus an x, y, and z-coordinate representing its center in the Cartesian system (see Materials and Methods). For each glomerulus, center-to-center distances were calculated in relation to every other glomerulus and subsequently averaged per glomerulus over the *in vivo* and *in vitro* datasets. We then normalized the Euclidean distances to the maximum glomerular distance per dataset and subtracted the normalized *in vivo* distance from the *in vitro* distance. Hence, a negative Δ *Distance* represents the approach of two glomeruli, while a positive Δ *Distance* reveals the increased interglomerular distance due to *in vitro* processing (Fig. 2B). Averaging the positive and negative distance changes per glomerulus over all *in vivo* and *in vitro* specimens, respectively (Fig. 2C, $n = 4$-7), shows various kinds of strong glomerular dislocations; for example, glomeruli VA2 and VM2 increase their distance to most other glomeruli in the *in vitro* dataset, while DL5 and DP1l show the opposite effect. Glomerulus VA1v is affected in both directions, as it ranks highest for an increased as well as decreased interglomerular distance change. Mapping these data onto the reconstructed *in vivo* AL illustrates the spatial distribution of the various effects of glomerular dislocation for the whole AL (Fig. 2D,E). One major reason for the strong geometrical modifications between the *in vivo* and *in vitro* AL is most likely the transection of the antennal nerve, a process in which the brain is extracted from the head capsule. Since the nerve provides tension to the AL, severing it deforms the whole AL neuropil (Fig. 1E).

Even though some glomeruli do not reveal pronounced interglomerular dislocation effects (e.g., DA4l, DM5, and VM7d), we cannot exclude that their position is affected without substantially changing their interglomerular distance. To estimate glomerular distortions independent of their distance, we determined the angle between the two position vectors of each possible glomerular combination for the *in vivo* and *in vitro* datasets (Fig. 2F,G). In order to obtain a glomerulus-specific estimation of the overall angle between *in vivo* and *in vitro* vectors, we calculated the average angle per glomerulus (Fig. 2H). Most glomeruli exhibit an angle above 30°, meaning that the positional arrangement of most glomeruli is considerably affected by the *in vitro* processing. Again, mapping these glomerular distortions on the reconstructed AL (Fig. 2I) reveals that the posterior area is affected strongest. In summary, due to the strong and so far unpredictable fixation artifacts in AL volume and geometry, a digital *in vivo* 3D atlas of the fly AL is essential in order to identify individual glomeruli in *in vivo* studies.

In vivo atlas of the antennal lobe

Previous *in vitro* studies established several AL atlases for *Drosophila* with varying nomenclature and numbers of glomeruli (Stocker et al., 1983; Laissue et al., 1999; Couto et al., 2005; Endo et al., 2007; Silbering et al., 2011). We are referring to the most recent nomenclature from Tanaka et al. (2012), who describe glomerulus VM7 as VM7d and the former unnamed glomerulus "1" (Couto et al., 2005) as its ventral counterpart VM7v. The split of glomerulus VC3 into VC3l and VC3m could not be confirmed at a morphological level, since both parts are innervated by OSNs expressing Or35a (Silbering et al., 2011). We therefore refer to this glomerulus as VC3. Even though no OR is yet known for glomerulus VA7m, we kept the anatomical division in the lateral and medial parts, since the two parts represent different subunits defined by the

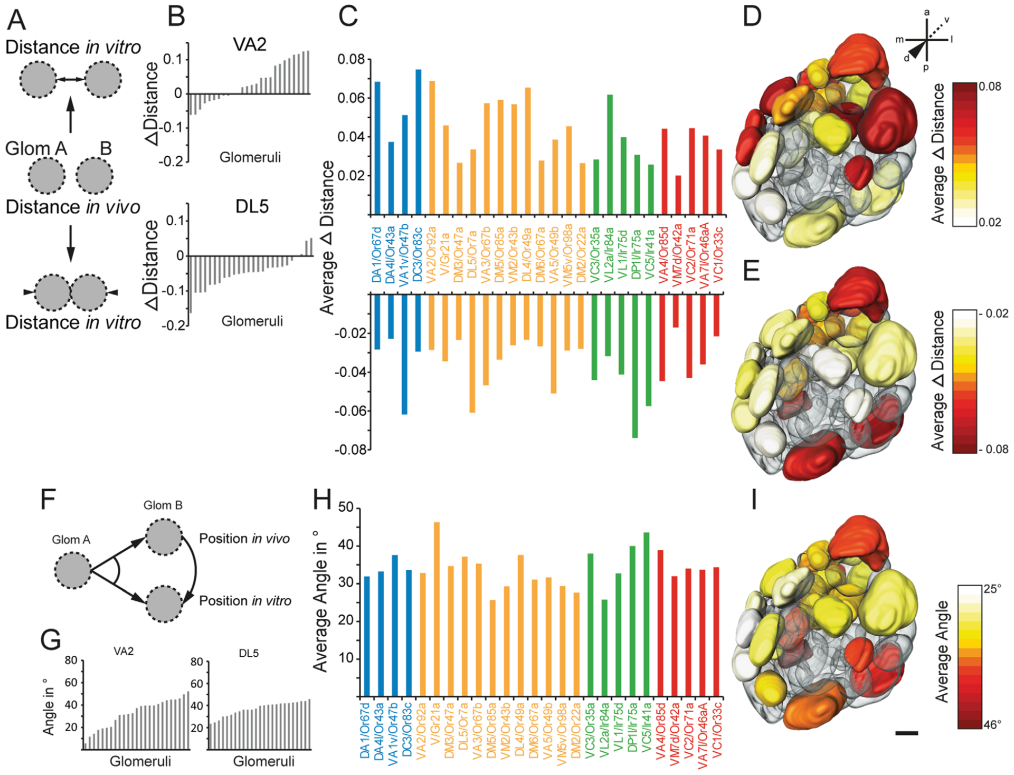

Figure 2. *In vitro* dissection and fixation leads to geometrical modifications of various glomeruli. **A:** Schematic of the investigated Euclidean distance changes between glomeruli as shown in B–E (for details, see Materials and Methods). **B:** Example of normalized center-to-center distance changes (Δ *Distance*) of two representative glomeruli in relation to all other glomeruli between the *in vivo* and *in vitro* dataset. **C:** Averaged positive (top) and negative (bottom) normalized distance changes per glomerulus in relation to all other glomeruli between all *in vivo* ($n = 4$) and *in vitro* specimens ($n = 7$). Positive values indicate an increased interglomerular distance; negative values represent a decrease. Various glomeruli display strong positive and/or negative distance changes underlining nonuniform dislocations of the glomerular arrangement. The color code indicates the classes of sensilla as shown in Figure 1. **D,E:** Positive (top) and negative (bottom) distance changes are heat-mapped onto the reconstructed *in vivo* AL. **F:** Schematic of the investigated angle between two position vectors of each glomerular pair as shown in (G–I). **G:** Example of calculated angles of two representative glomeruli between their positional vectors in relation to all other glomeruli of the *in vivo* and *in vitro* datasets. **H:** Averaged angles between the *in vivo* ($n = 4$) and *in vitro* ($n = 7$) positional vectors for each glomerulus. The positional arrangement of most glomeruli is considerably affected by dissection and *in vitro* processing. **I:** Averaged angles between *in vivo* and *in vitro* positional vectors are heat-mapped onto the reconstructed AL. For glomerular identities please see Fig. 5E. Scale bar = 20 μm.

convergence of OSNs expressing Or46aA to the VA7l part (Couto et al., 2005). Moreover, we fused glomerulus VP1 with glomerulus VM6, since they are morphologically not distinguishable and both are said to share most of their projection neurons (Yu et al., 2010), indicating their uniform nature. In addition, our *in vivo* AL atlas comprises the often neglected glomeruli VP1 and VP4 (Silbering et al., 2011; Kain et al., 2013), although their exact morphology is cryptic without the simultaneous expression of Ir40a-GAL4 that we employed for reliable identification. We also included the thermosensory glomeruli VP2 and VP3 in our AL atlas; these appear as part of the AL rather than as part of the proximal antennal protocerebrum as described previously (Gallio et al., 2011), since their input neurons are ascending along with the OSNs of other glomeruli.

By selectively expressing 34 receptor GAL4-lines combined with GCaMP3.0 into the END1-2 background (see Materials and Methods), we generated a new digital 3D atlas of the *in vivo Drosophila* AL (Fig. 3). First, we selected the most suitable confocal stack out of 13 scans of the END1-2 neuropil labeling (Fig. 3A) as a

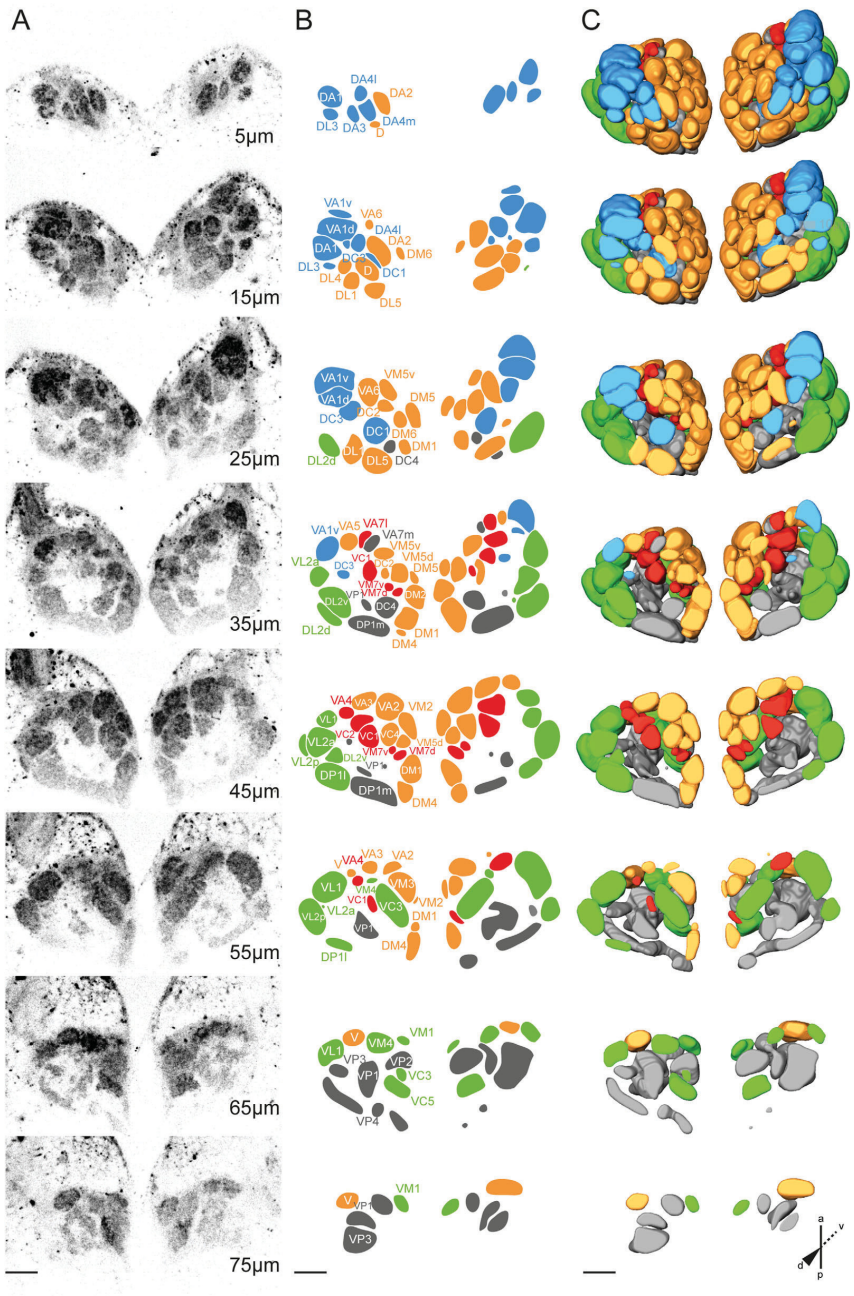

Figure 3. *In vivo* 3D atlas of the *Drosophila* antennal lobe. **A:** Representative confocal stack of an *in vivo* AL expressing the END1–2 neuropil labeling. Eight planes from dorsal to ventral (top to bottom) through a female AL are shown at 10-µm intervals displayed in an inverted gray scale. **B:** Identified and reconstructed glomeruli of the confocal stack shown in (A). **C:** Dorsal view on the 3D-reconstruction of the labels shown in (B). The glomeruli are successively removed as the scan moves from dorsal to ventral through the AL. The color code indicates the classes of sensilla as shown in Figure 1, extended by glomeruli that receive input from the grooved coeloconic sensilla of the sacculus and the aristal shaft (shown in gray). Scale bars = 20 µm.

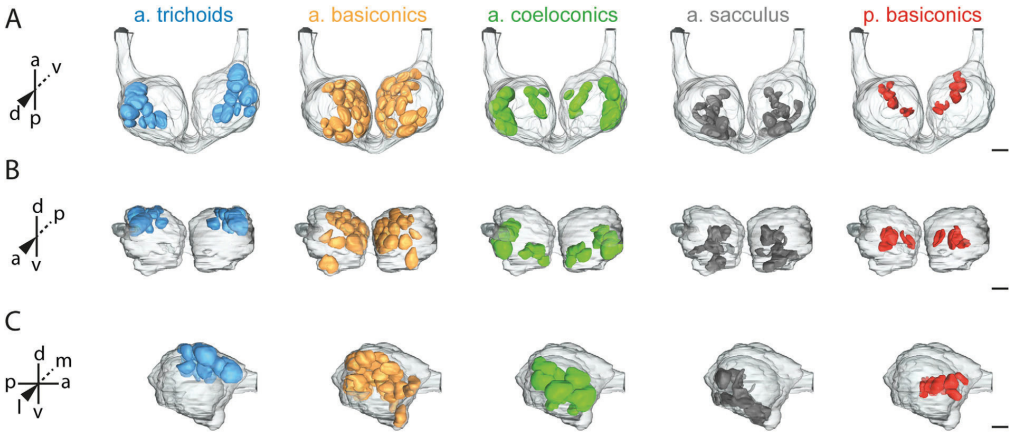

Figure 4. Segregation of the classes of sensilla in the AL. **A–C:** Innervation of glomeruli separately represented for each class of sensillum of the corresponding OSN class in a dorsal (A), frontal (B), and lateral (C) view. The color code refers to Fig. 3. For glomerular identities please see Figure 5E–G. Scale bars = 20 μm.

template for 3D reconstructions, based on the best signal-to-noise ratio throughout the entire scanned distance of ~100 μm. To securely identify the reconstructed glomeruli in the selected stack, in the initial scans we employed specific receptor GAL4-lines for 63% of the AL glomeruli and used the stereotypical OSN innervation patterns and their positions to verify glomerular identity. Based on the precise identification via the receptor GAL4-lines, we morphologically identified the remaining neuropils comprising a total of 54 glomeruli (Fig. 3B). The template scan was then properly reconstructed, improved through the OSN mapping and morphological assignment, and color-coded according to the class of sensilla projecting onto each glomerulus (Fig. 3C). In addition, we performed complete 3D glomerular reconstructions of three further specimens and used them as references. All 54 glomeruli that are included in the *in vivo* AL atlas could be identified unambiguously in all of these reference specimens.

Application of the *in vivo* AL atlas

Our *in vivo* AL atlas represents an accurate match for *in vivo* applications and provides a novel basis for reconsidering neuroanatomical features as exemplified by the glomerular clustering according to the class of sensilla of the OSN input (Couto et al., 2005). The discovery of ionotropic glutamate receptors in insects (IRs) (Benton et al., 2009) underlined this functional and morphological subdivision of the AL and revealed a clear segregation of glomeruli innervated by olfactory receptors (ORs) and IRs (Silbering et al., 2011). Revisiting this feature for the *in vivo* condition, the above-described segregation is present also in the live AL (Fig. 4). In addition, the glomerulus cluster that receives input from coeloconic sensilla can be further divided into two subtypes: Glomeruli that are innervated by OSNs from the sacculus expressing Ir40a and Ir64a (Ai et al., 2010; Silbering et al., 2011) are located separately from glomeruli receiving input from the remaining coeloconic sensilla. This segregation is most obvious in the lateral view of the AL (Fig. 4C), where glomeruli originating in the sacculus and situated most ventroposteriorly are followed in dorsoanterior direction by three layers of glomeruli receiving input from coeloconic, basiconic (antenna and palp), and trichoid sensilla.

As another example, we demonstrate the application of two of the most frequently used GAL4-lines in olfactory research: Orco-GAL4 and GH146-GAL4. The Orco-GAL4 line labels all OSNs that express the coreceptor Orco, formerly known as Or83b (Larsson et al., 2004); the enhancer trap line GH146-GAL4 labels the majority of uniglomerular projection neurons (PNs) in the AL (Stocker et al., 1997). Confocal *in vivo* scans of the Orco-GAL4 line combined with END1-2 and GCaMP3.0 reveal the clear innervation of the majority of glomeruli (39 glomeruli out of 54); the IR-positive glomeruli and the thermosensory center consisting of VP2 and VP3 are not labeled (Fig. 5A,B). The Orco-negative glomeruli group at the ventroposterior region of the AL, as they are congruent with the glomeruli innervated by coeloconic sensilla. Similarly, the innervation of the GH146-GAL4 line labels a total of 39 glomeruli; however, only

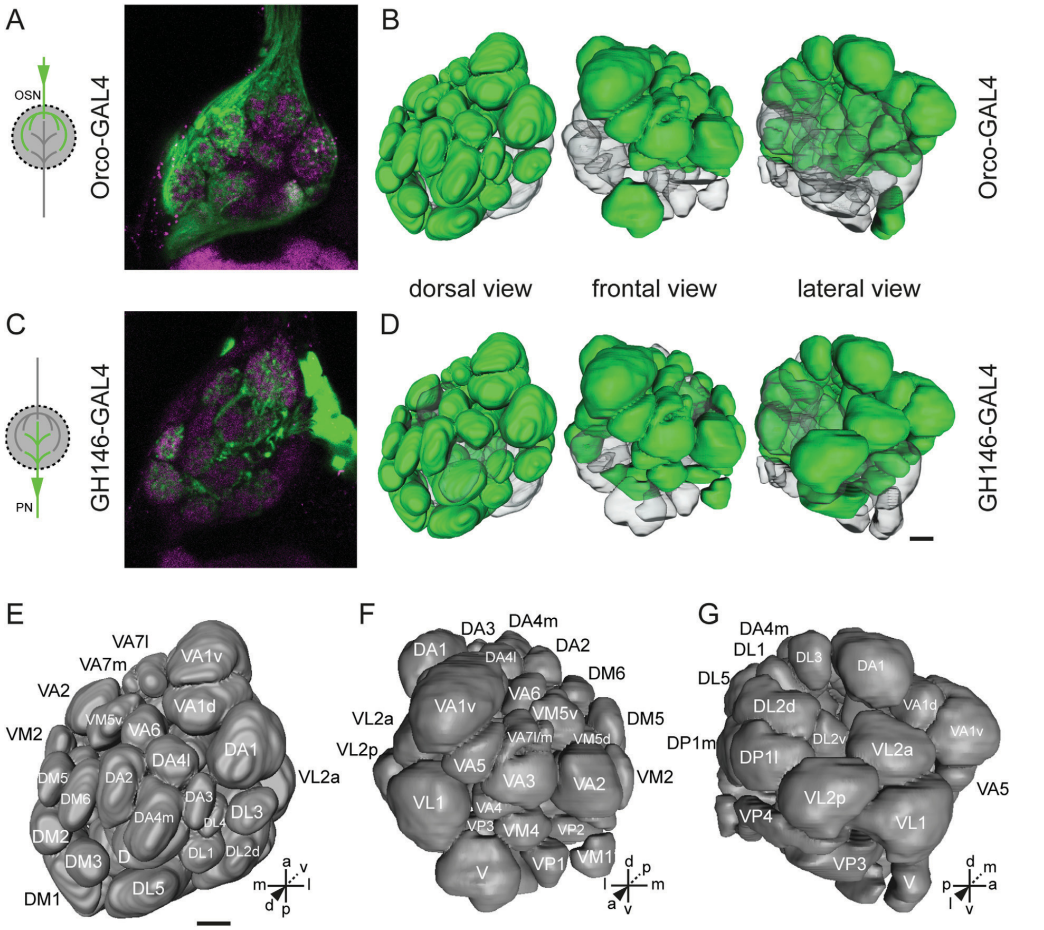

Figure 5. Characterization of the glomerular innervation patterns of two widely used GAL4-lines. **A:** Representative *in vivo* confocal scan of an AL expressing GCaMP3.0 under the control of the Orco promotor (green) combined with the END1–2 neuropil labeling (magenta) at 20 μm depth. The Orco-GAL4 line labels the majority of olfactory sensory neurons as depicted in the schematic on the left side. **B:** Glomerular innervations of the Orco-GAL4 line represented via the *in vivo* 3D AL atlas (green: innervated; transparent: not innervated). Depicted are the dorsal, frontal, and lateral views onto the AL. **C:** Representative *in vivo* confocal scan of an AL expressing GCaMP3.0 under the control of the GH146-GAL4 driver line (green) combined with the END1–2 neuropil labeling (magenta) at 30 μm depth. The GH146-GAL4 line labels the majority of projection neurons as depicted in the schematic on the left side. **D:** Glomerular innervations of the GH146-GAL4 line represented via the *in vivo* 3D AL atlas (green: innervated; transparent: not innervated). Depicted are the dorsal, frontal, and lateral views onto the AL. **E–G:** Complete glomerular assignment of the *in vivo* AL atlas from dorsal (E), frontal (F), and lateral views (G) corresponding to the perspectives in (B) and (D). Scale bars = 20 μm.

32 of which overlap the innervation of Orco-GAL4 (Fig. 5C,D; for glomerular identities, see Fig. 5E-G). Hence, if these two lines are employed simultaneously, functional studies that compare the input and output properties of specific glomeruli should be analyzed with caution. Although GH146-GAL4 is said to label one ventral PN innervating the whole AL (Marin et al., 2002), we were not able to observe any multiglomerular innervation. Due to the sparse glomerular innervation of multiglomerular PNs (Lai et al., 2008), the GCaMP3.0 expression level in this PN, which is below the detection level, can also be ignored for imaging experiments of the whole AL. For a detailed overview, all innervated glomeruli are listed for each GAL4-line in Table 1.

In summary, our *in vivo* AL atlas can be used to reliably identify glomeruli throughout the entire neuropil in

TABLE 1.
Glomeruli Innervated by the Orco-GAL4 and GH146-GAL4 Line

Glomerulus	Receptor type	Sensillum type	Orco-GAL4	GH146-GAL4
D	Or69a	Ab9	■	■
DA1	Or67d	At1	■	■
DA2	Or56a	Ab4	■	■
DA3	Or23a	At2	■	■
DA4l	Or43a	At3	■	■
DA4m	Or2a	At3	■	■
DC1	Or19a	At3	■	■
DC2	Or13a	Ab6	■	■
DC3	Or83c	At2	■	■
DC4	Ir64a	Sac III	■	■
DL1	Or10a	Ab1	■	■
DL2d	Ir75a/b/c	Ac3	■	■
DL2v	Ir75a/b/c	Ac3	■	■
DL3	Or65a	At4	■	■
DL4	Or49a(Or85f)	Ab10	■	■
DL5	Or7a	Ab4	■	■
DM1	Or42b	Ab1	■	■
DM2	Or22a	Ab3	■	■
DM3	Or47a	Ab5	■	■
DM4	Or59b	Ab2	■	■
DM5	Or85a(Or33b)	Ab2	■	■
DM6	Or67a	Ab10	■	■
DP1l	Ir75a	Ac2	■	■
DP1m	Ir64a	Sac III	■	■
V	Gr21a	Ab1	■	■
VA1d	Or88a	At4	■	■
VA1v	Or47b	At4	■	■
VA2	Or92a	Ab1	■	■
VA3	Or67b	Ab9	■	■
VA4	Or85d	Pb3	■	■
VA5	Or49b	Ab6	■	■
VA6	Or82a	Ab5	■	■
VA7l	Or46aA	Pb2	■	■
VA7m	?	?	■	■
VC1	Or33c	Pb2	■	■
VC2	Or71a	Pb1	■	■
VC3	Or35a	Ac3	■	■
VC4	Or67c	Ab7	■	■
VC5	Ir41a	Ac2	■	■
VL1	Ir75d	Ac1/2/4	■	■
VL2a	Ir84a	Ac4	■	■
VL2p	Ir31a	Ac1	■	■
VM1	Ir92a	Ac1	■	■
VM2	Or43b	Ab8	■	■
VM3	Or9a	Ab8	■	■
VM4	Ir76a	Ac4	■	■
VM5d	Or85b	Ab3	■	■
VM5v	Or98a	Ab7	■	■
VM7d	Or42a	Pb1	■	■
VM7v	Or59c	Pb3	■	■
VP1	Ir40a	Sac I	■	■
VP2	hot	Arista	■	■
VP3	cold	Arista	■	■
VP4	Ir40a	Sac I	■	■

These two lines refer to the olfactory sensory neurons and projection neurons, respectively. Black filled cells indicate innervation by the indicated line; white represents no innervation. Ab, antennal basiconic; Ac, antennal coeloconic; At, antennal trichoid; Pb, palp basiconic; Sac, sacculus; Or, olfactory receptor; Ir, ionotropic receptor; Gr, gustatory receptor.

the live fly brain; the atlas preserves the spatial arrangement of individual glomeruli as well as interglomerular differences regarding shape and size.

DISCUSSION

In vivo atlas for enhanced applicability

In this study we used a newly generated transgenic fly line, referred to as the END1-2 line, to provide *in vivo* neuropil labeling of the AL; this label is comparable to the nc82 immunostaining of *in vitro* whole mount brains (Fig. 1A-C) (Hofbauer, 1991; Laissue et al., 1999; Rein et al., 2002). The END1-2 line enables synaptically dense glomerular areas to be separated from synaptically sparse interglomerular areas (Boeckh et al., 1970; Tolbert and Hildebrand, 1981) by the expression of the presynaptic fusion protein *n*-synaptobrevin::DsRed in all neurons. By obtaining confocal stacks of this line and reconstructing individual glomeruli, we generated a 3D map of the AL of *Drosophila melanogaster* that accurately matches the AL in the living fly (Fig. 3). By taking advantage of the near-complete maps of receptor gene expression and OSN targeting (Couto et al., 2005; Fishilevich and Vosshall, 2005; Silbering et al., 2011), we verified the identity of 63% of AL glomeruli using specific receptor-GAL4 lines. This assisted identification allowed us to develop an *in vivo* AL atlas and a way to label neuropils that enables the orientation within and attribution of individual brain regions without *in vitro* processing. In addition, we demonstrate two applications of the new *in vivo* AL atlas by revisiting the segregation of glomeruli innervated by different types of sensilla (Fig. 4) (Couto et al., 2005), as well as by characterizing the glomerular innervation patterns of two of the most crucial GAL4-lines for targeting OSNs and PNs in the fly AL (Fig. 5).

In light of the number of glomeruli published over the last few years, which ranges from 35 (Stocker et al., 1990) to over 43 (Laissue et al., 1999) and up to 56 in current nomenclature (Tanaka et al., 2012), clearly the identification of glomeruli is not trivial. The subdividing of glomeruli, such as DL2, DP1, VA1, VA7, VC3, VL2 (Laissue et al., 1999), DA4, VM5, and VM7 (Couto et al., 2005) and the merging of others, such as VA1l and VA1m, VC3l and VC3m (Couto et al., 2005) as well as the addition of newly defined ones (e.g., VC5; Silbering et al., 2011) outline the challenge of distinguishing reliably between glomeruli. Consider glomerulus VM6, which cannot be distinguished from glomerulus VP1 by plain morphology. We merged the two glomeruli as VP1 since Yu et al. (2010) only observed PNs innervating both structures together via a twin-spot MARCM study. In addition, we were not able to assign glomerulus DL6,

which has been mentioned in two studies (Marin et al., 2005; Yu et al., 2010). However, its limited description to date leads us to assume that this glomerulus has been mislabeled and represents in fact glomerulus DC3. Hence, the new *in vivo* AL atlas of the vinegar fly consists of 54 glomeruli, of which 52 are innervated by chemosensory and two by thermosensory neurons (Gallio et al., 2011).

In vivo compared to *in vitro*

Our idea to create an *in vivo* AL atlas derived from the need to identify glomeruli in functional imaging experiments. Glomerular identification has proven challenging for *in vivo* data with the available *in vitro* atlases. Moreover, since there are not many investigations into the fixation artifacts of flexible neuropils such as the AL, we quantified the volumetric and geometrical modifications, such as shrinkage, dislocation, and distortion following *in vitro* processing. These three substantial effects of fixation on the AL were distributed dissimilarly across the AL neuropil (Figs. 1, 2). First, the heterogeneous shrinkage of glomeruli is most likely due to the different density of intraglomerular arborizations of OSNs, PNs, or LNs (Ignell et al., 2005), which leads to a small volumetric decrease in densely packed glomeruli, while sparsely innervated glomeruli are strongly affected.

Second, the dislocation of glomeruli during fixation affects mainly those glomeruli located anteriorly (VA1v, DA1, VA2) and posteriorly (DL5, DP1l), which reflects a longitudinal distortion of the entire AL neuropil. This global deformation is most likely based on the transection of the antennal nerve, which is required for *in vitro* dissection. In addition, the transection causes general changes in glomerular visibility: Under *in vivo* conditions the anterior glomeruli of the VA cluster are invisible when viewed from a dorsal perspective; they become visible in the surface layer following *in vitro* processing. The opposite effect happens for the posteriorly located glomeruli of the DL and DP clusters, as they are hidden beneath the DA glomeruli in the *in vitro* dissection.

Third, in addition to analyzing the dislocation of several glomeruli, we also investigated distortions regarding the relative positions of glomerular pairs. Again, we observed distortions mainly in glomerular pairs that are located anteriorly and posteriorly, which parallels the dislocation effect seen in individuals; however, the posterior glomeruli are more affected. These deformations highlight the rearrangement of most glomeruli around the ventroposterior basis, where the AL is attached to the protocerebrum. These diverse fixation artifacts emphasize the need for a thorough *in vivo* 3D AL atlas which has an enhanced application for characterizing GAL4 lines combined with the *in vivo* neuropil labeling in single- and multiphoton imaging experiments throughout the whole AL.

In vivo GAL4-line evaluations

As most of the ubiquitous GAL4-lines used for functional imaging studies are characterized by *in vitro* whole-mount brain immunochemistry, their maps suffer from the same issues as the initial identification of glomeruli described above. One can now screen any GAL4 line with the END1-2 neuropil label combined with mCD8-GFP (Lee and Luo, 1999) by maintaining the same conditions as in the actual *in vivo* experiment. END1-2, in contrast to ENG3 (Estes et al., 2000), can also be combined with various green fluorophores (Patterson and Lippincott-Schwartz, 2002; Tian et al., 2009) to visualize the neuropil while live measurements are running. For the characterization of new GAL4-lines labeling the olfactory pathway, we recommend identifying a reliable set of landmark glomeruli (such as DA1, DL5, DM2, VA2, VL1, and VM2) that is evenly spread over the whole AL neuropil.

Advantages and limitations of the new *in vivo* atlas

Our new approach for *in vivo* morphology based on END1-2 neuropil labeling has both advantages and limitations. The new method allowed us to depict the actual volume, distance, and angle artifacts influencing the *in vitro* atlases. The *in vivo* AL atlas does not suffer from those artifacts and its application in *in vivo* experiments is thus easier, especially as it has been generated from a perspective identical to the *in vivo* dissection for functional imaging experiments (Silbering et al., 2012; Strutz et al., 2012). On the other hand, this approach is limited by the age of flies used in the END1-2 staining: By using flies of 3-6 days after hatching, we obtained a clearly stained neuropil. However, stains made with older flies revealed an increasingly indistinct distribution of the DsRed labeling, which interferes with the identification of glomeruli (data not shown). Although we are not completely sure why older flies would have this effect, we assume that it represents a disassembly of the endocytotic recycling process of SNARE complexes (Südhof, 2004; Burgalossi et al., 2010). Disassembling the whole complex could lead to enriched levels of DsRed in the synaptic cleft. Alternatively, the fusion of DsRed to *n*-synaptobrevin might constrain vesicle recycling. Hence, to achieve the most distinct *in vivo* neuropil labeling, the age dependency should be kept in mind.

In summary, the new *in vivo* 3D digital atlas of the *Drosophila* AL represented here provides an invaluable

research tool for fly brain morphology and functional imaging studies. Publicly available and downloadable as a 3D PDF file, the atlas allows the AL or subgroups of glomeruli to be visualized from any angle. In addition, the *in vivo* neuropil labeling can be used to characterize the morphology of novel driver and enhancer trap lines in the commonly used GAL4 (Brand and Perrimon, 1993), LexA (Lai and Lee, 2006), and Q systems (Potter et al., 2010) for broad applications in *Drosophila* neuroscience.

ACKNOWLEDGMENTS

We thank Silke Trautheim and Regina Stieber for excellent technical assistance, Jürgen Rybak for help with the AMIRA software and advice on the article, Christine Miβbach for support regarding the antennal preparations, Michael Thoma for statistical advice, Enrico Garbe and Julia van Beesel for help with the *in vitro* 3D reconstructions, and Emily Wheeler for editorial assistance. Stocks obtained from the Bloomington Drosophila Stock Center (NIH P40OD018537) were used in this study.

CONFLICT OF INTEREST

The authors have no known or potential conflict of interest including any financial, personal, or other relationships with other people or organizations within the years of beginning the submitted work that could inappropriately influence or be perceived to influence the work.

ROLE OF AUTHORS

All authors had full access to all the data in the study and take responsibility for the integrity of the data and the accuracy of the data analysis. Study concept and design: Silke Sachse, Veit Grabe, Antonia Strutz, Bill S. Hansson. Acquisition of data: Veit Grabe, Amelie Baschwitz. Analysis and interpretation of data: Veit Grabe, Silke Sachse. Drafting of the article: Veit Grabe, Silke Sachse. Obtained funding: Silke Sachse, Bill S. Hansson. Material support (generation of GAL4-lines): Antonia Strutz. Critical revision of the article for important intellectual content: all authors. Study supervision: Silke Sachse.

LITERATURE CITED

Abuin L, Bargeton B, Ulbrich MH, Isacoff EY, Kellenberger S, Benton R. 2011. Functional architecture of olfactory ionotropic glutamate receptors. Neuron 69:44-60.

Ai M, Min S, Grosjean Y, Leblanc C, Bell R, Benton R, Suh GSB. 2010. Acid sensing by the Drosophila olfactory system. Nature 468:691-695.

Baird GS, Zacharias DA, Tsien RY. 2000. Biochemistry, mutagenesis, and oligomerization of DsRed, a red fluorescent protein from coral. Proc Natl Acad Sci U S A 97:11984-11989.

Benton R, Vannice KS, Gomez-Diaz C, Vosshall LB. 2009. Variant ionotropic glutamate receptors as chemosensory receptors in Drosophila. Cell 136:149-162.

Boeckh J, Sandri C, Akert K. 1970. Sensory inputs and synaptic connections in the insect CNS. Experimental degeneration in the antennal afferent pathway in the supraesophageal ganglia of flies and cockroaches. Z Zellforsch Mikrosk Anat 103:429-446.

Brand AH, Perrimon N. 1993. Targeted gene expression as a means of altering cell fates and generating dominant phenotypes. Development 118:401-415.

Burgalossi A, Jung S, Meyer G, Jockusch WJ, Jahn O, Taschenberger H, O'Connor VM, Nishiki T-I, Takahashi M, Brose N, Rhee J-S. 2010. SNARE protein recycling by αSNAP and βSNAP supports synaptic vesicle priming. Neuron 68:473-487.

Caron SJC, Ruta V, Abbott LF, Axel R. 2013. Random convergence of olfactory inputs in the Drosophila mushroom body. Nature 497:113-117.

Chou Y-H, Spletter ML, Yaksi E, Leong JCS, Wilson RI, Luo L. 2010. Diversity and wiring variability of olfactory local interneurons in the Drosophila antennal lobe. Nat Neurosci 13:439-449.

Couto A, Alenius M, Dickson BJ. 2005. Molecular, anatomical, and functional organization of the *Drosophila* olfactory system. Curr Biol 15:1535-1547.

Daniels RW, Gelfand MV, Collins CA, DiAntonio A. 2008. Visualizing glutamatergic cell bodies and synapses in Drosophila larval and adult CNS. J Comp Neurol 508:131-152.

Datta SR, Vasconcelos ML, Ruta V, Luo S, Wong A, Demir E, Flores J, Balonze K, Dickson BJ, Axel R. 2008. The Drosophila pheromone cVA activates a sexually dimorphic neural circuit. Nature 452:473-477.

de Bruyne M, Foster K, Carlson JR. 2001. Odor coding in the *Drosophila* antenna. Neuron 30:537-552.

DiAntonio A, Burgess RW, Chin AC, Deitcher DL, Scheller RH, Schwarz TL. 1993. Identification and characterization of Drosophila genes for synaptic vesicle proteins. J Neurosci 13:4924-4935.

Endo K, Aoki T, Yoda Y, Kimura K-i, Hama C. 2007. Notch signal organizes the Drosophila olfactory circuitry by diversifying the sensory neuronal lineages. Nat Neurosci 10: 153-160.

Fiala A, Spall T, Diegelmann S, Eisermann B, Sachse S, Devaud JM, Buchner E, Galizia CG. 2002. Genetically expressed cameleon in *Drosophila melanogaster* is used to visualize olfactory information in projection neurons. Curr Biol 12:1877-1884.

Fishilevich E, Vosshall LB. 2005. Genetic and functional subdivision of the *Drosophila* antennal lobe. Curr Biol 15: 1548-1553.

Galizia CG, Sachse S. 2010. Odor coding in insects. In: Menini A, editor. The neurobiology of olfaction. Boca Raton, FL: CRC Press. p 35-70.

Gallio M, Ofstad TA, Macpherson LJ, Wang JW, Zuker CS. 2011. The coding of temperature in the Drosophila brain. Cell 144:614-624.

Gao Q, Yuan B, Chess A. 2000. Convergent projections of *Drosophila* olfactory neurons to specific glomeruli in the antennal lobe. Nat Neurosci 3:780-785.

Hallem EA, Carlson JR. 2006. Coding of odors by a receptor repertoire. Cell 125:143-160.

Hansson BS, Knaden M, Sachse S, Stensmyr MC, Wicher D. 2010. Towards plant-odor-related olfactory neuroethology in *Drosophila*. Chemoecology 20:51-61.

Hofbauer A. 1991. Eine Bibliothek monoklonaler Antikörrper gegen das Gehirn von *Drosophila melanogaster* [Habilitation thesis]. Würzburg, Germany: University of Würzburg.

Ignell R, Dekker T, Ghaninia M, Hansson BS. 2005. Neuronal architecture of the mosquito deutocerebrum. J Comp Neurol 493:207-240.

Kain P, Boyle SM, Tharadra SK, Guda T, Pham C, Dahanukar A, Ray A. 2013. Odour receptors and neurons for DEET and new insect repellents. Nature 502:507-512.

Kondoh Y, Kaneshiro KY, Kimura K, Yamamoto D. 2003. Evolution of sexual dimorphism in the olfactory brain of Hawaiian *Drosophila*. Proc R Soc Lond B 270:1005-1013.

Kurtovic A, Widmer A, Dickson BJ. 2007. A single class of olfactory neurons mediates behavioural responses to a Drosophila sex pheromone. Nature 446:542-546.

Lai S-L, Lee T. 2006. Genetic mosaic with dual binary transcriptional systems in Drosophila. Nat Neurosci 9:703-709.

Lai S-L, Awasaki T, Ito K, Lee T. 2008. Clonal analysis of Drosophila antennal lobe neurons: diverse neuronal architectures in the lateral neuroblast lineage. Development 135: 2883-2893.

Laissue PP, Reiter C, Hiesinger PR, Halter S, Fischbach KF, Stocker RF. 1999. Three-dimensional reconstruction of the antennal lobe in *Drosophila melanogaster*. J Comp Neurol 405:543-552.

Larsson MC, Domingos AI, Jones WD, Chiappe ME, Amrein H, Vosshall LB. 2004. *Or83b* encodes a broadly expressed odorant receptor essential for *Drosophila* olfaction. Neuron 43:703-714.

Lee T, Luo L. 1999. Mosaic analysis with a repressible cell marker for studies of gene function in neuronal morphogenesis. Neuron 22:451-461.

Liang L, Li Y, Potter CJ, Yizhar O, Deisseroth K, Tsien Richard W, Luo L. 2013. GABAergic projection neurons route selective olfactory inputs to specific higher-order neurons. Neuron 79:917-931.

Ma Y, Smith D, Hof PR, Foerster B, Hamilton S, Blackband SJ, Yu M, Benveniste H. 2008. In vivo 3D digital atlas database of the adult C57BL/6J mouse brain by magnetic resonance microscopy. Front Neuroanat 2:1.

Marcucci F, Maier-Balough E, Zou D-J, Firestein S. 2011. Exuberant growth and synapse formation of olfactory sensory neuron axonal arborizations. J Comp Neurol 519: 3713-3726.

Marin EC, Jefferis GSXE, Komiyama T, Zhu H, Luo L. 2002. Representation of the glomerular olfactory map in the Drosophila brain. Cell 109:243-255.

Marin EC, Watts RJ, Tanaka NK, Ito K, Luo L. 2005. Developmentally programmed remodeling of the Drosophila olfactory circuit. Development 132:725-737.

Masse NY, Turner GC, Jefferis GSXE. 2009. Olfactory information processing in Drosophila. Curr Biol 19:R700-R713.

Ng M, Roorda RD, Lima SQ, Zemelman BV, Morcillo P, Miesenbock G. 2002. Transmission of olfactory information between three populations of neurons in the antennal lobe of the fly. Neuron 36:463-474.

Patterson GH, Lippincott-Schwartz J. 2002. A photoactivatable GFP for selective photolabeling of proteins and cells. Science 297:1873-1877.

Potter CJ, Tasic B, Russler EV, Liang L, Luo L. 2010. The Q system: a repressible binary system for transgene expression, lineage tracing, and mosaic analysis. Cell 141:536-548.

Rein K, Zöckler M, Mader MT, Grübel C, Heisenberg M. 2002. The drosophila standard brain. Curr Biol 12:227-231.

Ruta V, Datta SR, Vasconcelos ML, Freeland J, Looger LL, Axel R. 2010. A dimorphic pheromone circuit in Drosophila from sensory input to descending output. Nature 468: 686-690.

Ruthensteiner B, Heβ M. 2008. Embedding 3D models of biological specimens in PDF publications. Microsc Res Tech 71:778-786.

Rybak J, Kuss A, Hans L, Zachow S, Hege H-C, Lienhard M, Singer J, Neubert K, Menzel R. 2010. The digital bee brain: integrating and managing neurons in a common 3D reference system. Front Syst Neurosci 4.

Schubert M, Hansson BS, Sachse S. 2014. The banana code—natural blend processing in the olfactory circuitry of Drosophila melanogaster. Front Physiol 5:59.

Scott K, Brady R Jr, Cravchik A, Morozov P, Rzhetsky A, Zuker C, Axel R. 2001. A chemosensory gene family encoding candidate gustatory and olfactory receptors in *Drosophila*. Cell 104:661-673.

Seki Y, Rybak J, Wicher D, Sachse S, Hansson BS. 2010. Physiological and morphological characterization of local interneurons in the Drosophila antennal lobe. J Neurophysiol 104:1007-1019.

Shanbhag SR, Muller B, Steinbrecht RA. 1999. Atlas of olfactory organs of *Drosophila melanogaster*. 1. Types, external organization, innervation and distribution of olfactory sensilla. Int J Insect Morphol Embryol 28:377-397.

Silbering AF, Okada R, Ito K, Galizia CG. 2008. Olfactory information processing in the Drosophila antennal lobe: anything goes? J Neurosci 28:13075-13087.

Silbering AF, Rytz R, Grosjean Y, Abuin L, Ramdya P, Jefferis GSXE, Benton R. 2011. Complementary function and integrated wiring of the evolutionarily distinct Drosophila olfactory subsystems. J Neurosci 31:13357-13375.

Silbering AF, Bell R, Galizia CG, Benton R. 2012. Calcium imaging of odor-evoked responses in the Drosophila antennal lobe. JoVE:e2976.

Stocker RF, Singh RN, Schorderet M, Siddiqi O. 1983. Projection patterns of different types of antennal sensilla in the antennal glomeruli of *Drosophila melanogaster*. Cell Tissue Res 232:237-248.

Stocker RF, Lienhard MC, Borst A, Fischbach KF. 1990. Neuronal architecture of the antennal lobe in *Drosophila melanogaster*. Cell Tissue Res 262:9-34.

Stocker RF, Heimbeck G, Gendre N, de Belle JS. 1997. Neuroblast ablation in *Drosophila* P[GAL4] lines reveals origins of olfactory interneurons. J Neurobiol 32:443-456.

Stockinger P, Kvitsiani D, Rotkopf S, Tirian L, Dickson BJ. 2005. Neural circuitry that governs *Drosophila* male courtship behavior. Cell 121:795-807.

Stökl J, Strutz A, Dafni A, Svatos A, Doubsky J, Knaden M, Sachse S, Hansson BS, Stensmyr MC. 2010. A deceptive pollination system targeting drosophilids through olfactory mimicry of yeast. Curr Biol 20:1846-1852.

Strutz A, Voeller T, Riemensperger T, Fiala A, Sachse S. 2012. Calcium imaging of neural activity in the olfactory system of *Drosophila*. In: Martin J-R, editor. Genetically encoded functional indicators. New York: Springer Science+Business Media. p 43-70.

Südhof TC. 2004. The synaptic vesicle cycle. Annu Rev Neurosci 27:509-547.

Tanaka NK, Endo K, Ito K. 2012. Organization of antennal lobe-associated neurons in adult Drosophila melanogaster brain. J Comp Neurol 520:4067-4130.

Tian L, Hires SA, Mao T, Huber D, Chiappe ME, Chalasani SH, Petreanu L, Akerboom J, McKinney SA, Schreiter ER, Bargmann CI, Jayaraman V, Svoboda K, Looger LL. 2009. Imaging neural activity in worms, flies and mice with

improved GCaMP calcium indicators. Nat Meth 6:875-881.

Tolbert LP, Hildebrand JG. 1981. Organization and synaptic ultrastructure of glomeruli in the antennal lobes of the moth Manduca sexta: a study using thin sections and freeze-fracture. Proc R Soc Lond Ser B Biol Sci 213:279-301.

Vosshall LB, Stocker RF. 2007. Molecular architecture of smell and taste in Drosophila. Annu Rev Neurosci 30: 505-533.

Vosshall LB, Wong AM, Axel R. 2000. An olfactory sensory map in the fly brain. Cell 102:147-159.

Wang JW, Wong AM, Flores J, Vosshall LB, Axel R. 2003. Two-photon calcium imaging reveals an odor-evoked map of activity in the fly brain. Cell 112:271-282.

Wilson RI. 2013. Early olfactory processing in Drosophila: mechanisms and principles. Annu Rev Neurosci 36:217-241.

Wilson RI, Turner GC, Laurent G. 2004. Transformation of olfactory representations in the *Drosophila* antennal lobe. Science 303:366-370.

Wu JS, Luo L. 2006. A protocol for dissecting Drosophila melanogaster brains for live imaging or immunostaining. Nat Protocols 1:2110-2115.

Yao K-M, Samson M-L, Reeves R, White K. 1993. Gene elav of Drosophila melanogaster: a prototype for neuronal-specific RNA binding protein gene family that is conserved in flies and humans. J Neurobiol 24:723-739.

Yu H-H, Kao C-F, He Y, Ding P, Kao J-C, Lee T. 2010. A complete developmental sequence of a *Drosophila* neuronal lineage as revealed by twin-spot MARCM. PLoS Biol 8:e1000461.

Manuscript 3

Elucidating the neuronal architecture of olfactory glomeruli in the *Drosophila* antennal lobe

Veit Grabe, Amelie Baschwitz, Hany K.M. Dweck, Sofia Lavista-Llanos, Bill S. Hansson and Silke Sachse

Cell Reports 16, 3401–3413

Published, 20 September 2016 (DOI: 10.1016/j.celrep.2016.08.063)

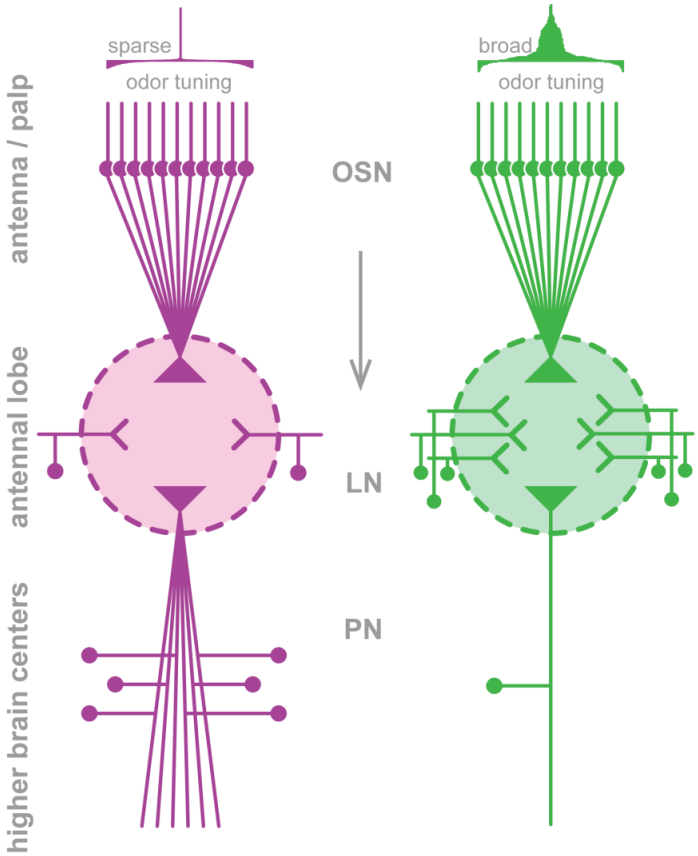

Cell Reports
Resource

OPEN ACCESS
CellPress

Elucidating the Neuronal Architecture of Olfactory Glomeruli in the *Drosophila* Antennal Lobe

Veit Grabe,[1,3] Amelie Baschwitz,[1,3] Hany K.M. Dweck,[1,2] Sofia Lavista-Llanos,[1] Bill S. Hansson,[1] and Silke Sachse[1,4,*]
[1]Department of Evolutionary Neuroethology, Max Planck Institute for Chemical Ecology, Hans-Knöll-Strasse 8, 07745 Jena, Germany
[2]Present address: Department of Molecular, Cellular, and Developmental Biology, Yale University, New Haven, CT 06520, USA
[3]Co-first author
[4]Lead Contact
*Correspondence: ssachse@ice.mpg.de
http://dx.doi.org/10.1016/j.celrep.2016.08.063

SUMMARY

Olfactory glomeruli are morphologically conserved spherical compartments of the olfactory system, distinguishable solely by their chemosensory repertoire, anatomical position, and volume. Little is known, however, about their numerical neuronal composition. We therefore characterized their neuronal architecture and correlated these anatomical features with their functional properties in *Drosophila melanogaster*. We quantitatively mapped all olfactory sensory neurons (OSNs) innervating each glomerulus, including sexually dimorphic distributions. Our data reveal the impact of OSN number on glomerular dimensions and demonstrate yet unknown sex-specific differences in several glomeruli. Moreover, we quantified uniglomerular projection neurons for each glomerulus, which unraveled a glomerulus-specific numerical innervation. Correlation between morphological features and functional specificity showed that glomeruli innervated by narrowly tuned OSNs seem to possess a larger number of projection neurons and are involved in less lateral processing than glomeruli targeted by broadly tuned OSNs. Our study demonstrates that the neuronal architecture of each glomerulus encoding crucial odors is unique.

INTRODUCTION

Species of divergent animal phyla with advanced olfactory systems share an important feature: all develop olfactory glomeruli (Strausfeld and Hildebrand, 1999). During recent decades, the wiring properties of these spherical compartments have been elucidated in great detail in the mammalian olfactory bulb as well as in the insect antennal lobe (AL) (Hansson et al., 2010; Mombaerts, 2006; Vosshall and Stocker, 2007; Wilson, 2013; Wilson and Mainen, 2006). In spite of this, little is known about the numerical neuronal composition of individual glomeruli. Given that different glomeruli do not accomplish uniform tasks, their neuronal architecture should not be homogeneous. Many studies in *Drosophila* provide evidence that each glomerulus represents a specific coding channel determined by the odor response profile of the olfactory receptor expressed by the innervating sensory neuron type (Ai et al., 2010; Dweck et al., 2015; Ebrahim et al., 2015; Hallem and Carlson, 2006; Kreher et al., 2008; Kurtovic et al., 2007; Ronderos et al., 2014; Silbering et al., 2011; Stensmyr et al., 2012; Suh et al., 2004). In order to determine whether each individual glomerulus represents indeed a unique structural coding unit, we characterized the complete neuronal architecture of each individual glomerulus of the *Drosophila* AL. Furthermore, we correlated these anatomical features with their functional properties. We used the genetic model organism *Drosophila melanogaster* because the different neuronal populations of the AL have been anatomically and functionally well characterized (Stocker et al., 1990) and can be selectively labeled and analyzed. In addition, a significant amount of data regarding specific odor-driven behavior has been produced lately (Duménil et al., 2016; Ebrahim et al., 2015; Grosjean et al., 2011; Knaden et al., 2012; Semmelhack and Wang, 2009; Stensmyr et al., 2012).

Olfactory sensory neurons (OSNs), in *Drosophila*, are housed in four different sensillum classes present on the third antennal segment and on the maxillary palp (Shanbhag et al., 1999) (Figures 1A and 1A′). Each OSN expresses one, in some instances two, specific olfactory receptors (Benton et al., 2009; Couto et al., 2005; Fishilevich and Vosshall, 2005). OSNs expressing the same olfactory receptor converge on one of the 52 glomeruli of the AL (Gao et al., 2000; Grabe et al., 2015; Vosshall et al., 2000) (Figure 1A′′). The AL represents the first olfactory center and conveys odor-induced activity patterns via projection neurons (PNs) to the protocerebrum (Vosshall and Stocker, 2007), where the olfactory information is integrated with other sensory modalities. OSNs synapse within each glomerulus of the AL via defined synapse numbers (Mosca and Luo, 2014) with most of the PNs and multiglomerular local interneurons (LNs) (Chou et al., 2010; Rybak et al., 2016; Seki et al., 2010). As mentioned above, several studies have characterized the molecular receptive range of most olfactory receptors and have thus provided us with a nearly complete functional characterization of the odor-tuning properties of OSNs targeting each glomerulus, which are accessible through

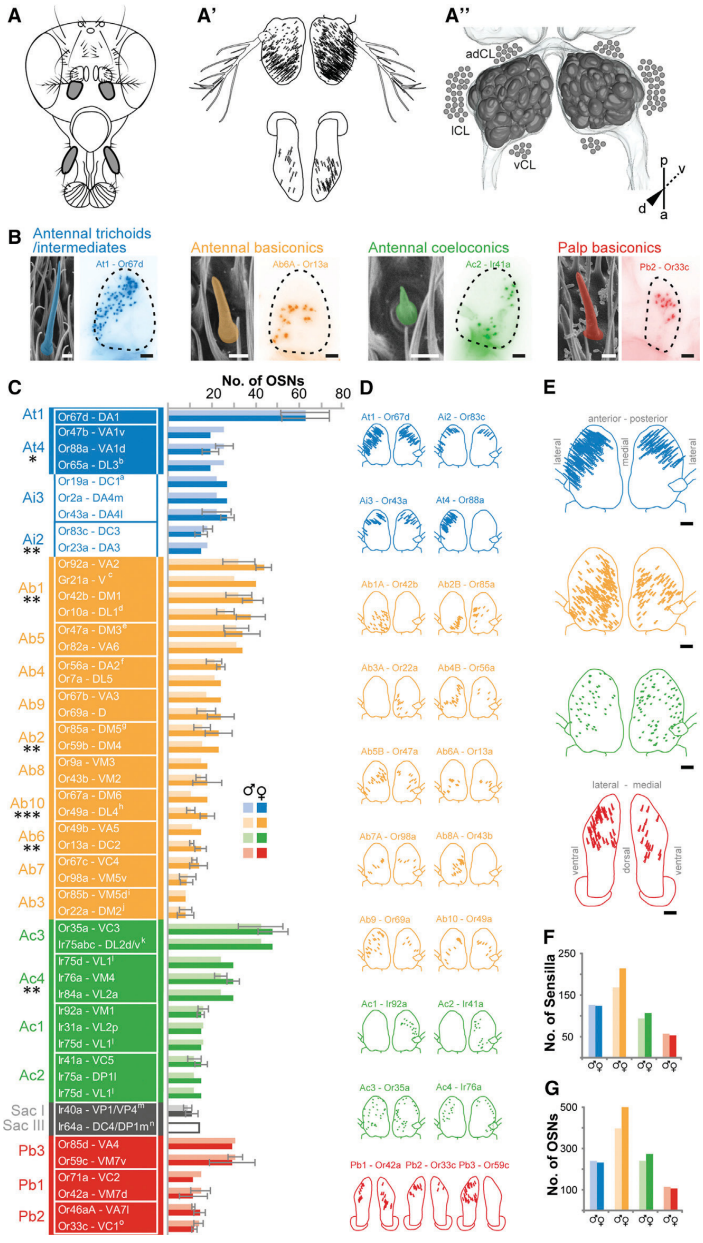

Figure 1. Each Glomerulus Receives Input from a Specific Number of OSNs

(A) Schematic of the *Drosophila* head in frontal view. The third antennal segments and maxillary palps—the major olfactory organs—are highlighted in gray and enlarged in (A′) (same perspective). (A′′) The antennal lobes, primary olfactory center in the brain, in dorsal view, including the three soma clusters (adCL, anterodorsal cluster; ICL, lateral cluster; vCL, ventral cluster).

(B) Electron microscopic scans of each sensillum class (left) and representative olfactory receptor mappings of the four sensillum classes (right). The scale bar in the scanning electron micrographs represents 2 μm; the scale bar in the fluorescence images represents 20 μm.

(C) Number of OSNs for each olfactory receptor and sensillum type. OSN numbers were acquired by quantifying at least one OSN type per sensillum type in males and females (indicated by error bars). Number of OSNs expressing Gr21a represents the mean of all counted Ab1 OSNs. Data represent median ± SD. Statistical differences between sexes were determined by Student's t test (*$p < 0.05$, **$p < 0.01$, ***$p < 0.001$; n = 5–30). Colors indicate the different sensilla classes as shown in (B). Data from males and females are shown by light (male) and dark (female) colors. [a]Coexpressing Or19b; [b]coexpressing Or65b and Or65c; [c]coexpressing Gr63a; [d]coexpressing Gr10a; [e]coexpressing Or33b; [f]coexpressing Or33a; [g]coexpressing Or33b; [h]coexpressing Or85f; [i]coexpressing Or98b; [j]coexpressing Or22b; [k]after Silbering et al. (2011): both parts of DL2 receive putative input from Ir75abc in Ac3; [l]after Silbering et al. (2011): receiving input from Ac1, Ac2 and Ac3; [m]data from Kain et al. (2013); [n]data from Ai et al. (2010); [o]coexpressing Or85e.

(D) Distribution of single sensillum types on the female antenna and palp.

(E) Distribution of all counted sensilla according to class. The scale bar represents 20 μm.

(F) Sex-specific differences of sensillum number per class.

(G) Sex-specific differences of OSN number per sensillum class.

the DoOR database (Galizia et al., 2010). Notably, several of these olfactory receptor types mediate information regarding unique and behaviorally highly relevant odors, such as sexual pheromones (Dweck et al., 2015; Ha and Smith, 2006; Kurtovic et al., 2007), oviposition cues (Dweck et al., 2013) and strongly aversive odors that signal stress (Suh et al., 2004), or unsuitable feeding and breeding sites (Ai et al., 2010; Ebrahim et al., 2015; Stensmyr et al., 2012). Beyond these functional differences, each glomerulus has a unique shape and size (Grabe et al., 2015; Laissue et al., 1999), suggesting that the number and composition of the innervating neurons are specific. This assumption is further supported by recent studies showing a diversified neurotransmitter repertoire in the AL (Busch et al., 2009; Carlsson et al., 2010; Liu and Wilson, 2013), as well as glomerulus-specific differences in the sensitivity to lateral inhibition (Hong and Wilson, 2015).

In the present study, we undertook a complete quantitative mapping of all receptor-specific OSNs and uniglomerular PNs that innervate each glomerulus, including sexually dimorphic distributions and glomerular volumes. By correlating these morphological features with functional properties, we provide evidence for a unique neuronal architecture of glomeruli encoding crucial odors.

RESULTS

Complete Quantitative Mapping of OSN Innervation

Although it has been shown that OSNs expressing a certain olfactory receptor occur in varying numbers, a uniform convergence of about 30:1 OSNs for each glomerulus has so far been assumed (Stocker, 2001; Vosshall and Stocker, 2007). This is because numerical OSN data have been available for only a limited set of olfactory receptor types (Dobritsa et al., 2003; Gao et al., 2000; Sachse et al., 2007). In order to determine the precise input convergence for all glomeruli in the *Drosophila* AL (Figure 1A″), we mapped and quantified the number of OSNs that express a certain olfactory receptor using specific *ORx-/IRx-GAL4* driver lines. In order to validate our methodological approach, we mapped the topographical distribution of sensilla on the antenna and the palp. To achieve this, we selected at least one OSN type per sensillum type, which has been described to be representative (Couto et al., 2005; Silbering et al., 2011) (Figures 1B and 1D). We observed a pattern of distribution of the different sensillum classes that confirmed what was previously found using single-sensillum recordings (de Bruyne et al., 1999, 2001) as well as immunohistochemistry (Fishilevich and Vosshall, 2005; Silbering et al., 2011). Moreover, our observed patterns of OSN types corresponds well with in situ hybridization data for specific OR and IR genes (Benton et al., 2009; Vosshall et al., 2000), confirming that our approach of labeling OSN types is reliable. Finally, our total numbers of the different sensillum classes for the antenna and the maxillary palps (Figures 1F and 1G) match well published data as further described below (de Bruyne et al., 2001; Shanbhag et al., 1999; Stocker, 2001).

In general, the basiconic sensilla were located almost everywhere on the third antennal segment, with higher density in the anterior proximal region; none were present at the distal tip (Figure 1E). The trichoid sensilla were located more distally, including the two intermediate types Ai2 and Ai3 (Dweck et al., 2013), which we still assigned to the trichoid sensillum group for simplicity. Coeloconic sensilla were evenly distributed with higher density at the posterior side. The basiconic sensilla on the maxillary palp were also evenly spread at the distal region of this appendage.

Next, we quantified the number of OSNs expressing each olfactory receptor type by counting at least one type per sensillum in males and females (Figure 1C; Table S1). For the number of sensory neurons in the different sacculus chambers (i.e., invaginations in the third antennal segment), we consulted recent studies (Ai et al., 2010; Kain et al., 2013). The remaining sensilla represent poreless hygro- or thermosensors (Gallio et al., 2011; Shanbhag et al., 1995) and were not included in our study. We observed OSN numbers ranging from 10 up to 65 per functional sensillum type; as an extreme example, Or67d, housed in the At4 sensillum, was expressed in the largest number of OSNs. As expected, the male antenna exhibited significantly more At4 sensilla than the female, because these sensilla house fruitless-positive OSNs and are involved in courtship behavior (Dweck et al., 2015; Kurtovic et al., 2007; Stockinger et al., 2005). Several other sensillum types, all of which were *fruitless* negative, were also present in sexually dimorphic numbers, occurring significantly more frequently in females than in males (Ab1, Ab2, Ab6, Ab10, and Ac4) or vice versa (Ai2; Figure 1C). Regarding the number of OSNs on the maxillary palps, we did not observe a clear sexual dimorphism, confirming previous studies (Stocker, 2001). Finally when we determined the total count of OSNs and sensilla on the antenna and the palp (Figures 1F and 1G), we observed that males had marginally more trichoid sensilla than females, while basiconic and coeloconic sensilla occured more frequently in females, as described earlier (Stocker, 2001).

We found a total of 417 ± 89 (average ± SD) sensilla per antenna and 57 ± 14 sensilla per palp housing 945 ± 201 and 113 ± 28 OSNs, respectively. These numbers are in line with former studies counting approximately 440 sensilla on the antenna and 60 on the palps, which house about 1,150 and 120 OSNs, respectively (Stocker, 2001). In order to verify whether our quantification with specific *ORx-/IRx-GAL4* lines is comprehensive, we labeled all OSNs on the maxillary palp by expressing the nuclear marker nls-GFP using the *Orco-Gal4* driver line (Larsson et al., 2004), as well as all coeloconic sensilla on the antenna via the *Ir8a-GAL4* line (Silbering et al., 2011). We counted 100 ± 4 (average ± SD) Orco-expressing OSNs on the maxillary palp and 130 ± 21 Ir8a-expressing OSNs on the antenna (n = 3–7 female flies). These numbers match reasonably well our specific quantifications for female flies, which resulted in 108 ± 19 OSNs on the palp and 107 ± 14 coeloconic sensilla on the antenna and confirms the reliability of our quantitative approach. Unfortunately, we could not reliably quantify the number of Orco-expressing OSNs on the antenna, becasue Orco is heterogeneously expressed in the different sensilla classes with high expression levels in the basiconic sensilla and low levels in the trichoids (Benton et al., 2006; Larsson et al., 2004). Because the maxillary palp has only basiconic sensilla, Orco is homogeneously expressed in all OSNs on this olfactory organ and could be used for reliable quantification.

The Number of OSNs Likely Determines Glomerular Volume

We next analyzed whether the number of olfactory input neurons correlates with the glomerular volume, as has been recently shown for a subset of glomeruli in the mouse olfactory bulb (Bressel et al., 2016). We therefore extended our previously published volumetric data set and obtained in vivo volume measurements for all glomeruli in males and females using the in vivo neuropil labeling via END1-2 (Grabe et al., 2015) (Figures 2A and 2E; Table S1; see Experimental Procedures for details). In order to adjust for inter-individual variability and sex-specific differences (Figure 2B), we compared the glomerular volume relative to the size of the summed glomerular volume per animal. We observed, for example, that glomeruli that receive input from trichoid sensilla account for about 20% or 25% of the complete AL

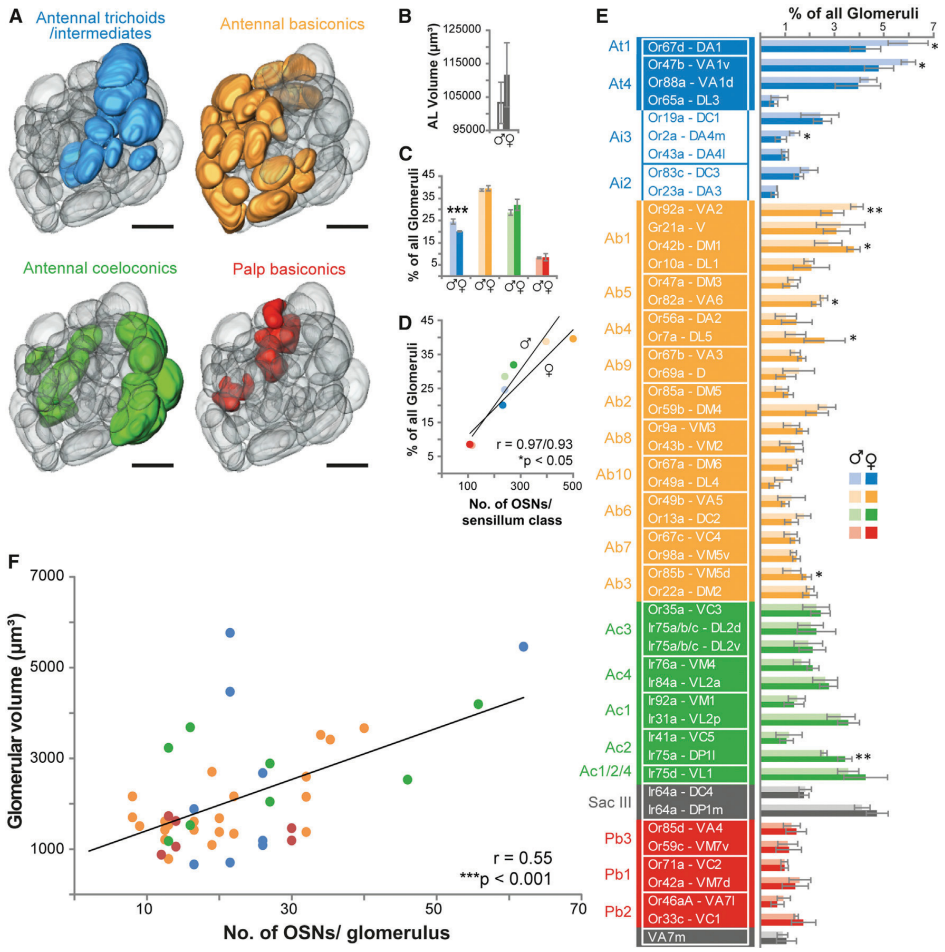

Figure 2. In Vivo Glomerular Volume Is Likely Determined by OSN Number

(A) Three-dimensional reconstructed ALs representing glomeruli separately for each class of sensillum of the corresponding OSN class. The scale bar represents 20 µm.

(B) Entire AL volume of males (empty column) and females (filled column). Data represent median ± SD.

(C) Percentage of AL volume of glomeruli innervated by each sensillum class separately in males and females. The colors indicate the sensillum classes as shown in Figure 1B. Data from males and females are indicated by light (male) and dark (female) colors. Statistical differences between sexes were determined by Student's t test (***p < 0.001).

(D) Correlation of OSN number per sensillum class and the respective glomerular volume for males and females (*p < 0.05, two-tailed probability of the Pearson correlation coefficient).

(E) Glomerulus-specific volumes shown as percentages of all labeled glomeruli per specimen. Data in (B), (C), and (E) represent median ± SD. Statistical differences between sexes were determined by Student's t test (*p < 0.05, **p < 0.01, ***p < 0.001; n = 4 for males and females each).

(F) Correlation of glomerular volume and OSN number (***p < 0.001, two-tailed probability of the Pearson correlation coefficient).

The color code refers to Figure 1B.

volume in females or males, respectively (Figure 2C). This volumetric proportion corresponds well to the proportion of OSNs expressing olfactory receptors housed in trichoid sensilla (23% in females and 26% in males). Extending this comparison to the remaining classes of sensilla, we observed a significant but shallow correlation between glomerular volume and OSN number (Figure 2D) that was also evident when we considered each glomerulus separately (Figure 2F). Hence, our data indicate

that the number of OSNs plays a role in determining glomerular volume.

Because we observed sex-specific differences for some OSN types, we wondered whether these differences become evident also in the volume of the target glomerulus. Sexual dimorphism in glomerular volume has so far been studied only for glomeruli that are involved in pheromone processing; glomeruli DA1 and VA1v, which encode the sexual pheromones *cis*-vaccenyl acetate and methyl laurate (Dweck et al., 2015; Kurtovic et al., 2007), are significantly larger in males than in females (Kondoh et al., 2003). Our volume measurements confirmed this finding and extended the list by several other glomeruli. Notably, we also observed gender-specific differences in glomeruli DA4m, VA2, and VA6, all of which are larger in males than in females, as well as in glomeruli DM1, DL5, DP1l, and VM5d, being larger in females than in males (Figure 2E; Table S1). For glomeruli VA1v and DM1, we also observed a dimorphic OSN quantity (Figure 1C). However, a sex-specific difference in glomerular volume was not always linked to a sex-specific difference in number of OSNs, implying that sensory input is the major, but not the only determinant of glomerular volume.

The Number of Excitatory Output Neurons Is Glomerulus Specific

Having shown that each glomerulus is targeted by a specific number of OSNs and that this number is correlated to the glomerular volume, we next asked whether each glomerulus is also innervated by a glomerulus-specific number of PNs. To quantify the number of output neurons for each glomerulus, we focused on uniglomerular, excitatory PNs by expressing photoactivatable GFP (Patterson and Lippincott-Schwartz, 2002) under the control of the enhancer trap line *GH146-GAL4* (Stocker et al., 1997) (Figure 3A). This line is described to label about 66% of total PNs (Stocker et al., 1997); these PNs project mainly via the medial AL tract (Ito et al., 2014) to the mushroom body calyx and farther, to the lateral horn (LH). A small proportion projects via the lateral AL tract to the LH and farther to the mushroom body calyx. Most GH146-positive PNs (i.e., 94%) are cholinergic (Shang et al., 2007). We applied repeated photoactivation of each labeled glomerulus in a minimum of three animals to gain a reliable estimate of the variability. When we quantified the excitatory output of all glomeruli that are labeled by *GH146-GAL4*, we observed two classes of glomeruli: the majority (i.e., 83%) is innervated by on average 2 ± 1 uniglomerular PNs, while the remaining glomeruli, which comprise glomeruli D, DA1, DA2, DC3, DL3, and VA1v, are innervated by on average 6 ± 2 PNs (Figure 3B; Table S1). Furthermore, we assigned each individual PN soma to the dorsomedial, lateral, or ventral cell cluster, revealing that a few glomeruli are innervated by PNs originating from more than one cluster, as described previously (Marin et al., 2002) (Table S2).

Infrequently, we also labeled one multiglomerular PN following photoactivation of some glomeruli. This PN belongs to the vPN group and it is described to innervate the entire AL (Marin et al., 2002). Possibly we do not label this vPN reliably because of its described sparse innervation in single glomeruli. Because we focused our study on uniglomerular PNs, we excluded this vPN from our quantification.

Since the *GH146-GAL4* line does not cover all uniglomerular and excitatory PNs in the AL (Lai et al., 2008), we might have underestimated the number of PNs per glomerulus. We therefore attempted to label all AL neurons by expressing photoactivatable GFP under the control of the pan-neuronal driver *elav*. However, because the cell bodies of PNs and LNs are located in the same cell clusters, labeled cell bodies could not be unambiguously assigned to PNs (data not shown). We therefore chose a different approach and quantified the number of all cholinergic uniglomerular PNs per glomerulus using the *ChA-GAL4* driver line (Salvaterra and Kitamoto, 2001) (Figure S1A). For this purpose, we photoactivated PNs in 28 glomeruli which were characterized either by being sparsely or densely innervated or by being GH146-negative (Grabe et al., 2015) (Figure S1B). Our analysis of all cholinergic PNs confirmed that our quantification of PNs per glomerulus was largely correct, except in six cases: we labeled one to three more uniglomerular PNs in the anterodorsal and lateral cell clusters in glomeruli VA1v, DA2, D, DM5, VM2, and DM6 using the enhancer trap line *GH146-GAL4* than we labeled using the *ChA-GAL4* line.

Interestingly, when we correlated glomerulus-specific PN quantities to the glomerular volume, a weak, but significant, correlation was visible (Figure 3C). Hence, uniglomerular PNs do have an impact on glomerular volume, although they have less impact than do the input neurons.

LN Innervation Is Lowest in Glomeruli Innervated by Trichoids

The remaining major neuronal population in the AL is represented by inhibitory and excitatory LNs. In order to quantify the glomerular innervation by LNs, we integrated a data set from Chou et al. (2010), in which most LNs had been thoroughly characterized with regard to their innervation frequency at the individual glomerular level, with our data. First, we analyzed the frequency of LN innervation related to each sensillum class (Figure 4A). Glomeruli innervated by OSNs housed in basiconic sensilla on the antenna or the palp or in coeloconic sensilla show a high LN innervation density of on average 83%, 87%, or 85%, respectively. Notably, glomeruli with OSN input from trichoid sensilla display a significantly lower LN innervation density, on average, 77% ($p < 0.05$, ANOVA followed by Tukey-Kramer multiple-comparisons test). Hence, glomerular innervation by LNs is not evenly distributed across the different sensillum types and might reflect a functional classification. Next, we analyzed whether the number of LNs contributes to the glomerular volume as observed for the OSNs and PNs, but we could not find any significant correlation (Figure 4B). Additionally, we did not observe any correlation between the LN density and the number of OSNs per glomerulus (Figure 4C). Instead, and interestingly, we found a significant negative correlation between LN density and the number of PNs (Figure 4D), indicating that glomeruli innervated by a high number of PNs receive a small number of LN dendrites.

Lifetime Sparseness Allows Linking Morphology to Function

Having quantified the three main neuronal populations for each glomerulus, we wondered whether the neuronal composition is

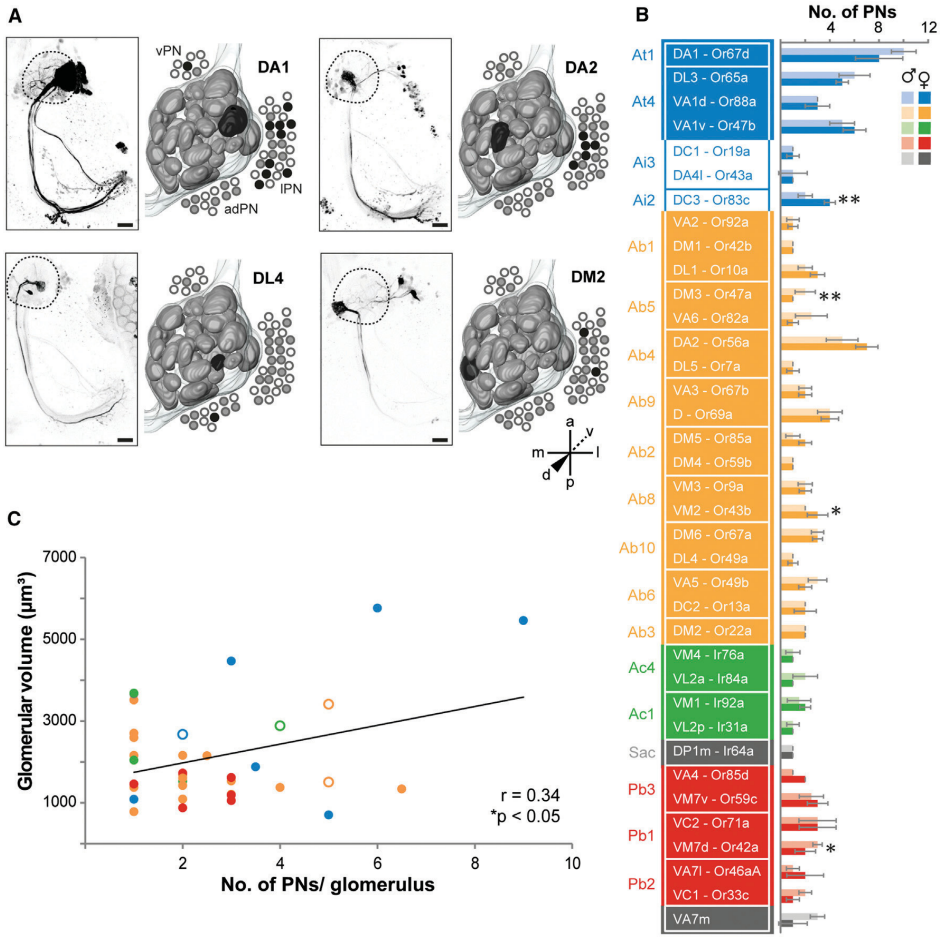

Figure 3. Number of Uniglomerular PNs per Glomerulus Is Specific

(A) Z projections of four different scans of brains expressing photoactivatable GFP in GH146-positive PNs after photoactivation of a specific glomerulus (DA1, DA2, DL4, and DM2). adPN, anterodorsal PN soma cluster; lPN, lateral PN soma cluster; vPN, ventral PN soma cluster. The scale bars represent 20 µm.

(B) Number of innervating PNs per glomerulus labeled with *GH146-GAL4;UAS-C3PA*. Data represent median ± SD. Statistical differences between sexes were determined by Student's t test (*p < 0.05, **p < 0.01; n = 3–10).

(C) Correlation of glomerular volume and PN number. Empty circles represent *ChA-GAL4;UAS-C3PA* based data (as shown in Figure S1). *p < 0.05 (two-tailed probability of the Pearson correlation coefficient).

The color code refers to Figure 1B.

reflected by the odor-tuning properties of each glomerulus. To quantify the selectivity of the response profile of a certain glomerulus, we calculated the lifetime sparseness of the olfactory receptor expressed in the OSNs innervating it (Bhandawat et al., 2007; Perez-Orive et al., 2002; Vinje and Gallant, 2000). We used the DoOR database (Galizia et al., 2010) for olfactory receptors that have been well characterized with an adequate odor set. However, several olfactory receptors have so far been tested only with a limited number of odors. In order to obtain a precise lifetime sparseness for all olfactory receptors, we extended the odor-tuning profile of 11 olfactory receptors via single-sensillum recordings (SSRs) by applying an odor set ranging from 37–474 different odors (Figure 5A; Table S3). By using our data set in addition to the odor response profiles that have already been published, we calculated the lifetime sparseness for each olfactory receptor, that is, for its corresponding glomerulus (Figure 5B; Table S1). Next, we correlated this measure to the glomerulus-specific numbers of the three main

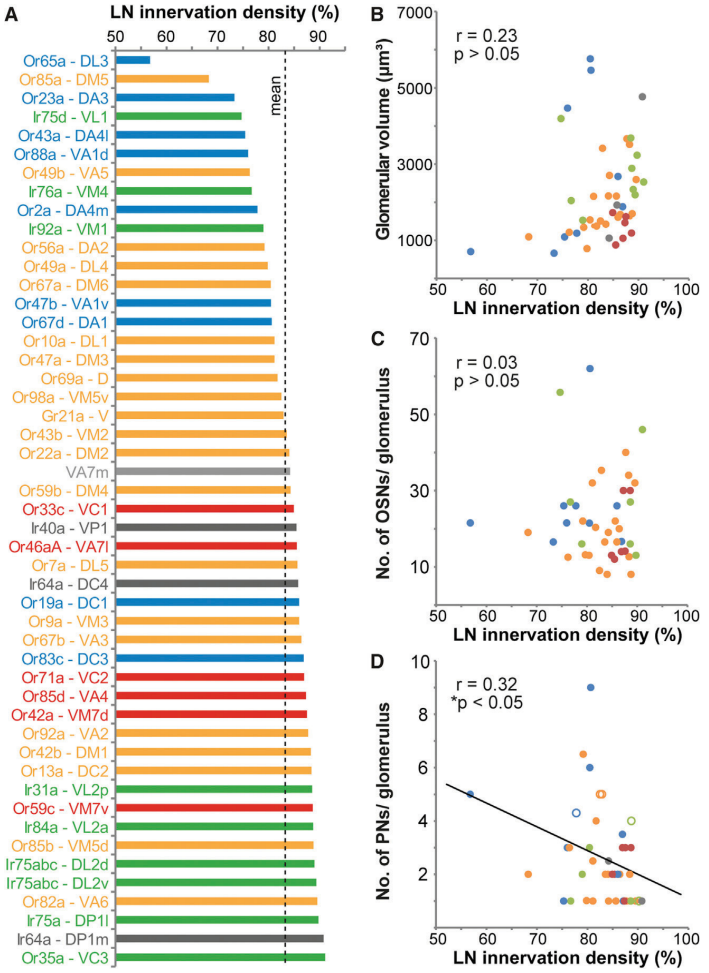

Figure 4. LN Innervation Density Is Negatively Correlated with PN Number

(A) Data set of the glomerulus-specific LN innervation frequency acquired via MARCM of several LN GAL4-Lines (data from Chou et al., 2010).

(B–D) Scatterplots representing the correlation of LN frequency with glomerular volume (B), OSN number (C), and PN number (D). *p < 0.05, two-tailed probability of the Pearson correlation coefficient.

The color code refers to Figure 1B.

neuronal populations in the AL. Although the number of OSNs does not show any correlation, we found a shallow, but significant, positive correlation with the number of PNs and a negative correlation to the LN innervation density (Figure 5C). However, because the number of PNs per glomerulus is not really continuous, the relationship between PN number and lifetime sparseness should be rather defined as two classes of glomeruli, implying that those glomeruli that have the highest sparseness seem to be innervated by more PNs than those glomeruli having a low sparseness. Hence the selectivity of a glomerulus seems to be represented not by the number of sensory input neurons innervating it but rather by the number of second-order neurons: glomeruli that are innervated by OSNs expressing a narrowly tuned olfactory receptor seem to have a higher number of PNs and are less frequently innervated by LNs, suggesting that these glomeruli perform less lateral processing. In summary, our data demonstrate that the neuronal composition of each glomerulus is specific and seems to reflect its odor-tuning profile.

DISCUSSION

Here we quantified the major neuronal populations for each individual glomerulus in the *Drosophila* AL. Using the functional characterization of a variety of olfactory receptors, our study demonstrates a correlation between functional specification and neuronal architecture. In recent decades, several neuroanatomical studies have investigated the pheromone system of several insect species; each study links a striking morphology to a specific function (Boeckh and Tolbert, 1993; Galizia et al., 1999; Hansson et al., 1992; Schneiderman et al., 1986). These studies provided evidence that the size of a glomerulus reflects its behavioral relevance. In addition, the volume of particular glomeruli in different drosophilids has been shown to be related to sensory specialization (Dekker et al., 2006; Linz et al., 2013). An enlargement in glomerular volume is correlated with either an increased number of total OSNs (Bressel et al., 2016) or an increase in their synapse number (Acebes and Ferrús, 2001). Indeed, recent ultrastructural studies have revealed that each OSN contributes an equal but specific number of synapses to a glomerulus (Mosca and Luo, 2014). In addition, it has long been known that different glomeruli receive input from various OSN numbers (de Bruyne et al., 2001; Shanbhag et al., 1999). However, the exact number of OSNs has been published only for very few olfactory receptor types so far (Dobritsa et al., 2003; Gao et al., 2000; Sachse et al., 2007). Our comprehensive OSN quantification shows that the volume of each glomerulus is most likely dictated by the number of OSNs and confirms a recent study in mice (Bressel et al., 2016). In addition, our data provide evidence that glomerular volume is also slightly correlated with the number of uniglomerular PNs.

We were able to precisely map 95% of sensillum classes and types by using 21 *OR-/IR-specific GAL4-lines* (Fishilevich and

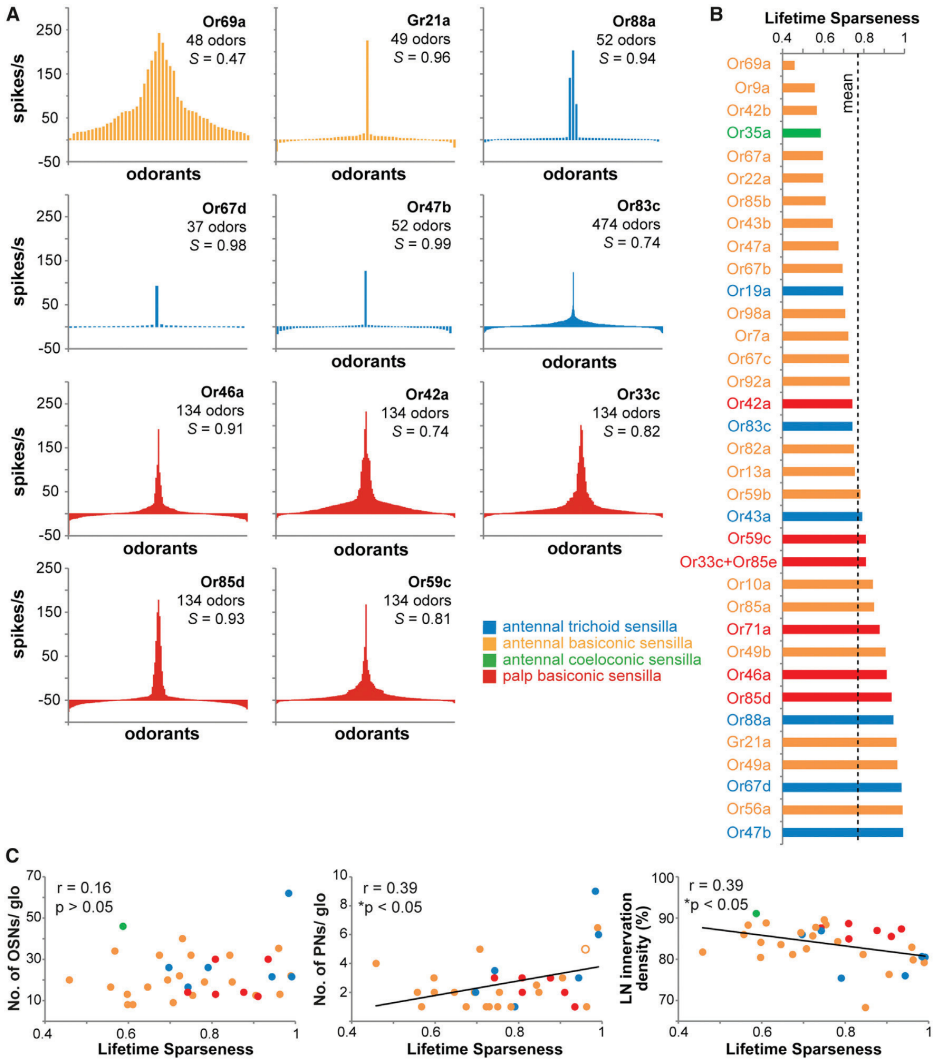

Figure 5. Odor-Tuning Properties Are Correlated with the Number of LNs and PNs per Glomerulus

(A) Odor response profiles of 11 olfactory receptors generated with SSR of the respective sensillum. Inset is the name of the olfactory receptor, the number of applied odors, and the lifetime sparseness, *S*. Color code refers to Figure 1B. Raw SSR data are listed in Table S3.

(B) Bar plot representing the lifetime sparseness for all olfactory receptor types.

(C) Scatterplots showing the correlation of the lifetime sparseness with number of OSNs (left), the number of PNs (middle), and the LN innervation frequency (right) per glomerulus. *p < 0.05 (two-tailed probability of the Pearson correlation coefficient).

Vosshall, 2005; Kurtovic et al., 2007; Silbering et al., 2011). The total number of sensilla per class corresponds to previously published reports and confirms that trichoid and basiconic sensilla are sexually dimorphic (Shanbhag et al., 1999; Stocker, 2001). We observed sexual dimorphism at the periphery of six sensillum types; these in turn comprise 18 olfactory receptor types. These types include olfactory receptors that are involved in courtship and mating (Or47b/Or88a/Or65a; Dweck et al., 2015; Lebreton et al., 2014), attraction behavior (Or83c; Ronderos et al., 2014), and CO_2 avoidance (Gr21a; Suh et al., 2004). Sexual dimorphism in the brain has been studied only at the glomerular level and not at the level of individual olfactory receptor types expressed in the

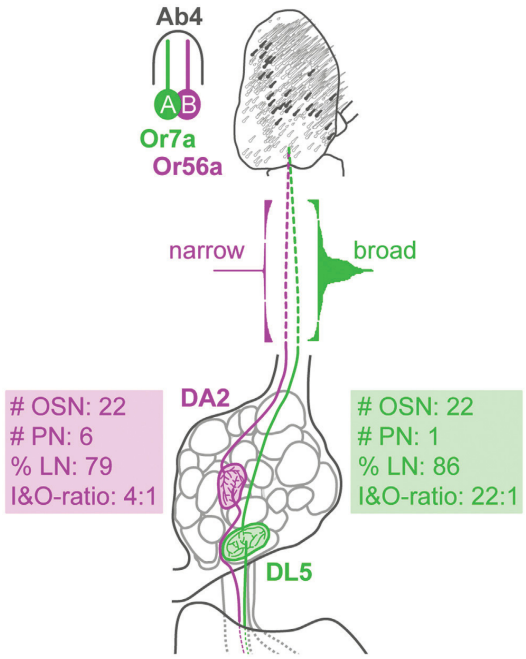

Figure 6. Glomerular Neuronal Architecture Reflects Functional Relevance

Schematic model displaying the morphological properties of two selected olfactory receptor pathways, Or56a/DA2 and Or7a/DL5, both of which descend from the Ab4 sensillum. The peripheral distribution of their sensilla over the odor response profile to their glomerular volume, convergence ratio, and LN innervation frequency (after Chou et al., 2010) are indicated. The color code refers to Figure 1B.

olfactory organs. Hence, our study demonstrates that the number of OSNs expressing a certain olfactory receptor type is different between the sexes, suggesting that those receptors might be involved in sex-specific behavior, such as courtship or oviposition. When we compared the female AL with the male AL, our data exceeded the number of dimorphic glomeruli described to date. Our data confirm that sexual dimorphism exists in the volumes of glomeruli DA1 and VA1v (Kondoh et al., 2003; Stockinger et al., 2005). We also agree that spatially adjacent glomeruli VA1d and DL3 are the same size in both sexes. We did not observe, however, that glomerulus VL2a is larger in males than in females, as it has been described (Stockinger et al., 2005), possibly because of the slight difference. In contrast to previous studies, we found sexual dimorphism in seven additional glomeruli, all of which are *fruitless* negative (Stockinger et al., 2005). These discrepancies might have a methodological basis. Although we quantified AL morphology under in vivo conditions, former studies analyzed glomerular volumes in brains that had been processed in vitro (Kondoh et al., 2003; Stockinger et al., 2005); such methodological disparities may cause unequal and unpredictable fixation artifacts in glomerular volume (Grabe et al., 2015). Our findings of additional, *fruitless* negative glomeruli with sex-specific volume differences suggest that other, so far unknown, factors might be involved. Future studies are needed to analyze whether these seven glomeruli are indeed involved in gender-specific behavior.

We observed that the majority of glomeruli is innervated by on average two uniglomerular PNs, while a few glomeruli relay their output via, on average, six uniglomerular PNs to higher brain centers. Our count of the number of PNs complements the previously published single cell clones of GH146-positive PNs (Jefferis et al., 2007; Marin et al., 2002, 2005; Wong et al., 2002) and confirms the estimated count of one to three uniglomerular PNs for most glomeruli (Wong et al., 2002). Notably, those glomeruli that exhibit the narrowest response profile seem to be innervated by the larger number of output neurons. These glomeruli are part of crucial pathways involved in reproduction and survival. For example, glomeruli DA1, VA1v, and VA1d are known to play a role in courtship and mating (Dweck et al., 2015; Kurtovic et al., 2007; Stockinger et al., 2005), while glomerulus DC3 is narrowly tuned to farnesol and mediates attraction behavior (Ronderos et al., 2014). Glomerulus DA2 encodes geosmin, the odor of toxic bacteria and mold, and evokes strong aversion in flies (Stensmyr et al., 2012). Glomerulus DL3 has so far not been deorphanized and will most likely have a very selected and narrow response profile. The olfactory system might therefore have evolved a strategy to ensure that highly essential odor cues are transferred reliably and quickly from the AL to higher brain centers. Indeed, it has recently been shown that higher PN numbers improve the detection accuracy and latency of odor stimuli (Jeanne and Wilson, 2015). In addition, large numbers of PNs might have the advantage of encoding diverse stimulus features, such as different intensities as suggested for the CO_2-encoding circuitry (Lin et al., 2013). We also demonstrate that narrowly tuned glomeruli are less frequently innervated by LNs, indicating that those glomeruli may be less integrated in the mainly inhibitory, interglomerular AL network than are broadly tuned glomeruli. This finding further underlines a straight feedforward network, ensuring fast processing and detection of key odorants. However, it must be kept in mind that the populations of OSNs, LNs, and PNs are not equal regarding their temporal response kinetics (Chou et al., 2010; de Bruyne et al., 2001; Laurent et al., 2001; Seki et al., 2010; Wilson et al., 2004). Hence, the final response of a glomerulus might not depend solely on neuron number but could be affected also by neuron-specific response dynamics.

Our main findings can be illustrated in the following representative example (Figure 6): glomeruli DL5 and DA2 receive input from 22 OSNs housed in the same basiconic sensillum type Ab4. The broad response profile of Or7a, whose OSNs target DL5 (Galizia et al., 2010), and the highly selective profile of Or56a targeting glomerulus DA2 and detecting geosmin (Stensmyr et al., 2012) represent two opposing input channels. DL5 is so far not affiliated with a specific behavioral task and seems to play a role in combinatorial coding of aversive odors (Knaden et al., 2012). The significance of glomerulus DA2 is supported by its high number of uniglomerular PNs, having potentially more random input sites on mushroom body Kenyon cells

OPEN ACCESS
CellPress

(Caron et al., 2013; Gruntman and Turner, 2013) and on third-order neurons in the LH, in contrast to glomerulus DL5, which has only a single PN. The difference in output quantity is linked to an inverse LN innervation frequency. Although glomerulus DA2 is innervated by fewer LNs than is DL5, both glomeruli most likely have different impacts on the AL network. These glomeruli have different volumes, which, although the overall OSN density per glomerulus is identical, might be due either to the different number of innervating LNs or to a differential density of synapses per OSN (Mosca and Luo, 2014). On the basis of our findings of a specific and heterogeneous glomerular architecture, we are in a position to speculate about the significance of glomeruli that have remained to date poorly characterized. Hence, we propose that glomeruli D (Or69a), DC3 (Or83c), and DL3 (Or65a) likely encode odor information that is as crucial as information encoded in the geosmin and pheromone pathways.

In conclusion, our study demonstrates that each glomerulus is a unique morphological and functional unit whose significance regarding odor detection and odor-guided behavior can be predicted. Future studies dedicated to elucidating the synaptic connectivity in more detail will reveal whether ultrastructural characteristics of individual glomeruli are also correlated with functional properties.

EXPERIMENTAL PROCEDURES

Flies

Flies were reared at 25°C and 70% humidity on a 12 hr/12 hr day/night cycle. We used the following fly lines ordered from the Bloomington *Drosophila* stock center (http://flystocks.bio.indiana.edu): *GH146-GAL4* (Stocker et al., 1997), *UAS-GCaMP3.0* (Tian et al., 2009), *UAS-nlsGFP*, *ChA-GAL4* (Salvaterra and Kitamoto, 2001), *Or10a-GAL4*, *Or13a-GAL4*, *Or22a-GAL4*, *Or33c-GAL4*, *Or35a-GAL4*, *Or42a-GAL4*, *Or42b-GAL4*, *Or43a-GAL4*, *Or43b-GAL4*, *Or46aA-GAL4*, *Or47a-GAL4*, *Or49a-GAL4*, *Or56a-GAL4*, *Or59c-GAL4*, *Or67c-GAL4*, *Or69a-GAL4*, *Or83c-GAL4*, *Or85a-GAL4*, *Or88a-GAL4*, *Or92a-GAL4*, *Or98a-GAL4*, and *Orco-GAL4* (all Fishilevich and Vosshall, 2005; Vosshall et al., 2000). Additional lines were kindly provided by Richard Benton (*Ir40a-GAL4*; *Ir41a-GAL4*, Silbering et al., 2011; *IR76a-GAL4*, Benton et al., 2009; *Ir92a-GAL4*; and *Ir8a-GAL4*, Abuin et al., 2011), Barry Dickson (*Or67d-GAL4*, Kurtovic et al., 2007), and Bob Datta (*UAS-C3PA*; Ruta et al., 2010).

Scanning Electron Microscopy

Flies were anesthetized in CO_2, placed in 5 ml 25% EtOH, and incubated for 12–24 hr at room temperature. In an EtOH row, the flies were further dehydrated in 50%, 75%, and two times 100% EtOH for 12–24 hr each at room temperature. Samples were then critical point dried. After mounting the samples with T. V. tube coat (Ted Pella) onto the SEM stubs, we sputter-coated them with a 25-nm-thick platinum coat. Images of the sensillum types on the third antennal segment and the maxillary palp were acquired using a LEO 1450 VP scanning electron microscope with 10 kV and 24 mm working distance (Carl Zeiss).

OSN Quantification and Mapping

To quantify the number of OSNs innervating each glomerulus, 3- to 6-day-old flies were anesthetized with CO_2, and their antennae or palps were collected. After the antennae or palps were covered with a solution of saline and Triton-X (Sigma-Aldrich), they were mounted in VectaShield (Vector Laboratories) and sealed with nail polish between a 22 × 22 mm and a 24 × 60 mm object slide, both 1 mm thick, to allow double-sided scanning. No spacer was needed, because the layer of nail polish provided enough space to fix the antennae or palp but not crush it. Scans of both sides of each antenna were carried out with an Axio Imager.Z1 (Carl Zeiss) using a 20× water immersion objective (W Plan-Apochromat 20×/0.8; Carl Zeiss) in combination with a GFP filter cube (HE 38, EX BP 470/40, BS FT 495, EM BP 525/50; Carl Zeiss). To reliably map the sensilla, an additional transmitted light scan of each antenna was acquired. This scan was used to register all antennae by hand, on the basis of the position of the arista and the sacculus. The quantification of OSN cell bodies was done in FIJI (ImageJ version 1.48r; NIH) software.

Confocal Microscopy, 3D Reconstruction, and Volume Quantification

The dissection of fly brains was carried out as previously described (Silbering et al., 2011; Strutz et al., 2012). Confocal scans were obtained using multiple-photon confocal laser scanning microscopy (MPCLSM) (Zeiss laser scanning microscopy [LSM] 710 NLO confocal microscope; Carl Zeiss) using a 40× water immersion objective (W Plan-Apochromat 40x/1.0 DIC M27; Carl Zeiss) in combination with the internal Argon 488 (LASOS) and Helium-Neon 543 (Carl Zeiss) laser lines. Reconstruction of whole ALs and of individual glomeruli was done using the segmentation software AMIRA version 5.5.0 (FEI Visualization Sciences Group). Identification of glomeruli was verified by the in vivo scans of the specific OR-lines crossed into the END1-2 background for in vivo neuropil labeling (Grabe et al., 2015). We analyzed scans of at least three specimens for each GAL4 receptor line and reconstructed them in using the segmentation software AMIRA 5.5.0 (FEI Visualization Sciences Group). Using information on the voxel size from the laser scanning microscopy scans as well as the number of voxels labeled for each neuropil in AMIRA, we calculated the volume of the glomeruli and the whole AL.

Photoactivation of PNs

In vivo labeling of single glomeruli of 4- to 6-day-old male and female flies of the genotype *+;GH146-GAL4/(CyO);UAS-C3PA/(TM6B)* using MPCLSM (Zeiss LSM 710 NLO confocal microscope; Carl Zeiss) equipped with an infrared Chameleon Ultra diode-pumped laser (Coherent). Flies were prepared as previously described (Strutz et al., 2012). Precise regions of interest (ROIs) in the center of each single glomerulus were continuously photoactivated for 5–15 min at a wavelength of 760 nm with a 40× water immersion objective (W Plan-Apochromat 40x/1.0 DIC M27; Carl Zeiss) with laser power of approximately 1.5 mW. In detail, after obtaining a pre-photoactivation scan of the whole AL, we identified the single target glomerulus, marked its volume with a precise ROI, photoactivated and subsequently labeled all GH146-positive PNs innervating it, including all corresponding somata in one of the three cell clusters surrounding the AL (Figure 3A) as well as all axonal projections to the mushroom body calyx and the LH. Z stacks of the pre- and post-activation states were scanned at 925 nm with 1,024 × 1,024 pixel resolution. The identification of glomeruli was based on the previously published screen of *GH146-GAL4/UAS-GCaMP3.0* under the same conditions (Grabe et al., 2015).

Single-Sensillum Recordings

Adult flies were immobilized in pipette tips, and the third antennal segment or the palps were placed in a stable position onto a glass coverslip. Sensilla were localized under a microscope (BX51WI; Olympus) at 100× magnification, and the extracellular signals originating from the OSNs were measured by inserting a tungsten wire electrode in the base of a sensillum. The reference electrode was inserted into the eye. Signals were amplified (10×; Syntech Universal AC/DC Probe; Syntech), sampled (10,667.0 samples/s), and filtered (100–3,000 Hz with 50/60 Hz suppression) via USB-IDAC connection to a computer (Syntech). Action potentials were extracted using Auto Spike 32 software (Syntech). Neuron activities were recorded for 10 s, starting 2 s before a stimulation period of 0.5 s. Responses from individual neurons were calculated as the increase (or decrease) in the action potential frequency (spikes per second) relative to the pre-stimulus frequency.

Lifetime Sparseness, *S*

Acquired responses were used to quantify a receptor's response profile by calculating its lifetime sparseness (Bhandawat et al., 2007; Perez-Orive et al., 2002; Vinje and Gallant, 2000). This is a non-parametric statistic providing a measure of the likeliness of an OSN to respond. The value ranges from $0 \leq S \leq 1$, where 0 means the OSN responds to every odor in the same

way and 1 means the OSN responds exclusively to one odor in the set. Calculation was carried out with following formula:

$$S = \left(\frac{1}{1-\frac{1}{N}}\right) * \left(1 - \frac{\left(\sum_{j=1}^{N} \frac{r_j}{N}\right)^2}{\sum_{j=1}^{N} \frac{r_j^2}{N}}\right),$$

where S is lifetime sparseness, N is the number of tested odors, and r_j is response to a given odor j. Any values of $r_j < 0$ were set to zero before computing lifetime sparseness. Used data sets are taken from Dweck et al. (2015), Ebrahim et al. (2015), and Hallem and Carlson (2006); the DoOR database (Galizia et al., 2010), and response profiles of 11 olfactory receptors acquired via SSR in this study (Table S3).

Statistical Methods

If not otherwise stated, data represent median ± SD. Statistical differences between groups were determined by Student's t test (*p < 0.05, **p < 0.01, ***p < 0.001).

Significance of the Pearson correlation coefficients were calculated using the online tool p-Value Calculator for Correlation Coefficients (http://www.danielsoper.com/statcalc).

SUPPLEMENTAL INFORMATION

Supplemental Information includes one figure and three tables and can be found with this article online at http://dx.doi.org/10.1016/j.celrep.2016.08.063.

AUTHOR CONTRIBUTIONS

V.G. and S.S. together conceived and designed the study. V.G. planned and carried out all experiments, with the exception of the quantification of PNs in females (Figure 3), which was done by A.B., and the SSR experiments (Figure 5), which were done by H.K.M.D. V.G. and S.S. analyzed and interpreted the results, prepared the figures, and wrote the paper. S.L.-L. helped to generate the END1-2 fly strain and provided neurogenetic advice. B.S.H. provided intellectual and financial support. All authors critically revised the article.

ACKNOWLEDGMENTS

We thank Silke Trautheim for excellent technical assistance, Jürgen Rybak for help with the AMIRA software, Christine Mißbach for support regarding the antennal preparations, Carolin Kathner and Julia van Beesel for help with the neuronal quantifications, and Emily Wheeler for editorial assistance. Stocks obtained from the Bloomington Drosophila Stock Center (NIH P40OD018537) were used in this study. We are grateful to the Hansson Department for comments on the manuscript. This study was funded by the Federal Ministry of Education and Research (BMBF research grant to S.S.) and the Max Planck Society (MPG).

Received: March 26, 2016
Revised: July 15, 2016
Accepted: August 18, 2016
Published: September 20, 2016

REFERENCES

Abuin, L., Bargeton, B., Ulbrich, M.H., Isacoff, E.Y., Kellenberger, S., and Benton, R. (2011). Functional architecture of olfactory ionotropic glutamate receptors. Neuron *69*, 44–60.

Acebes, A., and Ferrús, A. (2001). Increasing the number of synapses modifies olfactory perception in Drosophila. J. Neurosci. *21*, 6264–6273.

Ai, M., Min, S., Grosjean, Y., Leblanc, C., Bell, R., Benton, R., and Suh, G.S.B. (2010). Acid sensing by the Drosophila olfactory system. Nature *468*, 691–695.

Benton, R., Sachse, S., Michnick, S.W., and Vosshall, L.B. (2006). Atypical membrane topology and heteromeric function of *Drosophila* odorant receptors *in vivo*. PLoS Biol. *4*, e20.

Benton, R., Vannice, K.S., Gomez-Diaz, C., and Vosshall, L.B. (2009). Variant ionotropic glutamate receptors as chemosensory receptors in Drosophila. Cell *136*, 149–162.

Bhandawat, V., Olsen, S.R., Gouwens, N.W., Schlief, M.L., and Wilson, R.I. (2007). Sensory processing in the Drosophila antennal lobe increases reliability and separability of ensemble odor representations. Nat. Neurosci. *10*, 1474–1482.

Boeckh, J., and Tolbert, L.P. (1993). Synaptic organization and development of the antennal lobe in insects. Microsc. Res. Tech. *24*, 260–280.

Bressel, O.C., Khan, M., and Mombaerts, P. (2016). Linear correlation between the number of olfactory sensory neurons expressing a given mouse odorant receptor gene and the total volume of the corresponding glomeruli in the olfactory bulb. J. Comp. Neurol. *524*, 199–209.

Busch, S., Selcho, M., Ito, K., and Tanimoto, H. (2009). A map of octopaminergic neurons in the Drosophila brain. J. Comp. Neurol. *513*, 643–667.

Carlsson, M.A., Diesner, M., Schachtner, J., and Nässel, D.R. (2010). Multiple neuropeptides in the Drosophila antennal lobe suggest complex modulatory circuits. J. Comp. Neurol. *518*, 3359–3380.

Caron, S.J.C., Ruta, V., Abbott, L.F., and Axel, R. (2013). Random convergence of olfactory inputs in the Drosophila mushroom body. Nature *497*, 113–117.

Chou, Y.-H., Spletter, M.L., Yaksi, E., Leong, J.C.S., Wilson, R.I., and Luo, L. (2010). Diversity and wiring variability of olfactory local interneurons in the Drosophila antennal lobe. Nat. Neurosci. *13*, 439–449.

Couto, A., Alenius, M., and Dickson, B.J. (2005). Molecular, anatomical, and functional organization of the *Drosophila* olfactory system. Curr. Biol. *15*, 1535–1547.

de Bruyne, M., Clyne, P.J., and Carlson, J.R. (1999). Odor coding in a model olfactory organ: the *Drosophila* maxillary palp. J. Neurosci. *19*, 4520–4532.

de Bruyne, M., Foster, K., and Carlson, J.R. (2001). Odor coding in the *Drosophila* antenna. Neuron *30*, 537–552.

Dekker, T., Ibba, I., Siju, K.P., Stensmyr, M.C., and Hansson, B.S. (2006). Olfactory shifts parallel superspecialism for toxic fruit in Drosophila melanogaster sibling, D. sechellia. Curr. Biol. *16*, 101–109.

Dobritsa, A.A., van der Goes van Naters, W., Warr, C.G., Steinbrecht, R.A., and Carlson, J.R. (2003). Integrating the molecular and cellular basis of odor coding in the *Drosophila* antenna. Neuron *37*, 827–841.

Duménil, C., Woud, D., Pinto, F., Alkema, J.T., Jansen, I., Van Der Geest, A.M., Roessingh, S., and Billeter, J.-C. (2016). Pheromonal cues deposited by mated females convey social information about egg-laying sites in Drosophila melanogaster. J. Chem. Ecol. *42*, 259–269.

Dweck, H.K., Ebrahim, S.A., Kromann, S., Bown, D., Hillbur, Y., Sachse, S., Hansson, B.S., and Stensmyr, M.C. (2013). Olfactory preference for egg laying on citrus substrates in Drosophila. Curr. Biol. *23*, 2472–2480.

Dweck, H.K.M., Ebrahim, S.A.M., Thoma, M., Mohamed, A.A.M., Keesey, I.W., Trona, F., Lavista-Llanos, S., Svatoš, A., Sachse, S., Knaden, M., and Hansson, B.S. (2015). Pheromones mediating copulation and attraction in Drosophila. Proc. Natl. Acad. Sci. U S A *112*, E2829–E2835.

Ebrahim, S.A.M., Dweck, H.K.M., Stökl, J., Hofferberth, J.E., Trona, F., Weniger, K., Rybak, J., Seki, Y., Stensmyr, M.C., Sachse, S., et al. (2015). *Drosophila* avoids parasitoids by sensing their semiochemicals via a dedicated olfactory circuit. PLoS Biol. *13*, e1002318.

Fishilevich, E., and Vosshall, L.B. (2005). Genetic and functional subdivision of the *Drosophila* antennal lobe. Curr. Biol. *15*, 1548–1553.

Galizia, C.G., McIlwrath, S.L., and Menzel, R. (1999). A digital three-dimensional atlas of the honeybee antennal lobe based on optical sections acquired by confocal microscopy. Cell Tissue Res. *295*, 383–394.

Galizia, C.G., Münch, D., Strauch, M., Nissler, A., and Ma, S. (2010). Integrating heterogeneous odor response data into a common response model: a DoOR to the complete olfactome. Chem. Senses *35*, 551–563.

Gallio, M., Ofstad, T.A., Macpherson, L.J., Wang, J.W., and Zuker, C.S. (2011). The coding of temperature in the Drosophila brain. Cell *144*, 614–624.

Gao, Q., Yuan, B., and Chess, A. (2000). Convergent projections of *Drosophila* olfactory neurons to specific glomeruli in the antennal lobe. Nat. Neurosci. *3*, 780–785.

Grabe, V., Strutz, A., Baschwitz, A., Hansson, B.S., and Sachse, S. (2015). Digital in vivo 3D atlas of the antennal lobe of Drosophila melanogaster. J. Comp. Neurol. *523*, 530–544.

Grosjean, Y., Rytz, R., Farine, J.-P., Abuin, L., Cortot, J., Jefferis, G.S.X.E., and Benton, R. (2011). An olfactory receptor for food-derived odours promotes male courtship in Drosophila. Nature *478*, 236–240.

Gruntman, E., and Turner, G.C. (2013). Integration of the olfactory code across dendritic claws of single mushroom body neurons. Nat. Neurosci. *16*, 1821–1829.

Ha, T.S., and Smith, D.P. (2006). A pheromone receptor mediates 11-cis-vaccenyl acetate-induced responses in *Drosophila*. J. Neurosci. *26*, 8727–8733.

Hallem, E.A., and Carlson, J.R. (2006). Coding of odors by a receptor repertoire. Cell *125*, 143–160.

Hansson, B.S., Ljungberg, H., Hallberg, E., and Löfstedt, C. (1992). Functional specialization of olfactory glomeruli in a moth. Science *256*, 1313–1315.

Hansson, B.S., Knaden, M., Sachse, S., Stensmyr, M.C., and Wicher, D. (2010). Towards plant-odor-related olfactory neuroethology in *Drosophila*. Chemoecology *20*, 51–61.

Hong, E.J., and Wilson, R.I. (2015). Simultaneous encoding of odors by channels with diverse sensitivity to inhibition. Neuron *85*, 573–589.

Ito, K., Shinomiya, K., Ito, M., Armstrong, J.D., Boyan, G., Hartenstein, V., Harzsch, S., Heisenberg, M., Homberg, U., Jenett, A., et al.; Insect Brain Name Working Group (2014). A systematic nomenclature for the insect brain. Neuron *81*, 755–765.

Jeanne, J.M., and Wilson, R.I. (2015). Convergence, divergence, and reconvergence in a feedforward network improves neural speed and accuracy. Neuron *88*, 1014–1026.

Jefferis, G.S.X.E., Potter, C.J., Chan, A.M., Marin, E.C., Rohlfing, T., Maurer, C.R., Jr., and Luo, L. (2007). Comprehensive maps of Drosophila higher olfactory centers: spatially segregated fruit and pheromone representation. Cell *128*, 1187–1203.

Kain, P., Boyle, S.M., Tharadra, S.K., Guda, T., Pham, C., Dahanukar, A., and Ray, A. (2013). Odour receptors and neurons for DEET and new insect repellents. Nature *502*, 507–512.

Knaden, M., Strutz, A., Ahsan, J., Sachse, S., and Hansson, B.S. (2012). Spatial representation of odorant valence in an insect brain. Cell Rep. *1*, 392–399.

Kondoh, Y., Kaneshiro, K.Y., Kimura, K., and Yamamoto, D. (2003). Evolution of sexual dimorphism in the olfactory brain of Hawaiian *Drosophila*. Proc. Biol. Sci. *270*, 1005–1013.

Kreher, S.A., Mathew, D., Kim, J., and Carlson, J.R. (2008). Translation of sensory input into behavioral output via an olfactory system. Neuron *59*, 110–124.

Kurtovic, A., Widmer, A., and Dickson, B.J. (2007). A single class of olfactory neurons mediates behavioural responses to a Drosophila sex pheromone. Nature *446*, 542–546.

Lai, S.-L., Awasaki, T., Ito, K., and Lee, T. (2008). Clonal analysis of Drosophila antennal lobe neurons: diverse neuronal architectures in the lateral neuroblast lineage. Development *135*, 2883–2893.

Laissue, P.P., Reiter, C., Hiesinger, P.R., Halter, S., Fischbach, K.F., and Stocker, R.F. (1999). Three-dimensional reconstruction of the antennal lobe in *Drosophila melanogaster*. J. Comp. Neurol. *405*, 543–552.

Larsson, M.C., Domingos, A.I., Jones, W.D., Chiappe, M.E., Amrein, H., and Vosshall, L.B. (2004). *Or83b* encodes a broadly expressed odorant receptor essential for *Drosophila* olfaction. Neuron *43*, 703–714.

Laurent, G., Stopfer, M., Friedrich, R.W., Rabinovich, M.I., Volkovskii, A., and Abarbanel, H.D.I. (2001). Odor encoding as an active, dynamical process: experiments, computation, and theory. Annu. Rev. Neurosci. *24*, 263–297.

Lebreton, S., Grabe, V., Omondi, A.B., Ignell, R., Becher, P.G., Hansson, B.S., Sachse, S., and Witzgall, P. (2014). Love makes smell blind: mating suppresses pheromone attraction in Drosophila females via Or65a olfactory neurons. Sci. Rep. *4*, 7119.

Lin, H.-H., Chu, L.-A., Fu, T.-F., Dickson, B.J., and Chiang, A.-S. (2013). Parallel neural pathways mediate CO_2 avoidance responses in Drosophila. Science *340*, 1338–1341.

Linz, J., Baschwitz, A., Strutz, A., Dweck, H.K.M., Sachse, S., Hansson, B.S., and Stensmyr, M.C. (2013). Host plant-driven sensory specialization in Drosophila erecta. Proc. Biol. Sci. *280*, 20130626.

Liu, W.W., and Wilson, R.I. (2013). Glutamate is an inhibitory neurotransmitter in the Drosophila olfactory system. Proc. Natl. Acad. Sci. U S A *110*, 10294–10299.

Marin, E.C., Jefferis, G.S.X.E., Komiyama, T., Zhu, H., and Luo, L. (2002). Representation of the glomerular olfactory map in the Drosophila brain. Cell *109*, 243–255.

Marin, E.C., Watts, R.J., Tanaka, N.K., Ito, K., and Luo, L. (2005). Developmentally programmed remodeling of the Drosophila olfactory circuit. Development *132*, 725–737.

Mombaerts, P. (2006). Axonal wiring in the mouse olfactory system. Annu. Rev. Cell Dev. Biol. *22*, 713–737.

Mosca, T.J., and Luo, L. (2014). Synaptic organization of the Drosophila antennal lobe and its regulation by the Teneurins. Elife *3*, e03726.

Patterson, G.H., and Lippincott-Schwartz, J. (2002). A photoactivatable GFP for selective photolabeling of proteins and cells. Science *297*, 1873–1877.

Perez-Orive, J., Mazor, O., Turner, G.C., Cassenaer, S., Wilson, R.I., and Laurent, G. (2002). Oscillations and sparsening of odor representations in the mushroom body. Science *297*, 359–365.

Ronderos, D.S., Lin, C.-C., Potter, C.J., and Smith, D.P. (2014). Farnesol-detecting olfactory neurons in Drosophila. J. Neurosci. *34*, 3959–3968.

Ruta, V., Datta, S.R., Vasconcelos, M.L., Freeland, J., Looger, L.L., and Axel, R. (2010). A dimorphic pheromone circuit in Drosophila from sensory input to descending output. Nature *468*, 686–690.

Rybak, J., Talarico, G., Ruiz, S., Arnold, C., Cantera, R., and Hansson, B.S. (2016). Synaptic circuitry of identified neurons in the antennal lobe of Drosophila melanogaster. J. Comp. Neurol. *524*, 1920–1956.

Sachse, S., Rueckert, E., Keller, A., Okada, R., Tanaka, N.K., Ito, K., and Vosshall, L.B. (2007). Activity-dependent plasticity in an olfactory circuit. Neuron *56*, 838–850.

Salvaterra, P.M., and Kitamoto, T. (2001). Drosophila cholinergic neurons and processes visualized with Gal4/UAS-GFP. Brain Res. Gene Expr. Patterns *1*, 73–82.

Schneiderman, A.M., Hildebrand, J.G., Brennan, M.M., and Tumlinson, J.H. (1986). Trans-sexually grafted antennae alter pheromone-directed behaviour in a moth. Nature *323*, 801–803.

Seki, Y., Rybak, J., Wicher, D., Sachse, S., and Hansson, B.S. (2010). Physiological and morphological characterization of local interneurons in the Drosophila antennal lobe. J. Neurophysiol. *104*, 1007–1019.

Semmelhack, J.L., and Wang, J.W. (2009). Select Drosophila glomeruli mediate innate olfactory attraction and aversion. Nature *459*, 218–223.

Shanbhag, S.R., Singh, K., and Singh, R.N. (1995). Fine structure and primary sensory projections of sensilla located in the sacculus of the antenna of Drosophila melanogaster. Cell Tissue Res. *282*, 237–249.

Shanbhag, S.R., Muller, B., and Steinbrecht, R.A. (1999). Atlas of olfactory organs of *Drosophila melanogaster*. 1. Types, external organization, innervation and distribution of olfactory sensilla. Int. J. Insect Morphol. Embryol. *28*, 377–397.

Shang, Y., Claridge-Chang, A., Sjulson, L., Pypaert, M., and Miesenböck, G. (2007). Excitatory local circuits and their implications for olfactory processing in the fly antennal lobe. Cell *128*, 601–612.

Silbering, A.F., Rytz, R., Grosjean, Y., Abuin, L., Ramdya, P., Jefferis, G.S.X.E., and Benton, R. (2011). Complementary function and integrated wiring of the evolutionarily distinct Drosophila olfactory subsystems. J. Neurosci. *31*, 13357–13375.

Stensmyr, M.C., Dweck, H.K.M., Farhan, A., Ibba, I., Strutz, A., Mukunda, L., Linz, J., Grabe, V., Steck, K., Lavista-Llanos, S., et al. (2012). A conserved dedicated olfactory circuit for detecting harmful microbes in Drosophila. Cell *151*, 1345–1357.

Stocker, R.F. (2001). *Drosophila* as a focus in olfactory research: mapping of olfactory sensilla by fine structure, odor specificity, odorant receptor expression, and central connectivity. Microsc. Res. Tech. *55*, 284–296.

Stocker, R.F., Lienhard, M.C., Borst, A., and Fischbach, K.F. (1990). Neuronal architecture of the antennal lobe in *Drosophila melanogaster*. Cell Tissue Res. *262*, 9–34.

Stocker, R.F., Heimbeck, G., Gendre, N., and de Belle, J.S. (1997). Neuroblast ablation in *Drosophila* P[GAL4] lines reveals origins of olfactory interneurons. J. Neurobiol. *32*, 443–456.

Stockinger, P., Kvitsiani, D., Rotkopf, S., Tirián, L., and Dickson, B.J. (2005). Neural circuitry that governs Drosophila male courtship behavior. Cell *121*, 795–807.

Strausfeld, N.J., and Hildebrand, J.G. (1999). Olfactory systems: common design, uncommon origins? Curr. Opin. Neurobiol. *9*, 634–639.

Strutz, A., Voeller, T., Riemensperger, T., Fiala, A., and Sachse, S. (2012). Calcium imaging of neural activity in the olfactory system of Drosophila. In Genetically Encoded Functional Indicators, J.-R. Martin, ed. (Springer Science+Business Media), pp. 43–70.

Suh, G.S., Wong, A.M., Hergarden, A.C., Wang, J.W., Simon, A.F., Benzer, S., Axel, R., and Anderson, D.J. (2004). A single population of olfactory sensory neurons mediates an innate avoidance behaviour in *Drosophila*. Nature *431*, 854–859.

Tian, L., Hires, S.A., Mao, T., Huber, D., Chiappe, M.E., Chalasani, S.H., Petreanu, L., Akerboom, J., McKinney, S.A., Schreiter, E.R., et al. (2009). Imaging neural activity in worms, flies and mice with improved GCaMP calcium indicators. Nat. Methods *6*, 875–881.

Vinje, W.E., and Gallant, J.L. (2000). Sparse coding and decorrelation in primary visual cortex during natural vision. Science *287*, 1273–1276.

Vosshall, L.B., and Stocker, R.F. (2007). Molecular architecture of smell and taste in Drosophila. Annu. Rev. Neurosci. *30*, 505–533.

Vosshall, L.B., Wong, A.M., and Axel, R. (2000). An olfactory sensory map in the fly brain. Cell *102*, 147–159.

Wilson, R.I. (2013). Early olfactory processing in Drosophila: mechanisms and principles. Annu. Rev. Neurosci. *36*, 217–241.

Wilson, R.I., and Mainen, Z.F. (2006). Early events in olfactory processing. Annu. Rev. Neurosci. *29*, 163–201.

Wilson, R.I., Turner, G.C., and Laurent, G. (2004). Transformation of olfactory representations in the *Drosophila* antennal lobe. Science *303*, 366–370.

Wong, A.M., Wang, J.W., and Axel, R. (2002). Spatial representation of the glomerular map in the *Drosophila* protocerebrum. Cell *109*, 229–241.

Cell Reports, Volume *16*

Supplemental Information

Elucidating the Neuronal Architecture of Olfactory Glomeruli in the *Drosophila* Antennal Lobe

Veit Grabe, Amelie Baschwitz, Hany K.M. Dweck, Sofia Lavista-Llanos, Bill S. Hansson, and Silke Sachse

SUPPLEMENTAL FIGURE S1

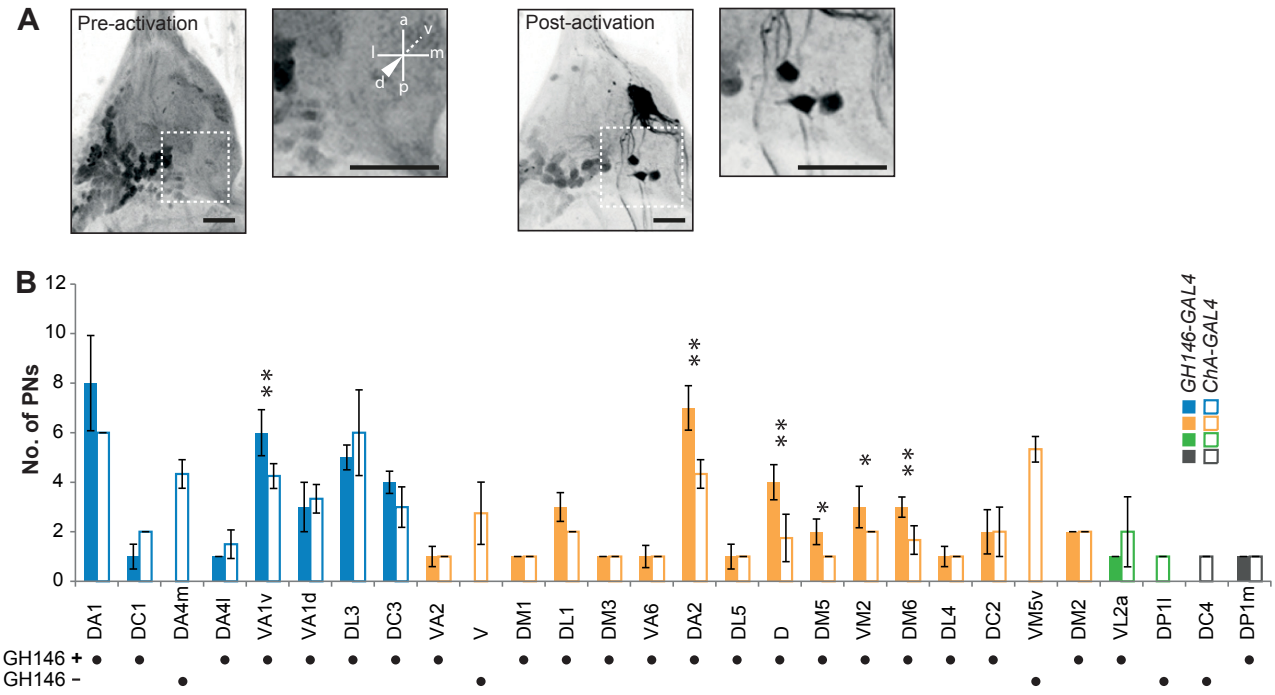

SUPPLEMENTAL FIGURE LEGEND

Supplemental Figure S1: Comparison between number of cholinergic and GH146-positive PNs per glomerulus.
(**A**) Left, Z-projection of a *ChA-GAL4/UAS-C3PA* scan of a left antennal lobe before photo-activation. Right, Z-projection of the same antennal lobe after photoactivation of glomerulus VM5v. The scale bar equals 20 µm. (**B**) Comparison between number of PNs labeled with photoactivation using the transgenic lines *GH146-GAL4* (filled bars) and *ChA-GAL4* (empty bars) for 28 glomeruli. Data represent median ± SD. Statistical differences between the two lines were determined by Student's t test, *p < 0.05, **p < 0.01, n = 3-6. The color code refers to Figure 1B.

SUPPLEMENTAL TABLES

Table S1: Glomerulus-specific dataset.

[a] Data from (Ai et al., 2010); [b] Data obtained by photoactivation with *ChA-GAL4*; [c] Alternative count with *ChA-GAL4* is 4 PNs (± 0.6); [d] Data from (Kain et al., 2013); [e] (Gallio et al., 2011); [f] (Ebrahim et al., 2015); [g] (Dweck et al., 2015); [h] Data from DoOR (Galizia et al., 2010); [i] (Hallem et al., 2006); [m] (Stensmyr et al., 2012).

Glomerulus	Sensillum	Receptor	OSNs (±SD)		*In vivo* glomerular volume (µm³ ±SD)		PNs (±SD)		Lifetime Sparseness (Source)
			females	males	females	males	females	males	
D	Ab9	Or69a	24 (6.1)	17.5 (4.3)	1170 (473)	1579 (552)	4 (0.7)	4 (1)	0.47 (novel)
DA1	At1	Or67d	62.5 (10.8)	62.25 (11)	4738 (732)	6182 (1037)	8 (1.9)	10 (1)	0.98 (novel)
DA2	Ab4	Or56a/Or33a	24 (1.9)	21 (3.6)	1630 (677)	1050 (361)	6.5 (1)	5 (1.3)	0.99[m]
DA3	At2	Or23a	15	18	629 (99)	692 (24)	GH146 negative		-
DA4l	At3	Or43a	27 (3)	22 (6.6)	1135 (119)	1041 (193)	1 (0)	1 (1.2)	0.79[h]
DA4m	At3	Or2a	27	22	935 (269)	1435 (275)	GH146 negative		-
DC1	At3	Or19a/b	27	22	2820 (593)	2532 (919)	1 (0.5)	1 (0)	0.70[h]
DC2	Ab6	Or13a	15 (2.5)	11 (1)	1415 (378)	1803 (239)	2 (0.9)	2 (0)	0.75[h]
DC3	At2	Or83c	15 (2.9)	18 (2.2)	1743 (311)	2017 (255)	4 (0.45)	2 (0.6)	0.74 (novel)
DC4	Sac III	Ir64a	15[a]		1975 (312)	1875 (300)	GH146 negative		
DL1	Ab1	Or10a/Gr10a	37.5 (6.5)	26 (4)	2267 (603)	2037 (277)	3 (0.6)	2 (0.6)	0.84[h]
DL2d	Ac3?	Ir75a/b/c	-	-	2591 (1045)	2077 (432)	GH146 negative		-
DL2v	Ac3?	Ir75a/b/c	-	-	2362 (655)	2025 (716)	GH146 negative		-
DL3	At4	Or65a/b/c	19.5	25.5	615 (177)	791 (329)	5 (1.1)	6 (1.3)	-
DL4	Ab10	Or49a/Or85f	18 (3.2)	10.5 (2)	622 (177)	946 (305)	1 (0.4)	1 (0)	0.96[f]
DL5	Ab4	Or7a	24	21	2865 (759)	1456 (334)	1 (0.6)	1 (0)	0.72[h]
DM1	Ab1	Or42b	38.5 (4.6)	32 (5.9)	4211 (493)	2821 (470)	1 (0)	1 (0)	0.57[h]
DM2	Ab3	Or22a/b	8 (3.9)	8 (2.9)	2241 (453)	2085 (267)	2 (0)	2 (0)	0.60[h]
DM3	Ab5	Or47a/Or33b	34 (8)	31 (5.4)	1336 (305)	1420 (296)	1 (0)	2 (0.8)	0.67[h]
DM4	Ab2	Or59b	23	15.5	2597 (693)	2806 (503)	1 (0)	1 (0)	0.78[h]
DM5	Ab2	Or85a/Or33b	23 (6)	15.5 (3.6)	1269 (253)	912 (313)	2 (0.5)	1 (0.6)	0.85[h]
DM6	Ab10	Or67a	18	10.5	1439 (236)	1631 (191)	3 (0.4)	3 (0.5)	0.60[h]
DP1l	Ac2	Ir75a	15	12	3805 (297)	2659 (244)	GH146 negative		-
DP1m	Sac III	Ir64a	15[a]		5288 (812)	4244 (331)	1 (0)	1 (0)	-
V	Ab1	Gr21a/Gr63a	39.8	30	3438 (644)	3392 (1106)	5.5 (0.57)[b]		0.96 (novel)
VA1d	At4	Or88a	19.5 (3.7)	25.5 (4)	4433 (1200)	4502 (179)	3 (1)	3 (0)	0.94 (novel)

VA1v	At4	Or47b	19.5	25.5	5347 (748)	6175 (409)	6 (0.9)	5 (1)	0.99 (novel)
VA2	Ab1	Or92a	43.5	32 (7.3)	3278 (738)	4051 (455)	1 (0.4)	1 (0.5)	0.73[h]
VA3	Ab9	Or67b	24	17.5	1886 (274)	1470 (250)	2 (0.5)	2 (0.5)	0.69[h]
VA4	Pb3	Or85d	29	30.5	1619 (437)	1307 (334)	2 (0)	1 (0)	0.93 (novel)
VA5	Ab6	Or49b	15	11	1126 (247)	1293 (484)	2 (0.5)	3 (0.75)	0.91[h]
VA6	Ab5	Or82a	34	31	2520 (218)	2667 (309)	1 (0.4)	2.5 (1.3)	0.75[h]
VA7l	Pb2	Or46a	14.5 (2.7)	11.5 (0.9)	784 (330)	972 (295)	1 (0.5)	1 (0)	0.91 (novel)
VA7m	-	-	-	-	1187 (489)	927 (229)	3 (0)	3 (0.6)	-
VC1	Pb2	Or33c/Or85e	12 (1)	14 (2.2)	1953 (593)	1497 (126)	1 (0.5)	2 (0.5)	0.82 (novel)
VC2	Pb1	Or71a	11.5	15	1090 (95)	1018 (152)	1 (0.5)	3 (1.5)	0.88[g]
VC3	Ac3	Or35a	47.5 (6.9)	42 (10.3)	2728 (539)	2332 (568)	GH146 negative		0.59[h]
VC4	Ab7	Or67c	14 (4)	12 (1.3)	1588 (332)	1263 (306)	GH146 negative		0.73[i]
VC5	Ac2	Ir41a	15 (2.7)	12 (2.4	1182 (240)	1173 (466)	GH146 negative		-
VL1	Ac1	Ir75d	15	16	4729 (914)	3657 (318)	GH146 negative		-
VL2a	Ac4	Ir84a	29.5	24	3081 (446)	2693 (512)	1 (0)[c]	2 (1)[c]	-
VL2p	Ac1	Ir31a	15	16	3989 (709)	3378 (684)	3 (0)	1 (0.5)	-
VM1	Ac1	Ir92a	15 (1.7)	16 (2.5)	1509 (391)	1543 (415)	2 (0.4)	1.5 (1)	-
VM2	Ab8	Or43b	18 (6.5)	15 (2.4)	1551 (423)	1296 (528)	3 (0.8)	2 (0)	0.65[h]
VM3	Ab8	Or9a	18	15	1898 (170)	1309 (328)	2 (0.5)	2 (0.6)	0.56[h]
VM4	Ac4	Ir76a	29.5 (2.8)	24 (2.9)	2382 (391)	1703 (302)	1 (0.5)	1 (0.6)	-
VM5d	Ab3	Or85b/Or98b	8	8	2097 (289)	1304 (370)	GH146 negative		0.61[i]
VM5v	Ab7	Or98a	8.5 (2.9)	9 (3.2)	1628 (46)	1385 (198)	5 (0.5)[b]		0.71[i]
VM7d	Pb1	Or42a	11.5 (6.5)	15 (4.5)	1578 (638)	1660 (531)	2 (0.8)	3 (0.4)	0.74 (novel)
VM7v	Pb3	Or59c	29 (10.4)	30.5 (3.2)	1296 (632)	1085 (562)	3 (0.8)	2.5 (1)	0.81 (novel)
VP1+VM6	Sac I	Ir40a	11 (2.8)[d]	9 (1.8)[d]	-	-	GH146 negative		-
VP2	Arista	hot	3[e]	3[e]	-	-	-	-	-
VP3	Arista	cold	3[e]	3[e]	-	-	-	-	-
VP4	Sac I	Ir40a	=VP1[d]	=VP1[d]	-	-	GH146 negative		-
all	**all**	**all**	**1047.8**	**934.25**	**111593**	**103168**	**80.5**	**83**	**-**

Table S2: Quantification of PN number per cell cluster.

Glomerulus	Sensillum	Receptor	# somata	adPN (±SD)	lPN (±SD)	vPN (±SD)
D	Ab9	Or69a	4	4 (0.8)		
DA1	At1	Or67d	9		8 (1.8)	1 (0)
DA2	Ab4	Or56a/Or33a	5.5	0.5 (1)	5 (1.3)	
DA4l	At3	Or43a	1	1 (0.8)		
DC1	At3	Or19a/b	1	1 (0.4)		
DC2	Ab6	Or13a	2	2 (0.7)		
DC3	At2	Or83c	3.5	3.5 (0.9)		
DL1	Ab1	Or10a/Gr10a	2.5	2.5 (0.5)		
DL3	At4	Or65a/b/c	5		5 (1)	
DL4	Ab10	Or49a/Or85f	1	1 (0.3)		
DL5	Ab4	Or7a	1	1 (0.3)		
DM1	Ab1	Or42b	1		1 (0)	
DM2	Ab3	Or22a/b	2		2 (0)	
DM3	Ab5	Or47a/Or33b	1	1 (0.7)		
DM4	Ab2	Or59b	1	1 (0)		
DM5	Ab2	Or85a/Or33b	2		2 (0.5)	
DM6	Ab10	Or67a	3	3 (0.4)		
DP1m	Sac III	Ir64a	1	1 (0)		
VA1d	At4	Or88a	3	3 (0.8)		
VA1v	At4	Or47b	5	4 (0.8)		1 (0.5)
VA2	Ab1	Or92a	1	1 (0.4)		
VA4	Pb3	Or85d	1		1 (0.5)	
VA5	Ab6	Or49b	3		3 (0.7)	
VA6	Ab5	Or82a	1	1 (1)		
VA7l	Pb2	Or46aA	2	2 (1.2)		
VA7m	-	-	2.5		2.5 (1)	
VC1	Pb2	Or33c/Or85e	2		2 (0.5)	
VC2	Pb1	Or71a	3		3 (1.4)	
VL2a	Ac4	Ir84a	1	1 (0.8)		
VL2p	Ac1	Ir31a	1	1 (0.4)		
VM1	Ac1	Ir92a	2		2 (0.7)	
VM2	Ab8	Or43b	2	2 (0.9)		
VM3	Ab8	Or9a	2	2 (0.6)		
VM4	Ac4	Ir76a	1	1 (0.4)		
VM7d	Pb1	Or42a	3	3 (0.8)		
VM7v	Pb3	Or59c	3	3 (0.9)		

Table S3: Odorant responses of 11 olfactory receptors acquired via SSR.

Firing rates for each olfactory receptor to 37 - 474 different odors (including CAS numbers) upon odor stimulation for 0.5 s; n = 3. (Please see Excel file)

CAS	Odor	Or67d	Or47b	Or88a	Or33c	Or69a	Or59c	Or85d	Or42a	Or83c	Or46a	Gr21a
1001-45-2	6-pentadecanone									-2,00		
10032-13-0	hexyl isovalerate									-2,50		
100-42-5	styrene									9,00		
100462-58-6	(Z,Z)-7,11-heptacosadiene	0,00	-1,50	1,50								
100-51-6	benzyl alcohol									7,00		
100-52-7	benzaldehyde									1,00		
100-66-3	anisole				1,00		5,00	-0,50	2,00	3,00	4,00	
101-48-4	phenylacetaldehyde dimethyl acetal				50,50		9,20	31,60	12,67	6,00	-4,00	
10233-13-3	isopropyl laurate									1,00		
102-69-2	tripropylamine									5,00		
102-76-1	triacetin									2,00		
10281-56-8	(-)-beta-citronellene									-7,00		
10321-71-8	4-methyl-2-pentenoic acid									-4,00		
103-36-6	ethyl cinnamate									0,00		
103-37-7	benzyl butyrate				-4,00		23,20	24,00	20,00	4,00	-5,00	
103-45-7	phenylethyl acetate				-1,00		22,00	189,75	0,00	-12,00	-0,50	
103-48-0	phenethyl isobutyrate									4,00		
103-48-0	phenyethyl isobutyrate				-1,92	26,67	-2,33	155,92	0,17		-5,92	0,67
10361-39-4	benzyl valerate				5,50		-2,40	-0,40	9,33	10,00	-5,50	
103-65-1	propyl benzene									-1,00		
103-82-2	phenylacetic acid									1,00		
104410-91-5	(Z,Z)-7,11-nonacosadiene	-0,40	-1,50	2,50								
104-50-7	gamma octalactone									17,00		
104-55-2	cinnamaldehyde									3,00		
104-61-0	gamma-nonalactone									11,00		
104-67-6	undecanoic -gamma-lactone									15,00		
104-76-7	2-ethyl-1-hexanol				-6,00	200,00	1,33	-4,00	-0,67	-6,00	4,00	-2,67
10482-56-1	alpha-terpineol				35,50		36,00	-6,00	125,33	-2,00	-11,50	
104-93-8	4-methyl anisole									2,00		
105-37-3	ethyl propionate									12,00		
105-43-1	3-methylpentanoic acid									4,00		
105-54-4	ethyl butyrate				6,00		3,60	6,00	74,33	6,00	0,00	
105-66-8	propyl butyrate									9,00		
105-68-0	Isoamyl propionate				12,00		24,00	2,40	25,00	3,00	11,00	
105-79-3	isobutyl hexanoate									0,00		
105-87-3	geranyl acetate									1,00		
106-22-9	beta-citronellol									38,00		
106-24-1	geraniol									22,00		
106-25-2	nerol				8,00	219,33	24,67	-16,00	32,67	28,00	-6,00	-5,33
106-27-4	isoamyl butyrate				6,50		20,40	2,80	30,00	10,00	6,50	
106-32-1	ethyl octanoate									1,00		
106-35-4	3-heptanone									-5,00		
106-36-5	propyl propionate									14,00		
106-42-3	p-xylene anhydrous									-4,00		
106-44-5	p-cresol				17,00		10,00	12,80	22,33	3,00	92,50	
106-51-4	p-benzoquinone									-9,00		
106-65-0	dimethyl succinate									0,00		
106-68-3	3-octanone				46,50		57,60	-14,00	52,67	6,00	15,00	
106-70-7	methyl hexanoate									11,00		
106-73-0	methyl heptanoate		-7,20	1,20								
107-02-8	acrolein									1,00		
107-10-8	propylamine									9,00		
107-15-3	ethylenediamine									3,00		
107-35-7	taurine									2,00		
1074-43-7	3-propyltoluene									1,00		
1078-61-1	3,4-dihydroxyhydrocinnamic acid									3,00		
107-87-9	2-pentanone									-1,00		
107-92-6	butyric acid									2,33		
107-98-2	1-methoxy-2-propanol									2,00		
108-01-0	2-dimethylaminoethanol									1,00		
108-21-4	isopropyl acetate									5,00		
108-29-2	gamma-valerolactone				72,50		4,80	1,60	191,33	12,00	-1,50	
108-38-3	m-xylene									1,00		
108-64-5	ethyl isovalerate									0,00		
108-65-6	propylene glycol monomethyl ether acetate									-2,00		
108-86-1	bromobenzene									3,00		
108-88-3	toluene									1,00		
108-93-0	cyclohexanol									19,00		
108-94-1	cyclohexanone				-7,00		-1,20	6,40	39,33	14,00	-1,00	
108-95-2	phenol				1,00		6,40	-2,40	27,33	6,00	191,50	
109-19-3	butyl isovalerate									12,00		
109-21-7	butyl butyrate				19,50		42,40	0,00	28,00	5,00	-6,00	
109-52-4	valeric acid									1,00		
109-60-4	propyl acetate				0,00		-2,40	2,80	119,67	-4,00	1,00	
109-73-9	butylamine									-10,00		
109-89-7	diethylamine									1,00		
109-94-4	ethyl formate									1,00		
110-13-4	2,5-hexanedione									3,00		
110-19-0	Isobutyl acetate									4,00		
110-27-0	Isopropyl myristate									1,00		
110-38-3	ethyl decanoate									17,00		
110-42-9	methyl decanoate		-7,60	3,20								
110-43-0	2-heptanone				4,00		14,00	64,40	126,33	21,00	5,00	
110-54-3	hexane				-2,08	14,00	2,40	2,00	13,17	1,00	-4,00	0,67
110-58-7	pentylamine									-5,00		
110-60-1	1,4-diaminobutane									1,00		
110-62-3	valeraldehyde									2,00		
110-63-4	1,4-butanediol									-3,00		
110-73-6	2-(ethylamino)ethanol									10,00		
110-93-0	6-methyl-5-hepten-2-one									2,00		
111-11-5	methyl octanoate									11,00		
111-13-7	2-octanone									1,00		
111-14-8	heptanoic acid									0,00		
111-25-1	1-bromohexane									-2,00		
111-26-2	hexylamine									-5,00		
111-27-3	1-hexanol				12,00		17,20	-3,20	29,33	9,00	15,50	
111-66-0	1-octene									2,00		
111-68-2	heptylamine									1,00		
111-70-6	1-heptanol									11,00		
111-71-7	1-heptanal									5,00		
111-76-2	ethylene glycol butyl ether									16,00		
111-82-0	methyl laurate	-1,20	126,00	80,00								
111-87-5	1-octanol									23,00		
1120-21-4	undecane									0,00		
112-05-0	nonanoic acid									1,00		
112-12-9	2-undecanone									19,00		
112-14-1	octyl acetate									21,00		
1122-62-9	2-acetylpyridine									-4,50		
112-29-8	1-bromodecane									-9,00		
112-30-1	1-decanol									2,50		
112-31-2	decanal	-0,40	-14,00	-3,00								
112-39-0	methyl palmitate	-0,40	0,00	202,00								
112-40-3	docosane									2,00		
1124-11-4	2,3,5,6-tetramethylpyrazine									-2,00		
1124-39-6	4-ethylcatechol									-3,00		

112-44-7	undecanal									11,00			
112-54-9	dodecyl aldehyde									13,00			
112-62-9	methyl oleate									6,00			
112-70-9	1-tridecanol									9,00			
112-72-1	1-tetradecanol									0,00			
112-80-1	oleic acid									-3,00			
112-88-9	1-octadecene									2,00			
112-92-5	1-octadecanol		1,60	-0,80						2,00			
112-95-8	eicosane	0,40	1,50	3,00									
1139-30-6	(-)-caryophyllene oxide				15,33	33,33	4,00	-4,00	-12,67	-1,00	-11,33	8,00	
115-95-7	linalyl acetate									1,00			
116-53-0	(±)-2-methylbutyric acid									-6,00			
117-39-5	quercetin				2,00		2,40	2,50	3,00		2,50		
118-58-1	benzyl salicylate				7,50		4,00	-1,20	22,67	1,00	5,00		
118-61-6	ethyl salicylate									15,00			
1191-16-8	prenyl acetate									5,00			
119-33-5	4-methyl-2-nitrophenol				34,50		-0,40	-14,80	-2,00	4,00	-6,00		
119-36-8	methyl salicylate				36,00		39,20	-6,40	4,67	5,00	45,50		
1195-79-5	fenchone				153,00		9,60	-4,80	25,67		-10,50		
119-64-2	1,2,3,4-tetrahydronaphthalene									-3,00			
120-50-3	isobutyl benzoate				9,50	96,67	0,00	0,87	7,17	12,00	-1,17	-2,67	
120-51-4	benzyl benzoate				9,00		1,60	2,40	11,33	0,00	37,00		
120-72-9	indol				-0,67	47,33	2,67	-14,67	3,33	2,00	-1,33	13,33	
120-92-3	cyclopentanone									4,00			
1211-29-6	methyl jasmonate									9,00			
121-32-4	ethyl vanillin				1,00		-2,00	1,20	4,67		4,00		
121-33-5	vanillin				1,00		0,80	1,50	1,00		1,50		
121-44-8	triethylamine									4,00			
122-03-2	cuminaldehyde				4,00	156,00	10,00	-11,33	0,67	3,00	-2,00	2,67	
1222-05-5	Abbalide									0,00			
122-63-4	Benzyl propionate									6,00			
122-70-3	phenylethyl propionate				4,00		2,40	198,80	25,33	14,00	-3,00		
122-78-1	phenylacetaldehyde									12,00			
122-99-6	phenoxyethanol				-3,50		0,50	0,00	-3,33		3,50		
122-99-6	2-phenoxyethanol									5,00			
123-05-7	2-ethyl hexanal									-1,00			
123-07-9	4-ethyl phenol				15,50		14,00	10,80	31,67	2,00	81,00		
123-32-0	2,5-dimethyl pyrazine									5,00			
123-35-3	myrcene				8,67	53,33	7,33	4,67	-3,33	8,00	5,33	-2,00	
123-38-6	propionaldehyde									2,00			
123-42-2	4-hydroxy-4-methyl-2-pentanone									6,00			
123-51-3	isoamyl alcohol				3,50		-2,40	7,60	24,33		-3,50		
123-54-6	acetylacetone									1,00			
123-66-0	ethyl hexanoate									22,00			
123-72-8	butyraldehyde									0,00			
123-75-1	pyrrolidine				2,67	20,67	2,67	4,67	2,67	-1,00	2,00	-0,67	
123-86-4	butyl acetate									0,00			
123-92-2	isoamyl acetate				9,00		3,20	6,80	37,33	16,00	-1,00		
123-93-3	2,2'-thiodiacetic acid									-6,00			
124-07-2	octanoic acid									5,00			
124-10-7	methyl myristate	0,40	0,00	140,00						5,00			
124-13-0	octanal									9,00			
124-19-6	nonanal	1,60	-8,50	-2,50									
124-38-9	carbone dioxide												220,00
124-76-5	isoborneol									6,00			
126-90-9	S-(+)linalool									7,00			
126-91-06	R-(-)linalool									2,00			
127-17-3	pyruvic acid									6,00			
127599-39-7	(Z,Z)-7,11-pentacosadiene	-0,40	1,50	1,50									
128-37-0	butylated hydroxytoluene				-9,00		-1,20	-0,40	7,33		-7,50		
13327-56-5	ethyl3-(methylthio)propionate				115,00		90,40	-8,00	44,33	5,00	-3,00		
1336-21-6	ammonium hydroxide solution									5,00			
134-20-3	methyl 2-aminobenzoate									-3,00			
134-62-3	N,N-diethyl-3-methylbenzamide (DEET)									11,00			
135-79-5	6-isopropylquinoline									4,00			
136-27-5	limonene				10,00		12,40	0,00	8,33		-6,00		
136-60-7	butyl benzoate				1,00		22,00	-3,60	11,33	3,00	-10,25		
137-32-6	2-methyl-1-butanol									6,00			
13877-91-3	ocimene				9,75	61,33	7,00	0,75	6,67	15,00	-2,00	0,67	
140-11-4	benzyl acetate				5,50		2,00	133,60	27,33	0,00	-3,00		
140-29-4	benzyl cyanide				-3,33	88,00	216,67	-14,00	231,33	23,00	-10,00	2,67	
14073-97-3	(-)-menthone				0,50		-0,60	-6,65	46,83	-14,00	-2,75		
141-12-8	neryl acetate									1,00			
141-78-6	ethyl acetate				0,00		4,80	-1,60	121,33	-2,00	0,00		
142-62-1	hexanoic acid									7,00			
142-83-6	trans,trans-2,4-hexadienal									-4,00			
142-91-6	isopropyl palmitate									3,00			
142-92-7	hexyl acetate									9,00			
143-07-7	dodecanoic acid		-1,20	0,80						5,00			
143-08-8	1-nonanol									5,50			
143-13-5	nonyl acetate									2,00			
143-28-2	oleyl alcohol		0,00	2,00									
1454-85-9	1-heptadecanol		-0,80	2,00									
1461-03-6	beta-himachalene				10,67	22,67	0,67	-4,00	-4,00	4,00	-2,67	2,00	
149-57-5	2-ethyl hexanoic acid									5,00			
1502-06-3	cyclodecanone									0,00			
1560-78-7	2-methyl tetracosane	0,00	0,50	1,00									
1560-81-2	2-methyl docosane	1,60	1,00	1,50									
1560-98-1	2-methyl octacosane	0,00	-4,00	2,00									
1561-02-0	2-methyl hexacosane	0,00	-1,00	0,50									
1569-60-4	(±)-6-methyl-5-hepten-2-ol									9,00			
15706-73-7	butyl 2-methylbutyrate									1,00			
15707-24-1	2,3-diethylpyrazine									3,00			
1576-95-0	cis-2-penten-1-ol									1,00			
1577-18-0	trans-3-hexenoic acid									1,00			
16423-19-1	geosmin									-2,00			
16491-36-4	cis-3-hexenyl butyrate									38,00			
17283-81-7	dihydro-beta-ionone									0,00			
1731-84-6	methyl nonanoate		-1,20	3,20									
1733-25-1	isopropyl tiglate				48,50		67,20	-6,40	32,67	0,00	0,00		
1758-88-9	2-ethyl-p-xylene									1,00			
1775-43-5	3-hexenoic acid, (3Z)-									-1,00			
18172-67-3	(1s)-(-)-beta-pinene									5,00		-1,33	
18362-97-5	isopropyl pentanoate				5,50		31,60	-12,00	19,67	0,00	2,00		
18368-91-7	2-ethylfenchol				17,42	26,00	7,53	-2,87	11,00	4,00	-8,42	-16,00	
1839-63-0	1,3,5-trimethylcyclohexane									-10,00			
18402-82-9	trans-3-octen-2-one									12,00			
19322-27-1	4-hydroxy-5-methyl-3-furanone									-1,00			
19870-74-7	methyl cedryl ether				6,00	22,00	0,67	-7,33	0,00	3,00	-2,00	0,00	
2004-38-9	1-heptacosanol		-5,20	2,80									
203719-54-4	(+)-limonene oxide				10,67	159,33	4,67	-1,33	14,00	36,00	-6,67	6,67	
2049-96-9	n-pentyl benzoate				1,00		2,00	5,60	5,33	5,00	-3,50		
2050-09-1	isoamyl valerate									5,00			
2067-33-6	5-bromovaleric acid									-0,50			
21061-10-9	cis-8 11 14-eicosatrienoic acid methyl ester		0,00	0,40									
2173-56-0	pentyl valerate									7,50			
2198-61-0	isopentyl hexanoate				2,00		-0,80	1,20	20,00	2,00	0,50		

22104-79-6	cis-2-nonen-1-ol										1,00		
2213-23-2	2,4-dimethylheptane										0,00		
2217-02-9	(1R)-(+)-fenchyl alcohol				200,50		26,00	-4,80	-0,67	5,00	-10,50		
22331-09-5	5-methyl tricosane	0,00	-0,50	3,00									
2315-68-6	propyl benzoate				11,00		32,80	-8,80	13,00	-1,00	18,50		
2344-70-9	4-phenyl-2-butanol				7,00		12,40	122,00	12,67	2,00	4,00		
2371-42-8	2-methylisoborneol									2,00			
2396-78-3	methyl trans-3-hexenoate									1,67			
2416-20-8	Z-11-hexadecenoic acid									2,00			
2445-67-2	isobutyl-2-methyl butyrate									10,00			
2497-18-9	trans-2-hexenyl acetate									19,00			
25152-85-6	cis-3-hexenyl benzoate				6,50		26,80	-0,80	20,33	-1,00	-3,00		
2623-87-2	4-bromobutyric acid									-10,00			
2628-17-3	4-vinyl phenol				7,50		-1,60	7,20	23,33	4,00	16,00		
2639-63-6	hexyl butyrate									19,00			
27519-02-4	(Z)-9-tricosene	0,80	-1,85	1,95									
27625-35-0	isoamyl 2-methylbutyrate									1,00			
2785-89-9	4-ethyl guaiacol				44,50		24,40	-4,00	20,67	0,00	0,50		
2896-60-8	4-ethylresorcinol				10,50		9,20	-0,80	14,67	0,00	3,00		
301-00-8	methyl linoleate									8,00			
3074-71-3	2,3-dimethyl heptane									3,00			
3142-72-1	2-methyl-2-pentenoic acid									12,00			
31501-11-8	cis-3-hexenyl hexanoate									12,00			
3240-09-3	5-methyl-5-hexen-2-one									4,00			
32665-23-9	isopropyl isopentanoate				19,50		36,80	-17,60	24,00	1,00	1,00		
331-39-5	caffeic acid									-6,00			
3338-55-4	z-beta-ocimene									-2,00			
334-48-5	decanoic acid									0,00			
33467-73-1	cis-3-hexenyl formate									2,00			
33467-74-2	cis-3-hexenyl propionate									8,00			
3350-30-9	cyclononanone									8,00			
3387-41-5	(+)-sabinene									2,00			
33880-83-0	beta-elemene									12,00			
3391-86-4	1-octen-3-ol									16,00			
3407-42-9	Sandenol									2,00			
35154-45-1	cis-3-hexenyl 3-methylbutanoate									-3,00			
35852-46-1	hexenyl-cis-3-valerate									0,00			
3658-80-8	dimethyl trisulfide									3,00			
36653-82-4	1-hexadecanol									7,00			
36759-47-4	decahydro-2-naphthol									-1,00			
3681-71-8	cis-3-hexenyl acetate									1,00			
3681-82-1	trans-3-hexenyl acetate									8,00			
3687-48-7	(R)-(-)-1-octen-3-ol									13,00			
37112-31-5	levoglucosenone									4,00			
373-49-9	palmitoleic acid		0,40	-0,80									
3796-70-1	geranyl acetone	0,00	-16,00	-4,50						47,00			
38462-23-6	maritima									12,00			
3856-25-5	(-)-a-copaene									-1,00			
3943-89-3	ethyl protocatechuate				2,50		2,40	1,00	1,00		1,00		
40716-66-3	trans-nerolidol									9,00			
41519-23-7	cis-3-hexenyl isobutyrate									1,00			
42125-10-0	cis-2-penten-1-yl acetate									2,00			
4224-70-8	6-bromohexanoic acid									1,00			
4229-91-8	2-n-propylfuran									2,00			
4276-49-7	1-bromoeicosane									-1,00			
431-03-8	2,3-butanedione									7,00			
4412-91-3	furan-3-methanol									2,00			
4437-20-1	furfuryl disulfide									-4,00			
4442-79-9	2-cyclohexylethanol				34,50		22,80	56,80	16,00	4,00	-3,00		
4602-84-0	farnesol				5,00	16,67	4,47	-3,07	11,33	123,00	1,83	-0,67	
462-94-2	cadaverine									7,00			
4630-07-3	valencene				28,00	53,00	6,00	-3,33	-8,00	9,00	11,33	-5,33	
464-43-7	(+)-borneol									9,00			
464-48-2	(-)-camphor									-2,00			
4674-50-4	(+)-nootkatone									5,00			
469-61-4	(-)-alpha-cedrene				-0,67	16,67	1,33	-4,67	8,00	1,00	-0,67	0,67	
470-82-6	eucalyptol									4,00			
475-20-7	(+)-longifolene				-1,33	17,33	1,33	-6,00	0,67	3,00	-10,67	2,00	
4906-24-5	acetoin acetate									1,00			
498-02-2	acetovanillone				-3,00		-1,00	2,50	-1,33	0,00	10,50		
498-15-7	(1S)-(+)-3-carene				97,33	55,33	0,00	0,00	2,00	0,00	-8,00	2,00	
4984-01-4	3,7-dimethyl-1-octene									1,00			
501-94-0	Tt				1,00		0,80	5,50	1,00		5,50		
501-97-3	3-(4-hydroxyphenyl)propionic acid									-4,00			
501-98-4	p-coumaric acid									-1,00			
502-47-6	citronellic acid									2,00			
502-61-4	farnesene				5,00		4,00	6,00	6,67	22,00	2,00		
502-69-2	6,10,14-trimethyl-2-pentadecanone									-1,00			
503-74-2	Ii				-2,00		9,20	0,80	22,00	2,00	0,00		
505-10-2	methionol				2,00		-4,00	6,80	24,00	-5,00	1,00		
506-42-3	Ee		0,40	1,20									
50-78-2	acetylsalicylic acid									4,00			
513-85-9	2,3-butanediol									8,50			
513-86-0	acetoin									2,00			
520-18-3	kaempferol				1,00		0,80	1,50	1,00		1,50		
5204-64-8	3-pentenoic acid									-1,00			
52078-42-9	(Z)-7-tricosene	1,20	-1,50	1,00									
529-44-2	myricetin				3,00		2,80	1,00	2,00		1,00		
53398-80-4	trans-2-hexenyl propionate									4,00			
53398-83-7	trans-2-hexenyl butyrate									2,00			
53398-86-0	n-caproic acid trans-2-hexen-1-yl ester									18,00			
535-77-3	m-cymene				6,00	48,67	0,67	-10,00	0,00	5,00	10,00	-2,00	
537-98-4	ferulic acid									-1,00			
5392-40-5	citral				18,00	241,33	4,00	-6,00	2,67	17,00	-2,67	5,33	
53939-28-9	Z-11-hexadecen-1-al									9,00			
539-90-2	isobutyl butyrate									15,00			
540-07-8	n-amyl hexanoate				-1,33	74,67	2,67	-8,67	2,00	12,00	-4,00	10,67	
5405-41-4	ethyl-3-hydroxy butyrate									3,00			
54-11-5	L-(-)-nicotine									2,00			
541-47-9	3,3-dimethyl acrylic acid									-1,00			
543-49-7	2-heptanol									3,00			
544-63-8	myristic acid		-2,00	1,20						-2,00			
544-76-3	hexadecane	-1,60	-0,50	1,00						1,00			
546-28-1	(+)-ß-cedrene				-0,67	18,00	2,00	-0,67	-2,00	0,00	-4,00	0,00	
547-63-7	methyl isobutyrate									0,50			
553-97-9	p-toluquinone									5,00			
554-12-1	methyl propionate									1,00			
554-84-7	3-nitrophenol									-3,00			
556-82-1	3-methyl-2-buten-1-ol									1,00			
55704-78-4	2,5-dimethyl-2,5-dihydroxy-1,4-dithiane									0,00			
563-80-4	3-methyl-2-butanone									2,00			
56539-66-3	3-methoxy-3-methyl-1-butanol									16,00			
5655-61-8	(-)-bornyl acetate				5,00	20,67	5,33	-2,67	1,33	13,50	-1,67	4,67	
565-63-9	2-methyl-cis-2-butenoic acid									6,00			
56683-54-6	z-11-hexadecen-1-ol									14,00			
56-84-8	L-aspartic acid									-2,00			
56-86-0	L-glutamic acid									-1,00			

57-06-7	allyl isothiocyanate										-1,00		
57-10-3	palmitic acid										-1,00		
57-11-4	stearic acid		-1,60	4,40							0,00		
57-55-6	1,2-propanediol				10,00		0,00	4,80	28,67	2,00	0,00		
5794-03-6	(+)-camphene				10,67	24,00	6,00	-4,00	8,67	3,00	0,67	1,33	
5794-04-7	(-)-camphene				14,00	17,33	3,33	0,00	9,33	-1,00	-4,67	-4,67	
5837-78-5	ethyl tiglate									2,00			
586-62-9	terpinolene				4,25	64,00	0,87	1,58	3,50	6,00	-0,75	7,33	
58917-26-3	(S)-6-methyl-5-hepten-2-ol									4,00			
58917-27-4	(R)-6-methyl-5-hepten-2-ol									5,00			
589-35-5	3-methyl-1-pentanol									-3,00			
589-59-3	isobutyl Isovalerate									-2,00			
589-91-3	4-methylcyclohexanol(cis+trans)									-1,00			
589-98-0	3-octanol									9,00			
590-90-9	4-hydroxy-2-butanone									-6,00			
591-23-1	3-methylcyclohexanol									13,00			
591-78-6	2-hexanone									-7,00			
593-45-3	octadecane	0,40	-1,50	3,00									
593-49-7	heptacosane	3,20	3,50	3,50						2,00			
5989-27-5	R-(+)-limonene				3,33	64,00	6,67	-6,67	5,33	-4,00	1,33	3,33	
5989-54-8	S-(-)-limonene				7,33	61,33	4,00	-4,00	10,00	11,00	1,33	3,33	
60047-17-8	linalool oxide									7,00			
60-12-8	2-phenylethanol									-1,00			
60-18-4	L-tyrosine									8,00			
60-24-2	2-mercaptoethanol				8,00		8,80	6,80	18,00	2,00	17,50		
6032-29-7	2-pentanol									2,00			
60-33-3	linoleic acid									5,00			
603-76-9	1-methylindole				14,00	179,33	8,67	-20,00	2,00	-16,00	-11,33	11,33	
60415-61-4	2-pentyl butyrate									3,00			
60763-41-9	alpha-pentylcinnamaldehyde diethyl acetal									4,00			
607-91-0	myristicin									-4,00			
611-14-3	2-ethyltoluene									4,00			
614-96-0	5-methylindole									-13,00			
616-25-1	1-penten-3-ol									18,00			
616-45-5	2-pyrrolidinone									4,00			
61692-84-0	Isobutyl tiglate				12,00		4,40	-2,40	21,67	10,00	10,50		
6186-98-7	cis-vaccenyl acetate	91,60	-1,50	0,50									
620-14-4	3-ethyl toluene									3,00			
620-17-7	3-ethylphenol				-0,50		0,50	-5,50	0,00	1,00	10,00		
622-96-8	4-ethyl toluene									3,00			
623-42-7	methyl butyrate									0,00			
623-70-1	ethyl crotonate									0,50			
624-92-0	dimethyl disulfide									6,00			
626-38-0	acetic acid-2-pentyl ester									0,00			
626-77-7	propyl hexanoate				13,50		22,80	-6,80	25,33	11,00	-4,50		
626-82-4	butyl hexanoate				-4,50		3,20	1,60	27,33	5,00	-5,00		
626-89-1	4-methyl-1-pentanol									3,50			
628-63-7	pentyl acetate									4,00			
628-99-9	2-nonanol				23,00		22,00	-10,80	17,33	12,00	63,50		
629-19-6	dipropyl disulfide									2,00			
629-50-5	tridecane	0,40	1,00	3,00									
629-59-4	tetradecane	1,20	0,00	4,00						-1,00			
629-62-9	pentadecane	0,00	-1,50	2,50									
629-72-1	1-bromopentadecane									4,00			
629-73-2	hexadecene	2,00	-5,50	0,50									
629-78-7	heptadecane	-0,40	1,50	2,00									
629-94-7	heneicosan	2,00	3,00	3,00						1,00			
629-96-9	1-eicosanol		0,00	2,40									
629-97-0	docosane	4,40	0,00	3,50						9,00			
629-99-2	pentacosane	0,80	2,00	5,00						2,00			
630-01-3	hexacosane	-1,20	-3,00	4,00						1,00			
630-02-4	octacosane	-1,60	2,50	2,00						11,00			
630-03-5	nonacosane	0,40	1,75	2,00									
63623-49-4	(Z)-7-pentacosene	0,40	1,00	1,00									
6378-65-0	hexyl hexanoate									5,00			
638-67-5	tricosane	0,40	-2,00	0,00						-2,00			
64-04-0	phenylethylamine									-1,00			
64-17-5	ethanol				1,67	2,67	7,00	3,93	15,00	8,00	-1,00	2,67	
64-18-6	formic acid									3,00			
64-19-7	acetic acid									0,00			
64275-73-6	cis-5-octen-1-ol				8,67	180,67	13,33	-12,67	6,00	-2,00	-14,00	-24,67	
646-07-1	4-methylvaleric acid									1,00			
646-31-1	tetracosane	2,00	-2,50	0,00						2,00			
65405-77-8	cis-3-hexenyl salicylate									5,00			
65405-80-3	cis-2-hexenyl crotonate									-11,00			
65-85-0	benzoic acid									-3,00			
659-70-1	isoamyl isovalerate									1,00			
659-76-5	1-pentadecanol									5,00			
661-19-8	1-docosanol		-1,60	2,80									
66-25-1	hexanal									-1,00			
675-20-7	d-valerolactam									2,00			
6753-98-6	alpha-humulene				6,00	29,33	2,00	-5,33	3,33	-5,00	-7,33	2,67	
67-56-1	methanol				0,00		-1,20	5,20	135,33		14,00		
67-71-0	dimethyl sulfone									1,00			
67883-79-8	cis-3-hexenyl tiglate				6,67	72,00	9,33	-2,67	-2,00	1,00	-2,67	8,00	
6789-80-6	cis-3-hexanal									12,00			
687-47-8	(-)-ethyl L-lactate									3,00			
6920-22-5	1,2-hexanediol									1,00			
695-06-7	gamma-hexalactone									13,50			
706-14-9	gamma-decanolactone									3,00			
71-23-8	1-propanol									5,00			
71-36-3	1-butanol									12,00			
71-41-0	1-pentanol									14,00			
71820-56-9	3-methyl-2-butenyl butanoate									7,00			
7452-79-1	ethyl 2-methylbutyrate									7,00			
75-04-7	ethylamine									12,00			
75-09-2	dichloromethane (DCM)				0,00	9,33	0,67	11,33	11,33	2,00	3,33	2,67	
7541-49-3	phytol									9,00			
75-47-8	iodoform									1,00			
75-50-3	trimethylamine									-2,00			
75-85-4	2-methyl-2-butanol									2,50			
76-22-2	(+) camphor									5,00			
76-49-3	bornyl acetate				1,33	13,33	2,67	-7,33	1,33	26,00	-0,67	7,33	
76649-23-5	vertenol-iso-butyrate									1,00			
77-83-8	ethyl 3-methyl-3-phenylglycidate									-3,00			
7785-26-4	(-)-alpha-pinene				47,33	37,33	5,33	2,00	0,67		-1,33		
7786-61-0	2-methoxy-4-vinylphenol				19,50		-0,40	4,20	16,00	3,00	6,25		
7787-20-4	(1R)-(-)-fenchone									5,00			
78-70-6	linalool									10,00			
78-79-5	isoprene									1,00			
78-81-9	isobutylamine									0,00			
78-83-1	isobutanol				5,00		1,20	-6,00	26,67	-1,00	3,50		
78-93-3	2-butanone				4,00		1,20	-2,40	56,67		7,50		
79-09-4	propionic acid									-13,00			
79-10-7	acrylic acid									3,00			
79-20-9	methyl acetate									14,00			
79-31-2	isobutyric acid									1,00			

79-33-4	L-(+)-lactic acid									-1,00			
79-41-4	methacrylic acid									1,00			
79-77-6	beta-ionene				189,33	126,67	-8,00	-16,67	-7,33		-10,00	6,67	
79-77-6	beta-ionone									0,00			
8001-28-3	croton oil									-2,00			
8006-87-9	sandalwood-oil									31,00			
80-56-8	alpha-pinene				35,33	26,67	10,00	-7,33	8,00	9,00	-4,67	6,00	
80-59-1	trans-2-methyl-2-butenoic acid									5,00			
80-71-7	2-hydroxy-3-methyl-2-cyclopenten-1-one									-3,00			
81-14-1	musk ketone									1,00			
821-55-6	2-nonanone				9,50		8,00	-3,60	27,67	2,00	12,50		
831-61-8	ethyl gallate				1,00		1,20	8,50	1,00		8,50		
83-34-1	skatole				11,00		4,40	-3,00	19,00	-4,00	-4,00		
83863-30-3	ylang ylang									12,00			
868-57-5	methyl 2-methylbutyrate									5,00			
871-83-0	2-methylnonane									-2,00			
872-05-9	1-decene									-3,00			
872-50-4	1-methyl-2-pyrrolidinone									1,00			
87-25-2	ethyl 2-aminobenzoate									-4,00			
87259-94-9	7-methyl tricosane	0,00	-4,00	1,50									
87-44-5	(-)-trans-caryophyllene				6,67	20,00	1,33	-7,33	2,67	1,00	-5,33	0,67	
878-13-7	cyclounedecanone									-6,00			
89026-29-9	3-methyl-2-butenyl-3-methyl butanoate									-1,00			
89-68-9	4-chloro-2-isopropyl-5-methylphenol									1,00			
90-02-8	salicylaldehyde									-2,00			
90-05-1	guaiacol				9,50		0,00	0,00	19,00	11,00	21,50		
91-20-3	naphthalene									5,00			
91-62-3	6-methylquinoline									0,00			
928-95-0	trans-2-hexen-1-ol									9,00			
928-96-1	cis-2-hexen-1-ol									4,00			
928-96-1	cis-3-hexen-1-ol									22,00			
928-97-2	trans-3-hexen-1-ol									-4,00			
93-15-2	methyl eugenol				12,00		-3,60	-1,20	8,00	-1,00	3,00		
93-16-3	methyl isoeugenol									5,00			
933-67-5	7-methylindole									-5,00			
93-55-0	propiophenone									1,00			
93-58-3	methyl benzoate				28,00		58,80	-5,20	15,33	3,00	110,00		
93-89-0	ethyl benzoate				-4,00		120,00	-8,00	12,67	15,00	-17,00		
939-48-0	isopropyl benzoate				4,11	166,67	44,53	-2,22	16,67	11,00	-0,72	6,00	
94-46-2	isoamyl benzoate				3,00		4,80	9,20	22,00	11,00	12,00		
95-16-9	benzothiazole									1,00			
95-20-5	2-methylindole									-7,00			
95-47-6	o-xylene									-1,00			
95-48-7	2-methylphenol				1,33	96,00	-2,00	-25,33	1,33	-13,00	-46,00	7,33	
95-50-1	o-dichlorobenzene									4,00			
95-63-6	1,2,4-trimethylbenzene									2,00			
96-48-0	4-hydroxybutanoic acid lactone									4,00			
97-42-7	(-)-carvyl acetate				6,50		1,20	-10,50	5,67	12,00	-0,50		
97-53-0	eugenol				15,50		11,20	-10,00	17,67	0,00	15,50		
97-54-1	isoeugenol				3,50		0,00	0,40	16,67	0,00	1,00		
97-64-3	ethyl lactate									1,00			
97-85-8	isobutyl isobutyrate									19,00			
97-96-1	2-ethylbutyraldehyde									-1,00			
98-00-0	furfuryl alcohol				16,50		40,40	29,20	12,00	5,00	22,50		
98-01-1	furfural									-1,00			
98-82-8	cumene									12,00			
98-85-1	phenylethanol				0,50		31,00	-6,00	2,00		19,50		
98-86-2	acetophenone				127,50		23,60	-2,80	56,00	5,00	-12,50		
99-83-2	alpha-phellandrene				16,67	38,00	2,00	1,33	14,00	-1,00	1,33	6,00	
99-85-4	gamma-terpinene				4,00	66,00	7,08	0,92	-0,67	1,00	3,92	7,33	
99-86-5	alpha-terpinene				6,67	68,67	11,33	-4,00	14,00	2,00	-1,33	-2,00	
99-87-6	p-cymene				-2,67	36,00	8,00	-6,00	-0,67	-1,00	6,67	0,67	
NA	(Z,Z)-7,11-octacosadiene	0,00	1,00	1,00									
	oil				3,00		-1,20	0,80	7,67	10,00	1,00		
	water				4,00		6,40	-1,20	18,00		2,00		

Manuscript 4

Parallel olfactory pathways support odor valence and intensity coding in the lateral horn of *Drosophila melanogaster*

Amelie Baschwitz, Jan Soelter, Natalia Marquez, Jürgen Rybak, Michael Schmuker, Bill S. Hansson, Silke Sachse

In preparation for eLife

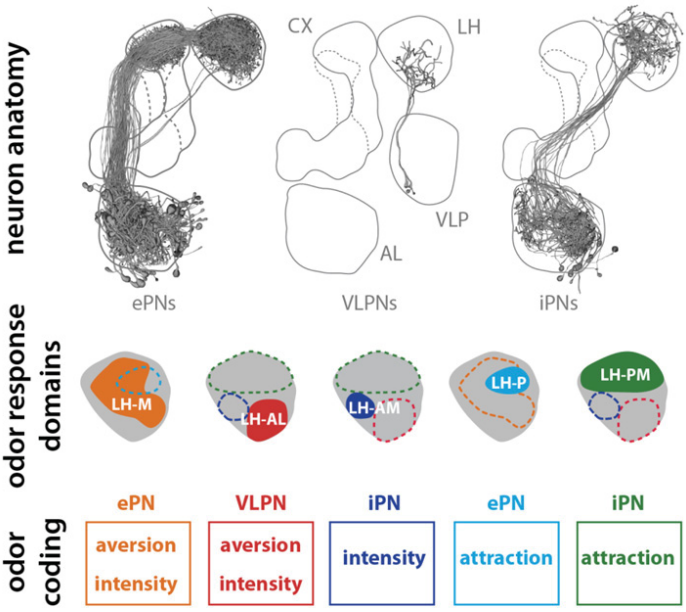

Parallel olfactory pathways support odor valence and intensity coding in the lateral horn of *Drosophila melanogaster*

Amelie Baschwitz [§1], Jan Sölter [§2], Natalia Marquez [1], Jürgen Rybak [1], Michael Schmuker [3], Bill S. Hansson [1], Silke Sachse *[1]

[§] These authors contributed equally to this work.

[1] Max Planck Institute for Chemical Ecology, Department of Evolutionary Neuroethology, Hans-Knöll-Str. 8, 07745 Jena, Germany

[2] Free University Berlin, Neuroinformatics & Theoretical Neuroscience, Department for Biology, Pharmacy and Chemistry, Königin-Luise-Strasse 1-3, 14195 Berlin, Germany

[3] University of Hertfordshire, School of Computer Science, College Lane, Hatfield, Herts AL10 9AB, United Kingdom

*Correspondence:

Dr. Silke Sachse, Department of Evolutionary Neuroethology,

Max Planck Institute for Chemical Ecology, Hans-Knöll-Str. 8, 07745 Jena, Germany.

Tel: +49-3641-571405, Fax: +49-3641-571402

Email: ssachse@ice.mpg.de

Key Words:

Drosophila melanogaster, excitatory projection neurons, odor response domains, lateral horn, odor valence, innate odor-guided behavior

Abstract

Vinegar flies show an innate odor-guided behavior to food, mating partners, oviposition sites, predators and harmful microbes. It is widely assumed that innate odor-guided behavior is mediated in the lateral horn (LH), a higher brain center of the protocerebrum. Two populations of projection neurons – excitatory (ePNs) and inhibitory (iPNs) – convey the odor information to the LH. A clear morphological and physiological separation in the LH according to the representation of specific odor features, such as valence and odor intensity, was previously demonstrated for iPNs. To investigate these properties in ePNs, we analyzed *in vivo* the terminal fields of all ePNs of the same origin, and the odor response patterns using functional calcium imaging. Additionally, we investigated the neural circuit of ePNs to third-order neurons of the ventrolateral protocerebrum that are inhibited by iPNs. Our study reveals that ePNs, similar to iPNs, categorize odor responses due to intensity and valence in the LH in two odor response domains. Furthermore, subpopulations of ePNs and iPNs innervating the same regions in the primary olfactory processing center also innervate the same areas in the LH. Thus, via parallel pathways ePNs and iPNs convey olfactory information categorized according to ecological relevance distinctly to the LH. As ePNs and iPNs synapse to the same set of third-order neurons they modulate – in opposite manner – the neural circuitry of innate odor-guided behavior.

Introduction

The vinegar fly *Drosophila melanogaster* encounters a plethora of odors while encountering the environment. The approach to or escape from an odor source are subject to innate preferences depending on specific odor features, such as odor identity, valence and intensity. Those specific odor features are extracted through neural processing of odor information in the fly´s brain. In the primary olfactory processing center, the antennal lobe (AL), odor features are represented by odor-specific and spatially restricted neuronal activity. Nevertheless, little is known about the representation of odor features in the higher brain center mediating innate preference, the lateral horn (LH). Due to the genetic accessibility the vinegar fly *Drosophila melanogaster* is an attractive model organism to examine the neural circuit in the LH.

The peripheral olfactory organs, antenna and maxillary palp, are equipped with hair-like structures called sensilla, which house olfactory sensory neurons (OSNs). OSNs expressing the same chemoreceptor transfer odor information to distinct subunits in the AL, called glomeruli. Within glomeruli, OSNs, projection neurons (PNs), and local interneurons (inter-) connect onto each other to modulate the received odor information. Two major PN populations exist in the olfactory system of *Drosophila*: excitatory, uniglomerular PNs (ePNs), and inhibitory, multiglomerular PNs (iPNs). Via the medial AL tract

(mALT; formerly inner antennocerebral tract iACT) ePNs innervate the higher brain centers the mushroom body calyx and the LH. A few ePNs innervate via the lateral AL tract (lALT; formerly outer antennocerebral tract, oACT) first the LH and then the mushroom body calyx (Jefferis et al., 2007; Stocker et al., 1997; Tanaka et al., 2012). In contrast, iPNs innervate via the mediolateral AL tract (mlALT; formerly middle antennocerebral tract, mACT) directly and solely the LH (Ito et al., 1997; Jefferis et al., 2007; Lai et al., 2008; Liang et al., 2013; Okada et al., 2009; Stocker et al., 1990; Tanaka et al., 2004). Furthermore, odor information is conveyed in parallel pathways by ePNs and iPNs to the LH (Wang et al., 2014). While the mushroom body calyx is essential for learning and memory (reviewed by (Davis, 2005; Heisenberg, 2003), the LH is described to be responsible for innate behavior (Heimbeck et al., 2001; Kido and Ito, 2002; Min et al., 2013; Strutz et al., 2014; Wang et al., 2003b; Xia and Tully, 2007).

So far, only few studies analyzed the morphological and physiological properties of neurons belonging to the neural circuit in the LH mediating innate odor-guided preference. The terminal fields of ePNs are distinct and highly stereotypic (Jefferis et al., 2007; Marin et al., 2002; Wong et al., 2002), whereas iPNs are separated in two groups due to the innervated area of the LH (Strutz et al., 2014). Depending on the innervated area subsets of ePNs are described to be spatially segregated either due to glomerular subgroups (Tanaka et al., 2004), ePNs responding to food and pheromone odors (Jefferis et al., 2007; Liang et al., 2013), as well as segregated in ePNs responding to attractive amines and ammonia or aversive carbon dioxide (Min et al., 2013). While functional analysis in iPNs revealed that they code either odor valence or intensity (Strutz et al., 2014), the representation of odors in the LH was investigated in ePNs only for few odors (Liang et al., 2013; Parnas et al., 2013) or simulated for food odors (Jefferis et al., 2007). The further relay of odor information to the several described types of third-order neurons, i.e. LH neurons (LHNs), was analyzed only for few LHN subsets (Cachero et al., 2010; Fişek and Wilson, 2014; Jefferis et al., 2007; Kohl et al., 2013; Lai et al., 2008; Ruta et al., 2010; Strutz et al., 2014; Tanaka et al., 2004; Yu et al., 2010). Hence, the neuronal properties of odor representations and their functional consequences are not fully understood. Therefore, we asked in this study whether ePNs can also be categorized morphologically and physiologically in subpopulations in the LH according to specific odor features, such as odor valence and intensity as described for iPNs. Furthermore, we investigated if ePNs are connected to third-order neurons of the ventrolateral protocerebrum (VLP), which are inhibited by iPNs (Liang et al., 2013; Strutz et al., 2014). To investigate the neural representation of ePNs we analyzed the *in vivo* innervation pattern in the LH of all ePNs innervating a specific glomerulus and the odor response patterns of several odors using functional calcium imaging. We compared the innervation patterns and the odor response patterns of ePNs with the previously published data of iPNs

(Strutz et al., 2014). Additionally, we investigated the neural circuit of ePNs with neurons of the VLP using microlesion during functional imaging.

Our study reveals that the stereotypical innervation patterns of ePNs retain the topographic map of the AL in the LH. Comparing the innervation pattern of ePNs and iPNs provides evidence that PNs that innervate overlapping regions in the AL also innervate overlapping regions in the LH. Furthermore, odor responses of ePNs in the LH can be separated due to the coding of odor valence and intensity in two odor response domains. Additionally, odor response domains coding the same odor features overlap in ePNs and iPNs. Both ePNs and iPNs responding to aversive odors connect to third-order neurons of the VLP.

We conclude that ePNs and iPNs receive odor information from the same subset of AL glomeruli and transfer this information via parallel pathways to the same regions in the LH. Via release of antagonistic neurotransmitters ePNs and iPNs modulate the odor responses of third-order neurons of the VLP.

Results

LH innervation of individual excitatory PNs are similar but not identical

The lateral horn (LH) is the target region of the axons of excitatory, uniglomerular projection neurons (ePNs) and of inhibitory, multiglomerular PNs (iPNs). About 90 of the estimated 120 ePNs are distinctly labeled by the enhancer trap line *GH146-GAL4* (Heimbeck et al., 2001; Stocker et al., 1997). Notably, *GH146-GAL4* labels in the ventral cell cluster around six PNs that express the inhibitory neurotransmitter gamma-aminobutyric acid (Wilson and Laurent, 2005). About 40 of the approximately 50 iPNs are distinctly labeled by *MZ699-GAL4* (Ito et al., 1997; Lai et al., 2008; Okada et al., 2009). In previous studies the morphology of ePNs was obtained *in vitro* by labeling all GH146+ neurons (Heimbeck et al., 2001; Stocker et al., 1997) or by selectively labeling single neurons using MARCM (Mosaic Analysis with a Repressible Cell Marker) (Jefferis et al., 2007; Marin et al., 2002; Wong et al., 2002). On the other hand, iPNs were analyzed *in vivo* using photoactivatable green fluorescent protein (pa-GFP) (Datta et al., 2008; Patterson and Lippincott-Schwartz, 2002; Ruta et al., 2010) to label single multiglomerular MZ699+ PNs (Strutz et al., 2014). To compare the morphology of all GH146+ PNs with the *in vivo* data of MZ699+ PNs we labeled *in vivo* all PNs innervating a specific glomerulus using the GAL4-UAS system to express pa-GFP under control of the *GH146-GAL4* line (Brand and Perrimon, 1993; Datta et al., 2008; Patterson and Lippincott-Schwartz, 2002; Ruta et al., 2010; Stocker et al., 1997; Strutz et al., 2014). This approach enables to analyze the LH innervation considering the proportion of terminal fields of PNs of single glomeruli. Notably, each glomerulus is innervated by a specific but varying number of GH146+ PNs ranging from only one up to eight PNs per glomeru-

lus (Figure 1-figure supplement 1; see also (Grabe et al., 2016)). Our *in vivo* data comprises about 185 reconstructed neurons that innervate 37 out of the total 54 glomeruli in the AL, which represents ≈69% of glomeruli innervated by GH146+ PNs (Grabe et al., 2015). For clarity GH146+ PNs were named by the glomerulus they innervate by applying the nomenclature and glomerular innervation described in (Grabe et al., 2015). Sister PNs innervate the same glomerulus. To simplify reading we abbreviate GH146+ PNs with ePNs and MZ699+ PNs with iPNs.

Labeling all ePNs revealed a dense innervation in almost the entire lateral horn, except a small anterior part (Figure 1B). The innervation patterns in the LH of ePNs originating in the same glomerulus were distinct and stereotypic concerning the main branches as described previously (Jefferis et al., 2007; Marin et al., 2002; Wong et al., 2002). To analyze the stereotypy of fine arborizations of individual ePNs, we compared the sister ePNs within one animal as well as in three different animals. Therefore, we performed 3D-reconstruction and subsequent registration to one reference brain for a subset of 21 glomeruli that were innervated by one up to three sister ePNs. Notably, while the main branches were highly stereotypic (Jefferis et al., 2007; Marin et al., 2002; Wong et al., 2002), the fine arborizations were not identical but similar (Figure 1C; Figure 1-figure supplement 1). The similarity of arborizations across three different animals was analyzed using the terminal points of registered neurons to generate density maps (Jefferis et al., 2007), which represent the spatial concentration of neuron terminals. Correlating the density maps demonstrate that terminal locations of some ePNs innervating the same specific glomerulus were similar across animals (e.g. DP1m and VM3, correlation coefficient ≈ 0.8), whereas some were slightly different (e.g. DA4l and DC1, correlation coefficient ≈ 0.6) (Figure 1D, Figure 1-figure supplement 2). To compare the similarity of the ePN innervations in the LH we correlated pairwise the density maps of neurons innervating the same glomerulus as well as of neurons innervating different glomeruli. Terminal branches of ePNs innervating the same glomerulus were highly similar to each other (correlation coefficient ≈ 0.8), whereas, ePNs originating from different glomeruli revealed different terminal fields (correlation coefficient ≈ 0.1; Figure 1E). Generally, analyzing the terminal fields of all ePNs innervating a specific glomerulus confirms the stereotypy of the main branches described in previous *in vitro* studies of single neurons (Jefferis et al., 2007; Marin et al., 2002; Wong et al., 2002). But comparing sister ePNs highlights the differences of fine arborizations.

Terminal fields of ePNs overlap

Since terminal fields of ePNs were significantly different for most glomeruli we aimed at categorizing all ePNs into subgroups according to their terminal fields similar to Jefferis et al. (Jefferis et al., 2007). Having confirmed the high stereotypy of ePNs in the LH for a subset of 21 glomeruli we decided to reconstruct the ePNs of the remaining 16 glomeruli

for one animal each. Unfortunately, it was not possible to separate reliably single neurons originating in glomeruli with more than three sister PNs, due to their close proximity, thus they were reconstructed as a group. Again, density maps were generated to compare the similarity of terminal fields of ePNs using hierarchical clustering (Figure 2A; Figure 2-Figure supplement 1). This resulted in five main groups, but the corresponding distance matrix revealed that defining cluster boundaries was arbitrary since similarities were not only found for neuron pairs within the same cluster. Notably, generating a Principal Component Analysis (PCA) of terminal fields revealed also no clear clusters of ePNs but an even distribution of overlapping ePN classes. Interestingly, in the PCA the spatial pattern of the ePNs in the LH is highly reminiscent of the AL map (Figure 2-Figure supplement 1). Previously, Marin et al. (Marin et al., 2002) described for a subset of ten ePN classes a tendency that adjacent ePNs in the AL have adjacent terminal fields. Comparing the spatial distribution of ePNs in the AL and the LH confirms that the neighborhood of ePNs in the LH is highly correlated to the neighborhood in the AL (Figure 2E; Distance correlation, r= 0.29; p= 4.8 e^{-14}). Although the orientation axis of neighboring glomeruli in the AL is rotated and tilted in the LH: anterior-dorsal glomeruli are represented in the anterior LH (e.g. DA1, VA6), and ventromedial glomeruli are represented in the posterior LH (e.g. VM3, VA4; Figure 2C). However, some glomeruli were not perfectly correlated e.g. VA4 is in the AL located next to VA3 and VA5 but the terminal fields were close to DM3 and DM1 (Figure 2B, D). Regarding the distribution of sensilla classes in the LH their topographic map from the AL is represented also rotated and tilted in the LH, but due to pronounced neuronal arborizations no clear boundaries exist (Figure 2-Figure supplement 1). Taken together, terminal fields of ePNs overlap each other, hence, hindering their clustering. Nevertheless, the neighborhood of ePNs in the AL is retained in the LH.

Parallel relay of odor information by ePNs and iPNs

The LH is targeted by axons of both ePNs and iPNs almost entirely overlapping with each other. On the one hand the innervation in the LH by ePNs is retaining the topographic map, and on the other hand iPNs are separated in two distinct groups regarding their LH innervation (Strutz et al., 2014). Those iPNs either innervate the anteromedial (accordingly the so-called LH-AM iPNs) or the posteromedial LH (accordingly the so-called LH-PM iPNs; Figure 3B). So far, nothing is known about the overlap for subsets of the PN populations of *GH146-GAL4* and *MZ699-GAL4*. Therefore, we registered the previously published iPNs (Strutz et al., 2014) onto the reference brain used for the registration of ePNs (Figure 3A).

Since ePNs exhibited an overlapping innervation in the LH, comparison of the density maps of iPNs with ePNs (Figure 3C) revealed that some ePNs overlapped with either the LH-AM (like D and VL2a), or the LH-PM (like DM3 and VA4). In rare cases ePNs (like

DC1 and VA3) overlapped with both clusters of the iPNs (Figure 3D, E). Interestingly, ePNs that overlapped in the LH with LH-PM iPNs innervated in the AL glomeruli that were mainly innervated by LH-PM neurons. And likewise, ePNs overlapping in the LH with LH-AM neurons innervated in the AL glomeruli that were predominantly innervated by LH-AM neurons (Fig.3D). Correlating glomerular origin and terminal fields confirmed similarity of terminal fields for ePNs and iPNs innervating similar regions in the AL (cosine distance ≈ 0.4). PNs innervating different regions in the AL had also different terminal fields (cosine distance ≈ 0.6). The innervation patterns of PNs within the same areas were significantly different to those of PNs within different areas (Mann-Whitney-U test p= 0.004; Figure 3F). In other words, excitatory uniglomerular and inhibitory multiglomerular PNs got their input from the same area in the AL and transferred the odor information via two parallel pathways to the same LH region.

ePN odor responses separate in two odor response domains

Having investigated the morphology of ePNs we next aimed to examine their odor coding properties in the LH. So far the odor responses of ePNs were extensively investigated only in the AL (e.g. (Knaden et al., 2012; Ng et al., 2002; Root et al., 2007; Schubert et al., 2014; Wang et al., 2003a) and the mushroom body calyx (e.g. (Fiala et al., 2002; Li et al., 2013; Wang et al., 2004). But to our knowledge the representation of odor information of ePNs in the LH was examined only for few odors in single planes using multiphoton calcium imaging (Liang et al., 2013; Parnas et al., 2013). As previously revealed iPNs represent odors in the LH only according to their valence and intensity (Strutz et al., 2014). Hence, we were interested if ePNs also categorize odors only by their valence and intensity or if the odor identity is retained in the LH activity patterns. Therefore, we performed widefield-calcium imaging experiments expressing the genetically encoded calcium indicator GCaMP3 under control of the GH146-GAL4 line (Stocker et al., 1997; Tian et al., 2009). We used an odor set that is largely overlapping with the odor set used for the investigation of iPNs (Strutz et al., 2014). Our odor set contained the blend balsamic vinegar and 18 pure odors of different ecological relevance: pheromones (11-*cis*-vaccenyl acetate (Ha and Smith, 2006; Kurtovic et al., 2007), methyl laurate (Dweck et al., 2015b), repellents (geosmin (Stensmyr et al., 2012), actinidin (Ebrahim et al., 2015), benzaldehyde (Semmelhack and Wang, 2009), 1-octanol (Knaden et al., 2012)), fruit odors (isoamyl acetate, acetophenone, γ-butyrolactone, 1-hexanol, 1-octen-3-ol), flower odor (linalool) and odors indicative for fermenting food (acetoine acetate, acetic acid (Becher, 2012), 2,3-butanedione, ethyl-4-guaiacol (Dweck et al., 2015a), propionic acid, and 2-phenethyl acetate).

Across animals the responses to different odors were very broad and seemed not to be odor specific. Only a separation in two spatial patterns for odors responses in the posterior part of the LH or responses in the almost entire LH was discernable. Notably, those

two spatial patterns were reproducible in all animals tested (Figure 4A; Figure 4-Figure supplement 1; n = 6-9). Depending on the odor concentration the response pattern changed in the breadth and the fluorescence intensity, but the shape and spatial position was maintained (Figure 4B). From higher to lower odor concentrations the fluorescence intensity of the responses decreased for e.g. hexanol and benzaldehyde dramatically with up to 100% difference in fluorescence intensity, but for e.g. propionic acid and balsamic vinegar the fluorescence intensity decreased only about 20% (Figure 4B and Figure 5A). Interestingly, responses to the pheromone 11-*cis*-vaccenyl acetate (Ha and Smith, 2006; Kurtovic et al., 2007) were detected mainly in the posterior LH. But Jefferis et al. predicted a specific "pheromone region" in the anterior-ventromedial part of the LH basing on the terminal fields of pheromone coding ePNs (Jefferis et al., 2007). Notably, the pheromone methyl laurate elicited responses in the same LH region as 11-*cis*-vaccenyl acetate (Dweck et al., 2015b).

Since the LH has a rather homogeneous morphology without any morphological landmarks, the functional data was analyzed using the non-negative Matrix Factorization (NMF) (Lee and Seung, 1999; Soelter et al., 2014; Strutz et al., 2014). NMF assembles odor activity patterns of similar spatial and temporal features to distinct odor response domains (ORDs). Two reliable and reproducible ORDs in ePNs were revealed for all tested animals, that are from now on defined as the lateral horn posterior (LH-P) and lateral horn medial region (LH-M). Very broad odor responses were clustered to the LH-M, whereas odor responses restricted to the posterior LH were clustered to the LH-P (Figure 4C, D). Almost all odors in different concentrations elicited responses above 20% fluorescence intensity in the LH-P ORD. In contrast, in the LH-M the elicited activity increased for higher odor concentration (Figure 5A). Statistical analyses of the odor response kinetics confirmed that odor representations in the LH-M ORD were concentration-dependent for most of the odors (Linear Regression, $r = 0.69$, $p = 4.97\ 10^{-9}$), while those in the LH-P were concentration-independent (Linear Regression, $r = 0.02$, $p = 0.09$; Figure 5B left).

To get a glimpse on the logic of the separation into the two ORDs we sorted the odors according to their hedonic valence in attractive or aversive odors determined by innate behavioral preference assays (Knaden et al., 2012; Steck et al., 2012; Stensmyr et al., 2012; Stensmyr et al., 2003; Strutz et al., 2014; Thoma et al., 2014). Surprisingly, the two aversive odors actinidin - representing the scent of a predatory wasp (Ebrahim et al., 2015) - and geosmin - indicating contaminated food (Stensmyr et al., 2012) - exhibited a response pattern more similar to attractive odors such as 11-*cis*-vaccenyl acetate or balsamic vinegar. Intriguingly, the attractive odor isoamyl acetate had a response pattern similar to aversive odors such as benzaldehyde, and activated the LH-M region (Figure 4 and Figure 5A). Overall, the LH-M ORD was mainly activated by odors eliciting aversive behavior, whereas attractive odors evoked strong neuronal activity in the LH-P region

(Mann-Whitney-U-test, Figure 5B right). Hence, there was a tendency of the separation of the LH for responses into attractive (LH-P) and aversive odors (LH-M) for ePNs.

Unequal processing of odor information in the AL

The spatial representation of odors in the LH for ePNs separated in only two ORDs is quite puzzling since the topographic map of the AL is retained in the LH. Probably the processing of odor information in the AL or LH results in broader PN responses reflected in only two ORDs. To examine the impact of processing, we took advantage of having the morphological data of all ePNs and OSN responses for some odors used in our odor set to simulate unprocessed odor patterns in the LH. Unfortunately, no known *Drosophila* pheromone is included in the DoOR data base (http://neuro.uni-konstanz.de/DoOR/2.0/) (Münch and Galizia, 2016). Thus, to predict the odor pattern for the pheromone methyl laurate we estimated values for the pheromone response depending on normalized spike count (Dweck et al., 2015b).

Interestingly, the predicted odor patterns were broad and not distinct for the different odors. In fact, for most of the odors the prediction reproduced patterns that were similar to the measured odor pattern, e.g. 1-hexanol and acetophenone. Nevertheless, for some odors the predicted odor patterns appeared to be shifted, e.g. the predicted pattern for methyl laurate was slightly shifted to the anterior LH, whereas for 2,3-butanedione it was slightly shifted to the posterior LH. In the cases of 1-octen-3-ol and isoamyl acetate the measured responses were broader than the predicted patterns (Figure 6A). Notably, also the prediction exhibited no specific pattern for the pheromone methyl laurate as it would be expected to be separated from general or food odors (Jefferis et al., 2007). Correlating the measured and simulated odor responses verifies that the differences are only slightly significant due to the unequal shifts of odor responses ($p=0.043$; Figure 6B). Consequently, the variety between simulated, unprocessed odor patterns and measured odor patterns is indicating different information processing for some odors. This confirms observations in the AL where odor information is transferred from first to second order neurons with varying degrees of processing (Bhandawat et al., 2007; Knaden et al., 2012; Ng et al., 2002; Olsen et al., 2007; Root et al., 2008; Silbering and Galizia, 2007; Wang et al., 2003a; Wang et al., 2014; Wilson et al., 2004).

ePNs synapse onto VLP neurons in the LH

Having elucidated that subsets of ePNs and iPNs innervate overlapping areas in the AL as well as in the LH, and that their odor responses can be separated due to odor valence and intensity we were curious whether they are functionally connected. Previous studies revealed that arborizations of ePNs, iPNs and VLP neurons overlap in the LH (Strutz et al., 2014). Furthermore, iPNs inhibit the third-order VLP neurons, which get their input (mainly) in the LH (Liang et al., 2013; Parnas et al., 2013; Strutz et al., 2014). Additional-

ly, Liang et al. (Liang et al., 2013) revealed that iPNs do not synapse onto ePNs. Yet, it is not known whether ePNs synapse onto iPNs or VLP neurons or both.

We therefore labeled synapses between the three different neuron populations using GFP reconstitution across synaptic partners (GRASP) (Feinberg et al., 2008). The $sGFP^{1-10}$ was either fused to the synaptic protein neurexin (Nrx) or to the pre-synaptic protein synaptobrevin (Syb) under control of *MZ699-GAL4* (Fan et al., 2013; Ito et al., 1997; Karuppudurai et al., 2014). Under control of *GH146-LexA* the $sGFP^{11}$ was expressed. Surprisingly, reconstitution of the GFP components resulted in labeling of synapses in the AL and the LH only for flies carrying the Nrx::$sGFP^{1-10}$ construct (Figure 7A, B). [As a control for the functionality of the Syb::$sGFP^{1-10}$ construct it was expressed under control of *Orco-GAL4* (Larsson et al., 2004) in flies also carrying $sGFP^{11}$ under control of LN1-LexA. This combination revealed abundant labeling of synapses in the AL (data not shown).] Thus, the missing labeling of presynapses of MZ699+ neurons onto GH146+ neurons implies that ePNs receive no input from iPNs or VLP neurons. Instead, the labeling of synapses by Nrx::$sGFP^{1-10}$ suggests connections from ePNs to iPNs and VLP neurons. To verify these connections we combined widefield calcium imaging for a subset of six odors in a concentration of 10^{-2} with microlesion of the PN-tracts mALT and mlALT. Imaging of ePNs revealed no differences in the response pattern after transection of mlALT (Figure 7 D, F, E; n = 6). This confirms observation that iPNs do not synapse onto ePNs (Liang et al., 2013). Notably, imaging of MZ699+ neurons revealed changes of odor responses after transection of the mALT (Figure 7 I; n = 7). Again we performed NMF to separate similar spatiotemporal activity patterns (Figure 7J). In this way we can demonstrate that only responses in the LH-AL were abolished after microlesion. This implies a connection of ePNs onto VLP neurons, since responses in the LH-AL domain derive exclusively from VLP neurons (Strutz et al., 2014). In contrast, responses in the LH-PM and LH-AM domain exhibited no changes after transection of the mALT suggesting that ePNs do not synapse onto iPNs (Figure 7 K-L).

ORDs deriving from distinct neuronal populations

In ePNs we could identify the LH-P ORD being activated by attractive odors as well as the LH-M ORD being activated by aversive odors and high odor concentrations. Neurons labeled by MZ699-GAL4 comprise three ORDs: one ORD in the anterolateral part of the LH (so-called LH-AL), one in the anteromedial part (LH-AM) and the third one in the posteromedial LH (LH-PM) (Strutz et al., 2014). While the LH-AM is intensity-dependent and valence-unspecific, the LH-PM is activated by attractive odors in a concentration-independent manner. The LH-AL represents the responses of third-order VLP neurons and encodes intensity and aversive odors. Since iPNs and VLP neurons overlap in the LH with ePNs (Strutz et al., 2014), as well as the ORDs of the three different neuron populations overlap (Figure 8A), we wondered whether the ORDs overlap regarding their

functional features. A correlation based on the odor-specific response profiles of the individual ORDs of iPNs, ePNs as well as VLP neurons exhibited a distinct clustering of the ORDs (Figure 8B, C). LH-P ePNs and LH-PM iPNs similarly represent attraction and spatially overlap almost entirely. LH-M ePNs and VLP neurons of the LH-AL encode aversion and high odor concentration. LH-AM iPNs encode only odor intensity (Figure 8D). LH-M overlaps completely with LH-AM and LH-AL, and also partially with LH-P and LH-PM. Thus, ORDs of the three different neuron populations overlap spatially and functionally. This segregated encoding of the same odor information (valence or concentration or both) as well as the overlap of terminal fields of the two different PN populations, ePNs and iPNs, supports the separation of the LH due to odor valence.

Discussion

The transfer of odor information from the AL to the LH by two neuronal populations of PNs (uniglomerular, excitatory ones (ePNs) and multiglomerular, inhibitory ones (iPNs)) raises the question of the relevance of two parallel pathways targeting the higher brain center. Here we used morphological and functional analyses to elucidate the properties of GH146+ ePNs regarding the representation of odor information in the higher olfactory neuropil, the LH, and compared it with previous findings of MZ699+ iPNs (Strutz et al., 2014).

We found that odor responses of ePNs in the LH can be segregated into two odor response domains (ORDs) according to the response patterns as well as the coding of odor valence and concentration. Notably, this odor representation in specific ORDs is in a similar manner described for iPNs (Strutz et al., 2014), i.e. ORDs of ePNs and iPNs coding same features are located in the same LH region. Regarding the output of ePNs and iPNs in the LH we could verify that both neuronal populations synapse on the same set of third-order neurons of the ventrolateral protocerebrum (VLP). Furthermore, subsets of ePNs and iPNs innervating the same LH area also overlap with each other in the AL. This is supporting the notion of a parallel pathway transferring odor information via two opposing neuronal populations that either excite or inhibit VLP neurons. In contrast to iPNs, the terminal fields of ePNs are evenly overlapping in the LH and thus cannot be clustered due to their innervated LH area. Notably, neighboring ePNs in the AL are also neighbors in the LH, thus the topographic map of the AL is retained. Furthermore, the major terminal arborizations are stereotypic and neuron-specific, while the fine branches of sister PNs reveal clear differences.

Coding of valence and concentration in the LH

Functional calcium imaging experiments revealed that ePNs, like iPNs, represent odor information in separated odor response domains (ORD) in the LH, which can be classified according to odor intensity and valence. Attractive odors are mainly represented in

the posterior LH region (ORD classified as LH-P ePNs or LH-PM iPNs), whereas, aversive odors are represented in a medial to anterior area (ORD classified as LH-M ePNs or LH-AM iPNs). Interestingly, while the region representing aversive odors is concentration-dependent, the region representing attractive odors is concentration-independent. Our approach applying non-negative matrix factorization (Lee and Seung, 1999; Soelter et al., 2014) reveals two ORDs in the LH that are highly stereotypic and reproducible for all odors tested. Thus, we defined two ORDs reflecting ecological relevance, but additional clusters or sub-clusters or both representing odor-specific response domains may exist. Furthermore, we used monomolecular compounds for calcium imaging except balsamic vinegar, which exhibited a similar response pattern as single odors eliciting attraction behavior. However, flies mainly encounter in their natural environment odor plumes of blends with attractive and aversive compounds. Thus, additional experiments are necessary to investigate the odor responses for mixtures of attractive and aversive odors to reveal if the LH processes information separately for the single compounds or if the LH rates the overall valence of the mixture.

The separation in “attractive“ and “aversive“ responses of ePNs in the LH is contradictory to predictions of separate regions for odor responses to food odors and pheromones (Jefferis et al., 2007; Liang et al., 2013). Odor responses of ePNs to pheromones are expected in the anterior LH where those pheromone-specific ePNs terminate. However, we could not assign this region being specific for pheromone responses since the pheromones methyl laurate and 11-*cis*-vaccenyl acetate elicited responses in the posterior LH similar to other attractive odors such as balsamic vinegar. The similarity in odor response patterns of balsamic vinegar and 11-*cis*-vaccenyl acetate may be caused by ePNs relaying responses to both odors (Lebreton et al., 2015). However, if further ePNs exist that respond to methyl laurate in addition to VA1d- and VA1v-ePNs has to be verified in future experiments. It is also possible that lateral excitation (Olsen et al., 2007; Root et al., 2007; Shang et al., 2007; Yaksi and Wilson, 2010) or lateral inhibition (Olsen et al., 2010; Olsen and Wilson, 2008b; Root et al., 2008) or both cause the unexpected response patterns for pheromones. Furthermore, comparison of the measured odor response patterns with our predictions basing on response data of sensory neurons (http://neuro.uni-konstanz.de/DoOR/2.0/) revealed slight shifts of some odor response patterns in the LH. These shifts also may underlie complex processing by lateral excitation or lateral inhibition or both (Bhandawat et al., 2007; Ng et al., 2002; Olsen and Wilson, 2008b; Root et al., 2008; Silbering and Galizia, 2007; Silbering et al., 2008; Wilson et al., 2004).

Knaden and co-workers (Knaden et al., 2012) described a separation of the AL for attractive odors to medial glomeruli and aversive odors to lateral glomeruli. Since the topographic map is retained in the LH (see below), but rotated and tilted, the medial glomeruli are represented in the posterior-dorsal LH, and lateral glomeruli are represented in the

anterior-ventral LH. This fits well to our separation of the LH into ORDs responding to attractive odors in the posterior LH and aversive odors in the medial to anterior LH (Figure 2-Figure supplement 2). A previous study described also a segregation of the LH in aversive and attractive odor responses that based on the different terminal fields of VM1-ePNs responding to attractive amines as well as ammonia, and V- and DC4-ePNs responding to aversive carbon dioxide and acids, respectively (Min et al., 2013). Unfortunately, we could not investigate the corresponding location of odor responses since we had not included amines and carbon dioxide in our odor set. Additionally, our morphological data set excluded ePNs innervating DC4 and V since they are not labeled by the *GH146-GAL4* line (Grabe et al., 2015). Thus, further experiments are needed to analyze the terminal fields and odor responses of ePNs that are not covered by the *GH146-GAL4* line.

Antagonistic modulation of third-order neurons by ePNs and iPNs

The responses to aversive odors by third-order neurons of the VLP are modulated via inhibition by iPNs. Furthermore, the odor responses of VLP neurons increased after ablation of the iPN input (Strutz et al., 2014). This raises the question about a possible connection of ePNs with those VLP neurons. Our GRASP-data revealed synapses between *GH146-GAL4* and *MZ699-GAL4* neurons in the AL and the LH. The GRASP-signals in the AL imply presynaptic connections of ePNs onto iPNs verifying previous observations (Wang et al., 2014). In the LH the GRASP-signals may either be synapses between ePNs-iPNs or ePNs-VLP neurons. Combining calcium imaging with microlesion of the ePN-tract mALT changed in iPNs the odor responses only in the anterior LH area. Those responses are assigned to the ORD LH-AL, which represents the responses of VLP neurons to odors of negative valence (Strutz et al., 2014). Conversely, odor responses in the ORDs LH-PM and LH-AM remained constant after microlesion of the ePN-tract mALT verifying that ePNs do not synapse onto iPNs in the LH. In line with this observation is that cutting of the iPN-tract mlALT exhibited persistent odor responses in ePNs confirming that iPNs do not synapse onto ePNs (this study, (Liang et al., 2013)). Thus, we conclude that ePNs and iPNs have no synaptic connections in the LH. However, both ePNs and iPNs synapse on the same set of third-order neurons of the VLP and modulate antagonistic the activity of those VLP neurons. The modulation might be dependent on the internal state of the fly but this has to be elucidated in further experiments.

In addition to VLP neurons ePNs and iPNs synapse onto other types of LHNs, which innervate different parts of the LH and connect to several higher brain centers (Cachero et al., 2010; Jefferis et al., 2007; Kohl et al., 2013; Lai et al., 2008; Ruta et al., 2010; Tanaka et al., 2004; Yu et al., 2010). Some of the LHNs are dimorphic (Kohl et al., 2013; Ruta et al., 2010; Yu et al., 2010) with sex specific odor responses (Kohl et al., 2013).

For other types of LHNs either broadly or narrowly tuned responses to fruit odors are described (Fişek and Wilson, 2014). If and how the coding of valence and intensity is relayed onto LHNs has to be investigated in further experiments.

Topographic map in the LH

Labeling *in vivo* all uniglomerular ePNs innervating the same glomerulus confirmed distinct stereotypic branching patterns with differences in their fine arborizations (Jefferis et al., 2007; Marin et al., 2002; Wong et al., 2002). Our comparison of the terminal fields revealed an overlapping innervation in the LH and not a clustering of ePNs with distinct terminal fields (Jefferis et al., 2007). This discrepancy may result from the different generation of density maps. Jefferis et al. (Jefferis et al., 2007) generated density maps integrating the morphology of single neurons labeled by MARCM, while we generated density maps basing on labeling of all ePNs per glomerulus (varying from one to eight; (Grabe et al., 2016)). Nevertheless, the overlapping innervation is highly correlated to the glomerular neighborhood in the AL, confirming that the topographic map is retained in the LH (Marin et al., 2002). We speculate that the topographic map is retained to implement the representation of the outer world as odotopic map in the LH. This odotopic map will be integrated with other sensory maps, such as of olfaction and vision as described in locusts (Gupta and Stopfer, 2012), to successfully navigate in an often hostile environment. In the fly the LH is linked with higher brain centers that represent e.g. the target of visual neurons, mechanosensory antennal neurons, or auditory sensory neurons. This enables a multimodal integration of several sensory types (Duistermars and Frye, 2010; Ruta et al., 2010; Tanaka et al., 2004).

Taken together, ePNs and iPNs work in a parallel pathway, however, they affect distinct aspects of olfactory information processing in the LH as described for parallel pathways in the mammalian visual system (Nassi and Callaway, 2009). While the retained topographic map enables ePNs to encode odor quality read out by LHNs (Fişek and Wilson, 2014), iPNs enhance the discrimination of odors via inhibition of postsynaptic neurons (Parnas et al., 2013). Furthermore, both ePNs and iPNs separate the LH due to odor valence and intensity and project onto third-order neurons of the VLP, which ePNs excite and iPNs inhibit. This parallel conveyance by two antagonistic PN populations may enhance the accuracy of the representation of odor valence and intensity. Moreover, the dual representation of olfactory information restricted to ecological relevance by two antagonistic PN populations might be a prerequisite to elicit innate behavior. Thus, our finding of the separation of the LH due to odor valence and intensity by ePNs and iPNs is a step further to understanding/unravel the neural circuitry causing innate behavior.

Material and Methods

Fly lines and rearing

Fly lines used were obtained from the Bloomington *Drosophila* stock center (http://flystocks.bio.indiana.edu/): *GH146-GAL4* (Stocker et al., 1997), *UAS-GCaMP3.0* (Tian et al., 2009), specific Or-GAL4 lines were used to reliably identify glomeruli (VA3, VA5, VC1, VC2, VA7l, VM7d, VM7v)*Or33c-GAL4, Or42a-GAL4, Or46a-GAL4, Or49b-GAL4, Or59c-GAL4, and Or67b-GAL4,* and *Or 71a-GAL4* (all (Fishilevich and Vosshall, 2005; Vosshall et al., 2000)), *GH146-QF,QUAS-mtdTomato* (Potter et al., 2010). Additional lines were kindly provided by Bob Datta for photoactivation (*UAS-C3PA*, (Ruta et al., 2010)) and Kei Ito (*MZ699-GAL4*, (Okada et al., 2009)). For calcium imaging flies of the genotypes *+;GH146-GAL4/(CyO);UAS-GCaMP3.0/(TM2)* were used, and *+;+/UAS-GC3.0;GH146-QF,QUAS-mtdTomato/MZ699-GAL4* for microlesion experiments. Flies carrying *UAS-Syb::GFP*$^{1\text{-}10}$ (Karuppudurai et al., 2014), *UAS-Nrx::GFP*$^{1\text{-}10}$ and *LexAop-CD4::GFP*^{11} (Fan et al., 2013) were used for analyses on synaptic connections.

Flies were reared on standard corn meal molasses medium (1 l of fly food consists of 918 ml water, 95 g polenta, 11 g brewer's yeast, 2.4 ml propionic acid, 3.3 ml nipagine (16%), 118 g sugar beet molasses and 4.1 g agarose) in a climate chamber with 12/12 hrs light/dark cycle, 70 % relative humidity and 23°C.

***In vivo* Preparation**

For *in vivo* photoactivation as well as calcium imaging experiments 4-6 d old female flies, anesthetized for at least 15 min on ice, were fixed in a custom-made stage (one-sided beveled plastic block of ≈ 8 cm^3) with a drill hole for the fly´s body. On the upper edge of the drill hole, one half of a 3.05 µm thin copper grid (Athene Grids ©) with a slit of 125 µm was glued. Into this slit the neck of the fly was gently pushed. A minute needle in front of the head fixed with wax onto the custom-made stage and 3-component silicon (Protemp^{TM}II, 3M Deutschland GmbH, Neuss, Germany) coated on the back of the head prevented the fly to escape. A fine wire, fixed with wax to a trimmed plastic coverslip, was placed in the flexible ptilinal suture to stretch the antennae. The coverslip, fixed with wax to the beveled side of the stage, was bended by turning screws, which passed through the block, to tense the wire. A punched plastic plate (1 mm in diameter) was placed on the head and fixed with wax to the stage. With two-component silicone (Kwik-Sil™, WPI Inc, Sarasota, FL) the gap between head and margin of the plastic plate was sealed. Ringer solution (NaCl 7.6 g/l, KCl 0.37 g/l, $MgCl_2$ $6H_2O$ 0.41 g/l; $CaCl_2$ 2 H_2O 0.29 g/l; saccharose 12.32 g/l; HEPES 1.19 g/l; pH 7.3) was used to prevent the brain from drying out during imaging. With a stab knife (Sharpoint, Surgical Specialties Corporation, Reading, PA) a window was cut in the head capsule, thus tracheae and fat bodies could be removed getting a clear view onto the brain.

Photoactivation for neuronal tracing

Photoactivation was performed with a MPCLSM 710 NLO (Zeiss, Germany) equipped with an infrared laser (Chameleon Ultra II, Coherent, Santa Clara, CA) as previously de-

scribed (Grabe et al., 2016). In brief, a 40x water immersions objective (W Plan-Apochromat 40x/1.0 DIC M27; Carl Zeiss, Germany) was used to continuously irradiate a glomerulus in 3 planes in succession for approx. 15-25 min with 760 nm laser wavelength. The region for activation was of similar shape as the glomerulus´ boarder but a little bit smaller. After a break of approx. 5-15 min for diffusion of the photoconverted protein through the entire neuron the brain was scanned with 925 nm in 1 µm steps (1024x1024, 8-bit). For the scanning procedure in some cases the body was removed to eliminate movement (Figure 1).

Neuronal reconstruction, registration and anatomical analyses

Confocal scans of labeled neurons were used for 3D-reconstruction with the skeleton tool of the segmentation software AMIRA 5.6.0 (FEI Company, Hillsboro, OR). The reconstructed neurons were registered onto an *in vivo* reference brain based on reconstructed labelfields of the different neuropils (i.e. AL, mushroom body calyx and LH (Rybak et al., 2010). For comparison MZ699-PNs (Strutz et al., 2014) were re-registered onto a reference brain basing on the *GH146-GAL4* line.

The morphology of reconstructed ePNs was analyzed based on the full morphology in the LH similar to (Jefferis et al., 2007): For each ePN we used the point cloud from the neuronal reconstruction from Amira, while we used the terminal points for iPNs (according to (Strutz et al., 2014). We calculated density maps for the LH by applying a Gaussian kernel (size +/- 7 sigma) to this data set for each voxel in a grid of equally spaced voxels with 5 microns per side covering the space (272:353, 236:316, 50:132) in the master coordinate system. We first calculated density maps for each animal (Figure 1D) that were averaged across animals for further analyses (Figure 2, Figure 3). To quantify spatial relationships between different neuronal types we calculated the spatial overlap between the 3D density maps (map1, map2, ….) where d_{vox} is the density per voxel as follows:

$$similarity\ (map1, map2) = \sum_{vox} \frac{d_{vox}^{map1} * d_{vox}^{map2}}{\sqrt{\sum_{vox}(d_{vox}^{map1})^2}\sqrt{\sum_{vox}(d_{pvox}^{map2})^2}}$$

Using Principal Component Analysis (PCA) the pairwise similarity matrix of the density maps did not show any distinct and stable clustering in subgroups as assumed (Figure 2 – supplement 1). We also performed a hierarchical clustering of the similarity matrix (Figure 2 – supplement 1) that yielded four main clusters, which are similar to the clusters published by (Jefferis et al., 2007). However, a closer look at the full distance matrix revealed that individual clusters are not clearly spatially separated and are arbitrary at the borders of each cluster (Figure 2 – supplement 1B; e.g. glomerulus DM2 is grouped in the red cluster, but shares strong similarities with the other DM glomeruli in the green

cluster). We therefore sorted and colored each PN class as a continuous representation according to their position in the first axis of the PCA (Figure 2A, B, C, D). To compare the similarity of our data set of ePN types obtained *in vivo* with the ePN types obtained *in vitro* (kindly provided by GSXE Jefferis, published in (Jefferis et al., 2007)) we correlated the cosine distances of neuronal arborizations *in vivo* to the correlation distances of neuronal arborizations *in vitro* (Figure 2 – supplement 1).

To quantify the relationship between the target areas in the LH and the neighborhood of innervated glomeruli we correlated the spatial overlap in the LH with the spatial distance of origin (i.e. the Euclidian distances of innervated glomeruli) (Figure 2E). Euclidean distances in the AL were calculated based on the 3D-coordinated of the *in vivo* AL atlas (Grabe et al., 2015).

Predictions for odor activity patterns in the LH were calculated by summing the density maps for each ePN class weighted by the published odor response profiles for each innervated glomerulus from the DoOR database (Münch and Galizia, 2016) (Figure 6).

Odor delivery system

All odor concentrations are prepared as v/v dilutions in mineral oil (in total 2 ml)(Roth, Karlsruhe, Germany) and were freshly prepared after approximately 30 puffs or after one month. Odors were used in three different concentrations (v/v 10^{-2}, 10^{-4}, 10^{-6}) except for geosmin and actinidin that were used in lower concentrations (v/v 10^{-4}, 10^{-6}, 10^{-8}) since they are described to elicit strong odor responses in the AL (Ebrahim et al., 2015; Stensmyr et al., 2012). 50-ml glass bottles with custom-made lid insert (POM; HL Kunststofftechnik, Landsberg, Germany) were equipped with push-in adapter (jenpneumatik & Schlauchtechnik GmbH, Jena, Germany) for the tubing system. Odors were delivered via Teflon-tubes (jenpneumatik & Schlauchtechnik GmbH, Jena, Germany) and were changed for each odor to avoid contamination.

Odors were delivered via a custom-made two-way bottle system with a charcoal-filtered constant air stream (1 l/min) split into a humidified constant air stream and an odor stimulus (0.1 l/min; flow-meter by Key Instruments, Hatfield, PA) adjoining in a peek-tube (Arthur Krüger GmbH, Barsbüttel, Germany) in ≈5 cm from the opening of the peek-tube (4 mm in diameter). The opening was positioned in 1 cm distance directed onto the fly. Behind the chamber with the fly was an air extraction system (flow rate 5 l/min) to prevent contamination of the room air. The recordings lasted 10 s with a frame rate of 4 Hz. Odor application after 2 s for 2 s was regulated with a Stimulus Controller CS 55 (Syntech GmbH, Germany). In each experiment the odors were given in random order with an inter-stimulus interval of at least 90 s. Between experiments the Teflon-tubes were cleaned with a constant air stream of 55°C.

#	odor	CAS-number	company
1	acetic acid	64-19-7	Sigma-Aldrich
2	acetophenone	98-86-2	Fluka
3	balsamic vinegar	-	Mamma Gina
4	benzaldehyde	100-52-7	Sigma-Aldrich
5	isoamyl acetate	123-92-2	Sigma-Aldrich
6	1-octen-3-ol	3391-86-4	SAFC
7	propionic acid	79-09-4	Fluka
8	actinidin	-	provided by HKM Dweck
9	acetoin acetate	4906-24-5	alfa aesar
10	2,3-butanedione	431-03-8	Fluka
11	11-cis-vaccenyl acetate	-	PheroBank BV
12	ethyl-4-guaiacol	2785-89-9	Sigma-Aldrich
13	geosmin	16423-19-1	Sigma-Aldrich
14	methyl laurate	111-82-0	Sigma-Aldrich
15	γ-butyrolactone	96-48-0	Sigma-Aldrich
16	1-hexanol	111-27-3	Sigma-Aldrich
17	linalool	78-70-6	Sigma-Aldrich
18	1-octanol	111-87-5	Sigma-Aldrich
19	2-phenethyl acetate	103-45-7	Sigma-Aldrich

Functional calcium imaging

Calcium imaging was performed on a wide-field microscope (Olympus BX-W51WI) with a 60x/ 1.0 NA water immersion objective (LUMPlanFL N 60x/1.00 W, Olympus) equipped with a Polychrome V (TILL Photonics, FEI Company, Hillsboro, OR) to generate 475 nm wavelength for measuring, as well as a CCD-camera (Sensicam, PCO AG, Germany) for image acquisition with symmetrical binning of 4 (0.625 × 0.625 µm/pixel). Imaging data was obtained using TillVision 4.0 (TillPhotonics, FEI Company,Hillsboro, OR). Flies were imaged focusing ≈30 µm below the most dorsal point where the mediolateral Al tract enters the LH (Figures 4 and 7).

Microlesion

For the microlesion experiments a reduced odor set with 7 odors (11-cis-vaccenyl acetate, benzaldehyde, isoamyl acetate, 1-octen-3-ol, balsamic vinegar and propionic acid, all at 10^{-2}, as well as 1-octen-3-ol at 10^{-6}) was used for calcium imaging. Transections of either the medial antennal lobe tract (mALT) or the mediolateral antennal lobe tract (mlALT) were monitored via fast z-scans with 925 nm before and after the lesion. The elliptical regions for lesion were continuously illuminated with 800 nm for 25 s. To completely cut the tracts lesion was carried out from the most dorsal to the most ventral point of the tracts by means of changes in z-position (Δz = 10 µm (mlALT) and Δz = 20 µm (mALT)). After a recovery of 5 min the imaging procedure was continued (Figure 7).

Imaging data analysis – Non-Negative Matrix Factorization (NMF)

Image processing was done with Fiji (Version 20121127 Image J 1.49r) including movement correction using the plugin StackReg, the calculation of relative fluorescence changes ($\Delta F/F_0$; F_0 is the averaged value of frames 0-8 of each measurement), false color-coded fluorescent changes in raw-data images were maximum intensity projections of frames 13-19 (Figure 4A, figure 7D, K).

For further analyses, a Gaussian low-pass filter (σ = 2px) was applied to compensate for remaining movement artifacts and pixel noise. The resulting concatenated time-series of the recordings is denoted as measurement matrix **Y** with element $\mathbf{Y}_{t,p}$ being the t^{th} observed value of pixel p. Analogous to our LH study on iPNs (Strutz et al., 2014), we used the automatic method non-negative matrix factorization (NMF) to extract Ca^{2+} signals that exhibit common spatial or temporal features since the LH does not provide any morphological landmarks (Lee and Seung, 1999). NMF, like other matrix factorization techniques (e.g. PCA and Independent Component Analysis (ICA)), decompose the measurement matrix **Y** into *k* components, $\mathbf{Y} = \sum_k x_k * a_k^T + \mathbf{R}$. The time-course a_k of each component contains a common underlying time-course of all pixels and each pixel participation x_k declares how strongly each pixel is involved in this time-course. The residual matrix **R** contains the unexplained data. In order to perform NMF, we employed the software framework from Soelter et al. (Soelter et al., 2014) with the following parameters: $\square_{sm} = 0$ and $\square_{de} = 10^{-4}$. For each animal, we performed decomposition into $k = 2$ components, which consisted each of a spatial activity pattern and the corresponding temporal odor-evoked response. The averaged response between 1 and 3 s after odor onset was used as the component-specific response strength for each odor (R_o^{comp}). To identify odor-evoked patterns across animals, we clustered components according to their odor response profiles using the cosine similarity (Figure 4C) (Soucy et al., 2009):

$$similarity\ (comp1, comp2) = \sum_o \frac{R_o^{comp1} * R_o^{comp2}}{\sqrt{\sum_o (R_o^{comp1})^2}\sqrt{\sum_o (R_o^{comp2})^2}}$$

For clustering we used the hierarchical clustering according to the UPGMA method. We first started to analyze the first odor set that included all odors at the highest concentration (i.e. 10^{-2}). The odor-evoked responses clearly clustered into two response patterns (orange and blue clusters in Fig. 4C) with each cluster containing exactly one component of one animal. In addition the spatial areas of the components in each cluster were highly similar between animals. The clustering was stable towards changes of included animals. We defined therefore the two components as two odor response domains (ORDs). The two ORDs were highly stereotypic and could be identified in every animal measured. We performed the same analysis with an initial decomposition of *k = 3* or *k = 4* components, but subsequent clustering did not result into more than two distinct and reproducible clusters and therefore no additional ORDs could be detected (data not shown). The two ORDs were sufficient to explain most of the data's variance (80.4% ± 2.3%, error is standard deviation across individuals). A validation of our NMF-based results with spatial ICA yielded qualitatively similar results (data not shown). We analyzed the other three odor sets and the microlesion experiments (Figure 7) using the same approach, i.e. NMF with *k = 2* and subsequent hierarchical clustering. To decompose the activity patterns of iPNs during the microlesion experiments (Figure 7F-J), we used *k = 3* in line with the results of Strutz et al.(Strutz et al., 2014). To determine the coding properties of extracted ORDs (Figure 5B) we calculated the mean response of each animal within a time window of 1-3 s after stimulus onset. Median responses over all animals defined the standard stimulated response r_{ORD}^{o} of an ORD to an odor *o*.

Immunohistochemistry for GRASP

We used flies between 5-10 days after eclosion. Brains were dissected in Ringer's solution, fixed with 4% paraformaldehyde in saline phosphate-buffer solution (PBS; pH 7.4) containing 0.3% Triton X-100 (PBST) for 30 min on ice, and washed three times for 15 min with PBST. After incubation with blocking solution containing 0.1% bovine serum albumine (BSA) and 5% normal donkey serum (NDS) or 5% normal goat serum for 1 h at room temperature (RT), brains were incubated in primary antibody for 1-2 days at 4°C. The following primary antibodies were used: mouse anti-GFP20 (Sigma, G6539) diluted 1:250; guinea pig anti-BrpN-Term ((Andlauer et al., 2014) gift from Stephan Sigrist) 1:100; rat anti N-cadherin (Developmental Studies Hybridoma Bank, DN-Ex #8) dilution 1:20. Then brains were washed three times 15 min and incubated overnight at 4°C in secondary antibody. The following secondary antibodies were used at 1:250 dilutions: donkey anti mouse Alexa Fluor 488 (Jackson ImmunoResearch Europe Ltd., 715-545-151), donkey anti guinea pig Alexa Fluor 647 (Jackson ImmunoResearch Europe Ltd., 706-605-148), goat anti mouse Alexa Fluor 488 (Invitrogen, A11001), goat anti rat Cy3 (Life technologies, A21094). Brains were mounted in Vectashield (Vector, Burlingame, CA) after washing (three times 20 to 30 min) with PBST. Whole brains were scanned

with a Zeiss LSM 880 confocal microscope (Carl Zeiss, Jena, Germany) using a 40X water immersion objective (C-Apochromat 40x/1.2 W Corr M27, Carl Zeiss). Z-stacks were obtained with 0.4-0.6 µm intervals at 1024 x 1024 pixel resolution. Z-projections of confocal images were made after adjustment of contrast and brightness using Fiji software (http://fiji.sc/wiki/index.php/Fiji) (Figure 7A).

Supplemental information

Supplemental Information includes four figures (Figure 1 Supplement 1, Figure 1 Supplement 2, Figure 2 Supplement 1, Figure 2 Supplement 2).

Figure Legends

Figure 1. Stereotypic terminal arborizations of ePNs

(A) Schematic of the olfactory neuropils and the main projection neuron tracts. Excitatory, uniglomerular GH146+ projection neurons (ePNs) relay odor information via the mALT and lALT from the AL to the LH, while inhibitory, multiglomerular projection neurons (iPNs) relay odor information from the AL to the LH only via the mlALT. Abbreviations: AL antennal lobe, CX mushroom body calyx, LH lateral horn, a anterior, d dorsal, l lateral, m medial, p posterior, v ventral, mALT medial antennal lobe tract, mlALT mediolateral antennal lobe tract, lALT lateral antennal lobe tract.

(B) Confocal scan of all ePNs and a single ePN labeled using photoactivatable GFP (left). 3D-reconstruction and registration of labeled single neurons to a reference brain (right) enable comparison of the innervation patterns of the different ePN types in the LH. Scale bars, 50 µm.

(C) LH-innervation of one up to three ePNs innervating the same glomerulus in three different animals (left) and the superimposing of all labeled ePNs from different animals reveals similarity in the main branches but differences in their fine arborizations. See Figure 1-Figure supplement 1 for registered neurons of all ePN types.

(D) Images of density maps basing on the neuronal arborizations in the LH for 21 ePN types exhibit high similarity of the same ePN types across three different animals in dorsal view. See Figure 1-Figure supplement 2 for lateral and posterior view of density maps.

(E) Density maps are used to calculate similarities of ePNs originating in the same glomerulus as well as of different origin. The terminal areas in the LH of ePNs innervating the same glomerulus are stronger correlated than ePNs innervating different glomeruli (Kolmogorov-Smirnov-Test, $p = 4.1\ 10^{-42}$).

Figure 2. The topographic map of the AL is retained in the LH

(A) Density maps of all 37 ePN types labeled by *GH146-GAL4* sorted by their similarity of the LH innervation from posterior (red) to anterior (blue; according to Figure 2B). See Figure 2-Figure supplement 1 for lateral and posterior view of density maps.

(B) PCA of terminal fields exhibit an even distribution of overlapping ePN classes in the LH. Color-code (from red to blue) based on the first axis of the PCA (i.e. PC1). The three dimensions of the PCA explain 78% of the variance of terminal fields.

(C) From the AL ePNs (color coded as in (A)) transfer the topographic map to the LH with a tilted and rotated orientation.

(D) Separation of the AL glomeruli according to neighboring terminal fields of ePNs color-coded as in (A).

(E) Terminal fields of ePNs in the LH are highly correlated to the distances of innervated glomeruli in the AL confirming that the topographic map of the AL is retained in the LH ($r = 0.29$, $p = 5\ 10^{-14}$). Abbreviations: AL antennal lobe, CX mushroom body calyx, LH lateral horn, a anterior, d dorsal, l lateral, m medial, p posterior, v ventral

Figure 3. ePNs and iPNs innervating similar areas in the AL target overlapping areas in the LH

(A) Reconstructions of all ePN types labeled by *GH146-GAL4* (gray) and the two iPN-populations LH-AM (green) and LH-PM (magenta) labeled by *MZ699-GAL4*.

(B) Different views of terminal fields of LH-AM and LH-PM iPNs (left) and their corresponding density maps with superimposed outline in dorsal, posterior and lateral view (right).

(C) Density maps of ePNs (gray) with superimposed outline of density maps of iPNs reveals overlap of ePNs either with LH-AM- or LH-PM-iPN types in the LH.

(D) Varying overlap of terminal fields of ePN and iPN types in the LH. Similarity of innervated regions in the LH reflects glomeruli innervation in the AL (represented by black dots).

(E) Representative examples of single ePNs overlapping with LH-PM or LH-AM iPN types.

(F) Correlation of glomerular origin and terminal fields between ePNs and iPNs. PNs of similar AL origin target similar terminal fields, while PNs of different origin do not overlap in the LH (Mann-Whitney-U test, $p = 0.004$). Box plots give the median (white bold line), quartiles (box), 95% confidence intervals (whiskers),

and specific values of the PN types (individual dots). Abbreviations: AL antennal lobe, CX mushroom body calyx, LH lateral horn, a anterior, d dorsal, l lateral, m medial, p posterior, v ventral

Figure 4. Stereotypic odor response profile of ePNs

(A) Widefield Ca^{2+}-imaging in ePNs expressing GCaMP3.0 under the control of *GH146-GAL4*, revealed stereotypic odor response patterns for several odors that are reproducible across animals. All false color-coded images are individually scaled to the individual maxima (indicated by red numbers in the lower right corner) and superimposed onto the raw fluorescence images. Values below the $\Delta F/F_0$ threshold of 50% are omitted to illustrate the specificity of the signals. (n = 6-9)

(B) Odor response patterns are concentration-dependent and show broader calcium-responses with increasing odor concentration.

(C) Odor response profiles in the LH cluster into two regions. See Figure 4-Figure supplement 1 for cluster of all animals tested with highest odor concentration.

(D) Using non-negative matrix factorization (NMF) the spatial and temporal responses can be extracted into two separate odor response domains (ORDs): LH-M (medial) and LH-P (posterior).

Figure 5. ORDs represent odor valence and concentration

(A) Median time traces of all odors and concentrations tested in calcium imaging experiments reveal different calcium responses due to odor identity for the two odor response domains (ORDs). Shadows represent upper and lower quartiles. (n = 6-9)

(B) Scheme of the colored ORDs (left). Correlation of calcium responses of the two ORDs LH-P and LH-M to odor concentration and odor valence. Responses in the ORD LH-M are concentration-dependent (Linear regression, r = 0.69, p = $4.97\ 10^{-9}$) and are stronger to aversive odors (Mann-Whitney-U test, p = 0.0215). Responses in the ORD LH-P are concentration-independent (Linear regression, r = 0.02, p = 0.09) and are stronger to attractive odors (Mann-Whitney-U test, p = 0.0176). Box plots give the median (gray bold line), quartiles (box), 95% confidence intervals (whiskers), and specific values of the tested odorants (individual dots).

Figure 6. Simulated and measured odor responses are similar

(A) Measured odor responses using calcium imaging (upper row). All false color-coded images are individually scaled to the individual maxima (indicated by red numbers in the lower right corner). Predicted odor responses in the LH of ePNs

calculated on previously published OSN response profiles (DoOr Data base) and the terminal fields of reconstructed ePNs (lower row). See Methods for details.

(B) Simulated and measured odor responses are significantly correlated, and therefore confirming the similarity between predicted and measured odor-evoked response patterns ($r = 0.37$; $p = 0.012$).

Figure 7. ePNs synapse onto VLP neurons

(A) GFP Reconstitution Across Synaptic Partners (GRASP) exhibit putative synaptic connections of ePNs, iPNs and VLP neurons in flies *carrying MZ699-Gal4>UAS-Nrx::GFP$^{1-10}$* and *GH146-LexA>LexAop-CD4::GFP^{11}*. Immunostaining against the reconstituted GFP20 (green) and nc82 neuropil labeling (magenta).

(B) GRASP experiments reveal the absence of presynapses of iPNs and VLP neurons onto ePNs in flies carrying *MZ699-Gal4>UAS-Syb::GFP$^{1-10}$* and *GH146-LexA>LexAop-CD4::GFP^{11}*. Immunostaining against the reconstituted GFP^{20} (green) and N-Cadherin neuropil labeling (magenta).

(C) Scheme of transection of the mlALT-tract. Flies expressing the genetically encoded calcium reporter GCaMP3.0 allowed visualization of odorant-evoked activities of ePNs using *GH146-GAL4* line before and after laser transection of iPNs to examine their functional interaction.

(D) Odor response pattern of ePNs before and after transection (pre/post) exhibit changes of fluorescence in different regions of the LH. False color-coded images are individually scaled to the individual maxima (indicated by red numbers in the lower right corner) and superimposed onto the raw fluorescence images. Values below the $\Delta F/F_0$ threshold of 50% are omitted to illustrate the specificity of the signals. (n = 6)

(E) Extracted odor response domains (ORDs) of ePNs using non-negative matrix factorization (NMF). See Methods for details.

(F) Transection of mlALT resulted in constant Ca^{2+} fluorescence signals in the two ORDs of ePNs to example odors.

(G) Median time traces of all odors and concentrations tested in calcium imaging experiments combined with transection of the mlALT-tract reveal constant activities after transection except for balsamic vinegar (two-tailed paired t-test; $p = 0.04$). Shadows represent upper and lower quartiles (n = 6).

(H) Scheme of transection of the mALT-tract in calcium imaging experiments to examine the functional connection of ePNs onto iPNs and VLP neurons.

(I) Odor response patterns of iPNs before and after transection of ePNs (pre/post) of *MZ699-GAL4; G-CaMP3.0* flies in widefield Ca^{2+}-imaging. Transection revealed changes of odor response patterns only in the LH-AL region that represents the activity of VLP neurons. All false color-coded images are individually scaled to the individual maxima (indicated by red numbers in the lower right corner) and superimposed onto the raw fluorescence images. Values below the $\Delta F/F_0$ threshold of 50% are omitted to illustrate the specificity of the signals. (n = 7)

(J) Extracted ORDs of iPNs using non-negative matrix factorization (NMF). See Methods for details.

(K) Transection of mALT resulted in a significant decrease of Ca^{2+} fluorescence signals in the LH-AL ORD of iPNs to the tested odors (two-tailed paired t-test; $p_{isoamyl\ acetate} = 0.00042$; $p_{benzaldehyde} = 0.00291$), while the other two ORDs, LH-PM and LH-AM, remain unaffected.

(L) Median time traces of all odors and concentrations tested in calcium imaging experiments combined with transection of the mALT-tract reveal only for the LH-AL ORD different activities after transection. Shadows represent upper and lower quartiles (n = 7). Abbreviations: AL antennal lobe, CX mushroom body calyx, LH lateral horn, a anterior, d dorsal, l lateral, m medial, p posterior, v ventral, mALT medial antennal lobe tract, mlALT mediolateral antennal lobe tract, VLP ventrolateral protocerebrum.

Figure 8. ORDs in the LH overlap

(A) Scheme of odor response domain (ORD) with outlines of ePNs, iPNs and VLP neurons superimposed on a widefield image (left). All three neuron populations innervate via different tracts the LH. Scheme of the five different ORDs deriving from the three neuron populations (right).

(B) Odor response profiles of several odors reveal functional overlap of ORDs of ePNs, iPNs and VLP neurons.

(C) Functional cluster analysis of ORDs according to their odor response profiles (shown in B). ORDs cluster according to the coding of odor intensity and valence.

(D) Single ORDs differently represent odor intensity or valence or both. Abbreviations: a anterior, d dorsal, l lateral, m medial, p posterior, v ventral, mALT medial antennal lobe tract, mlALT mediolateral antennal lobe tract, lALT lateral antennal lobe tract, VLPb bundle of neurons of the ventrolateral protocerebrum, VLPN ventrolateral protocerebrum neurons.

Figure 1-Figure supplement 1. Stereotypical LH arborizations of all analyzed ePN types

(A) All registered neurons labeled by photoactivation of the transgenic line *+;GH146-GAL4;UAS-C3PA* in dorsal, lateral and posterior view. Abbreviations: AL antennal lobe, CX mushroom body calyx, LH lateral horn, a anterior, d dorsal, l lateral, m medial, p posterior, v ventral, mALT medial antennal lobe tract, mlALT mediolateral antennal lobe tract, VLP ventrolateral protocerebrum. Scale bar, 50 µm

(B) Individual representation of all ePN types. Registered ePN types without separated reconstruction of sister neurons and that derive from reconstruction of one animal are shown in gray. Reconstructed sister neurons of registered ePN types that derive from reconstructions of three animals are shown in a different color each. Glomeruli DA1 and VA1v contain also PNs deriving from the ventral soma cluster.

Figure 1-Figure supplement 2. Density maps of the LH in lateral and posterior view

(A+B) Density maps of neuronal arborizations of 21 ePN types for three animals each in lateral and posterior view. Abbreviations: a anterior, d dorsal, l lateral, m medial, p posterior, v ventral

Figure 2-Figure supplement 1. Density maps and ePN clusters

(A) Density maps of neuronal arborizations of all ePN types in dorsal, lateral and posterior view. Color code (red to blue) represents the similarity of ePN density maps according to the first axis of the PCA shown in Figure 2B. Abbreviations: a anterior, d dorsal, l lateral, m medial, p posterior, v ventral

(B) Clustermatrix of all ePN types based on density maps reveals four clusters and the DA1-ePNs. Notably, no clear borders exist: several ePN types are similar to ePN types that are located in a different cluster. For example, VC1 belongs to the fourth cluster (violet) but is also very similar to ePN types in the second cluster (red) such as glomeruli VM7d, VA5 and DC1.

(C) Clustered ePN types in a PCA space confirm the ambiguous separation of innervated LH areas.

(D) Cosine distances of neuronal arborizations of ePN types obtained *in vivo* (data in this study) are highly correlated to correlation distances of neuronal arborizations of ePN types obtained *in vitro* (kindly provided by GSXE Jefferis, published in Jefferis 2007) ($r = 0.57$, $p = 3.4\ 10^{-36}$).

Figure 2-Figure supplement 2. Sensilla classes

(A) Pheromone-responsive ePNs (DA1, VA1d and VA1v) are located in the anterior LH in comparison to the remaining ePN types. Abbreviations: AL antennal lobe,

CX mushroom body calyx, LH lateral horn, a anterior, d dorsal, l lateral, m medial, p posterior, v ventral.

(B) ePN types color-coded according to sensilla classes of corresponding sensory neurons in dorsal, posterior and lateral view.

(C) ePN types color-coded as attractive (cyan; DM4, DM5, and DM2) and aversive (magenta ; D, DA4, DC3, DL1, DL4, and DL5) according to Knaden 2012 in dorsal, posterior and lateral view.

References

Andlauer, T.F., Scholz-Kornehl, S., Tian, R., Kirchner, M., Babikir, H.A., Depner, H., Loll, B., Quentin, C., Gupta, V.K., Holt, M.G*., et al.* (2014). Drep-2 is a novel synaptic protein important for learning and memory. eLife *3*.

Becher, P.G., Flick, G., Rozpędowska, E., Schmidt, A., Hagman, A., Lebreton, S., Larsson, M. C., Hansson, B. S., Piškur, J., Witzgall, P., et al. (2012). Yeast, not fruit volatiles mediate *Drosophila melanogaster* attraction, oviposition and development. Funct. Ecol. *26*, 822-828.

Bhandawat, V., Olsen, S.R., Gouwens, N.W., Schlief, M.L., and Wilson, R.I. (2007). Sensory processing in the *Drosophila* antennal lobe increases reliability and separability of ensemble odor representations. Nature neuroscience *10*, 1474-1482.

Brand, A.H., and Perrimon, N. (1993). Targeted gene expression as a means of altering cell fates and generating dominant phenotypes. Development *118*, 401-415.

Cachero, S., Ostrovsky, A.D., Yu, J.Y., Dickson, B.J., and Jefferis, G.S. (2010). Sexual dimorphism in the fly brain. Current biology : CB *20*, 1589-1601.

Datta, S.R., Vasconcelos, M.L., Ruta, V., Luo, S., Wong, A., Demir, E., Flores, J., Balonze, K., Dickson, B.J., and Axel, R. (2008). The *Drosophila* pheromone cVA activates a sexually dimorphic neural circuit. Nature *452*, 473-477.

Davis, R.L. (2005). Olfactory memory formation in *Drosophila*: from molecular to systems neuroscience. Annual review of neuroscience *28*, 275-302.

Duistermars, B.J., and Frye, M.A. (2010). Multisensory integration for odor tracking by flying *Drosophila*: Behavior, circuits and speculation. Communicative & integrative biology *3*, 60-63.

Dweck, H.K., Ebrahim, S.A., Farhan, A., Hansson, B.S., and Stensmyr, M.C. (2015a). Olfactory proxy detection of dietary antioxidants in *Drosophila*. Current biology : CB *25*, 455-466.

Dweck, H.K., Ebrahim, S.A., Thoma, M., Mohamed, A.A., Keesey, I.W., Trona, F., Lavista-Llanos, S., Svatos, A., Sachse, S., Knaden, M., and Hansson, B.S. (2015b). Pheromones mediating copulation and attraction in *Drosophila*. Proceedings of the National Academy of Sciences of the United States of America *112*, E2829-2835.

Ebrahim, S.A., Dweck, H.K., Stokl, J., Hofferberth, J.E., Trona, F., Weniger, K., Rybak, J., Seki, Y., Stensmyr, M.C., Sachse, S.*, et al.* (2015). *Drosophila* Avoids Parasitoids by Sensing Their Semiochemicals via a Dedicated Olfactory Circuit. PLoS biology *13*, e1002318.

Fan, P., Manoli, D.S., Ahmed, O.M., Chen, Y., Agarwal, N., Kwong, S., Cai, A.G., Neitz, J., Renslo, A., Baker, B.S., and Shah, N.M. (2013). Genetic and neural mechanisms that inhibit *Drosophila* from mating with other species. Cell *154*, 89-102.

Feinberg, E.H., Vanhoven, M.K., Bendesky, A., Wang, G., Fetter, R.D., Shen, K., and Bargmann, C.I. (2008). GFP Reconstitution Across Synaptic Partners (GRASP) defines cell contacts and synapses in living nervous systems. Neuron *57*, 353-363.

Fiala, A., Spall, T., Diegelmann, S., Eisermann, B., Sachse, S., Devaud, J.M., Buchner, E., and Galizia, C.G. (2002). Genetically expressed cameleon in *Drosophila melanogaster* is used to visualize olfactory information in projection neurons. Current biology : CB *12*, 1877-1884.

Fişek, M., and Wilson, R.I. (2014). Stereotyped connectivity and computations in higher-order olfactory neurons. Nature neuroscience *17*, 280-288.

Fishilevich, E., and Vosshall, L.B. (2005). Genetic and functional subdivision of the *Drosophila* antennal lobe. Current biology : CB *15*, 1548-1553.

Grabe, V., Baschwitz, A., Dweck, H.K., Lavista-Llanos, S., Hansson, B.S., and Sachse, S. (2016). Elucidating the Neuronal Architecture of Olfactory Glomeruli in the *Drosophila* Antennal Lobe. Cell reports *16*, 3401-3413.

Grabe, V., Strutz, A., Baschwitz, A., Hansson, B.S., and Sachse, S. (2015). Digital *in vivo* 3D atlas of the antennal lobe of *Drosophila melanogaster*. The Journal of comparative neurology *523*, 530-544.

Gupta, N., and Stopfer, M. (2012). Functional analysis of a higher olfactory center, the lateral horn. The Journal of neuroscience : the official journal of the Society for Neuroscience *32*, 8138-8148.

Ha, T.S., and Smith, D.P. (2006). A pheromone receptor mediates 11-*cis*-vaccenyl acetate-induced responses in *Drosophila*. The Journal of neuroscience : the official journal of the Society for Neuroscience *26*, 8727-8733.

Heimbeck, G., Bugnon, V., Gendre, N., Keller, A., and Stocker, R.F. (2001). A central neural circuit for experience-independent olfactory and courtship behavior in *Drosophila melanogaster*. Proceedings of the National Academy of Sciences of the United States of America *98*, 15336-15341.

Heisenberg, M. (2003). Mushroom body memoir: from maps to models. Nature reviews. Neuroscience *4*, 266-275.

Ito, K., Awano, W., Suzuki, K., Hiromi, Y., and Yamamoto, D. (1997). The *Drosophila* mushroom body is a quadruple structure of clonal units each of which contains a virtually identical set of neurones and glial cells. Development *124*, 761-771.

Jefferis, G.S., Potter, C.J., Chan, A.M., Marin, E.C., Rohlfing, T., Maurer, C.R., Jr., and Luo, L. (2007). Comprehensive maps of *Drosophila* higher olfactory centers: spatially segregated fruit and pheromone representation. Cell *128*, 1187-1203.

Karuppudurai, T., Lin, T.-Y., Ting, C.-Y., Pursley, R., Melnattur, Krishna V., Diao, F., White, Benjamin H., Macpherson, Lindsey J., Gallio, M., Pohida, T., and Lee, C.-H. (2014). A Hard-Wired Glutamatergic Circuit Pools and Relays UV Signals to Mediate Spectral Preference in *Drosophila*. Neuron *81*, 603-615.

Kido, A., and Ito, K. (2002). Mushroom bodies are not required for courtship behavior by normal and sexually mosaic *Drosophila*. Journal of neurobiology *52*, 302-311.

Knaden, M., Strutz, A., Ahsan, J., Sachse, S., and Hansson, B.S. (2012). Spatial representation of odorant valence in an insect brain. Cell reports *1*, 392-399.

Kohl, J., Ostrovsky, A.D., Frechter, S., and Jefferis, G.S. (2013). A bidirectional circuit switch reroutes pheromone signals in male and female brains. Cell *155*, 1610-1623.

Kurtovic, A., Widmer, A., and Dickson, B.J. (2007). A single class of olfactory neurons mediates behavioural responses to a *Drosophila* sex pheromone. Nature *446*, 542-546.

Lai, S.L., Awasaki, T., Ito, K., and Lee, T. (2008). Clonal analysis of *Drosophila* antennal lobe neurons: diverse neuronal architectures in the lateral neuroblast lineage. Development *135*, 2883-2893.

Larsson, M.C., Domingos, A.I., Jones, W.D., Chiappe, M.E., Amrein, H., and Vosshall, L.B. (2004). Or83b encodes a broadly expressed odorant receptor essential for *Drosophila* olfaction. Neuron *43*, 703-714.

Lebreton, S., Trona, F., Borrero-Echeverry, F., Bilz, F., Grabe, V., Becher, P.G., Carlsson, M.A., Nassel, D.R., Hansson, B.S., Sachse, S., and Witzgall, P. (2015). Feeding regulates sex pheromone attraction and courtship in *Drosophila* females. Scientific reports *5*, 13132.

Lee, D.D., and Seung, H.S. (1999). Learning the parts of objects by non-negative matrix factorization. Nature *401*, 788-791.

Li, H., Li, Y., Lei, Z., Wang, K., and Guo, A. (2013). Transformation of odor selectivity from projection neurons to single mushroom body neurons mapped with dual-color calcium imaging. Proceedings of the National Academy of Sciences of the United States of America *110*, 12084-12089.

Liang, L., Li, Y., Potter, C.J., Yizhar, O., Deisseroth, K., Tsien, R.W., and Luo, L. (2013). GABAergic projection neurons route selective olfactory inputs to specific higher-order neurons. Neuron *79*, 917-931.

Marin, E.C., Jefferis, G.S., Komiyama, T., Zhu, H., and Luo, L. (2002). Representation of the glomerular olfactory map in the *Drosophila* brain. Cell *109*, 243-255.

Min, S., Ai, M., Shin, S.A., and Suh, G.S. (2013). Dedicated olfactory neurons mediating attraction behavior to ammonia and amines in *Drosophila*. Proceedings of the National Academy of Sciences of the United States of America *110*, E1321-1329.

Münch, D., and Galizia, C.G. (2016). DoOR 2.0--Comprehensive Mapping of *Drosophila melanogaster* Odorant Responses. Scientific reports *6*, 21841.

Nassi, J.J., and Callaway, E.M. (2009). Parallel processing strategies of the primate visual system. Nature reviews. Neuroscience *10*, 360-372.

Ng, M., Roorda, R.D., Lima, S.Q., Zemelman, B.V., Morcillo, P., and Miesenbock, G. (2002). Transmission of olfactory information between three populations of neurons in the antennal lobe of the fly. Neuron *36*, 463-474.

Okada, R., Awasaki, T., and Ito, K. (2009). Gamma-aminobutyric acid (GABA)-mediated neural connections in the *Drosophila* antennal lobe. The Journal of comparative neurology *514*, 74-91.

Olsen, S.R., Bhandawat, V., and Wilson, R.I. (2007). Excitatory interactions between olfactory processing channels in the *Drosophila* antennal lobe. Neuron *54*, 89-103.

Olsen, S.R., Bhandawat, V., and Wilson, R.I. (2010). Divisive normalization in olfactory population codes. Neuron *66*, 287-299.

Olsen, S.R., and Wilson, R.I. (2008). Lateral presynaptic inhibition mediates gain control in an olfactory circuit. Nature *452*, 956-960.

Parnas, M., Lin, A.C., Huetteroth, W., and Miesenbock, G. (2013). Odor discrimination in *Drosophila*: from neural population codes to behavior. Neuron *79*, 932-944.

Patterson, G.H., and Lippincott-Schwartz, J. (2002). A photoactivatable GFP for selective photolabeling of proteins and cells. Science *297*, 1873-1877.

Potter, C.J., Tasic, B., Russler, E.V., Liang, L., and Luo, L. (2010). The Q system: a repressible binary system for transgene expression, lineage tracing, and mosaic analysis. Cell *141*, 536-548.

Root, C.M., Masuyama, K., Green, D.S., Enell, L.E., Nassel, D.R., Lee, C.H., and Wang, J.W. (2008). A presynaptic gain control mechanism fine-tunes olfactory behavior. Neuron *59*, 311-321.

Root, C.M., Semmelhack, J.L., Wong, A.M., Flores, J., and Wang, J.W. (2007). Propagation of olfactory information in *Drosophila*. Proceedings of the National Academy of Sciences of the United States of America *104*, 11826-11831.

Ruta, V., Datta, S.R., Vasconcelos, M.L., Freeland, J., Looger, L.L., and Axel, R. (2010). A dimorphic pheromone circuit in *Drosophila* from sensory input to descending output. Nature *468*, 686-690.

Rybak, J., Kuss, A., Lamecker, H., Zachow, S., Hege, H.C., Lienhard, M., Singer, J., Neubert, K., and Menzel, R. (2010). The Digital Bee Brain: Integrating and Managing Neurons in a Common 3D Reference System. Frontiers in systems neuroscience *4*.

Schubert, M., Hansson, B.S., and Sachse, S. (2014). The banana code-natural blend processing in the olfactory circuitry of *Drosophila melanogaster*. Frontiers in physiology *5*, 59.

Semmelhack, J.L., and Wang, J.W. (2009). Select *Drosophila* glomeruli mediate innate olfactory attraction and aversion. Nature *459*, 218-223.

Shang, Y., Claridge-Chang, A., Sjulson, L., Pypaert, M., and Miesenbock, G. (2007). Excitatory local circuits and their implications for olfactory processing in the fly antennal lobe. Cell *128*, 601-612.

Silbering, A.F., and Galizia, C.G. (2007). Processing of odor mixtures in the *Drosophila* antennal lobe reveals both global inhibition and glomerulus-specific interactions. The Journal of neuroscience : the official journal of the Society for Neuroscience *27*, 11966-11977.

Silbering, A.F., Okada, R., Ito, K., and Galizia, C.G. (2008). Olfactory information processing in the *Drosophila* antennal lobe: anything goes? The Journal of neuroscience : the official journal of the Society for Neuroscience *28*, 13075-13087.

Soelter, J., Schumacher, J., Spors, H., and Schmuker, M. (2014). Automatic segmentation of odor maps in the mouse olfactory bulb using regularized non-negative matrix factorization. NeuroImage *98*, 279-288.

Soucy, E.R., Albeanu, D.F., Fantana, A.L., Murthy, V.N., and Meister, M. (2009). Precision and diversity in an odor map on the olfactory bulb. Nature neuroscience *12*, 210-220.

Steck, K., Veit, D., Grandy, R., Badia, S.B., Mathews, Z., Verschure, P., Hansson, B.S., and Knaden, M. (2012). A high-throughput behavioral paradigm for *Drosophila* olfaction - The Flywalk. Scientific reports *2*, 361.

Stensmyr, M.C., Dweck, H.K., Farhan, A., Ibba, I., Strutz, A., Mukunda, L., Linz, J., Grabe, V., Steck, K., Lavista-Llanos, S.*, et al.* (2012). A conserved dedicated olfactory circuit for detecting harmful microbes in *Drosophila*. Cell *151*, 1345-1357.

Stensmyr, M.C., Giordano, E., Balloi, A., Angioy, A.M., and Hansson, B.S. (2003). Novel natural ligands for *Drosophila* olfactory receptor neurones. The Journal of experimental biology *206*, 715-724.

Stocker, R.F., Heimbeck, G., Gendre, N., and de Belle, J.S. (1997). Neuroblast ablation in *Drosophila* P[GAL4] lines reveals origins of olfactory interneurons. Journal of neurobiology *32*, 443-456.

Stocker, R.F., Lienhard, M.C., Borst, A., and Fischbach, K.F. (1990). Neuronal architecture of the antennal lobe in *Drosophila melanogaster*. Cell and tissue research *262*, 9-34.

Strutz, A., Soelter, J., Baschwitz, A., Farhan, A., Grabe, V., Rybak, J., Knaden, M., Schmuker, M., Hansson, B.S., and Sachse, S. (2014). Decoding odor quality and intensity in the *Drosophila* brain. eLife *3*, e04147.

Tanaka, N.K., Awasaki, T., Shimada, T., and Ito, K. (2004). Integration of chemosensory pathways in the *Drosophila* second-order olfactory centers. Current biology : CB *14*, 449-457.

Tanaka, N.K., Endo, K., and Ito, K. (2012). Organization of antennal lobe-associated neurons in adult *Drosophila melanogaster* brain. The Journal of comparative neurology *520*, 4067-4130.

Thoma, M., Hansson, B.S., and Knaden, M. (2014). Compound valence is conserved in binary odor mixtures in *Drosophila melanogaster*. The Journal of experimental biology *217*, 3645-3655.

Tian, L., Hires, S.A., Mao, T., Huber, D., Chiappe, M.E., Chalasani, S.H., Petreanu, L., Akerboom, J., McKinney, S.A., Schreiter, E.R.*, et al.* (2009). Imaging neural activity in worms, flies and mice with improved GCaMP calcium indicators. Nature methods *6*, 875-881.

Vosshall, L.B., Wong, A.M., and Axel, R. (2000). An olfactory sensory map in the fly brain. Cell *102*, 147-159.

Wang, J.W., Wong, A.M., Flores, J., Vosshall, L.B., and Axel, R. (2003a). Two-photon calcium imaging reveals an odor-evoked map of activity in the fly brain. Cell *112*, 271-282.

Wang, K., Gong, J., Wang, Q., Li, H., Cheng, Q., Liu, Y., Zeng, S., and Wang, Z. (2014). Parallel pathways convey olfactory information with opposite polarities in *Drosophila*. Proceedings of the National Academy of Sciences of the United States of America *111*, 3164-3169.

Wang, Y., Chiang, A.S., Xia, S., Kitamoto, T., Tully, T., and Zhong, Y. (2003b). Blockade of neurotransmission in *Drosophila* mushroom bodies impairs odor attraction, but not repulsion. Current biology : CB *13*, 1900-1904.

Wang, Y., Guo, H.F., Pologruto, T.A., Hannan, F., Hakker, I., Svoboda, K., and Zhong, Y. (2004). Stereotyped odor-evoked activity in the mushroom body of *Drosophila* revealed by green fluorescent protein-based Ca^{2+} imaging. The Journal of neuroscience : the official journal of the Society for Neuroscience *24*, 6507-6514.

Wilson, R.I., and Laurent, G. (2005). Role of GABAergic inhibition in shaping odor-evoked spatiotemporal patterns in the *Drosophila* antennal lobe. The Journal of neuroscience : the official journal of the Society for Neuroscience *25*, 9069-9079.

Wilson, R.I., Turner, G.C., and Laurent, G. (2004). Transformation of olfactory representations in the *Drosophila* antennal lobe. Science *303*, 366-370.

Wong, A.M., Wang, J.W., and Axel, R. (2002). Spatial representation of the glomerular map in the *Drosophila* protocerebrum. Cell *109*, 229-241.

Xia, S., and Tully, T. (2007). Segregation of odor identity and intensity during odor discrimination in *Drosophila* mushroom body. PLoS biology *5*, e264.

Yaksi, E., and Wilson, R.I. (2010). Electrical coupling between olfactory glomeruli. Neuron *67*, 1034-1047.

Yu, J.Y., Kanai, M.I., Demir, E., Jefferis, G.S., and Dickson, B.J. (2010). Cellular organization of the neural circuit that drives *Drosophila* courtship behavior. Current biology : CB *20*, 1602-1614.

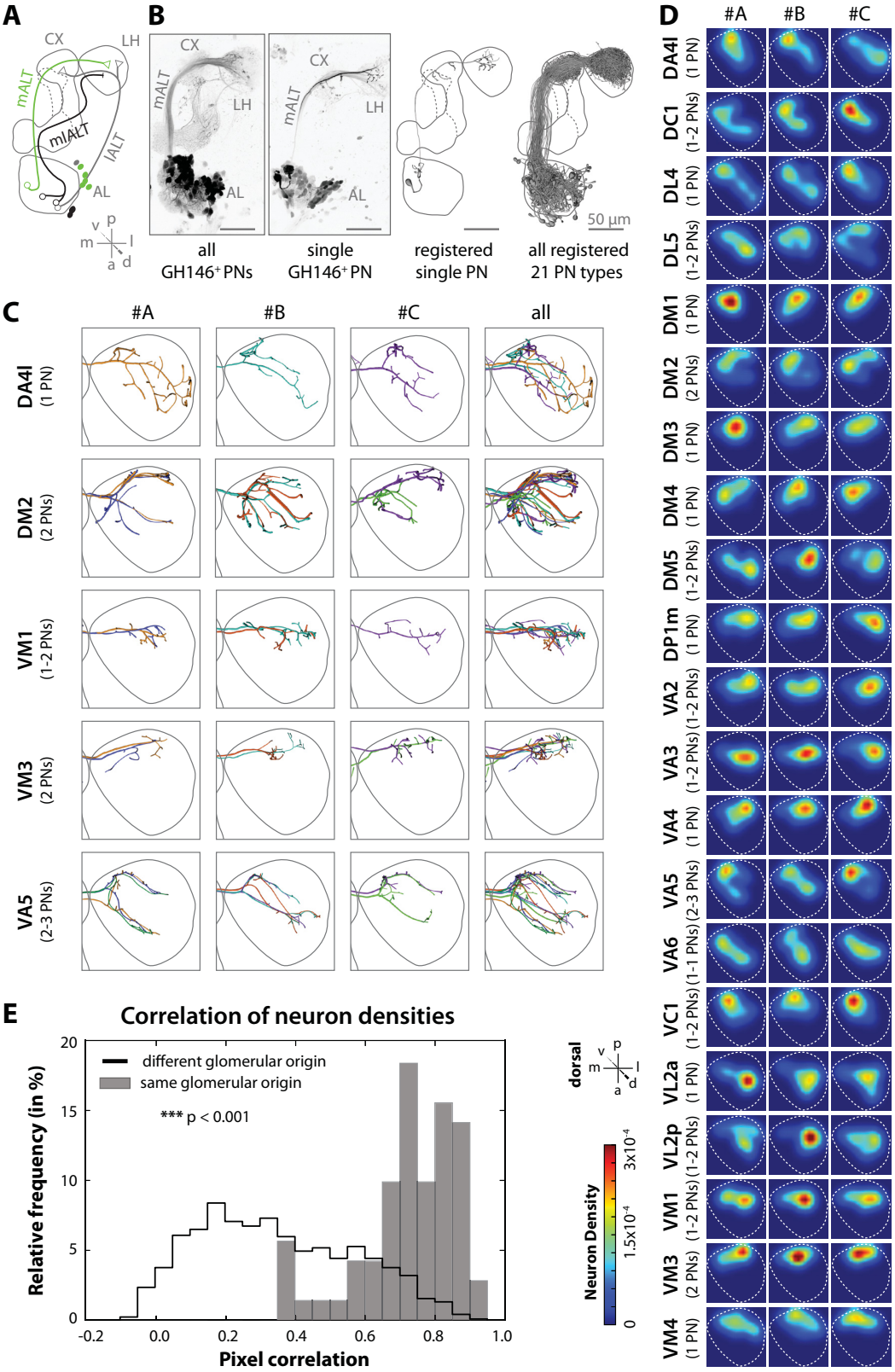
A
B
CX
LH
mALT
mlALT
lALT
AL
v p m l a d
all GH146+ PNs
single GH146+ PN
registered single PN
all registered 21 PN types
50 µm
C
#A
#B
#C
all
DA4l (1 PN)
DM2 (2 PNs)
VM1 (1-2 PNs)
VM3 (2 PNs)
VA5 (2-3 PNs)
D
#A
#B
#C
DA4l (1 PN)
DC1 (1-2 PNs)
DL4 (1 PN)
DL5 (1-2 PNs)
DM1 (1 PN)
DM2 (2 PNs)
DM3 (1 PN)
DM4 (1 PN)
DM5 (1-2 PNs)
DP1m (1 PN)
VA2 (1-2 PNs)
VA3 (1-2 PNs)
VA4 (1 PN)
VA5 (2-3 PNs)
VA6 (1-1 PNs)
VC1 (1-2 PNs)
VL2a (1 PN)
VL2p (1-2 PNs)
VM1 (1-2 PNs)
VM3 (2 PNs)
VM4 (1 PN)
E
Correlation of neuron densities
different glomerular origin
same glomerular origin
*** p < 0.001
Relative frequency (in %)
Pixel correlation
dorsal
Neuron Density
3x10-4
1.5x10-4
0

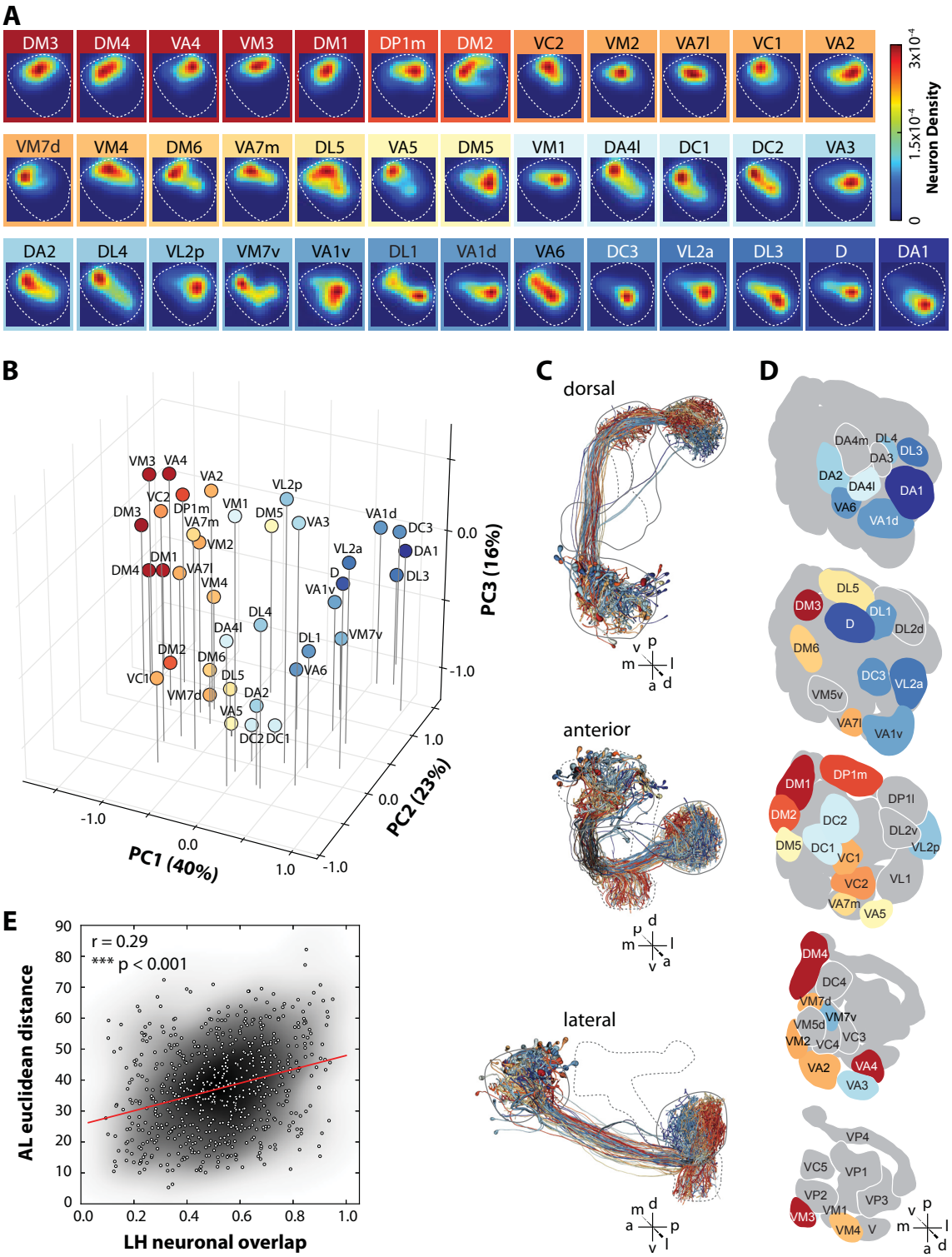
A
DM3 DM4 VA4 VM3 DM1 DP1m DM2 VC2 VM2 VA7l VC1 VA2
VM7d VM4 DM6 VA7m DL5 VA5 DM5 VM1 DA4l DC1 DC2 VA3
DA2 DL4 VL2p VM7v VA1v DL1 VA1d VA6 DC3 VL2a DL3 D DA1
Neuron Density
3x10-4
1.5x10-4
0
B
PC1 (40%)
PC2 (23%)
PC3 (16%)
C
dorsal
anterior
lateral
D
E
r = 0.29
*** p < 0.001
AL euclidean distance
LH neuronal overlap

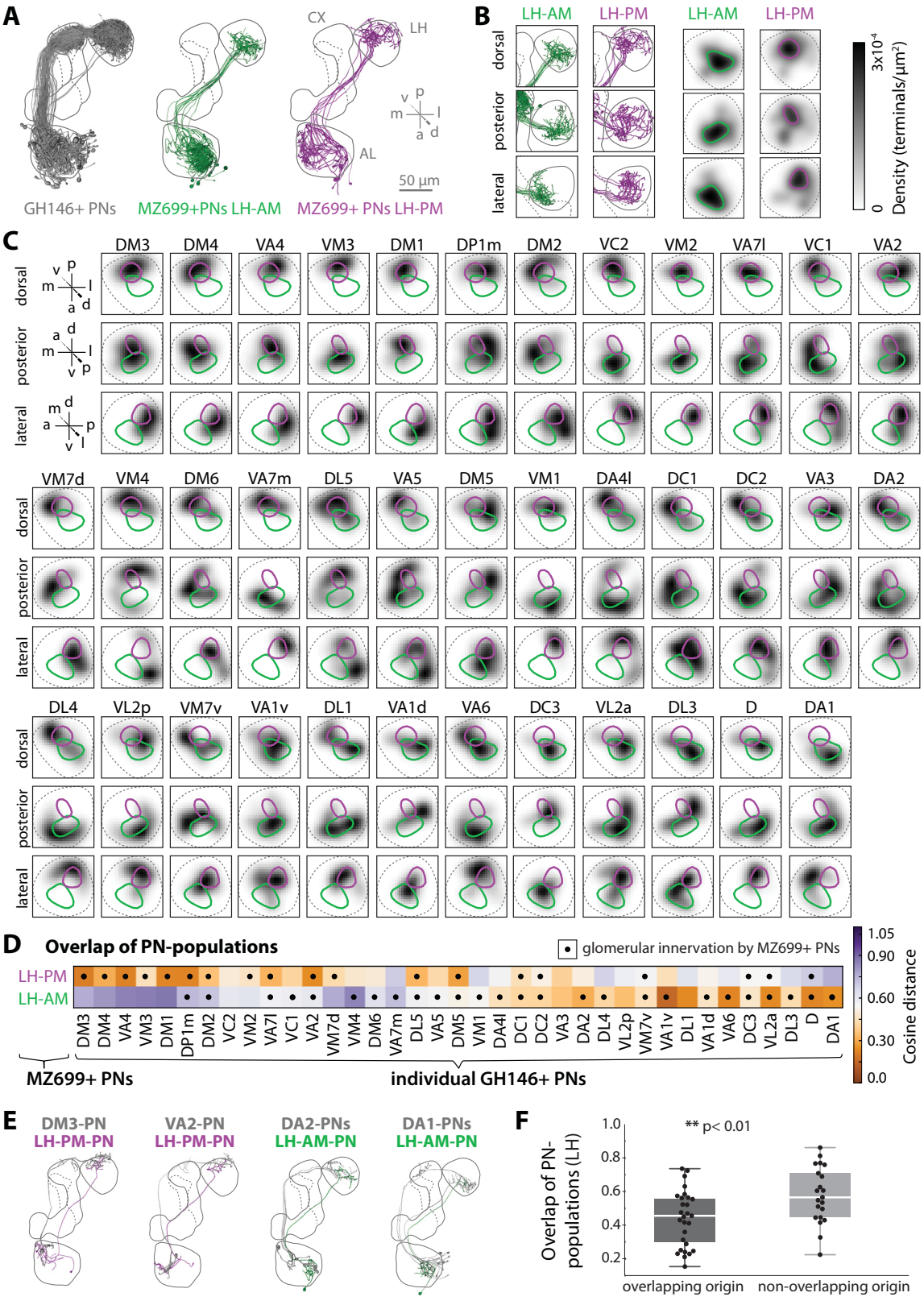
A
CX
LH
AL
50 µm
GH146+ PNs
MZ699+PNs LH-AM
MZ699+ PNs LH-PM
B
LH-AM
LH-PM
LH-AM
LH-PM
dorsal
posterior
lateral
3x10-4
0
Density (terminals/µm2)
C
DM3 DM4 VA4 VM3 DM1 DP1m DM2 VC2 VM2 VA7l VC1 VA2
VM7d VM4 DM6 VA7m DL5 VA5 DM5 VM1 DA4l DC1 DC2 VA3 DA2
DL4 VL2p VM7v VA1v DL1 VA1d VA6 DC3 VL2a DL3 D DA1
D
Overlap of PN-populations
glomerular innervation by MZ699+ PNs
LH-PM
LH-AM
MZ699+ PNs
individual GH146+ PNs
1.05
0.90
0.60
0.30
0.0
Cosine distance
E
DM3-PN LH-PM-PN
VA2-PN LH-PM-PN
DA2-PNs LH-AM-PN
DA1-PNs LH-AM-PN
F
** p< 0.01
Overlap of PN-populations (LH)
1.0
0.8
0.6
0.4
0.2
overlapping origin
non-overlapping origin

Baschwitz et al.
Figure 4

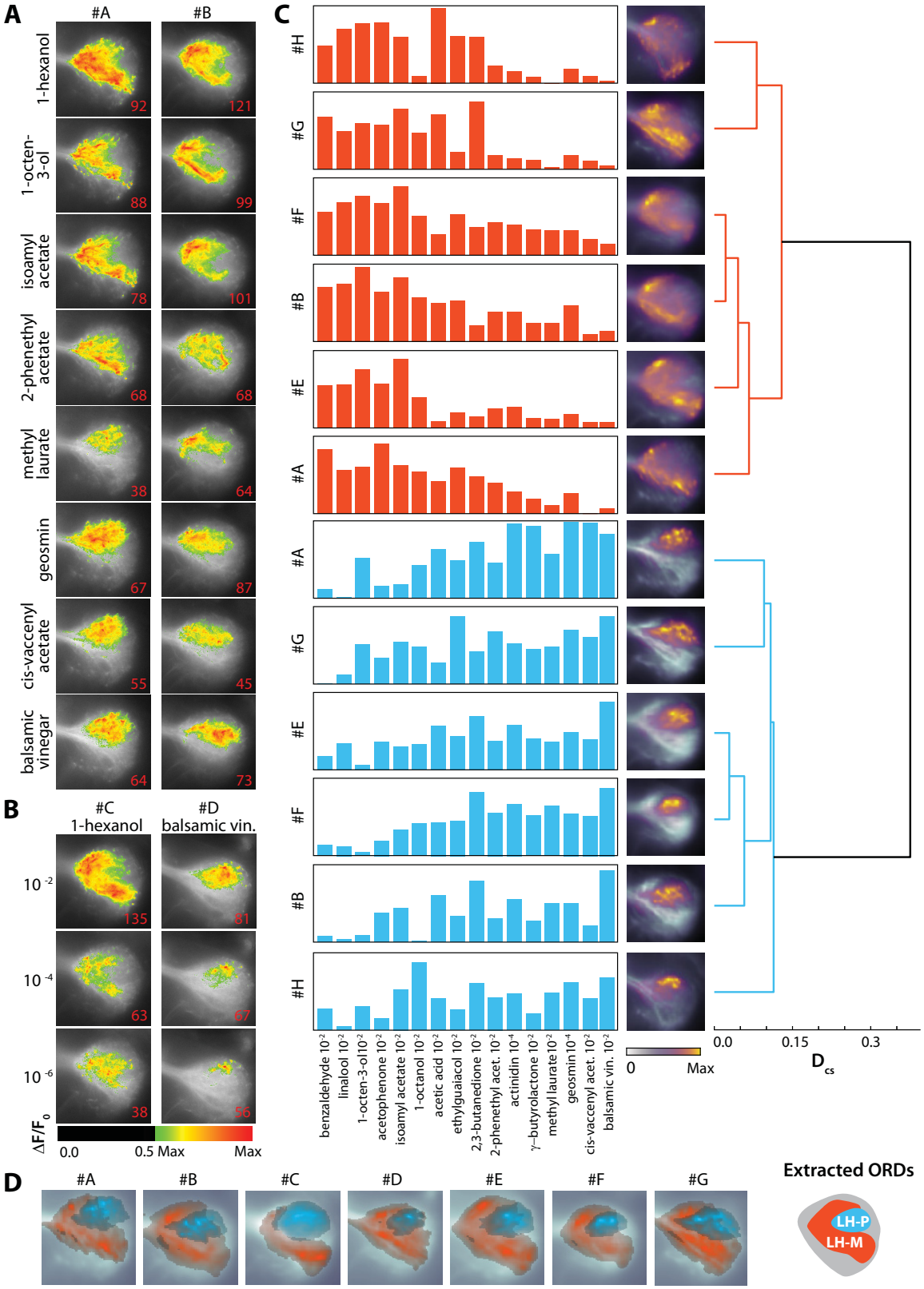

Baschwitz et al.
Figure 5

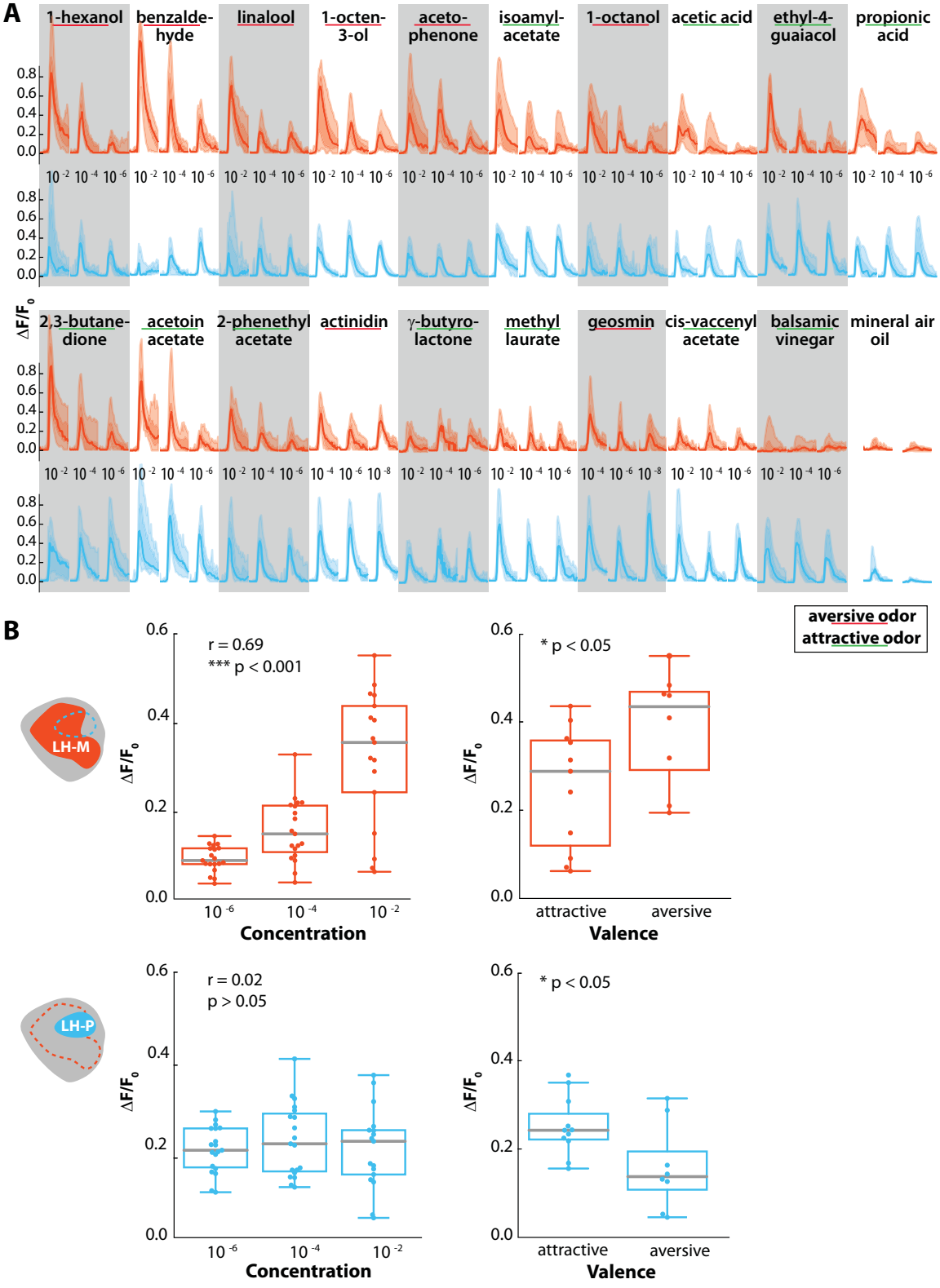

Baschwitz et al.
Figure 6

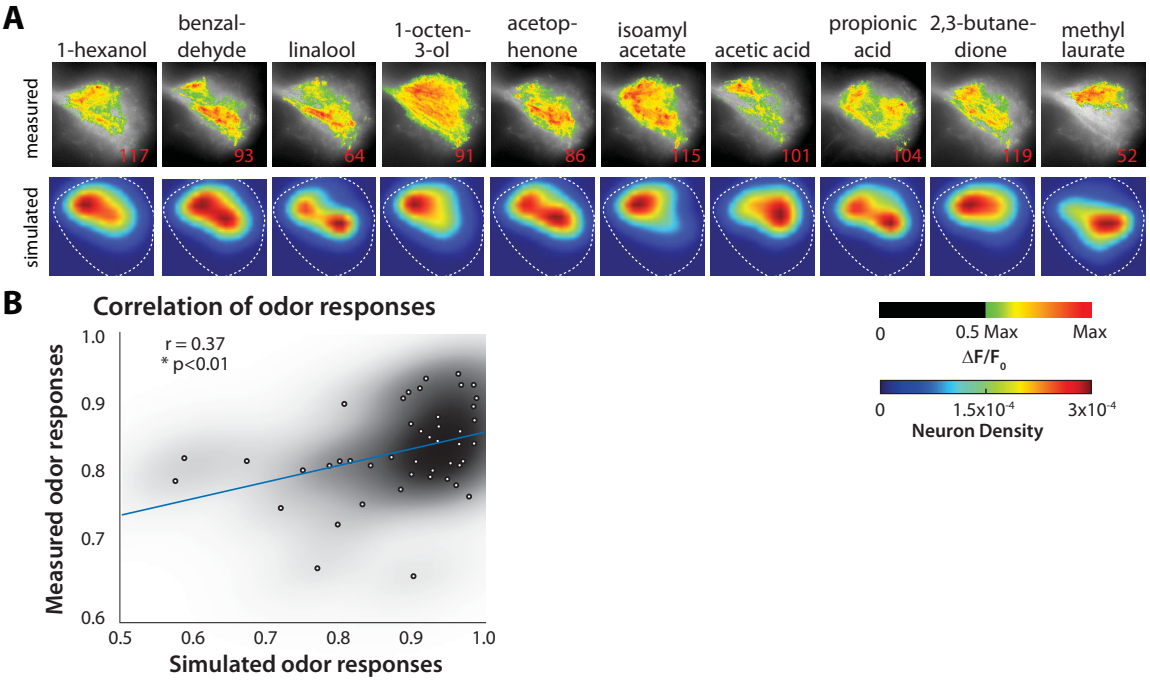

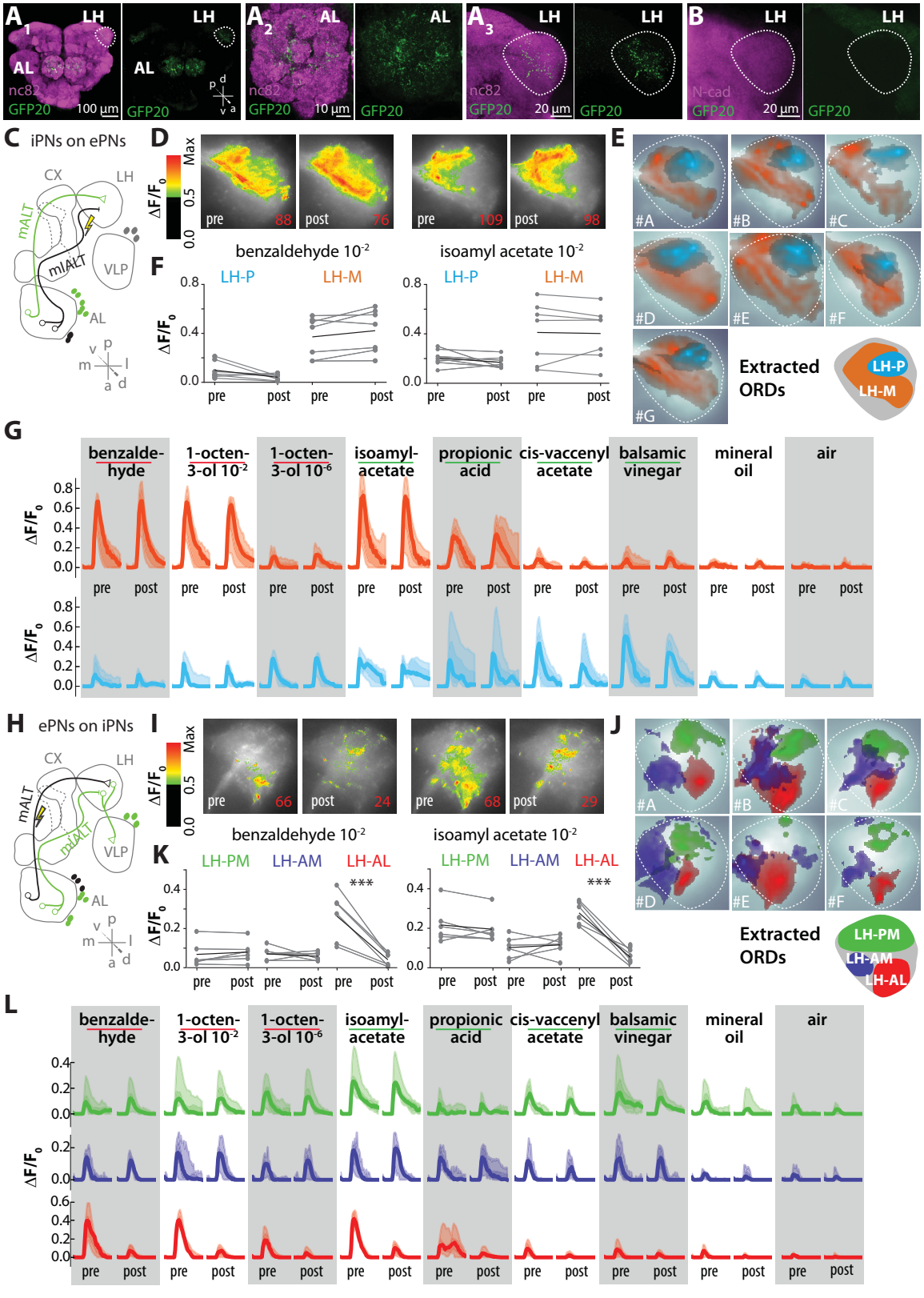
A1
LH
AL
nc82
GFP20
100 µm
A2
10 µm
A3
20 µm
B
N-cad
C iPNs on ePNs
CX
mALT
VLP
D
Max
ΔF/F0
pre
post
88
76
109
98
E
#A
#B
#C
#D
#E
#F
#G
Extracted ORDs
LH-P
LH-M
F
benzaldehyde 10-2
isoamyl acetate 10-2
G
benzalde-hyde
1-octen-3-ol 10-2
1-octen-3-ol 10-6
isoamyl-acetate
propionic acid
cis-vaccenyl acetate
balsamic vinegar
mineral oil
air
H ePNs on iPNs
I
66
24
68
29
J
K
LH-PM
LH-AM
LH-AL
***
L

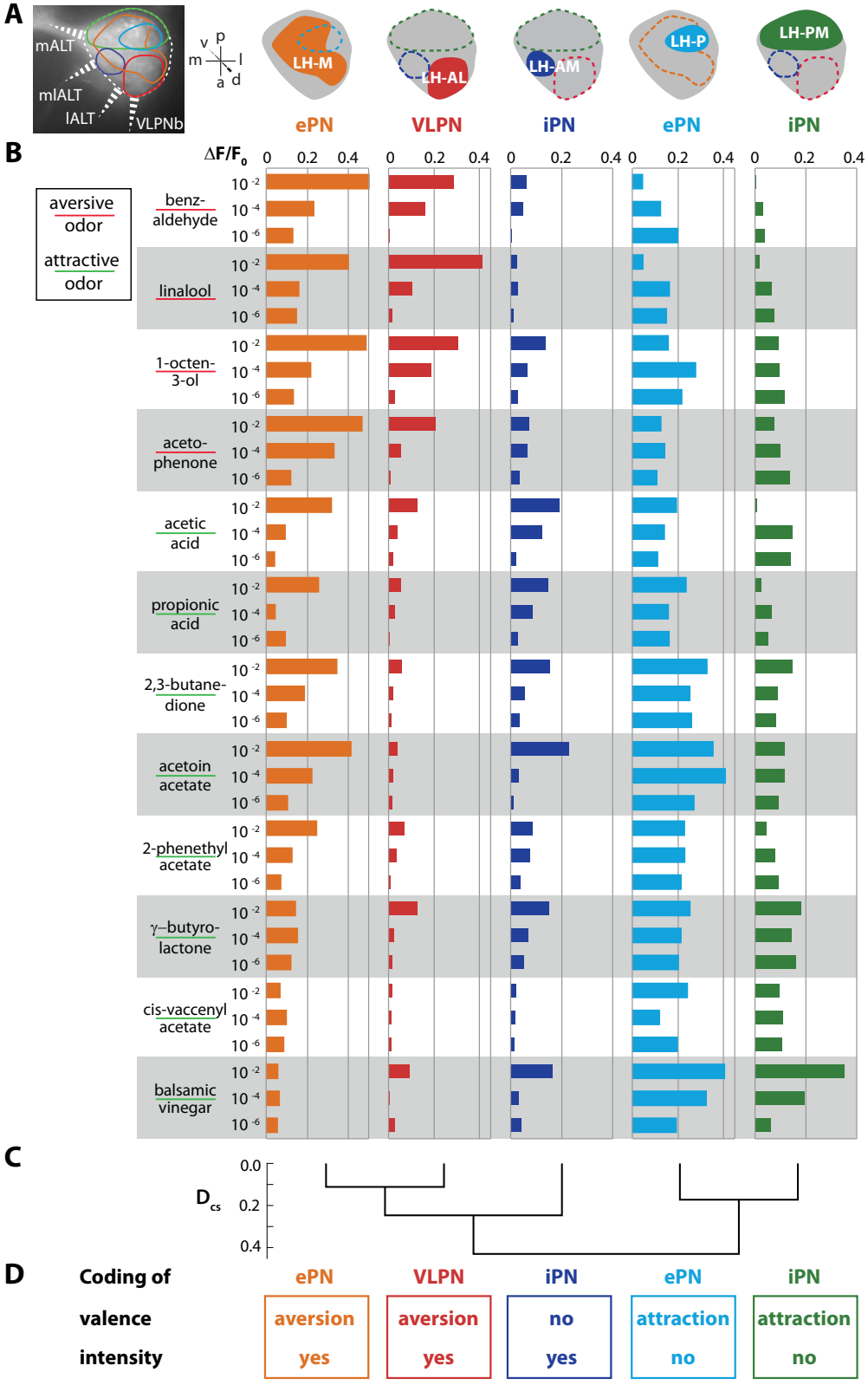
A
mALT
mlALT
lALT
VLPNb
v p
m l
a d
LH-M
LH-AL
LH-AM
LH-P
LH-PM
ePN
VLPN
iPN
ePN
iPN
B
ΔF/F0
0 0.2 0.4
aversive odor
attractive odor
benz-aldehyde
linalool
1-octen-3-ol
aceto-phenone
acetic acid
propionic acid
2,3-butane-dione
acetoin acetate
2-phenethyl acetate
γ–butyro-lactone
cis-vaccenyl acetate
balsamic vinegar
10 -2
10 -4
10 -6
C
Dcs
0.0
0.2
0.4
D
Coding of
valence
intensity
ePN
VLPN
iPN
ePN
iPN
aversion
yes
aversion
yes
no
yes
attraction
no
attraction
no

Baschwitz et al.

Figure 1 Supplement 1

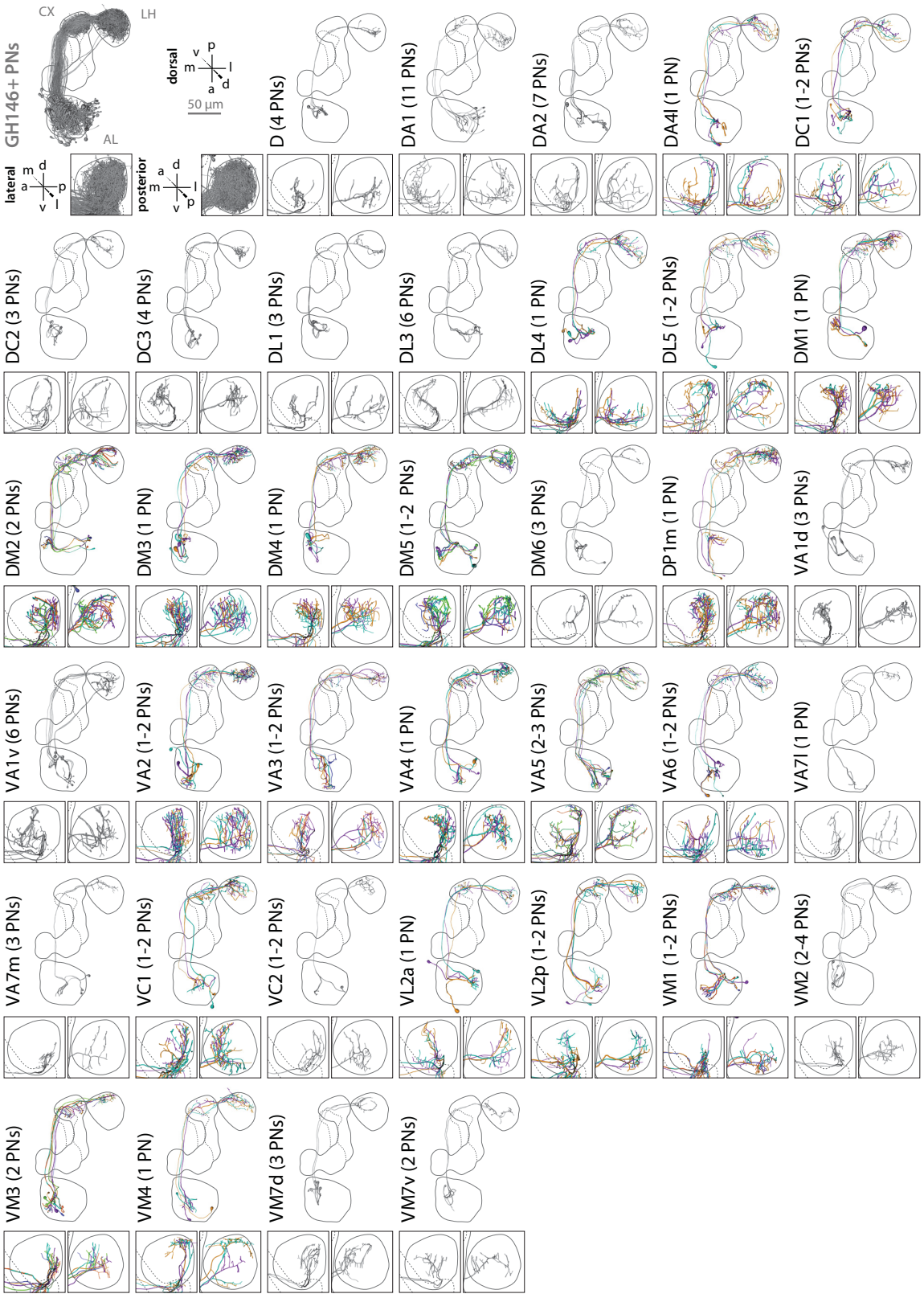

Baschwitz et al.
Figure 1 - Figure Supplement 2

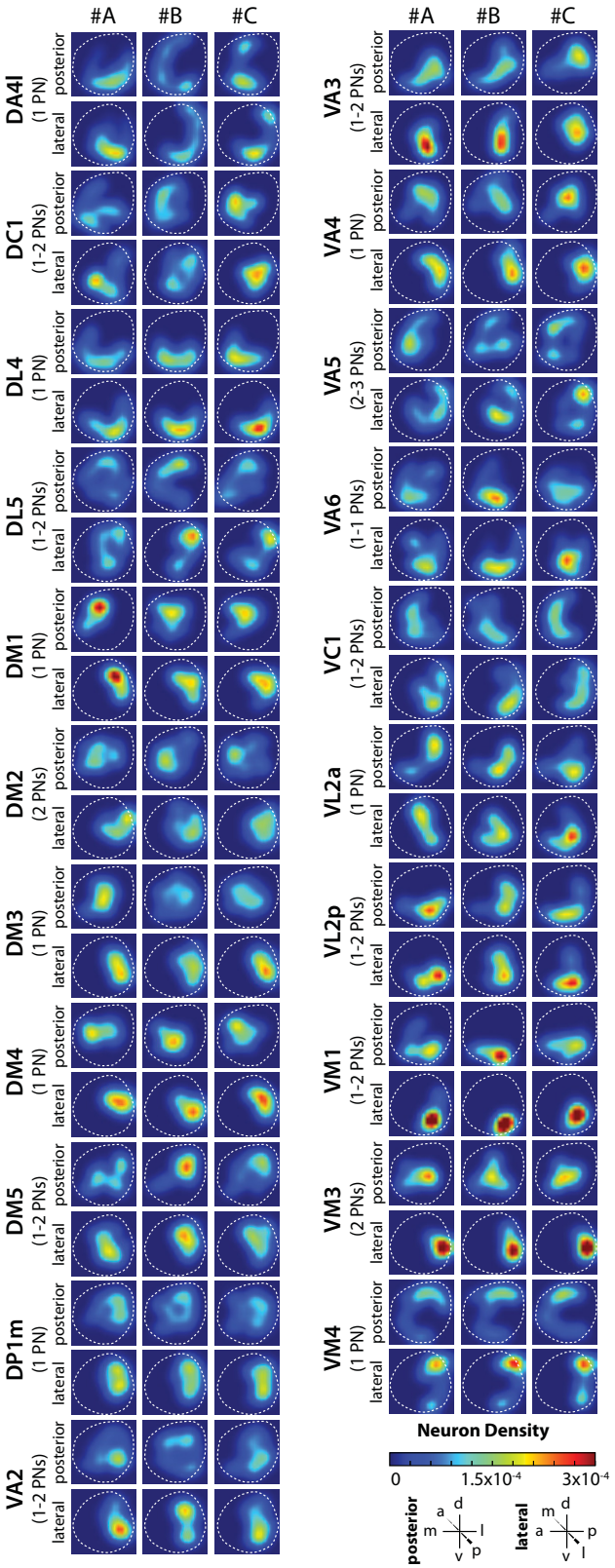

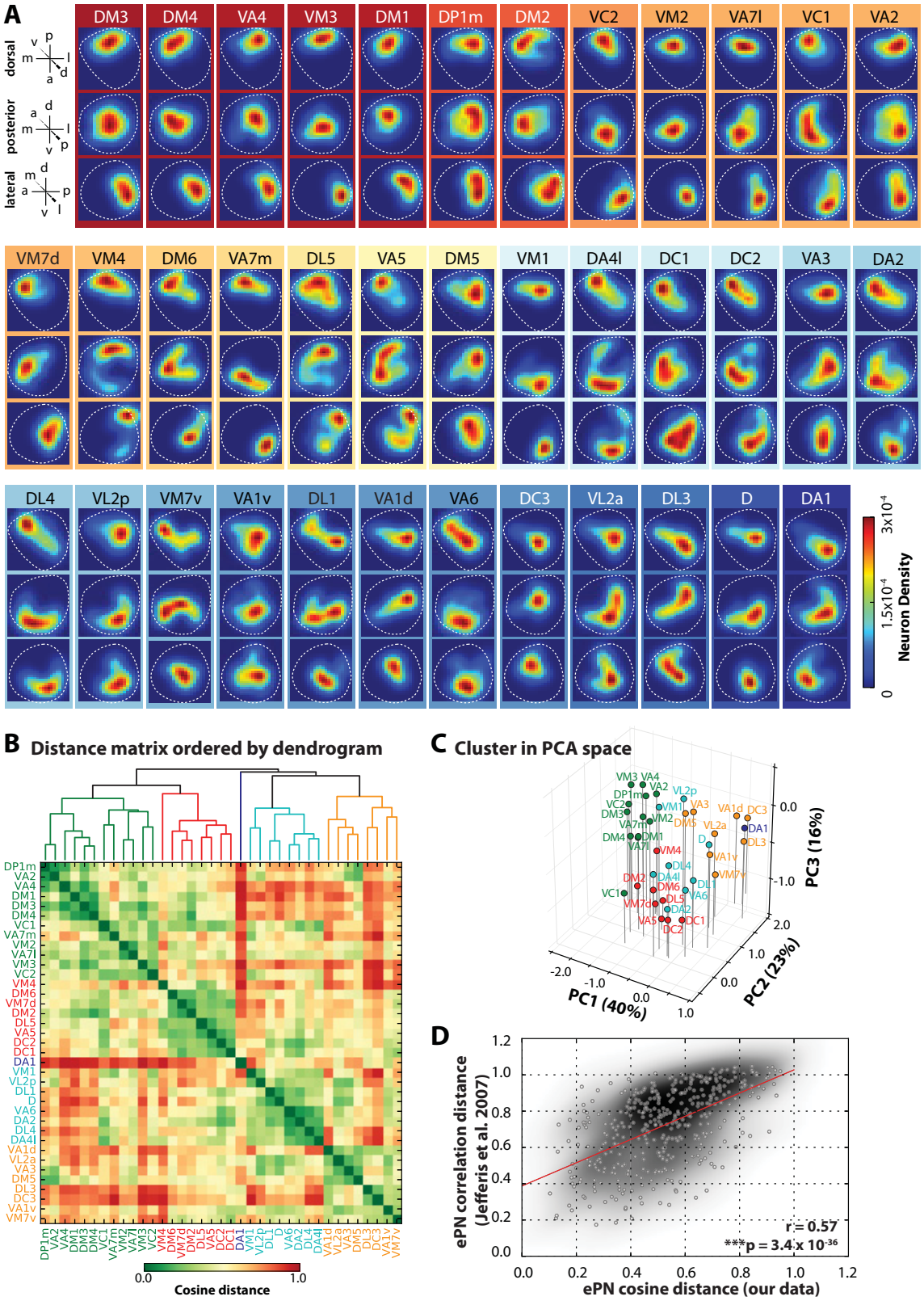
A
dorsal
posterior
lateral
DM3 DM4 VA4 VM3 DM1 DP1m DM2 VC2 VM2 VA7l VC1 VA2
VM7d VM4 DM6 VA7m DL5 VA5 DM5 VM1 DA4l DC1 DC2 VA3 DA2
DL4 VL2p VM7v VA1v DL1 VA1d VA6 DC3 VL2a DL3 D DA1
3x10-4
1.5x10-4
0
Neuron Density
B Distance matrix ordered by dendrogram
Cosine distance
C Cluster in PCA space
PC1 (40%)
PC2 (23%)
PC3 (16%)
D
ePN correlation distance (Jefferis et al. 2007)
ePN cosine distance (our data)
r = 0.57
***p = 3.4 x 10-36

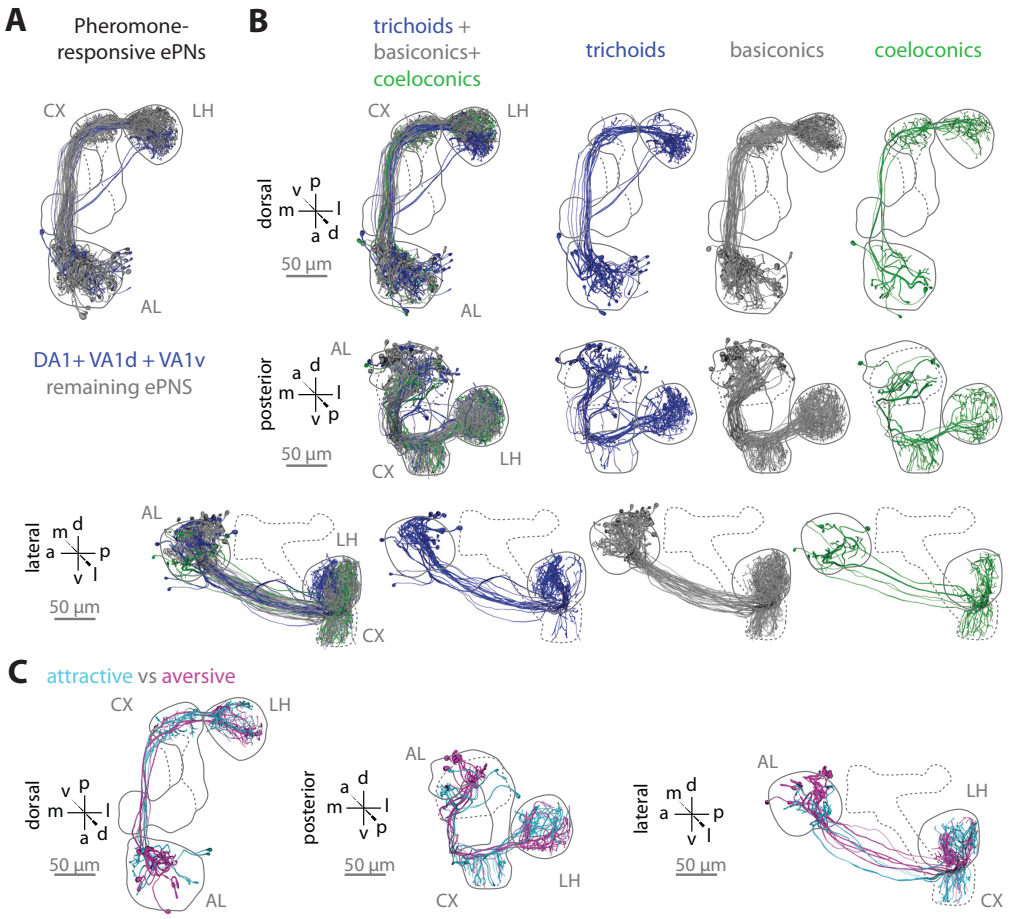
A
Pheromone-responsive ePNs
CX
LH
AL
DA1+ VA1d + VA1v
remaining ePNS
B
trichoids +
basiconics+
coeloconics
trichoids
basiconics
coeloconics
dorsal
posterior
lateral
50 µm
C
attractive vs aversive

General Discussion

The aim of this dissertation was the comparative investigation of the morphological and functional characteristics of different neuron populations within the olfactory pathways in the vinegar fly *Drosophila melanogaster*. This investigation embraced the impact of the different neuron populations on the neuropil structure of the primary olfactory processing center, the antennal lobe (AL), and the secondary olfactory processing center, the lateral horn (LH). Moreover, the functional properties of two types of projection neurons (PNs) were analyzed considering the coding of odor information in the LH.

The examination of the olfactory neural circuitry was enabled by the use of several state-of-the-art techniques including the generation of a new transgenic fly line to label neuropil structures *in vivo*. On the one hand, this neuropil staining permitted the immediate 3D-reconstruction of higher brain centers and the registration of labeled neurons in order to compare their axonal as well as dendritic arborizations (Manuscripts 1 and 4). On the other hand, based on the neuropil labeling an *in vivo* atlas of the AL was generated for improved and simplified identification of glomeruli (Manuscript 2). We used the atlas to identify the glomeruli innervated by single multiglomerular inhibitory projection neurons (iPNs; Manuscript 1). Furthermore, this atlas simplified the identification of glomeruli of interest to label *in vivo* all uniglomerular excitatory projection neurons (ePNs) innervating those specific glomeruli (Manuscripts 3 and 4). The *in vivo* labeling of specific single neurons and all neurons innervating distinct glomeruli was performed by photoactivation of the endogenously expressed photoactivatable green fluorescent protein (pa-GFP). 3D-reconstruction and registration of labeled neurons onto a reference brain enabled their thorough morphological examination (Manuscripts 1 and 4). Moreover, functional properties of ePNs and iPNs were examined using wide-field calcium imaging in the LH. The obtained global odor responses were analyzed by applying the improved pattern recognition algorithm non-negative matrix factorization (NMF). Neuronal connections between different neuron populations were investigated by the use of GFP reconstitution across synaptic partners (GRASP). Furthermore, by ablation of distinct neuron populations the functional connectivity was verified (Manuscripts 1 and 4).

Elucidating olfactory pathways within the antennal lobe

The investigation of morphological and physiological properties of the neuron populations of interest as well as their contribution to the formation of neuropil structures is a prerequisite to unravel neural circuits. Nevertheless, morphological analyses are mainly conducted by *in vitro* techniques as immuno-labeling and in-situ hybridization (Couto et al., 2005; Fishilevich and Vosshall, 2005; Laissue et al., 1999; Rein et al., 2002). In contrast, physiological analyses comprise a comprehensive collection of *in vivo* methods like photolesioning, single cell recordings as well as functional imaging (Caron et al., 2013;

Chou et al., 2010; Datta et al., 2008; Fiala et al., 2002; Liang et al., 2013; Ng et al., 2002; Ruta et al., 2010; Schubert et al., 2014; Seki et al., 2010; Silbering et al., 2008; Wilson et al., 2004) (Manuscripts 1 and 4). Applying the available *in vitro* atlases on *in vivo* functional imaging data to map response patterns is challenging since the neuropils underlie unequal geometrical as well as volumetric modifications due to dissection and fixation artefacts (Chiang et al., 2011; Ma et al., 2008). In manuscript 2 we, therefore, developed a genetically encoded fusion protein (END1-2) that is mimicking the *in vitro* staining with the antibody nc82 to label neuropil structures *in vivo* (Hofbauer, 1991). We used the expression of END1-2 and the subsequent 3D-reconstruction of confocal brain scans to establish an *in vivo* atlas (Rybak et al., 2010). Furthermore, the reconstructed *in vivo* brain enabled us to investigate precisely the impact of the fixation procedure on geometric and volumetric modifications that occur in reconstructed *in vitro* brains. To reliably assign the identity of glomeruli in our 3D-*in vivo* atlas we used the labeling of specific chemosensory receptors (CRs) expressed under control of GAL4, and the END1-2 neuropil staining (Abuin et al., 2011; Couto et al., 2005; Dobritsa et al., 2003; Fishilevich and Vosshall, 2005; Goldman et al., 2005; Larsson et al., 2004; Vosshall, 2001). First of all, the *in vivo* labeling of AL glomeruli revealed a volumetric decrease of the AL by 43% in stained *in vitro* brains. Notably, the difference of individual glomerular volumes ranged from almost no change up to 60% reduction of the size in comparison to the *in vitro* neuropil staining. This non-uniform shrinkage may depend on the different innervation frequency as well as the different innervation density by olfactory sensory neurons (OSNs), PNs and local interneurons (LNs) (Ignell et al., 2005)(Manuscript 3). Second, the positions of glomeruli were affected by the transection of the antennal nerve that resulted in changed distances as well as in changed angles between glomeruli pairs. These remarkable differences of geometric and volumetric properties of AL glomeruli obtained *in vivo* in comparison to the *in vitro* situation highlights the necessity of an *in vivo* AL atlas.

The *in vivo* scans of the AL stained with END1-2 have the same orientation without deformation of the AL as observed in functional imaging due to the identical preparation. Consequently, our improved AL atlas simplifies the identification of activated glomeruli for the mapping of neuronal activity in functional imaging experiments gained *in vivo*. In addition, the *in vivo* neuropil staining enables to assign the innervated AL glomeruli by specific neuron populations without further fixation and staining, i.e. it is less time consuming. Moreover, the END1-2 staining supports the identification and characterization of innervation patterns in other neuropils than the AL. For example, we compared terminal fields of single iPNs in the LH based on 3D-reconstructions of the stained neuropil structures and their subsequent registration onto a reference brain (Manuscript 1). Furthermore, the integration of the END1-2 construct in the fly genome permits a neuropil staining and instantaneous neuron specific expression of reporter proteins under control of binary transcription systems.

The acquisition of the *in vivo* AL atlas encouraged us to investigate the basis and the significance of the different sizes and shapes of AL glomeruli. Based on simple averaging it was commonly assumed that each glomerulus is innervated by 20 OSNs and 3 PNs but only for few glomeruli the actual numbers are published (Ai et al., 2010; Dobritsa et al., 2003; Gao et al., 2000; Ramaekers et al., 2005; Ruta et al., 2010; Sachse et al., 2007; Vosshall and Stocker, 2007). Only the enormous diversity of glomerular innervation by LNs is comprehensively investigated (Chou et al., 2010; Das et al., 2011; Seki et al., 2010) . Comparison of one OSN type in different *Drosophila* species revealed an impact of the OSN number on the volume of the innervated glomerulus (Dekker et al., 2006; Linz et al., 2013). To verify this, we investigated quantitatively and qualitatively the neuron populations in the AL as well as their impact on the glomerular volume (Manuscript 3).

OSNs expressing a specific CR were labeled to gain for each OSN type the accurate number of neurons varying from 10 to 65 in males and females. Furthermore, we investigated the distribution of all sensilla subtypes on the olfactory organs of the fly according to the expressed CRs. On one hand, this verified the previously published distribution patterns of sensilla subtypes, on the other hand, this confirmed the reliability of our approach to endogenously label OSN types (Benton et al., 2009; de Bruyne et al., 1999; de Bruyne et al., 2001; Fishilevich and Vosshall, 2005; Shanbhag et al., 1999; Silbering et al., 2011; Stocker, 2001; Vosshall et al., 2000).

The number of ePNs innervating individual glomeruli was investigated in flies expressing pa-GFP under control of the enhancer trap line *GH146-GAL4*, which labels about two-thirds of all ePNs (Datta et al., 2008; Patterson and Lippincott-Schwartz, 2002; Stocker et al., 1997). Photoactivation of each glomerulus revealed numbers varying from one up to ten ePNs per glomerulus. The glomerular innervation frequency by LNs also varied from approximately 57 up to 95% of all LNs (Chou et al., 2010). Those varying numbers of OSNs, ePNs and LNs for different glomeruli already hint at a unique architecture of each single glomerulus. Correlating the glomerular volume with the distinct numbers of OSNs, ePNs and LNs indeed revealed a significant impact of the number of OSNs and ePNs on the volume. When comparing the number of OSNs, ePNs and LNs with each other only ePNs and LNs exhibited a significant inverse correlation, i.e. glomeruli with a high number of ePNs were innervated by few LNs. Interestingly, glomeruli with a high number of ePNs showed responses to odors of considerable ecological relevance. Those include, for example, the glomeruli processing responses to the pheromones 11-*cis*-vaccenyl acetate (DA1 (Ha and Smith, 2006; Kurtovic et al., 2007) and DL3 (Lebreton et al., 2014)), as well as methyl laurate (VA1d (Dweck et al., 2015b)), or to the aversive cue geosmin emitted by bacteria or mold (DA2 (Stensmyr et al., 2012)). To correlate the number of OSNs, ePNs and LNs of a glomerulus with its odor tuning profile we calculated the lifetime sparseness of olfactory chemoreceptors. To this end, we used available

online data (http://neuro.uni-konstanz.de/DoOR/2.0/; (Münch and Galizia, 2016)) and we gained novel data for eleven so far scarcely investigated CRs using single sensillum recordings. CRs and the corresponding glomeruli revealing a high lifetime sparseness (i.e. high odor-selectivity) are innervated by many ePNs but by few LNs. This supports that channels for specific odors get less lateral processing and convey reliably via more PNs this important information to the higher brain centers (Hong and Wilson, 2015; Jeanne and Wilson, 2015; Root et al., 2008; Seki et al., 2010). Closer examination of our data indicates that the D-glomerulus innervated by OSNs expressing OR69a may be a further candidate of a channel for specific ecological relevance. The D-glomerulus is innervated by few LNs and four ePNs, which is more than the average of two ePNs. However, the odor tuning profile of OR69a is rather broad. Current investigations suggest for the odor processing channel of the D-glomerulus a combinatorial coding of a putative pheromone and odors emanating from food preferred by *Drosophila melanogaster* (Lebreton et al., 2017).

Our extensive investigation of the OSN numbers in male and female flies revealed also differences for some OSN types between the sexes that were so far not described. Furthermore, sexual differences are noted in the volume of few glomeruli and the number of ePNs. Interestingly, not all dimorphic OSNs and ePNs express the sex-specific *fruitless* gene, which governs the neural circuitry of courtship (Stockinger et al., 2005). However, the cause and the impact of those sex-dependent quantitive differences on the processing of odor information as well as the elicited behavior have to be investigated. It is possible that those processing channels exhibiting sex-specific quantitive differences can elicit sex-specific behavior independent of *fruitless*-expression in the sensory neurons because of their postsynaptic connection to *fruitless*-positive neurons. For example, it was shown recently that a *fruitless*-negative processing channel assembles together with higher-order *fruitless*-positive neurons a neural circuit that prevents interspecies courtship (Fan et al., 2013). Moreover, dimorphic differences in the number of neuron types may reveal processing channels governing sex-specific behaviors apart from courtship. For example, in the case of OR49a-expressing OSNs the higher number in female flies may be attributed to their relevance in avoiding unsuitable places for oviposition (Ebrahim et al., 2015).

The contribution of iPNs on the glomerular architecture was not investigated in our study due to their complex innervation patterns. Since they innervate glomeruli only sparsely the impact might be low. Besides, our study excluded also the barely investigated atypical PNs that bilaterally innervate the AL or that target higher brain centers additionally to the mushroom body calyx and the LH (Tanaka et al., 2012). Further examination of those types of PNs is necessary to determine their impact on the glomerular architecture. This will help to identify the rationale of why some glomeruli are innervated only by few OSNs despite displaying a huge volume. For example the glomeruli VL1, VL2p and DP1m are

almost as big as the pheromone processing glomeruli but are innervated by about 60% less OSNs. Another possibility is that OSNs innervating those glomeruli exhibit a very high amount of synapses that increase the glomerular volume (Acebes and Ferrus, 2001; Mosca and Luo, 2014).

Elucidating olfactory pathways beyond the antennal lobe

In manuscripts 2 and 3 we established a tool for *in vivo* labeling of the neuropil and subsequently applied it to investigate the neuronal architecture of the AL glomeruli. Investigations described in manuscripts 1 and 4 focused on the two main populations of projection neurons – multiglomerular inhibitory and uniglomerular excitatory ones. We investigated the characteristics of their arborizations, and we examined their functional principles for the parallel convey of odor information to the lateral horn.

The iPNs were so far scarcely investigated regarding their morphological and functional properties. The enhancer trap line *MZ699-GAL4* labels about 45 out of the 50 iPNs and almost all of those iPNs are multiglomerular and secrete the neurotransmitter gamma-aminobutyric acid (GABA) (Ito et al., 1997; Lai et al., 2008; Liang et al., 2013; Okada et al., 2009; Parnas et al., 2013). To analyze the glomerular innervations of single iPNs we expressed pa-GFP under control of *MZ699-GAL4* and the END1-2 neuropil staining (Datta et al., 2008; Ito et al., 1997; Patterson and Lippincott-Schwartz, 2002; Ruta et al., 2010). In general, labeling all MZ699-positive iPNs revealed an overall sparse innervation of 40 out of the 54 AL glomeruli. This is contradictory to a previous study assigning an innervation of all glomeruli by MZ699-positive iPNs (Tanaka et al., 2012). Those differences in glomerular innervation can most likely be attributed to the application of different methods for the analysis. In comparison to our approach, Tanaka and colleagues used the *in vitro* immuno-labeling, which substantially enhances the staining but also suffers from fixation artefacts (Manuscript 2). Nevertheless, it seems likely that MZ699-positive iPNs innervate all glomeruli since immuno-labeling enhances the fluorescence of very thin arborizations.

Confocal scans of labeled single neurons were subsequently used for 3D-reconstruction and registration (Rybak et al., 2010). Notably, none of the analyzed iPNs exhibited identical glomerular innervations but in some cases iPNs innervated similar subsets of glomeruli. Strikingly, the examined iPNs revealed a separated innervation of mainly ventro- and dorsomedial glomeruli or of mainly anterodorsal and lateral glomeruli. These two separated groups innervated in the LH also segregated areas hinting towards a different role in odor processing and further relay to different third-order neurons in the LH. Hence, we analyzed the representation of several odors by iPNs in the LH using wide-field functional imaging of flies expressing the calcium indicator GCaMP3 under control of *MZ699-GAL4* (Ito et al., 1997; Tian et al., 2009). Odors elicited responses of varying

intensities in three different regions of the LH with concentration-dependent shifts in the response patterns. To analyze these response patterns we conducted NMF that revealed odor response domains (ORDs) with similar spatiotemporal odor response profiles found in all tested animals (Lee and Seung, 1999; Soelter et al., 2014; Soucy et al., 2009). Three ORDs were extracted with one domain in the posterior LH responding to attractive odors, one in the medial LH coding odor concentration and one in the anterolateral LH representing aversive odors and concentration. The latter domain might also represent the neuronal activity of third-order neurons of the ventrolateral protocerebrum (VLP). Those VLP neurons (VLPNs) are also labeled by the *MZ699-GAL4* line and innervated the anterior part of the LH. To examine the activity of VLPNs we conducted functional imaging experiments combined with microlesion of either the iPN tract to abolish iPN input in the LH or the VLPN tract to abolish VLPN activity. Ablating the iPN tract diminished responses in the posterior and medial odor response domains, whereas responses in the anterolateral domain slightly increased. This reveals that responses in the posterior and medial domain derive only from iPN activity, whereas responses in the anterolateral domain derive from VLPN activity. Furthermore, this confirms that iPNs inhibit the activity of VLPNs (Liang et al., 2013).

The impact of iPNs on odor-guided behavior was elucidated in the T-maze using flies with silenced iPNs. The loss of inhibition by iPNs led to a reduced attraction to all tested odors and concentrations. Thus iPNs contribute to odor attraction. Notably, glomeruli that are estimated to be responsible for processing of aversive odors were not innervated by MZ699-positive iPNs according to our *in vivo* labeling (Knaden et al., 2012). However, regarding the described innervation of all glomeruli by MZ699-positive iPNs *in vitro* those glomeruli may be innervated only weakly (Tanaka et al., 2012). Thus, our analyses revealed in the LH a coding of attractive odors and odor concentration as well as a contribution to attraction behavior by MZ699-positive iPNs. However, the connection to other lateral horn neurons (LHNs) than to VLPNs as well as the relay of odor valence and intensity has to be analyzed in further experiments (see below).

In manuscript 4 we aimed at a morphological and functional investigation of ePNs comparable to our findings of iPNs: a separation of ePNs in groups representing odor valence and intensity. To examine ePNs we used the enhancer trap line *GH146-GAL4* that labels about 90 of the estimated 120 ePNs (Stocker et al., 1997).

To compare the innervation patterns in the LH of ePNs and iPNs, we needed *in vivo* data of ePNs. Available data on the morphology of ePNs consist of *in vitro* scans of single ePNs. Similar to our results in manuscript 2 that *in vitro* data suffer from fixation artefacts the comparison of available *in vitro* data of ePNs with our *in vivo* data of iPNs was not possible. Therefore, we reconstructed all ePNs *in vivo* innervating distinct glomeruli acquired by photoactivation (Datta et al., 2008; Patterson and Lippincott-Schwartz, 2002;

Ruta et al., 2010; Rybak et al., 2010). This way, we could confirm the high stereotypy of ePNs innervating the same glomerulus (Jefferis et al., 2007; Marin et al., 2002; Wong et al., 2002). Additionally, the reconstructions of sister ePNs (i.e. ePNs innervating the same glomerulus in the same animal) revealed that fine arborizations were not identical but similar. Since our data set of ePNs included two more glomeruli and all sister ePNs, a re-examination of their clustering by hierarchical clustering (Jefferis et al., 2007) resulted in five main groups. However, defining cluster boundaries was ambiguous since the corresponding distance matrix revealed that similarities were not only found for neuron pairs within the same cluster. In a principal component analysis (PCA) the ePNs were evenly distributed without any clustering at all. Notably, the distribution of ePNs in the PCA was highly reminiscent to the distribution of innervated glomeruli in the AL. Therefore, we correlated the spatial distribution of glomeruli in the AL – gained in manuscript 2 – with the spatial distribution of the corresponding ePNs in the LH. This revealed that ePNs innervating neighboring glomeruli in the AL also innervated neighboring areas in the LH. Thus, the topographic map of the AL was retained but rotated in the LH confirming observations in a previous study (Marin et al., 2002). Comparison of the innervation of ePNs and iPNs in the AL and the LH revealed that ePNs and iPNs overlapping in the AL also were overlapping in the LH. Consequently, ePNs and iPNs getting input from the same AL region relayed the odor information to the same region in the LH via two parallel pathways.

The representation of odors in the LH was in previous studies analyzed or simulated only for a few odors (Jefferis et al., 2007; Liang et al., 2013; Parnas et al., 2013). To study the global representation of odors in all ePNs we again used wide-field calcium imaging. This revealed two different response patterns that were – by applying NMF – attributed to two ORDs that separately code attractive and aversive odors. Comparing the ORDs of ePNs and iPNs coding attractive odors revealed their spatial overlap. Aversive odors and high odor concentrations were coded in overlapping ORDs of ePNs and VLPNs. In iPNs the odor intensity was coded separately in an ORD that overlapped with the ePN ORD coding aversive odors and odor intensity. The spatial and functional overlap of ORDs in ePNs and iPNs support the segregation of the LH according to odor valence.

In manuscript 1 we verified the connection of iPNs onto VLPNs and that iPNs were not connecting onto ePNs (Liang et al., 2013; Parnas et al., 2013). Since the connection of ePNs onto iPNs and VLPNs was so far not investigated we labeled putative synapses between those three neuron populations using *MZ699-GAL4* and *GH146-GAL4* lines for the GRASP technique (Feinberg et al., 2008). Indeed, this way we could visualize synapses of ePNs onto iPNs and VLPNs in the LH. Notably, this approach could not differentiate between synapses of either ePNs and iPNs, or ePNs and VLPNs, or both. In order to attribute the labeled synapses to the neuronal partners we performed calcium im-

aging experiments combined with microlesion that revealed synaptic connections of ePNs onto VLPNs only.

In conclusion, ePNs and iPNs form a parallel pathway for the transfer of odor information from the same area in the AL to the same LH region, the segregation of the LH according to odor valence, and the antagonistic connection to the same set of third-order neurons of the VLP. Like the parallel pathways in the visual system of mammals and *Drosophila* the two antagonistic PN populations relay in parallel different features of olfactory information to the LH (Nassi and Callaway, 2009; Otsuna et al., 2014). The combinatorial coding of odor quality by ePNs is retained in the topographic map and enables the readout by LHNs (Fişek and Wilson, 2014). The concentration-dependent inhibition of postsynaptic neurons via iPNs enhances the discrimination of odors (Parnas et al., 2013). This dual representation of olfactory information may improve the accuracy of the representation of odor valence and intensity. Consequently, our systematic descriptions of the coding of ecological relevance by two antagonistic PN populations permit a deeper understanding of the neural circuitry governing innate behavior in *Drosophila melanogaster*.

Future perspectives to unravel the neural circuitry governing innate behavior

To unravel complex neural circuits it is necessary to investigate the morphological and physiological properties of all involved members. An assumption of separated coding areas in the LH for pheromones and food odors has been based solely on separately innervated areas in the LH of PNs coding those different odor classes (Jefferis et al., 2007). However, global functional imaging of iPNs and ePNs revealed a separation of the LH according to the coding of odor valence and intensity. Interestingly, pheromones were represented by both ePNs and iPNs in the odor response domains that responded mainly to attractive odors. This supports the separation of the LH due to coding of aversive or attractive stimuli, and not for pheromones versus food odors. It is not clear why responses to the pheromones 11-*cis*-vaccenyl acetate and methyl laurate were in functional imaging not detected in the anterior LH region innervated by DA1- and VA1d-PNs. Although, it was shown that 11-*cis*-vaccenyl acetate elicits responses in LHNs, which innervate the anterior LH and connect onto DA1-PNs (Kohl et al., 2013). Most likely the responses to pheromones were relayed to the LH by other ePN types additional to DA1- and VA1d-PNs (Lebreton et al., 2015).

Generally, our findings of separated odor representations according to odor valence and intensity in the LH provide an essential progress in analyzing innate behavior. Further analysis of odor processing in the LH, the connections of PNs as well as the transfer of the separated responses according to odor valence and intensity to the different types of

third-order neurons are necessary. Of the diverse types of LHNs only few sets were so far examined (Cachero et al., 2010; Fişek and Wilson, 2014; Jefferis et al., 2007; Kohl et al., 2013; Lai et al., 2008; Ruta et al., 2010; Tanaka et al., 2004; Yu et al., 2010) (Manuscripts 1 and 4). Several higher brain centers responsible for the processing of e.g. visual, auditory and mechanosensory stimuli are connected by LHNs constituting a prerequisite for the multimodal integration of sensory stimuli (Duistermars and Frye, 2010; Gupta and Stopfer, 2012; Ruta et al., 2010; Tanaka et al., 2004).

The enhancer trap lines *MZ699-GAL4* and *GH146-GAL4* label not exclusively all iPNs or ePNs thus analyses of odor responses and innervation patterns in AL and LH of missing PNs are necessary. In line with this, further analyses of the remaining VLPNs are necessary. This can be accomplished by using different lines of the several thousand newly generated transgenic fly lines (Jenett et al., 2012) or by generating more specific fly lines. Moreover, the development of sophisticated tools like photoconvertable calcium indicators such as GCaMP and GR-GECO (Ai et al., 2015; Hoi et al., 2013), or multicolor functional imaging (Akerboom et al., 2013) will help to analyze the functional connection of different neuron populations. Furthermore, the improvement of optical imaging facilities enables the analysis of the activity of specific neuron populations in freely behaving flies (Grover et al., 2016).

In this dissertation I contributed to the knowledge of the connectivity map of odor processing channels as well as to the odor coding strategies in the AL and the LH. This was accomplished by establishing an *in vivo* neuropil staining and by generating an *in vivo* AL atlas based on this staining (Manuscript 2). The application of both innovations improved the comparability of morphological and physiological imaging data (Manuscripts 1 and 4). Furthermore, the quantification of the different neuron types, which innervate individual AL glomeruli, highlighted the uniqueness of each processing channel according to the ratio of the connected neuron types. This ratio is associated with the coding of ecological relevance through the individual processing channels (Manuscript 3). Furthermore, investigations described in this dissertation elucidated the morphological and functional characteristics of projection neurons that relay the processed odor information to the higher brain (Manuscripts 1 and 4). The multiglomerular iPNs constituted two groups that separately innervated the AL and the LH. In comparison, the innervation patterns of uniglomerular ePNs retained the topographic map of the AL in the LH. Both, ePNs and iPNs represented in the LH odor information categorized by odor valence and intensity. Moreover, in the anterior LH ePNs and iPNs synapsed onto and modulated antagonistically a subset of VLPNs. How the odor information of the individual processing channels is conveyed to LHNs and how then an innate odor-guided behavior is elicited will be investigated in the coming decades by the help of existing genetic and technical tools, as well as by those tools in development. Odor-guided behavior can be modulated depending on the internal state of the fly, the context of the perceived odors as well as the fly´s

experience (Beshel and Zhong, 2013; Bräcker et al., 2013; Heisenberg, 2015; Lin et al., 2014b; Owald and Waddell, 2015; Root et al., 2011; Su and Wang, 2014). To comprehensively unravel the neural circuit governing innate behavior it will be necessary to scrutinize these adjustments as well as the interplay of the involved neuron types.

Summary

In its natural environment the vinegar fly *Drosophila melanogaster* encounters a plethora of different odors. To some odors flies show an innate preference, like to the smell of food or pheromones, or an innate avoidance, like to the smell of predators or contaminated food. This innate odor-guided behavior is governed by the interplay of several neuron populations in the olfactory system. Those neuron populations extract the relevant odor information and thus enable the evaluation of the encountered odors. However, the rationale and significance of the odor processing by different neuron populations onto the elicited innate odor-guided behavior is not fully understood. To unravel the principles of neural circuits *Drosophila melanogaster* is a versatile model organism due to the gigantic genetic tool box for selective examination of diverse neuron populations.

In this dissertation I aimed at a deeper understanding of the contribution of the individual odor processing channels to innate odor-guided behavior as well as the odor coding strategies. This was accomplished by the use of state-of-the-art *in vivo* techniques including a newly generated fly line, establishing an *in vivo* atlas of the antennal lobe (AL), the labeling of single cells by photoactivation, the 3D-reconstruction and registration of single cells for anatomical comparisons, as well as functional investigations of different neuron populations and the examination of their synaptic connections.

To investigate the glomerular anatomy of the primary olfactory processing center a new fly line was generated for a permanent and endogenous labeling of the neuropil. Based on this labeling an *in vivo* AL atlas was established (Manuscript 2). The comparative investigation of the neuropil architecture in the *in vivo* and *in vitro* situation verified the ample influence of the dissection and fixation procedure on the size and the position of glomeruli. Furthermore, the detailed examination of each of the neuropil subunits of the primary olfactory processing center, the glomeruli, revealed a quantitatively unique innervation by sensory neurons, projection neurons (PNs) and local interneurons (Manuscript 3). Processing channels that code ecological relevance exhibit a lower innervation by modulatory local interneurons and consequently may be subject to a lower degree of lateral processing. To those channels belong DA1-neurons and VA1d-neurons that process the reception of pheromones, or the DA2-neurons that process the reception of geosmin emitted by toxic microbes.

How odors are represented in the lateral horn (LH) by the two main populations of excitatory (ePNs) and inhibitory projection neurons (iPNs) was investigated morphologically and physiologically (Manuscripts 1 and 4). This was accomplished by photolabeling with subsequent 3D-reconstruction and registration of single neurons, as well as functional calcium imaging combined with microablation. Both PN populations encode odor valence and intensity in separate regions of the LH. Furthermore, subsets of ePNs and iPNs in-

nervating the same region of the AL also innervate the same region in the LH: consequently, they receive the same odor information and transfer it to the same output region. Both neuron populations connect to the same set of third-order neurons of the ventrolateral protocerebrum but with antagonistic modulation. These findings support the notion of a parallel relay of odor information via two projection neuron populations to the LH that improves the accuracy of the represented odor categorized by its valence and intensity. Furthermore, the characterization of the coding strategies of PNs in the LH and the comparative investigation of different odor processing channels will help to unravel the neural circuitry of innate odor-guided behavior. In addition, this neural circuitry will be deciphered by future studies assigning the connectivity to further neurons of the LH as well as investigating the relay of the coding of odor valence and intensity.

Zusammenfassung

Bei der Erkundung der Umgebung offenbart die Essigfliege *Drosophila melanogaster* eine angeborene Präferenz zu Gerüchen, die Nahrungsquellen signalisieren, genauso wie zu Pheromonen, die von Artgenossen oder Fortpflanzungspartnern sekretiert werden. Des Weiteren zeigen Essigfliegen eine instinktive Abneigung gegenüber dem Geruch ihrer Feinde bzw. gegenüber ungenießbarer Nahrung. Dieses angeborene Verhalten, ausgelöst durch bestimmte Düfte, wird durch das Zusammenspiel verschiedener Neuronenpopulationen des olfaktorischen Systems reguliert. Die verschiedenen Neuronenpopulationen extrahieren relevante Duftinformationen und ermöglichen dadurch die Bewertung der wahrgenommenen Düfte. Dennoch sind die Grundprinzipien und die Bedeutung der Duftverarbeitung durch verschiedene Neuronenpopulationen für das Auslösen von angeborenem Verhalten zu Düften noch nicht vollständig verstanden. Zur Untersuchung neuronaler Verschaltungen ist *Drosophila melanogaster* als Modellorganismus aufgrund der umfangreichen Möglichkeiten zur selektiven, genetischen Manipulation von Neuronenpopulationen vielseitig einsetzbar.

Das Ziel dieser Dissertation war die Entschlüsselung der Beiträge einzelner Neuronenpopulationen zur Verarbeitung von Duftinformationen, die relevant für das Auslösen angeborener Verhalten notwendig ist, sowie die zugrundeliegende Kodierung von Duftinformationen. Dies wurde mittels modernster Methoden erreicht, welche die Entwicklung einer Fliegenlinie, die Etablierung eines *in vivo* Atlasses der Gewebestrukturen des primären Geruchszentrums, dem Antennallobus, die photo-optische Markierung einzelner Neurone und deren anatomischer Vergleich durch anschließende 3D-Rekonstruktion und Registrierung sowie die Aktivitätsmessung verschiedener Neuronenpopulationen und deren neuronale Verschaltungen einschließen.

Die Anatomie der glomerulären Gewebestrukturen des primären Geruchszentrums wurde im lebenden Organismus einer neuen Fliegenlinie, die eine endogene Fluoreszenzmarkierung der Gehirnstrukturen ermöglicht, untersucht. Basierend auf dieser Markierung wurde ein *in vivo* Atlas des Antennallobus etabliert (Manuskript 2). Die vergleichenden, anatomischen Studien der Gehirnstrukturen des primären Geruchszentrums im lebenden Organismus bzw. im präparierten Zustand verdeutlichen die umfangreichen Einflüsse der Sezierung und Fixierung auf die Position der Neuropiluntereinheiten, den Glomeruli. Des Weiteren wurde die charakteristische Innervationshäufigkeit sensorischer Neurone, Projektionsneurone und lokaler Interneurone für die einzelnen Glomeruli im primären Geruchszentrum dokumentiert (Manuskript 3). Neuronengruppen zur Verarbeitung wichtiger sensorischer Informationen der Umwelt weisen eine erhöhte Neuronenzahl zur Weiterleitung sowie eine geringere Anzahl modulierender lokaler Interneurone auf. Dazu gehört die Informationsverarbeitung von Pheromonen durch Neurone, die sich

jeweils in den Glomeruli DA1 und VA1d miteinander verschalten, sowie die Neurone des DA2-Glomerulus zur Verarbeitung des Geruchs toxischer Mikroorganismen.

Die Repräsentation von Duftmerkmalen im höheren Gehirnzentrum, dem lateralen Horn, durch die zwei Hauptgruppen stimulierender und hemmender Projektionsneurone wurde in den Manuskripten 1 und 4 untersucht. Dies erfolgte mittels photo-optischer Markierung von Einzelneuronen und deren anschließende 3D-Rekonstruktion und Registrierung sowie durch Messung von Neuronenaktivität und deren Weiterleitung. Beide Projektionsneuronenpopulationen kodieren die Valenz und Intensität von Düften in jeweils getrennten Regionen des lateralen Horns. Die stimulierenden und hemmenden Projektionsneurone, die dasselbe Areal im primären Gehirnzentrum innervieren, übertragen zur selben Region des höheren Gehirnzentrums dieselbe Duftinformation. Dort verschalten sich die Projektionsneurone mit derselben Gruppe nachgeschalteter Neurone des benachbarten Hirnzentrums, des sogenannten ventrolateralen Protocerebrums. Diese Ergebnisse bekräftigen die Ansicht einer parallelen Informationsweiterleitung mit Hilfe zweier Projektionsneuronenpopulationen zum lateralen Horn zur präziseren Darstellung von Düften kategorisiert in Abhängigkeit ihrer Valenz und Intensität. Die Charakterisierung der Verschlüsselungsstrategien von Projektionsneuronen im lateralen Horn sowie die vergleichende Untersuchung der unterschiedlichen Verarbeitungswege von Düften unterstützt die Aufklärung der neuronalen Schaltkreise, die dem durch bestimmte Gerüche hervorgerufenen, angeborenen Verhalten zugrunde liegen. Wie die Verschaltung zu Neuronen anderer, benachbarter Hirnregionen aussieht, muss in weiteren Experimenten erfolgen. Dabei ist auf die Kodierung von Valenz und Intensität von Düften ein besonderes Augenmerk zu richten.

References

Abuin, L., Bargeton, B., Ulbrich, M.H., Isacoff, E.Y., Kellenberger, S., and Benton, R. (2011). Functional architecture of olfactory ionotropic glutamate receptors. Neuron *69*, 44-60.

Acebes, A., and Ferrus, A. (2001). Increasing the number of synapses modifies olfactory perception in *Drosophila*. The Journal of neuroscience : the official journal of the Society for Neuroscience *21*, 6264-6273.

Adams, M.D., Celniker, S.E., Holt, R.A., Evans, C.A., Gocayne, J.D., Amanatides, P.G., Scherer, S.E., Li, P.W., Hoskins, R.A., Galle, R.F.*, et al.* (2000). The genome sequence of *Drosophila melanogaster*. Science *287*, 2185-2195.

Ai, M., Mills, H., Kanai, M., Lai, J., Deng, J., Schreiter, E., Looger, L., Neubert, T., and Suh, G. (2015). Green-to-Red Photoconversion of GCaMP. PloS one *10*, e0138127.

Ai, M., Min, S., Grosjean, Y., Leblanc, C., Bell, R., Benton, R., and Suh, G.S. (2010). Acid sensing by the *Drosophila* olfactory system. Nature *468*, 691-695.

Akerboom, J., Carreras Calderon, N., Tian, L., Wabnig, S., Prigge, M., Tolo, J., Gordus, A., Orger, M.B., Severi, K.E., Macklin, J.J.*, et al.* (2013). Genetically encoded calcium indicators for multi-color neural activity imaging and combination with optogenetics. Frontiers in molecular neuroscience *6*, 2.

Akerboom, J., Rivera, J.D., Guilbe, M.M., Malave, E.C., Hernandez, H.H., Tian, L., Hires, S.A., Marvin, J.S., Looger, L.L., and Schreiter, E.R. (2009). Crystal structures of the GCaMP calcium sensor reveal the mechanism of fluorescence signal change and aid rational design. The Journal of biological chemistry *284*, 6455-6464.

Andlauer, T.F., Scholz-Kornehl, S., Tian, R., Kirchner, M., Babikir, H.A., Depner, H., Loll, B., Quentin, C., Gupta, V.K., Holt, M.G.*, et al.* (2014). Drep-2 is a novel synaptic protein important for learning and memory. eLife *3*.

Aso, Y., Hattori, D., Yu, Y., Johnston, R.M., Iyer, N.A., Ngo, T.T., Dionne, H., Abbott, L.F., Axel, R., Tanimoto, H., and Rubin, G.M. (2014a). The neuronal architecture of the mushroom body provides a logic for associative learning. eLife *3*, e04577.

Aso, Y., Sitaraman, D., Ichinose, T., Kaun, K.R., Vogt, K., Belliart-Guerin, G., Placais, P.Y., Robie, A.A., Yamagata, N., Schnaitmann, C.*, et al.* (2014b). Mushroom body output neurons encode valence and guide memory-based action selection in *Drosophila*. eLife *3*, e04580.

Babin, A., Kolly, S., Schneider, F., Dolivo, V., Zini, M., and Kawecki, T.J. (2014). Fruit flies learn to avoid odours associated with virulent infection. Biology letters *10*, 20140048.

Becher, P.G., Flick, G., Rozpędowska, E., Schmidt, A., Hagman, A., Lebreton, S., Larsson, M. C., Hansson, B. S., Piškur, J., Witzgall, P., et al. (2012). Yeast, not fruit volatiles mediate *Drosophila melanogaster* attraction, oviposition and development. Funct. Ecol. *26*, 822-828.

Begon, M. (1982). Yeasts and *Drosophila*. The Genetics and Biology of *Drosophila* (eds M. Ashburner, H. L. Carson & J. Thompson. Academic Press, London. *3a*, 345–384.

Benton, R., Vannice, K.S., Gomez-Diaz, C., and Vosshall, L.B. (2009). Variant ionotropic glutamate receptors as chemosensory receptors in *Drosophila*. Cell *136*, 149-162.

Beshel, J., and Zhong, Y. (2013). Graded encoding of food odor value in the *Drosophila* brain. The Journal of neuroscience : the official journal of the Society for Neuroscience *33*, 15693-15704.

Bhandawat, V., Olsen, S.R., Gouwens, N.W., Schlief, M.L., and Wilson, R.I. (2007). Sensory processing in the *Drosophila* antennal lobe increases reliability and separability of ensemble odor representations. Nature neuroscience *10*, 1474-1482.

Bräcker, L.B., Siju, K.P., Varela, N., Aso, Y., Zhang, M., Hein, I., Vasconcelos, M.L., and Grunwald Kadow, I.C. (2013). Essential role of the mushroom body in context-dependent CO(2) avoidance in *Drosophila*. Current biology : CB *23*, 1228-1234.

Brand, A.H., and Perrimon, N. (1993). Targeted gene expression as a means of altering cell fates and generating dominant phenotypes. Development *118*, 401-415.

Budick, S.A., and Dickinson, M.H. (2006). Free-flight responses of *Drosophila melanogaster* to attractive odors. The Journal of experimental biology *209*, 3001-3017.

Butcher, N.J., Friedrich, A.B., Lu, Z., Tanimoto, H., and Meinertzhagen, I.A. (2012). Different classes of input and output neurons reveal new features in microglomeruli of the adult *Drosophila* mushroom body calyx. The Journal of comparative neurology *520*, 2185-2201.

Butenandt, A., and Hecker, E. (1961). Synthese des Bombykols, des Sexual-Lockstoffes des Seidenspinners, und seiner geometrischen Isomeren. Angewandte Chemie *73*, 349-416.

Cachero, S., Ostrovsky, A.D., Yu, J.Y., Dickson, B.J., and Jefferis, G.S. (2010). Sexual dimorphism in the fly brain. Current biology : CB *20*, 1589-1601.

Caron, S.J., Ruta, V., Abbott, L.F., and Axel, R. (2013). Random convergence of olfactory inputs in the *Drosophila* mushroom body. Nature *497*, 113-117.

Chen, T.W., Wardill, T.J., Sun, Y., Pulver, S.R., Renninger, S.L., Baohan, A., Schreiter, E.R., Kerr, R.A., Orger, M.B., Jayaraman, V.*, et al.* (2013). Ultrasensitive fluorescent proteins for imaging neuronal activity. Nature *499*, 295-300.

Chiang, A.S., Lin, C.Y., Chuang, C.C., Chang, H.M., Hsieh, C.H., Yeh, C.W., Shih, C.T., Wu, J.J., Wang, G.T., Chen, Y.C.*, et al.* (2011). Three-dimensional reconstruction of brain-wide wiring networks in *Drosophila* at single-cell resolution. Current biology : CB *21*, 1-11.

Chou, Y.H., Spletter, M.L., Yaksi, E., Leong, J.C., Wilson, R.I., and Luo, L. (2010). Diversity and wiring variability of olfactory local interneurons in the *Drosophila* antennal lobe. Nature neuroscience *13*, 439-449.

Clyne, P.J., Warr, C.G., Freeman, M.R., Lessing, D., Kim, J., and Carlson, J.R. (1999). A novel family of divergent seven-transmembrane proteins: candidate odorant receptors in *Drosophila*. Neuron *22*, 327-338.

Couto, A., Alenius, M., and Dickson, B.J. (2005). Molecular, anatomical, and functional organization of the *Drosophila* olfactory system. Current biology : CB *15*, 1535-1547.

Das, A., Chiang, A., Davla, S., Priya, R., Reichert, H., Vijayraghavan, K., and Rodrigues, V. (2011). Identification and analysis of a glutamatergic local interneuron lineage in the adult *Drosophila* olfactory system. Neural systems & circuits *1*, 4.

Datta, S.R., Vasconcelos, M.L., Ruta, V., Luo, S., Wong, A., Demir, E., Flores, J., Balonze, K., Dickson, B.J., and Axel, R. (2008). The *Drosophila* pheromone cVA activates a sexually dimorphic neural circuit. Nature *452*, 473-477.

Davis, R.L. (2005). Olfactory memory formation in *Drosophila*: from molecular to systems neuroscience. Annual review of neuroscience *28*, 275-302.

de Belle, J.S., and Heisenberg, M. (1994). Associative odor learning in *Drosophila* abolished by chemical ablation of mushroom bodies. Science *263*, 692-695.

de Bruyne, M., Clyne, P.J., and Carlson, J.R. (1999). Odor coding in a model olfactory organ: the *Drosophila* maxillary palp. The Journal of neuroscience : the official journal of the Society for Neuroscience *19*, 4520-4532.

de Bruyne, M., Foster, K., and Carlson, J.R. (2001). Odor coding in the *Drosophila* antenna. Neuron *30*, 537-552.

Dekker, T., Ibba, I., Siju, K.P., Stensmyr, M.C., and Hansson, B.S. (2006). Olfactory shifts parallel superspecialism for toxic fruit in *Drosophila melanogaster* sibling, D. *sechellia*. Current biology : CB *16*, 101-109.

Denk, W., Strickler, J.H., and Webb, W.W. (1990). Two-photon laser scanning fluorescence microscopy. Science *248*, 73-76.

DiAntonio, A., Burgess, R.W., Chin, A.C., Deitcher, D.L., Scheller, R.H., and Schwarz, T.L. (1993). Identification and characterization of *Drosophila* genes for synaptic vesicle proteins. The Journal of neuroscience : the official journal of the Society for Neuroscience *13*, 4924-4935.

Dobritsa, A.A., van der Goes van Naters, W., Warr, C.G., Steinbrecht, R.A., and Carlson, J.R. (2003). Integrating the molecular and cellular basis of odor coding in the *Drosophila* antenna. Neuron *37*, 827-841.

Duffy, J.B. (2002). GAL4 system in *Drosophila*: a fly geneticist's Swiss army knife. Genesis *34*, 1-15.

Duistermars, B.J., and Frye, M.A. (2010). Multisensory integration for odor tracking by flying *Drosophila*: Behavior, circuits and speculation. Communicative & integrative biology *3*, 60-63.

Dweck, H.K., Ebrahim, S.A., Farhan, A., Hansson, B.S., and Stensmyr, M.C. (2015a). Olfactory proxy detection of dietary antioxidants in *Drosophila*. Current biology : CB *25*, 455-466.

Dweck, H.K., Ebrahim, S.A., Kromann, S., Bown, D., Hillbur, Y., Sachse, S., Hansson, B.S., and Stensmyr, M.C. (2013). Olfactory preference for egg laying on citrus substrates in *Drosophila*. Current biology : CB *23*, 2472-2480.

Dweck, H.K., Ebrahim, S.A., Thoma, M., Mohamed, A.A., Keesey, I.W., Trona, F., Lavista-Llanos, S., Svatos, A., Sachse, S., Knaden, M., and Hansson, B.S. (2015b). Pheromones mediating copulation and attraction in *Drosophila*. Proceedings of the National Academy of Sciences of the United States of America *112*, E2829-2835.

Ebrahim, S.A., Dweck, H.K., Stokl, J., Hofferberth, J.E., Trona, F., Weniger, K., Rybak, J., Seki, Y., Stensmyr, M.C., Sachse, S.*, et al.* (2015). *Drosophila* Avoids Parasitoids by Sensing Their Semiochemicals via a Dedicated Olfactory Circuit. PLoS biology *13*, e1002318.

Enjin, A., Zaharieva, E.E., Frank, D.D., Mansourian, S., Suh, G.S., Gallio, M., and Stensmyr, M.C. (2016). Humidity Sensing in *Drosophila*. Current biology : CB *26*, 1352-1358.

Fan, P., Manoli, D.S., Ahmed, O.M., Chen, Y., Agarwal, N., Kwong, S., Cai, A.G., Neitz, J., Renslo, A., Baker, B.S., and Shah, N.M. (2013). Genetic and neural mechanisms that inhibit *Drosophila* from mating with other species. Cell *154*, 89-102.

Feinberg, E.H., Vanhoven, M.K., Bendesky, A., Wang, G., Fetter, R.D., Shen, K., and Bargmann, C.I. (2008). GFP Reconstitution Across Synaptic Partners (GRASP) defines cell contacts and synapses in living nervous systems. Neuron *57*, 353-363.

Fiala, A., Spall, T., Diegelmann, S., Eisermann, B., Sachse, S., Devaud, J.M., Buchner, E., and Galizia, C.G. (2002). Genetically expressed cameleon in *Drosophila melanogaster* is used to visualize olfactory information in projection neurons. Current biology : CB *12*, 1877-1884.

Fişek, M., and Wilson, R.I. (2014). Stereotyped connectivity and computations in higher-order olfactory neurons. Nature neuroscience *17*, 280-288.

Fishilevich, E., and Vosshall, L.B. (2005). Genetic and functional subdivision of the *Drosophila* antennal lobe. Current biology : CB *15*, 1548-1553.

Frye, M.A., and Dickinson, M.H. (2004). Motor output reflects the linear superposition of visual and olfactory inputs in *Drosophila*. The Journal of experimental biology *207*, 123-131.

Gallio, M., Ofstad, T.A., Macpherson, L.J., Wang, J.W., and Zuker, C.S. (2011). The coding of temperature in the *Drosophila* brain. Cell *144*, 614-624.

Gao, Q., and Chess, A. (1999). Identification of candidate *Drosophila* olfactory receptors from genomic DNA sequence. Genomics *60*, 31-39.

Gao, Q., Yuan, B., and Chess, A. (2000). Convergent projections of *Drosophila* olfactory neurons to specific glomeruli in the antennal lobe. Nature neuroscience *3*, 780-785.

Goldman, A.L., Van der Goes van Naters, W., Lessing, D., Warr, C.G., and Carlson, J.R. (2005). Coexpression of two functional odor receptors in one neuron. Neuron *45*, 661-666.

Grabe, V., Baschwitz, A., Dweck, H.K., Lavista-Llanos, S., Hansson, B.S., and Sachse, S. (2016). Elucidating the Neuronal Architecture of Olfactory Glomeruli in the *Drosophila* Antennal Lobe. Cell reports *16*, 3401-3413.

Grabe, V., Strutz, A., Baschwitz, A., Hansson, B.S., and Sachse, S. (2015). Digital *in vivo* 3D atlas of the antennal lobe of *Drosophila melanogaster*. The Journal of comparative neurology *523*, 530-544.

Grover, D., Katsuki, T., and Greenspan, R.J. (2016). Flyception: imaging brain activity in freely walking fruit flies. Nature methods *13*, 569-572.

Gupta, N., and Stopfer, M. (2012). Functional analysis of a higher olfactory center, the lateral horn. The Journal of neuroscience : the official journal of the Society for Neuroscience *32*, 8138-8148.

Ha, T.S., and Smith, D.P. (2006). A pheromone receptor mediates 11-*cis*-vaccenyl acetate-induced responses in *Drosophila*. The Journal of neuroscience : the official journal of the Society for Neuroscience *26*, 8727-8733.

Hallem, E.A., and Carlson, J.R. (2006). Coding of odors by a receptor repertoire. Cell *125*, 143-160.

Hallem, E.A., Ho, M.G., and Carlson, J.R. (2004). The molecular basis of odor coding in the *Drosophila* antenna. Cell *117*, 965-979.

Hansson, B.S., Knaden, M., Sachse, S., Stensmyr, M.C., and Wicher, D. (2010). Towards plant-odor-related olfactory neuroethology in *Drosophila*. Chemoecology *20*, 51-61.

Heimbeck, G., Bugnon, V., Gendre, N., Keller, A., and Stocker, R.F. (2001). A central neural circuit for experience-independent olfactory and courtship behavior in *Drosophila melanogaster*. Proceedings of the National Academy of Sciences of the United States of America *98*, 15336-15341.

Heisenberg, M. (2003). Mushroom body memoir: from maps to models. Nature reviews. Neuroscience *4*, 266-275.

Heisenberg, M. (2015). Outcome learning, outcome expectations, and intentionality in *Drosophila*. Learn Mem *22*, 294-298.

Heisenberg, M., Borst, A., Wagner, S., and Byers, D. (1985). *Drosophila* mushroom body mutants are deficient in olfactory learning. Journal of neurogenetics *2*, 1-30.

Hires, S.A., Tian, L., and Looger, L.L. (2008). Reporting neural activity with genetically encoded calcium indicators. Brain cell biology *36*, 69-86.

Hofbauer, A. (1991). Eine Bibliothek monoklonaler Antikörper gegen das Gehirn von *Drosophila melanogaster*. Habilitation thesis. University of Würzburg,Würzburg, Germany.

Hoi, H., Matsuda, T., Nagai, T., and Campbell, R.E. (2013). Highlightable Ca^{2+} indicators for live cell imaging. Journal of the American Chemical Society *135*, 46-49.

Honegger, K.S., Campbell, R.A., and Turner, G.C. (2011). Cellular-resolution population imaging reveals robust sparse coding in the *Drosophila* mushroom body. The Journal of neuroscience : the official journal of the Society for Neuroscience *31*, 11772-11785.

Hong, E.J., and Wilson, R.I. (2015). Simultaneous encoding of odors by channels with diverse sensitivity to inhibition. Neuron *85*, 573-589.

Huang, J., Zhang, W., Qiao, W., Hu, A., and Wang, Z. (2010). Functional connectivity and selective odor responses of excitatory local interneurons in *Drosophila* antennal lobe. Neuron *67*, 1021-1033.

Ignell, R., Dekker, T., Ghaninia, M., and Hansson, B.S. (2005). Neuronal architecture of the mosquito deutocerebrum. The Journal of comparative neurology *493*, 207-240.

Ignell, R., Root, C.M., Birse, R.T., Wang, J.W., Nassel, D.R., and Winther, A.M. (2009). Presynaptic peptidergic modulation of olfactory receptor neurons in *Drosophila*. Proceedings of the National Academy of Sciences of the United States of America *106*, 13070-13075.

Ito, K., Awano, W., Suzuki, K., Hiromi, Y., and Yamamoto, D. (1997). The *Drosophila* mushroom body is a quadruple structure of clonal units each of which contains a virtually identical set of neurones and glial cells. Development *124*, 761-771.

Ito, K., and Awasaki, T. (2008). Clonal unit architecture of the adult fly brain. Advances in experimental medicine and biology *628*, 137-158.

Jeanne, J.M., and Wilson, R.I. (2015). Convergence, Divergence, and Reconvergence in a Feedforward Network Improves Neural Speed and Accuracy. Neuron *88*, 1014-1026.

Jefferis, G.S., Potter, C.J., Chan, A.M., Marin, E.C., Rohlfing, T., Maurer, C.R., Jr., and Luo, L. (2007). Comprehensive maps of *Drosophila* higher olfactory centers: spatially segregated fruit and pheromone representation. Cell *128*, 1187-1203.

Jenett, A., Rubin, G.M., Ngo, T.T., Shepherd, D., Murphy, C., Dionne, H., Pfeiffer, B.D., Cavallaro, A., Hall, D., Jeter, J.*, et al.* (2012). A GAL4-driver line resource for *Drosophila* neurobiology. Cell reports *2*, 991-1001.

Jones, W.D., Cayirlioglu, P., Kadow, I.G., and Vosshall, L.B. (2007). Two chemosensory receptors together mediate carbon dioxide detection in *Drosophila*. Nature *445*, 86-90.

Kandel, E.R., Dudai, Y., and Mayford, M.R. (2014). The molecular and systems biology of memory. Cell *157*, 163-186.

Karuppudurai, T., Lin, T.-Y., Ting, C.-Y., Pursley, R., Melnattur, Krishna V., Diao, F., White, Benjamin H., Macpherson, Lindsey J., Gallio, M., Pohida, T., and Lee, C.-H. (2014). A Hard-Wired Glutamatergic Circuit Pools and Relays UV Signals to Mediate Spectral Preference in *Drosophila*. Neuron *81*, 603-615.

Kazama, H., and Wilson, R.I. (2008). Homeostatic matching and nonlinear amplification at identified central synapses. Neuron *58*, 401-413.

Kido, A., and Ito, K. (2002). Mushroom bodies are not required for courtship behavior by normal and sexually mosaic *Drosophila*. Journal of neurobiology *52*, 302-311.

Knaden, M., Strutz, A., Ahsan, J., Sachse, S., and Hansson, B.S. (2012). Spatial representation of odorant valence in an insect brain. Cell reports *1*, 392-399.

Kohl, J., Ostrovsky, A.D., Frechter, S., and Jefferis, G.S. (2013). A bidirectional circuit switch reroutes pheromone signals in male and female brains. Cell *155*, 1610-1623.

Kreher, S.A., Kwon, J.Y., and Carlson, J.R. (2005). The molecular basis of odor coding in the *Drosophila* larva. Neuron *46*, 445-456.

Kurtovic, A., Widmer, A., and Dickson, B.J. (2007). A single class of olfactory neurons mediates behavioural responses to a *Drosophila* sex pheromone. Nature *446*, 542-546.

Kwon, J.Y., Dahanukar, A., Weiss, L.A., and Carlson, J.R. (2007). The molecular basis of CO_2 reception in *Drosophila*. Proceedings of the National Academy of Sciences of the United States of America *104*, 3574-3578.

Lai, S.L., Awasaki, T., Ito, K., and Lee, T. (2008). Clonal analysis of *Drosophila* antennal lobe neurons: diverse neuronal architectures in the lateral neuroblast lineage. Development *135*, 2883-2893.

Lai, S.L., and Lee, T. (2006). Genetic mosaic with dual binary transcriptional systems in *Drosophila*. Nature neuroscience *9*, 703-709.

Laissue, P.P., Reiter, C., Hiesinger, P.R., Halter, S., Fischbach, K.F., and Stocker, R.F. (1999). Three-dimensional reconstruction of the antennal lobe in *Drosophila melanogaster*. The Journal of comparative neurology *405*, 543-552.

Larsson, M.C., Domingos, A.I., Jones, W.D., Chiappe, M.E., Amrein, H., and Vosshall, L.B. (2004). Or83b encodes a broadly expressed odorant receptor essential for *Drosophila* olfaction. Neuron *43*, 703-714.

Leal, W.S. (2013). Odorant reception in insects: roles of receptors, binding proteins, and degrading enzymes. Annual review of entomology *58*, 373-391.

Lebreton, S., Borrero-Echeverry, F., Gonzalez, F., Solum, M., Wallin, E., Hedenstroem, E., Hansson, B.S., Gustavsson, A.-L., Bengtsson, M., Birgersson, G.*, et al.* (2017). The *Drosophila* pheromone Z4-11Al is encoded together with habitat olfactory cues and mediates species-specific communication. bioRxiv.

Lebreton, S., Grabe, V., Omondi, A.B., Ignell, R., Becher, P.G., Hansson, B.S., Sachse, S., and Witzgall, P. (2014). Love makes smell blind: mating suppresses pheromone attraction in *Drosophila* females via Or65a olfactory neurons. Scientific reports *4*, 7119.

Lebreton, S., Trona, F., Borrero-Echeverry, F., Bilz, F., Grabe, V., Becher, P.G., Carlsson, M.A., Nassel, D.R., Hansson, B.S., Sachse, S., and Witzgall, P. (2015). Feeding regulates sex pheromone attraction and courtship in *Drosophila* females. Scientific reports *5*, 13132.

Lee, D.D., and Seung, H.S. (1999). Learning the parts of objects by non-negative matrix factorization. Nature *401*, 788-791.

Li, H., Li, Y., Lei, Z., Wang, K., and Guo, A. (2013). Transformation of odor selectivity from projection neurons to single mushroom body neurons mapped with dual-color calcium imaging. Proceedings of the National Academy of Sciences of the United States of America *110*, 12084-12089.

Li, Q., and Liberles, S.D. (2015). Aversion and attraction through olfaction. Current biology : CB *25*, R120-129.

Liang, L., Li, Y., Potter, C.J., Yizhar, O., Deisseroth, K., Tsien, R.W., and Luo, L. (2013). GABAergic projection neurons route selective olfactory inputs to specific higher-order neurons. Neuron *79*, 917-931.

Liang, L., and Luo, L. (2010). The olfactory circuit of the fruit fly *Drosophila melanogaster*. Science China. Life sciences *53*, 472-484.

Lin, A.C., Bygrave, A.M., de Calignon, A., Lee, T., and Miesenbock, G. (2014a). Sparse, decorrelated odor coding in the mushroom body enhances learned odor discrimination. Nature neuroscience *17*, 559-568.

Lin, H.H., Lai, J.S., Chin, A.L., Chen, Y.C., and Chiang, A.S. (2007). A map of olfactory representation in the *Drosophila* mushroom body. Cell *128*, 1205-1217.

Lin, S., Owald, D., Chandra, V., Talbot, C., Huetteroth, W., and Waddell, S. (2014b). Neural correlates of water reward in thirsty *Drosophila*. Nature neuroscience *17*, 1536-1542.

Linz, J., Baschwitz, A., Strutz, A., Dweck, H.K., Sachse, S., Hansson, B.S., and Stensmyr, M.C. (2013). Host plant-driven sensory specialization in *Drosophila erecta*. Proceedings. Biological sciences / The Royal Society *280*, 20130626.

Liu, W.W., and Wilson, R.I. (2013). Glutamate is an inhibitory neurotransmitter in the *Drosophila* olfactory system. Proceedings of the National Academy of Sciences of the United States of America *110*, 10294-10299.

Luo, L., Callaway, E.M., and Svoboda, K. (2008). Genetic dissection of neural circuits. Neuron *57*, 634-660.

Ma, Y., Smith, D., Hof, P.R., Foerster, B., Hamilton, S., Blackband, S.J., Yu, M., and Benveniste, H. (2008). *In vivo* 3D Digital Atlas Database of the Adult C57BL/6J Mouse Brain by Magnetic Resonance Microscopy. Frontiers in neuroanatomy *2*, 1.

Marin, E.C., Jefferis, G.S., Komiyama, T., Zhu, H., and Luo, L. (2002). Representation of the glomerular olfactory map in the *Drosophila* brain. Cell *109*, 243-255.

Masters, B.R., So, P.T., and Gratton, E. (1997). Multiphoton excitation fluorescence microscopy and spectroscopy of *in vivo* human skin. Biophysical journal *72*, 2405-2412.

Masuda-Nakagawa, L.M., Tanaka, N.K., and O'Kane, C.J. (2005). Stereotypic and random patterns of connectivity in the larval mushroom body calyx of *Drosophila*. Proceedings of the National Academy of Sciences of the United States of America *102*, 19027-19032.

Matz, M.V., Fradkov, A.F., Labas, Y.A., Savitsky, A.P., Zaraisky, A.G., Markelov, M.L., and Lukyanov, S.A. (1999). Fluorescent proteins from nonbioluminescent Anthozoa species. Nature biotechnology *17*, 969-973.

Min, S., Ai, M., Shin, S.A., and Suh, G.S. (2013). Dedicated olfactory neurons mediating attraction behavior to ammonia and amines in *Drosophila*. Proceedings of the National Academy of Sciences of the United States of America *110*, E1321-1329.

Miyawaki, A., Llopis, J., Heim, R., McCaffery, J.M., Adams, J.A., Ikura, M., and Tsien, R.Y. (1997). Fluorescent indicators for Ca^{2+} based on green fluorescent proteins and calmodulin. Nature *388*, 882-887.

Morgan, T.H. (1910). Sex Limited Inheritance in *Drosophila*. Science *32*, 120-122.

Mosca, T.J., and Luo, L. (2014). Synaptic organization of the *Drosophila* antennal lobe and its regulation by the Teneurins. eLife *3*, e03726.

Münch, D., and Galizia, C.G. (2016). DoOR 2.0--Comprehensive Mapping of *Drosophila melanogaster* Odorant Responses. Scientific reports *6*, 21841.

Murthy, M., Fiete, I., and Laurent, G. (2008). Testing odor response stereotypy in the *Drosophila* mushroom body. Neuron *59*, 1009-1023.

Nakai, J., Ohkura, M., and Imoto, K. (2001). A high signal-to-noise $Ca^{(2+)}$ probe composed of a single green fluorescent protein. Nature biotechnology *19*, 137-141.

Nassi, J.J., and Callaway, E.M. (2009). Parallel processing strategies of the primate visual system. Nature reviews. Neuroscience *10*, 360-372.

Neuhaus, E.M., Gisselmann, G., Zhang, W., Dooley, R., Stortkuhl, K., and Hatt, H. (2005). Odorant receptor heterodimerization in the olfactory system of *Drosophila melanogaster*. Nature neuroscience *8*, 15-17.

Ng, M., Roorda, R.D., Lima, S.Q., Zemelman, B.V., Morcillo, P., and Miesenbock, G. (2002). Transmission of olfactory information between three populations of neurons in the antennal lobe of the fly. Neuron *36*, 463-474.

Okada, R., Awasaki, T., and Ito, K. (2009). Gamma-aminobutyric acid (GABA)-mediated neural connections in the *Drosophila* antennal lobe. The Journal of comparative neurology *514*, 74-91.

Olsen, S.R., Bhandawat, V., and Wilson, R.I. (2007). Excitatory interactions between olfactory processing channels in the *Drosophila* antennal lobe. Neuron *54*, 89-103.

Olsen, S.R., Bhandawat, V., and Wilson, R.I. (2010). Divisive normalization in olfactory population codes. Neuron *66*, 287-299.

Olsen, S.R., and Wilson, R.I. (2008a). Cracking neural circuits in a tiny brain: new approaches for understanding the neural circuitry of *Drosophila*. Trends in neurosciences *31*, 512-520.

Olsen, S.R., and Wilson, R.I. (2008b). Lateral presynaptic inhibition mediates gain control in an olfactory circuit. Nature *452*, 956-960.

Otsuna, H., Shinomiya, K., and Ito, K. (2014). Parallel neural pathways in higher visual centers of the *Drosophila* brain that mediate wavelength-specific behavior. Frontiers in neural circuits *8*, 8.

Owald, D., and Waddell, S. (2015). Olfactory learning skews mushroom body output pathways to steer behavioral choice in *Drosophila*. Current opinion in neurobiology *35*, 178-184.

Parnas, M., Lin, A.C., Huetteroth, W., and Miesenbock, G. (2013). Odor discrimination in *Drosophila*: from neural population codes to behavior. Neuron *79*, 932-944.

Patterson, G.H., and Lippincott-Schwartz, J. (2002). A photoactivatable GFP for selective photolabeling of proteins and cells. Science *297*, 1873-1877.

Pelosi, P., Iovinella, I., Felicioli, A., and Dani, F.R. (2014). Soluble proteins of chemical communication: an overview across arthropods. Frontiers in physiology *5*, 320.

Perez-Orive, J., Mazor, O., Turner, G.C., Cassenaer, S., Wilson, R.I., and Laurent, G. (2002). Oscillations and sparsening of odor representations in the mushroom body. Science *297*, 359-365.

Potter, C.J., Tasic, B., Russler, E.V., Liang, L., and Luo, L. (2010). The Q system: a repressible binary system for transgene expression, lineage tracing, and mosaic analysis. Cell *141*, 536-548.

Ramaekers, A., Magnenat, E., Marin, E.C., Gendre, N., Jefferis, G.S., Luo, L., and Stocker, R.F. (2005). Glomerular maps without cellular redundancy at successive levels of the *Drosophila* larval olfactory circuit. Current biology : CB *15*, 982-992.

Rein, K., Zockler, M., Mader, M.T., Grubel, C., and Heisenberg, M. (2002). The *Drosophila* standard brain. Current biology : CB *12*, 227-231.

Riemensperger, T., Pech, U., Dipt, S., and Fiala, A. (2012). Optical calcium imaging in the nervous system of *Drosophila melanogaster*. Biochimica et biophysica acta *1820*, 1169-1178.

Robertson, H.M., Warr, C.G., and Carlson, J.R. (2003). Molecular evolution of the insect chemoreceptor gene superfamily in *Drosophila melanogaster*. Proceedings of the National Academy of Sciences of the United States of America *100 Suppl 2*, 14537-14542.

Root, C.M., Ko, K.I., Jafari, A., and Wang, J.W. (2011). Presynaptic facilitation by neuropeptide signaling mediates odor-driven food search. Cell *145*, 133-144.

Root, C.M., Masuyama, K., Green, D.S., Enell, L.E., Nassel, D.R., Lee, C.H., and Wang, J.W. (2008). A presynaptic gain control mechanism fine-tunes olfactory behavior. Neuron *59*, 311-321.

Root, C.M., Semmelhack, J.L., Wong, A.M., Flores, J., and Wang, J.W. (2007). Propagation of olfactory information in *Drosophila*. Proceedings of the National Academy of Sciences of the United States of America *104*, 11826-11831.

Ruta, V., Datta, S.R., Vasconcelos, M.L., Freeland, J., Looger, L.L., and Axel, R. (2010). A dimorphic pheromone circuit in *Drosophila* from sensory input to descending output. Nature *468*, 686-690.

Rybak, J., Kuss, A., Lamecker, H., Zachow, S., Hege, H.C., Lienhard, M., Singer, J., Neubert, K., and Menzel, R. (2010). The Digital Bee Brain: Integrating and Managing Neurons in a Common 3D Reference System. Frontiers in systems neuroscience *4*.

Sachse, S., Rueckert, E., Keller, A., Okada, R., Tanaka, N.K., Ito, K., and Vosshall, L.B. (2007). Activity-dependent plasticity in an olfactory circuit. Neuron *56*, 838-850.

Sato, K., Pellegrino, M., Nakagawa, T., Vosshall, L.B., and Touhara, K. (2008). Insect olfactory receptors are heteromeric ligand-gated ion channels. Nature *452*, 1002-1006.

Schlief, M.L., and Wilson, R.I. (2007). Olfactory processing and behavior downstream from highly selective receptor neurons. Nature neuroscience *10*, 623-630.

Schneider, D., Kasang, G., and Kaissling, K.E. (1968). [Determination of the olfactory threshold of Bombyx mori with tritium-labelled bombycol]. Die Naturwissenschaften *55*, 395.

Schubert, M., Hansson, B.S., and Sachse, S. (2014). The banana code-natural blend processing in the olfactory circuitry of *Drosophila melanogaster*. Frontiers in physiology *5*, 59.

Schultzhaus, J.N., Saleem, S., Iftikhar, H., and Carney, G.E. (2016). The role of the *Drosophila* lateral horn in olfactory information processing and behavioral response. Journal of insect physiology *98*, 29-37.

Sejourne, J., Placais, P.Y., Aso, Y., Siwanowicz, I., Trannoy, S., Thoma, V., Tedjakumala, S.R., Rubin, G.M., Tchenio, P., Ito, K.*, et al.* (2011). Mushroom body efferent neurons responsible for aversive olfactory memory retrieval in *Drosophila*. Nature neuroscience *14*, 903-910.

Seki, Y., Rybak, J., Wicher, D., Sachse, S., and Hansson, B.S. (2010). Physiological and morphological characterization of local interneurons in the *Drosophila* antennal lobe. Journal of neurophysiology *104*, 1007-1019.

Semmelhack, J.L., and Wang, J.W. (2009). Select *Drosophila* glomeruli mediate innate olfactory attraction and aversion. Nature *459*, 218-223.

Shanbhag, S.R., Muller, B., and Steinbrecht, R.A. (1999). Atlas of olfactory organs of *Drosophila melanogaster* - 1. Types, external organization, innervation and distribution of olfactory sensilla. Int J Insect Morphol *28*, 377-397.

Shanbhag, S.R., Muller, B., and Steinbrecht, R.A. (2000). Atlas of olfactory organs of *Drosophila melanogaster* 2. Internal organization and cellular architecture of olfactory sensilla. Arthropod structure & development *29*, 211-229.

Shang, Y., Claridge-Chang, A., Sjulson, L., Pypaert, M., and Miesenbock, G. (2007). Excitatory local circuits and their implications for olfactory processing in the fly antennal lobe. Cell *128*, 601-612.

Silbering, A.F., and Galizia, C.G. (2007). Processing of odor mixtures in the *Drosophila* antennal lobe reveals both global inhibition and glomerulus-specific interactions. The Journal of neuroscience : the official journal of the Society for Neuroscience *27*, 11966-11977.

Silbering, A.F., Okada, R., Ito, K., and Galizia, C.G. (2008). Olfactory information processing in the *Drosophila* antennal lobe: anything goes? The Journal of neuroscience : the official journal of the Society for Neuroscience *28*, 13075-13087.

Silbering, A.F., Rytz, R., Grosjean, Y., Abuin, L., Ramdya, P., Jefferis, G.S., and Benton, R. (2011). Complementary function and integrated wiring of the evolutionarily distinct *Drosophila* olfactory subsystems. The Journal of neuroscience : the official journal of the Society for Neuroscience *31*, 13357-13375.

Soelter, J., Schumacher, J., Spors, H., and Schmuker, M. (2014). Automatic segmentation of odor maps in the mouse olfactory bulb using regularized non-negative matrix factorization. NeuroImage *98*, 279-288.

Soucy, E.R., Albeanu, D.F., Fantana, A.L., Murthy, V.N., and Meister, M. (2009). Precision and diversity in an odor map on the olfactory bulb. Nature neuroscience *12*, 210-220.

Steck, K., Veit, D., Grandy, R., Badia, S.B., Mathews, Z., Verschure, P., Hansson, B.S., and Knaden, M. (2012). A high-throughput behavioral paradigm for *Drosophila* olfaction - The Flywalk. Scientific reports *2*, 361.

Stensmyr, M.C., Dweck, H.K., Farhan, A., Ibba, I., Strutz, A., Mukunda, L., Linz, J., Grabe, V., Steck, K., Lavista-Llanos, S*., et al.* (2012). A conserved dedicated olfactory circuit for detecting harmful microbes in *Drosophila*. Cell *151*, 1345-1357.

Stensmyr, M.C., Giordano, E., Balloi, A., Angioy, A.M., and Hansson, B.S. (2003). Novel natural ligands for *Drosophila* olfactory receptor neurones. The Journal of experimental biology *206*, 715-724.

Stocker, R.F. (1994). The organization of the chemosensory system in *Drosophila melanogaster*: a review. Cell and tissue research *275*, 3-26.

Stocker, R.F. (2001). *Drosophila* as a focus in olfactory research: mapping of olfactory sensilla by fine structure, odor specificity, odorant receptor expression, and central connectivity. Microscopy research and technique *55*, 284-296.

Stocker, R.F., Heimbeck, G., Gendre, N., and de Belle, J.S. (1997). Neuroblast ablation in *Drosophila* P[GAL4] lines reveals origins of olfactory interneurons. Journal of neurobiology *32*, 443-456.

Stocker, R.F., Lienhard, M.C., Borst, A., and Fischbach, K.F. (1990). Neuronal architecture of the antennal lobe in *Drosophila melanogaster*. Cell and tissue research *262*, 9-34.

Stockinger, P., Kvitsiani, D., Rotkopf, S., Tirian, L., and Dickson, B.J. (2005). Neural circuitry that governs *Drosophila* male courtship behavior. Cell *121*, 795-807.

Stökl, J., Strutz, A., Dafni, A., Svatos, A., Doubsky, J., Knaden, M., Sachse, S., Hansson, B.S., and Stensmyr, M.C. (2010). A deceptive pollination system targeting drosophilids through olfactory mimicry of yeast. Current biology : CB *20*, 1846-1852.

Strutz, A., Soelter, J., Baschwitz, A., Farhan, A., Grabe, V., Rybak, J., Knaden, M., Schmuker, M., Hansson, B.S., and Sachse, S. (2014). Decoding odor quality and intensity in the *Drosophila* brain. eLife *3*, e04147.

Su, C.Y., Menuz, K., and Carlson, J.R. (2009). Olfactory perception: receptors, cells, and circuits. Cell *139*, 45-59.

Su, C.Y., and Wang, J.W. (2014). Modulation of neural circuits: how stimulus context shapes innate behavior in *Drosophila*. Current opinion in neurobiology *29*, 9-16.

Suh, G.S., Wong, A.M., Hergarden, A.C., Wang, J.W., Simon, A.F., Benzer, S., Axel, R., and Anderson, D.J. (2004). A single population of olfactory sensory neurons mediates an innate avoidance behaviour in *Drosophila*. Nature *431*, 854-859.

Swarup, S., Williams, T.I., and Anholt, R.R. (2011). Functional dissection of Odorant binding protein genes in *Drosophila melanogaster*. Genes, brain, and behavior *10*, 648-657.

Tanaka, N.K., Awasaki, T., Shimada, T., and Ito, K. (2004). Integration of chemosensory pathways in the *Drosophila* second-order olfactory centers. Current biology : CB *14*, 449-457.

Tanaka, N.K., Endo, K., and Ito, K. (2012). Organization of antennal lobe-associated neurons in adult *Drosophila melanogaster* brain. The Journal of comparative neurology *520*, 4067-4130.

Tanaka, N.K., Tanimoto, H., and Ito, K. (2008). Neuronal assemblies of the *Drosophila* mushroom body. The Journal of comparative neurology *508*, 711-755.

Thoma, M., Hansson, B.S., and Knaden, M. (2014). Compound valence is conserved in binary odor mixtures in *Drosophila melanogaster*. The Journal of experimental biology *217*, 3645-3655.

Tian, L., Hires, S.A., Mao, T., Huber, D., Chiappe, M.E., Chalasani, S.H., Petreanu, L., Akerboom, J., McKinney, S.A., Schreiter, E.R.*, et al.* (2009). Imaging neural activity in worms, flies and mice with improved GCaMP calcium indicators. Nature methods *6*, 875-881.

Tully, T., and Quinn, W.G. (1985). Classical conditioning and retention in normal and mutant *Drosophila melanogaster*. Journal of comparative physiology. A, Sensory, neural, and behavioral physiology *157*, 263-277.

Turner, G.C., Bazhenov, M., and Laurent, G. (2008). Olfactory representations by *Drosophila* mushroom body neurons. Journal of neurophysiology *99*, 734-746.

van der Goes van Naters, W., and Carlson, J.R. (2007). Receptors and neurons for fly odors in *Drosophila*. Current biology : CB *17*, 606-612.

van Thor, J.J. (2009). Photoreactions and dynamics of the green fluorescent protein. Chemical Society reviews *38*, 2935-2950.

Venken, K.J., Simpson, J.H., and Bellen, H.J. (2011). Genetic manipulation of genes and cells in the nervous system of the fruit fly. Neuron *72*, 202-230.

Vieira, F.G., and Rozas, J. (2011). Comparative genomics of the odorant-binding and chemosensory protein gene families across the Arthropoda: origin and evolutionary history of the chemosensory system. Genome biology and evolution *3*, 476-490.

Vinje, W.E., and Gallant, J.L. (2000). Sparse coding and decorrelation in primary visual cortex during natural vision. Science *287*, 1273-1276.

Vogt, R.G., Rogers, M.E., Franco, M.D., and Sun, M. (2002). A comparative study of odorant binding protein genes: differential expression of the PBP1-GOBP2 gene cluster in *Manduca sexta* (*Lepidoptera*) and the organization of OBP genes in *Drosophila melanogaster* (*Diptera*). The Journal of experimental biology *205*, 719-744.

Vosshall, L.B. (2001). The molecular logic of olfaction in *Drosophila*. Chemical senses *26*, 207-213.

Vosshall, L.B., Amrein, H., Morozov, P.S., Rzhetsky, A., and Axel, R. (1999). A spatial map of olfactory receptor expression in the *Drosophila* antenna. Cell *96*, 725-736.

Vosshall, L.B., and Stocker, R.F. (2007). Molecular architecture of smell and taste in *Drosophila*. Annual review of neuroscience *30*, 505-533.

Vosshall, L.B., Wong, A.M., and Axel, R. (2000). An olfactory sensory map in the fly brain. Cell *102*, 147-159.

Wang, J.W., Wong, A.M., Flores, J., Vosshall, L.B., and Axel, R. (2003a). Two-photon calcium imaging reveals an odor-evoked map of activity in the fly brain. Cell *112*, 271-282.

Wang, K., Gong, J., Wang, Q., Li, H., Cheng, Q., Liu, Y., Zeng, S., and Wang, Z. (2014). Parallel pathways convey olfactory information with opposite polarities in *Drosophila*. Proceedings of the National Academy of Sciences of the United States of America *111*, 3164-3169.

Wang, Y., Chiang, A.S., Xia, S., Kitamoto, T., Tully, T., and Zhong, Y. (2003b). Blockade of neurotransmission in *Drosophila* mushroom bodies impairs odor attraction, but not repulsion. Current biology : CB *13*, 1900-1904.

Wang, Y., Guo, H.F., Pologruto, T.A., Hannan, F., Hakker, I., Svoboda, K., and Zhong, Y. (2004). Stereotyped odor-evoked activity in the mushroom body of *Drosophila*

revealed by green fluorescent protein-based Ca^{2+} imaging. The Journal of neuroscience : the official journal of the Society for Neuroscience *24*, 6507-6514.

Wicher, D., Schafer, R., Bauernfeind, R., Stensmyr, M.C., Heller, R., Heinemann, S.H., and Hansson, B.S. (2008). *Drosophila* odorant receptors are both ligand-gated and cyclic-nucleotide-activated cation channels. Nature *452*, 1007-1011.

Wilson, R.I., and Laurent, G. (2005). Role of GABAergic inhibition in shaping odor-evoked spatiotemporal patterns in the *Drosophila* antennal lobe. The Journal of neuroscience : the official journal of the Society for Neuroscience *25*, 9069-9079.

Wilson, R.I., Turner, G.C., and Laurent, G. (2004). Transformation of olfactory representations in the *Drosophila* antennal lobe. Science *303*, 366-370.

Wong, A.M., Wang, J.W., and Axel, R. (2002). Spatial representation of the glomerular map in the *Drosophila* protocerebrum. Cell *109*, 229-241.

Xia, S., and Tully, T. (2007). Segregation of odor identity and intensity during odor discrimination in *Drosophila* mushroom body. PLoS biology *5*, e264.

Xu, P., Atkinson, R., Jones, D.N., and Smith, D.P. (2005). *Drosophila* OBP LUSH is required for activity of pheromone-sensitive neurons. Neuron *45*, 193-200.

Yaksi, E., and Wilson, R.I. (2010). Electrical coupling between olfactory glomeruli. Neuron *67*, 1034-1047.

Yao, C.A., Ignell, R., and Carlson, J.R. (2005). Chemosensory coding by neurons in the coeloconic sensilla of the *Drosophila* antenna. The Journal of neuroscience : the official journal of the Society for Neuroscience *25*, 8359-8367.

Yao, K.M., Samson, M.L., Reeves, R., and White, K. (1993). Gene *elav* of *Drosophila melanogaster*: a prototype for neuronal-specific RNA binding protein gene family that is conserved in flies and humans. Journal of neurobiology *24*, 723-739.

Yasuyama, K., and Salvaterra, P.M. (1999). Localization of choline acetyltransferase-expressing neurons in *Drosophila* nervous system. Microscopy research and technique *45*, 65-79.

Yu, J.Y., Kanai, M.I., Demir, E., Jefferis, G.S., and Dickson, B.J. (2010). Cellular organization of the neural circuit that drives *Drosophila* courtship behavior. Current biology : CB *20*, 1602-1614.

Zhao, Y., Araki, S., Wu, J., Teramoto, T., Chang, Y.F., Nakano, M., Abdelfattah, A.S., Fujiwara, M., Ishihara, T., Nagai, T., and Campbell, R.E. (2011). An expanded palette of genetically encoded Ca^{2+} indicators. Science *333*, 1888-1891.

Glossary

adCL	anterodorsal cell cluster
AL	antennal lobe
CRs	chemosensory receptors
CSPs	chemosensory proteins
CX	mushroom body calyx
DsRed	red fluorescent protein found in the coral *Discosoma striata*
ELAV	embryonic lethal abnormal vision; protein involved in the development of the central nervous system
END1-2	fusion protein composed of ELAV, *n*-synaptobrevin and DsRed
GABA	gamma-aminobutyric acid
GAL4-UAS	yeast binary transcription system, like the Q-system and LexA-LexAop
GECIs	genetically encoded calcium (or chloride) indicators
GFP	green fluorescent protein
GRASP	GFP reconstitution across synaptic partners
ePNs	excitatory projection neurons
iPNs	inhibitory projection neurons
IRs	ionotropic receptors
KCs	Kenyon cells
lCL	lateral cell cluster
LH	lateral horn
LHNs	lateral horn neurons
LNs	local interneurons
NMF	non-negative matrix factorization
n-synaptobrevin	neuronal synaptic vesicle protein
OBPs	odorant binding proteins
ODEs	odor degrading enzymes
Orco	olfactory receptor co-receptor (formerly called OR83b)
ORDs	odor response domains
ORs	olfactory receptors
OSNs	olfactory sensory neurons
pa-GFP	photoactivatable green fluorescent protein
PCA	principal component analysis

PNs	projection neurons
SSR	single sensillum recordings
UAS	upstream activating sequence
vCL	ventral cell cluster
VLP	ventrolateral protocerebrum
VLPNs	ventrolateral protocerebrum neurons

Declaration of independent assignment

I declare in accordance with the conferral of the degree of doctor from the School of Biology and Pharmacy of Friedrich-Schiller-University Jena that the submitted thesis was written only with the assistance and literature cited in the text.

People who assisted in experiments, data analysis and writing of the manuscripts are listed as co-authors of the respective manuscripts. I was not assisted by a consultant for doctorate theses.

The thesis has not been previously submitted whether to the Friedrich-Schiller-University, Jena or to any other university.

_____ _____

Place, date Signature

Acknowledgements

First of all, I want to thank Prof. Bill S. Hansson and Dr. Silke Sachse for giving me the opportunity to do my PhD in that great environment of the “Hansson department”. During the last years I learned under your supervision a lot about the neurobiology of olfaction in insects and the methods to investigate the olfactory system.

I thank the International Max Planck Research School (IMPRS for the exploration of ecological interactions with molecular and chemical techniques) for the funding, the great courses offered on soft and hard skills, and the opportunity to meet all those impressive young scientists within the IMPRS.

Dr. Michael Schmuker danke ich für die konstruktiven Beiträge zu den verschiedenen Projekten und den daraus hervorgegangenen Papern sowie als Mitglied in meinen Thesis Committee Meetings.

Ich danke Dr. Jan Sölter für die „Opferung“ seiner wenigen Freizeit, um die morphologischen und physiologischen Daten zu analysieren und mir die dazugehörigen bioinformatischen Grundlagen (soweit möglich) zu erklären. Seine Ideen und Ratschläge zu den Möglichkeiten der Datenauswertung haben sehr viele tolle Ergebnisse hervorgebracht.
- Jan, ich wünsche dir noch einen tollen Urlaub!

For teaching me the dissection of fly brains, the immunohistochemistry, the confocal laser scanning microscopy and the reconstruction of neurons and neuropils already during my student assistance I want to thank Dr. Yoichi Seki and Dr. Jürgen Rybak. Furthermore, I thank Dr. Sofia Lavista-Llanos for the introduction into and the help with fly genetics during the last years.

Bei Dr. Antonia Strutz und Dr. Veit Grabe bedanke ich mich für die Einarbeitung und Unterrichtung in Multiphotonenmikroskopie und funktionellem Imaging sowie für die alltägliche Unterstützung bei Fragen und Problemen bei meinen Experimenten.

Für die Hilfe im Fliegenlabor, beim Präparieren und vielen weiteren Unterstützungen bei der Laborarbeit, danke ich Silke Trautheim. Ebenso bedanke ich mich bei Regina Stieber-Rödiger, Kerstin Weniger, Sylke Dietel-Gläßer, Sabine Kaltofen und Sascha Bucks für die Unterstützung bei Fragen und Problemen im Laboralltag.

Swetlana Laubrich danke ich für die Unterstützung bei administrativen Anliegen.

Für die technische Umsetzung von Versuchsaufbauten und deren kontinuierliche Entwicklung bedanke ich mich bei Daniel Veit und dem Werkstattteam. Des Weiteren danke ich dem IT-Department bei der Hilfe zu meinen kleinen und großen Problemen mit Software, PC & Co.

I am especially grateful to the members of the research group Olfactory Coding, all Journal Clubbers as well as all former and current members of the “Hansson department”. Thank you for the fruitful discussions on scientific issues and beyond, as well as for the awesome time in this nice multi-cultural working environment with lots of cakes and sweets.

Ein extra Dankeschön geht an PD Dr. Dieter Wicher, Dr. Veit Grabe und Dr. Michael Thoma für die Kommentare zum Skript und besonders die Motivation während der letzten Etappe.
- Ohne euch hätte ich das ganze wohl nicht mehr fertig gemacht!
In line with this I thank Dr. Richard Fandino for the correction of my proper “denglisch“ of the (almost) final version of this dissertation.

Regina, ohne dich wäre ich verhungert oder hätte drei Tage lang immer Dasselbe essen müssen, falls ich mich mal zum Kochen motivieren konnte. Aber zum Glück hast du mich mit Kartoffelbrei & Würstchen-Gulasch (und vielen anderen Leckereien!) aufgepäppelt. Elisa hat diese anspruchsvolle Aufgabe in deiner Elternzeit übernommen, sodass ich die letzte Etappe bis zum Einreichen der Doktorarbeit nicht verhungert bin.

Sascha, Daniel, Veit, Micha, Tom, Christopher, Alex, Roman u.a. danke ich für die zahlreichen zynischen Kommentare und Gespräche, ohne die ich mich wohl schon längst für verrückt erklärt hätte.
In line with this I thank Fabio for sharing with me the view of realism (with a tendency to pessimism and sarcasm).
- It was a pleasure for me attending that marvellous time of epic failures!

Elisa+Flosch+Alma, Christopher+Tim, Sina, Fabio, Jan+Frank, Alex+Sinead, Regi+RoRö+ Nora+Niklas, Veit+Franzi+Ida, Ahmed, Lydia, Tom u.a. vielen Dank für die lustigen Stunden bei Movie Nights, Volleyball, Dinner, Spex- und Hat-Vorbereitungen, Christmas Movies, Drachen-boot, Partys u.v.m.

Meiner Familie, Mathias, Maria, Anna, Isa, Gerald und darüber hinaus gilt mein Dank allen namentlich nicht erwähnten Verwandten, Freunden und Bekannten, für die Unterstützung, Motivation sowie jegliche Ablenkung nach etlichen missglückten Experimenten in den letzten Jahren.

Mathias, die Doktorarbeit ist fertig („yippie yeah“) und du kannst endlich deine XXX machen!

Curriculum Vitae

Personal Information

Amelie Baschwitz

Eichendorffweg 2

07745 Jena, Germany

Born May, 9th 1985 in Altenburg (Thüringen), Germany

Education

11.2011 – present	***PhD student***
11.2011 – 11.2014	***Stipend of the International Max Planck Research School***
	Max Planck Institute for Chemical Ecology in Jena, Germany
	Department of Evolutionary Neuroethology
	Research Group Olfactory coding
	Thesis advisors: Prof. Bill S. Hansson, Dr. Silke Sachse, Dr. Michael Schmuker
	Thesis Title:
	Elucidating the olfactory pathways within and beyond the antennal lobe in *Drosophila melanogaster*
10.2005 - 09.2011	***Diploma in Biochemistry***
	Friedrich – Schiller – University Jena, Germany
	Thesis advisors: Prof. Bill S. Hansson, Dr. Silke Sachse
	Thesis Title:
	Characterization of inhibitory olfactory projection neurons in *Drosophila melanogaster*

Scientific employment

10.2008 - 03.2011	Student assistent at MPI CE Jena by Dr. Y. Seki
	Reconstruction and volume measuring of neurons in *Drosophila*

Publications

2016 Grabe V., Baschwitz, A., Dweck, H. K. M., Lavista-Llanos, S., Hansson, B. S., Sachse, S.

Elucidating the neuronal architecture of olfactory glomeruli in the *Drosophila* antennal lobe. Cell Reports, 16

2015 Grabe, V., Strutz, A., Baschwitz, A., Hansson, B. S., Sachse, S.

A digital *in vivo* 3D atlas of the antennal lobe of *Drosophila melanogaster*. The Journal of Comparative Neurology, 523(3)

2014 Strutz, A., Soelter, J., Baschwitz, A., Farhan, A., Grabe, V., Rybak, J., Knaden, M., Schmuker, M., Hansson, B. S., Sachse, S.

Decoding odor quality and intensity in the *Drosophila* brain. eLife, 3

2013 Linz, J., Baschwitz, A., Strutz, A., Dweck, H., Sachse, S., Hansson, B. S., Stensmyr, M. C.

Host plant-driven sensory specialization in *Drosophila erecta*. Proceedings of the Royal Society B: Biological Sciences, 280

Oral Presentations

04.2014 *Drosophila* als Modellorganismus - Erforschung der Neurobiologie des Riechens

Presentation of current research topics in the Department of Evolutionary Neuroethology and guided tour through the laboratories for pupil of the Goetheschule Ilmenau

03.2014 Numerical integration of input & output neurons in the primary olfactory center of the fruit fly

13. IMPRS Symposium, MPI for Chemical Ecology, Dornburg, DE

09.2013 Quantitative analysis of the input-output connectivity of the *Drosophila* antennal lobe

13th European Symposium for Insect Taste and Olfaction (ESITO), Villasimius, IT

09.2012 Coding of odor valence in neural circuits of *Drosophila*

Chemical Ecology 2012 Mini-Symposium, Rothamsted, GB

Additional Qualifications

09.2016 Project Management, Speaker: Peter Wagner

09.2016 Time and Self-Management for Scientists, Speaker: Matthias Schwarzkopf

06.2016 Experimental Design Workshop, Speaker: Andrew Davis

05.2016 Communication - How to Manage Your Supervisors, Speakers: Dr. Alexander Schiller, Dr. Daniel Mertens

10.2015 Scientific writing, Speaker: Brian Cusack/Science Craft

03.2015 Gene Safety Project Leader Certificate, Speaker: Monika Wetzker and invited Speakers

07.2014	Introductory workshop on neural and behavioral modeling in *Drosophila*, Speakers: Prof. Thomas Nowotny, Dr. Ruben Moreno Bote, Dr. Greg Stephens
06.2014	Research Funding - Third Party Grant Proposals, Speaker: Dr. Jan Kellmann
05.2013	Functional imaging of neuronal activity, Speaker: Dr. Silke Sachse
02.2013	Innovative Morphology and Phylogeny, Speaker: Prof. Rolf Beutel
02./03.2013	Introduction into the statistical program R, Speaker: Dr. Grit Kunert
11./12.2012	Frontiers of Chemical Ecology, Speakeren: Dr. Shannon Olsson and invited Speakers
06.2012	Adobe Illustrator, Speaker: Nico Überschaar
03.2012	Multiphoton microscopy: a powerful bioimaging technique, Speaker: Prof. Dr. Rachel Grange
01.2012	How to prepare a scientific poster, Speaker: Dr. Karin Groten

Grants

Travel Grant of the European Science Foundation (ESF) for:

Flies, Worms and Robots: Combining Perspectives on Minibrains and Behaviour,

Sant Feliu de Guixols, Spain, 8 - 13 November 2014

Jena, February 1, 2017

Amelie Baschwitz